Development and Characterization of Low Cost Ceramic Membrane for Liquid Phase Separation Applications

Monash P.

(Reg. No: 06610703)

Thesis submitted for the degree of Doctor of Philosophy

Department of Chemical Engineering

Indian Institute of Technology Guwahati

Guwahati, India

April, 2011

Declaration

This is to certify that the thesis entitled, **Development and Characterization of Low Cost Ceramic Membrane for Liquid Phase Separation Applications**, being submitted for the award of degree of Doctor of Philosophy, is an authentic record of the research carried out by me in the Department of Chemical Engineering, Indian Institute of Technology Guwahati, India, under the supervision of Dr. G. Pugazhenthi. The work documented in this thesis has not been submitted to any other university or institute for the award of any degree.

.

Mr. Monash P.
Research Scholar,
Department of Chemical Engineering,
Indian Institute of Technology Guwahati,
India.

Date:

Department of Chemical Engineering

Indian Institute of Technology Guwahati

India

Certificate

This is to certify that the thesis entitled, **Development and Characterization of Low Cost Ceramic Membrane for Liquid Phase Separation Applications**, being submitted by **Mr. Monash P.** for the award of degree of Doctor of Philosophy, is an authentic record of the research carried out by him in the Department of Chemical Engineering, Indian Institute of Technology Guwahati, India, under my supervision. The work documented in this thesis has not been submitted to any other university or institute for the award of any degree.

_____.

(Signature of Thesis Supervisor)

Dr. G. Pugazhenthi
Associate Professor,
Department of Chemical Engineering,
Indian Institute of Technology Guwahati,
India.

Date:

ABSTRACT

A porous membrane support is prepared with low cost ceramic materials by a simple uniaxial compaction method. The effect of sintering temperature (850-1000°C) on porosity, mean pore size, pore size distribution, shrinkage, flexural strength and pure water permeability was investigated. The raw materials and sintered supports were characterized using thermo gravimetric analysis (TGA), particle size distribution (PSD), X-ray diffraction (XRD) and scanning electron micrograph (SEM) analysis. Based on the characterization results, the support sintered at 950˚C (porosity = 44%, flexural strength = 28 MPa, average pore diameter = 1.01 μm, and water permeability = 4.46×10^{-6} m/s kPa) is considered as the optimum support (referred as support-I) for membrane applications. Subsequently, the effect of TiO_2 (3g and 6g) addition on the properties of the optimized support (support-I) is also examined and no substantial changes is observed for the TiO_2 added membrane supports. All the membrane supports are investigated for the separation of oil and BSA from its solution. A higher rejection value of 90-99% is obtained for separation of oil through these supports. However, less rejection is observed for BSA. To improve the separation performance, a selective γ-Al_2O_3 layer (thickness = 2.6 μm, pore diameter = 5.4-13.6 nm) is developed on the support-I by dip-coating using a stable boehmite sol (d_{avg} =30.9 nm) synthesized from inexpensive aluminium chloride. The boehmite sol and the γ-Al_2O_3-clay (clay refers to support-I) composite membrane are characterized with TGA, XRD, SEM, Fourier transform infrared spectroscopy (FTIR), dynamic light scattering (DLS) and liquid displacement techniques. The separation performance of the membrane is investigated using BSA and electrolyte ($AlCl_3$ and $MgCl_2$) solution by varying the process parameters such as pH, applied pressure and feed concentration.

The separation results confirm that the rejection and permeability mainly depend on electrostatic attraction/repulsion between the membrane and the solute molecules (BSA, electrolyte). The intrinsic rejection is estimated using Spiegler-Kedem model and the higher rejection (99% for BSA, 72% for $MgCl_2$ and 88% for $AlCl_3$) and permeate flux (3.4×10^{-5} m/s for BSA, 9.6×10^{-5} m/s for $MgCl_2$ and 4.4×10^{-5} m/s for $AlCl_3$) values confirm that the fabricated γ-Al_2O_3-clay composite membrane is potential for liquid phase separation applications. The estimated cost of the membrane (26.04 \$/m^2) suggests that this could be an alternate for high cost commercial ceramic membranes.

ACKNOWLEDGEMENTS

First of all my deepest gratitude goes to **Dr. G. Pugazhenthi** for his guidance and constant support. I would also like to thank my doctoral committee members **Dr. Anil Verma, Dr. Pallab Ghosh and Dr. Kannan Pakshirajan** for their advice and valuable inputs. Their comments and suggestions have all helped me to accomplish the thesis work. I would like to specially thank Dr. Pakshirajan for engaged me as a Senior Research Fellow in his CSIR research project.

I would also like to thank other faculty members who supported me from their perspective. I would like to take this opportunity to specially thank **Dr. Ramgopal Uppaluri** for his valuable comments and feedback helped me to bring this thesis to the present form.

I would like to thank our department scientific officers and staffs Mr. Subodh, Ms. Sumedha Sharma, Mr. Kaustavmoni Deka, Mr. Lukumoni Borah (looks), Mr. Prasun Bhattacharjee, Mr. Balen Mahanta and Mr. Pankaj for their support.

I would appreciate the support given by the Central Instrument Facility (CIF) staffs Mr. Senapati, Mr. Chandan Borgohain, Mr. Madhurjya Borah and Mr. Singh. I would also thank Mr. Indrajit Talukdar and Mr. Kaustubh Acharyya from the Centre for Nanotechnology for XRD and DLS analysis.

Special thanks to Dr. P. Saravanan and Dr. P. Gopinath for their advice and inputs at initial stages of my research. The days are lively with their presence and I never felt that I am away from my hometown. I am intellectually indebted to Mr. J. Anto Pradeep and Mr. P. Aadaleesan for their ideas and conversations.

I would also like to thank my seniors Dr. Bishwanath Saha, Dr. Siva Shankar, Dr. Subham Paul, Dr. Pradeep Chowdhary, Dr. Debasis Ghosh and Dr. Barun Nandi for their advice and suggestions. I would like to acknowledge my friends Mr. Biraj Kumar Kakatti, Mr. Subramanian, Mr. Gunin Saikia, Mr. Sakthivel and Mr. Karthick who helped me by providing scientific instruments for the characterization of my samples.

Special thanks to Mr. N. Vinothkumar for his help at the crucial time. I would also thank other friends Ramakrishnan, Santhosh Kumar, Murugadoss, Ashok Kumar, Eswaran, Anandaraj, Murugavelh and Vasanth for their love and support.

I am forever indebted to my parents Mr. G. Purushothaman, Ms. Jagatha and Ms. Kalaiselvi for their endless patience. Last, but not least, I want to thank my brothers Mr. P. Logesh and Mr. P. Magesh for their constant encouragement and belief throughout my life.

Many other people, not mentioned here but present in my soul, I greatly acknowledge their support to accomplish my doctoral study.

Guwahati, April 2011 (Monash P.)

CONTENTS

LIST OF FIGURES

भारतीय प्रौद्योगिकी संस्थान गुवाहाटी
Indian Institute of Technology Guwahati

LIST OF TABLES

NOMENCLATURE

A	Effective membrane area (m^2)
C_f	Concentration of the feed solution (ppm)
C_m	Concentration of solute at the membrane surface (ppm)
C_p	Concentration of the permeate solution (ppm).
D_{avg}	Average pore diameter (μm),
d_{XRD}	Crystallite size (nm)
F	Flow parameter
F_p	Load at the fracture point (kN)
J or J_v	Solute or permeate flux rate (m/s)
J_w	Pure water flux (m/s)
$\frac{J}{\Delta P}$	Permeability (m/s kPa)
K	Shape constant
L	Span length (mm)
L_p	Hydraulic permeability (m/s kPa)
m_A	Mass of the water saturated support (g)
m_D	Mass of the dry membrane support (g)
m_w	Mass of the membrane support when pores filled with water (g)
P_m	Solute permeability of the membrane (m/s kPa)
Q	Volume of water permeated (m^3)
R	Universal gas constant

R_{int}	Intrinsic or real rejection (%)
R or R_{obs}	Observed rejection (%)
r_m	Mean pore radius (μm),
$\Delta C (= C_m - C_p)$	Difference in the concentration of the solute at the membrane surface and in the permeate
ΔP	Transmembrane pressure (kPa)
ΔT	Sampling time (s)
Δx or t	Thickness of the membrane or membrane support (μm or mm)
λ	CuKα radiation wave length (Å)
β	Full width at half maximum (Radians)
θ	Diffraction angle (°) or Contact angle (°)
ε	Porosity (%)
σ_{fl}	Flexural strength (MPa)
μ	Viscosity (cP or kPa s),
$\Delta\pi$	Osmotic pressure difference (kPa)
γ	Interfacial tension between the two fluids (mN/m)
σ	Membrane reflection coefficient (dimensionless)

Chapter 1

INTRODUCTION

1.1 DEFINITION

Membrane can be defined in several ways, however, the International Union of Pure and Applied Chemistry (IUPAC) defines the membrane as "a structure, having lateral dimensions much greater than its thickness, through which mass transfer may occur under a variety of driving forces" (Koros *et al.,* 1996). A simplified working definition of a membrane can be conveniently stated as a permselective barrier (active or passive) that permits or restricts preferential passage of one or more selected species or components (ions and molecules) present in a gaseous and liquid mixture or solution, under the influence of a driving force (Ho and Sirkar 1992; Hsieh 1996; Baker 2004). Generally, the driving force for the separation could be pressure gradient (ΔP), concentration gradient (ΔC), electrical potential gradient (ΔE) and temperature gradient (ΔT). In some membrane separation operations, more than one driving force can be applied. In such cases, anyone of the above mechanism is dominant (Ho and Sirkar 1992; Tsuru 2001). The stream leaving a membrane module with penetrated

components is called as the permeate stream and the stream that leaves the membrane module without passing through the membrane is called as a retentate or raffinate stream (Koros *et al.,* 1996; Tsuru 2001).

1.2 CLASSIFICATION OF MEMBRANE PROCESSES

Many types of membrane processes exist that can be classified into various groups based on various criteria (Hsieh 1996). Generally membrane classification is either based on the mode of operation or driving force. Operationally, membrane processes can be classified into either dead-end or cross flow mode. This is according to the direction of the feed stream relative to the orientation of the membrane surface (Hsieh 1996; Koros *et al.,* 1996). A schematic of the membrane process operated in different modes is shown in Fig. 1.1. In dead-end filtration mode, both the feed and permeate stream flow is perpendicular to the membrane surface and only outlet for upstream fluid is through the membrane. Generally, it is a batch separation process widely used in laboratory for the characterization of membranes. In cross flow filtration the fluid on the upstream side of the membrane moves parallel to the membrane surface and the fluid on the downstream side of the membrane moves away from the membrane in the direction normal to the membrane surface. This concept is widely used for the majority of the membrane separation applications. Any stagnant and accumulated rejected species on the membrane surface can be removed by the shear force exerted by the flowing feed stream. Due to this reason, permeation rate is enhanced. Cross flow filtration can be operated in co-current or counter-current mode using a sweep stream. In co-current flow, the fluid on the upstream and downstream sides moves parallel to the membrane surface and in the same direction.

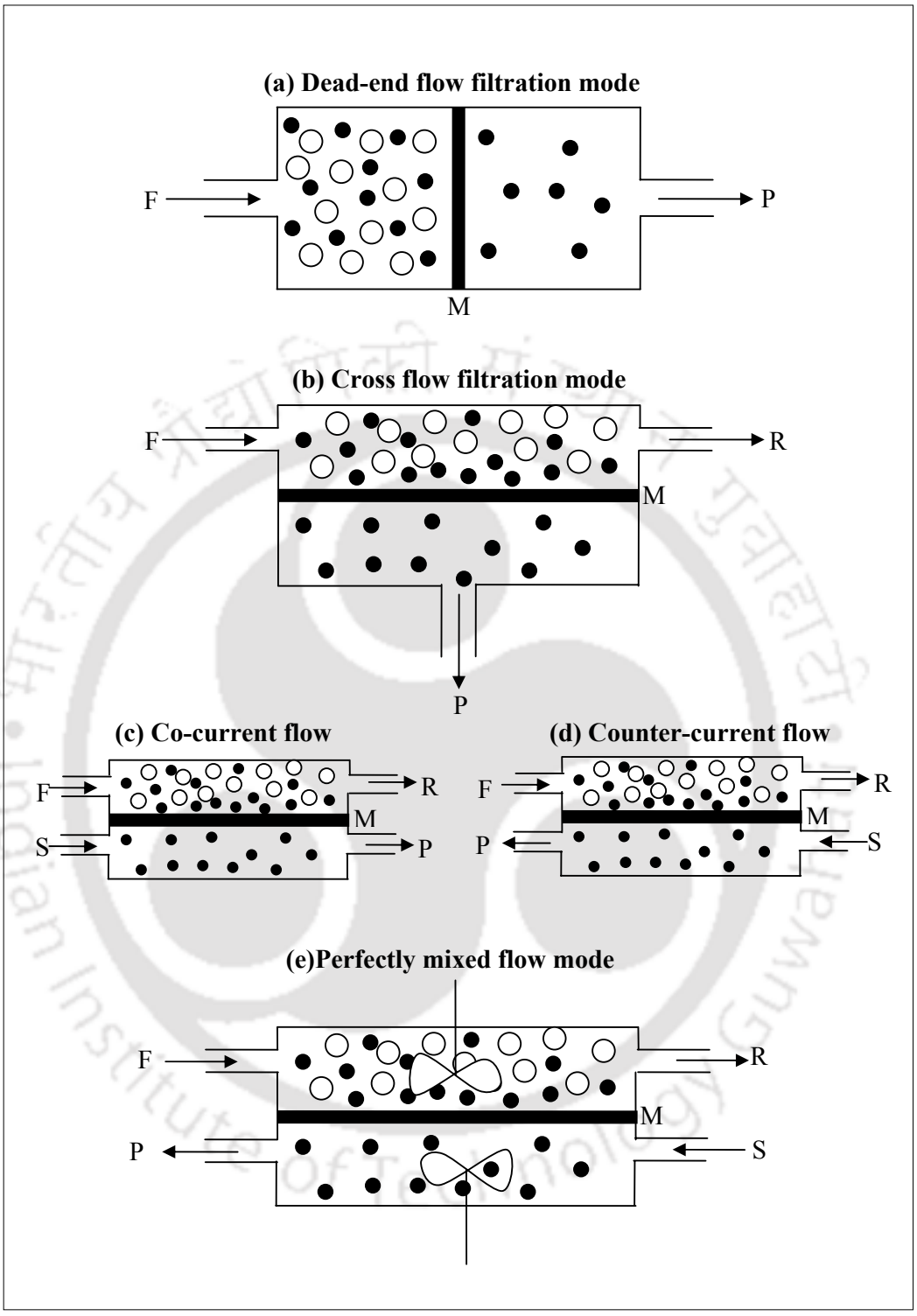

Fig. 1.1 Schematic of different modes of operation in a membrane process.

F- Feed; M-Membrane; P- Permeate; R-Retentate; S-Sweep stream

In the case of counter current flow, the upstream and downstream fluid moves parallel to the membrane surface but in opposite directions. When the upstream and downstream fluid of the membrane unit is well-mixed individually, the flow is called as completely or perfectly mixed flow.

Dead-end filtration can be used for treating feed streams containing less than 0.1% solids and the cross flow filtration can be used to treat the feed streams containing 0.5% solids (Baker 2004). Both dead-end and cross flow mode filters can be used within these limits depending on the particular characteristics of the application. A semi dead-end filtration can be used for a feed stream containing very low solid loading or concentration such as removal of bacterial and virus from water. Initially the membrane unit is operated as a dead-end filter to maintain a useful flow across the filter (Baker 2004). When the pressure required to maintain the useful flow across the membrane filter reaches its maximum, the membrane is operated in cross-flow mode with backflushing using air or permeate solution. After a short period of backflushing in cross flow mode to remove material deposited on the membrane, the system is switched back to the dead-end operation (Baker 2004).

The classification of the membrane separation process based on driving force is represented schematically in Fig. 1.2 (Mulder 1996; Li 2007). Pressure driven membranes have a wide and diverse range of applications. The driving force is the pressure gradient that provides the energy to separate the feed molecules. Pressure driven membrane processes are very popular because of their simplicity, cost effectiveness and higher feed processing rate.

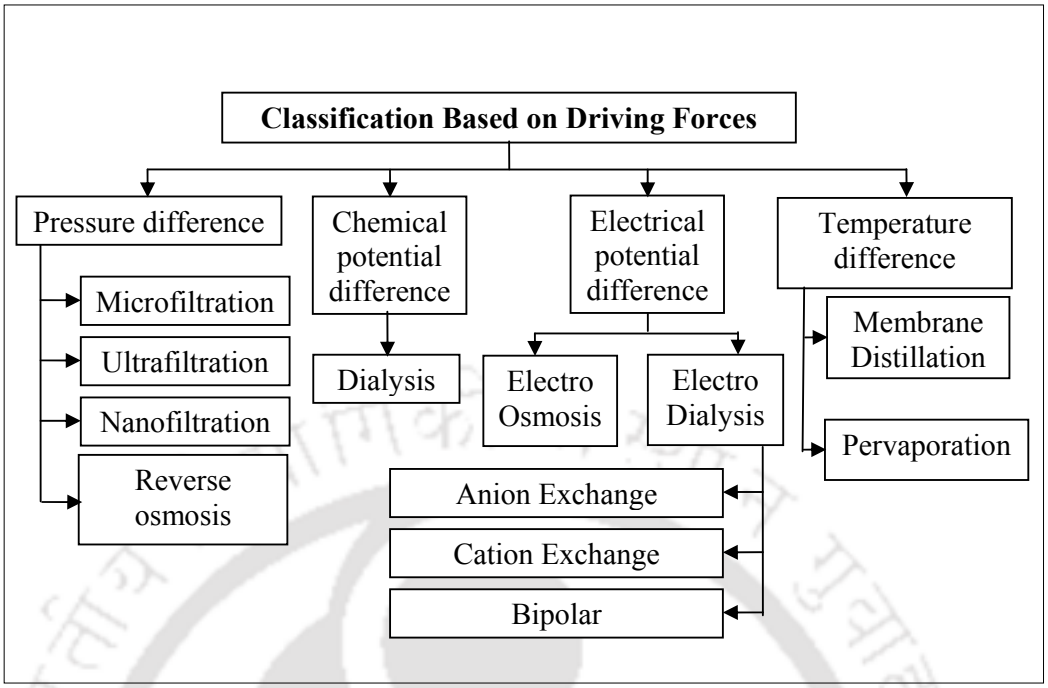

Fig. 1.2 Classification of membranes based on driving forces.

Table 1.1 Characteristics of the pressure driven membrane processes

Process	Pore size (nm)	Pressure (bar)	Materials retained	Materials passed
MF	> 100	< 2	Particles (bacteria, yeast, etc.)	Water, salts and macromolecules
UF	2-100	1-10	Macromolecules, colloids, lattices solutes M_W > 10,000	water, salts and sugars
NF	< 2	5-20	Solutes M_W > 500, di and multivalent ions	Water, sugars and monovalent ions
RO		15-80	All dissolved and suspended solutes (sugars, salts etc.,)	Water

Pressure driven membrane processes are classified as microfiltration (MF) (where suspended particles and dissolved macromolecules larger than 0.1 μm are rejected), ultrafiltration (UF) (where particles and dissolved macromolecules smaller than 0.1 μm and larger than 2 nm are rejected), nanofiltration (NF) (where particles less than 2 nm are rejected) and reverse osmosis (RO) (liquid-phase separation process in which applied transmembrane pressure causes selective movement of solvent against its osmotic pressure difference). The characteristics of these processes are given in Table 1.1 (Koros *et al.,* 1996; Mulder 1996).

Dialysis is a membrane process in which the transport of solutes is driven primarily by concentration difference, ie., chemical potential difference, rather than by pressure or electrical-potential difference, across the thickness of a membrane. Dialysis membrane is commonly used for kidney dialysis, in which the driving force is created by the higher concentration of the impurities in the blood compared to the buffer (Baker 2004; Li 2007). The electrical potential difference membrane process is classified as electro-dialysis (in which ions are driven through an ion-selective membrane under the influence of an electric field) and electro-osmosis (in which water is transported across the thickness of an ion-exchange membrane under an applied electric field).

An overview of the typical membranes separation processes along with their fields of application and corresponding driving forces are given in Table 1.2 (Hsieh 1996; Nasef and Hegazy 2004).

Table 1.2 Overview of the typical membrane separation processes along with their field of application and the driving forces

Membrane process	Driving force (Membrane type)	Phases involved	Field of application
Dialysis	ΔC (Dense)	Liquid/ liquid	Purification of polymer solutions, hemodialysis, controlled-release, alcohol reduction in beer
Reverse osmosis	ΔP (Dense)	Liquid/ liquid	Desalination
Microfiltration	ΔP (Porous)	Solid/ liquid	Clarification of beverages, cell harvesting, reduction of bacteria and particulate turbidity, production of ultra-pure water for semiconductor industry
Ultrafiltration	ΔP (Porous)	Liquid/ liquid	Purification and concentration of juices and polymer solution, protein recovery and waste water purification in dairy industry, starch recovery and pharmaceuticals
Nanofiltration	ΔP (Porous)	Liquid/ liquid	Desalination of brackish and sea water, purification of waste water, metal recovery from galvanic industry waste water, concentration of juice and milk
Electrodialysis	ΔE (Dense/ porous)	Liquid/ liquid	Production of salt and ion free water from seawater, reduction of acidity of citrus juices, chloro-alkali, production of sulfuric acid
Pervaporation	ΔP, ΔC and ΔT (Dense)	Liquid/ vapor/ liquid	Dehydration of organic solvents, separation of isomer solvents, recovery from water
Membrane distillation	ΔP, ΔC and ΔT (Dense)	Liquid/ vapor/ liquid	Liquid production of pure water, solvent recovery
Gas separation	ΔP (Dense/ composite)	Gas/gas	Natural gas purification, oxygen enrichment
ΔC = Concentration difference; ΔP = Pressure difference; ΔE = Electrical Potential difference; ΔT = Temperature			

Electro-dialysis membranes are ion exchange membranes which are classified into three basic categories such as anion exchange (membrane containing fixed cationic charges and mobile anions that can be exchanged with other anions present in an external fluid in contact with the membrane), cation exchange (membrane containing fixed anionic charges and mobile cations which can be exchanged with other cations present in an external fluid in contact with the membrane) and bipolar (synthetic membrane containing two oppositely charged ion-exchanging layers in contact with each other) membranes depending on the type of ionic groups attached to the polymer matrix (Li 2007). Most of the inorganic ion-exchange membranes are made up of zeolites.

The type and concentration of the fixed ionic charges determine the permselectivity and electrical resistance of the membrane. Further, they also have a significant effect on the mechanical properties of the membrane. Temperature driven membranes are classified into pervaporation and membrane distillation. Their separation also depends on the pressure and concentration difference. Pervaporation is a membrane based separation process in which both the feed and retentate streams are liquid phases while permeate emerges at the downstream side of the membrane is a vapor (Baker 2004). In membrane distillation process, liquid and gas phases are separated by a porous membrane, whose pores are not wetted by the liquid phase (Baker 2004).

1.3 MEMBRANE CLASSIFICATION BASED ON NATURE

Membrane classification based on the nature is schematically represented in Fig. 1.3. Membranes are classified into two types, namely natural or biological and synthetic membranes.

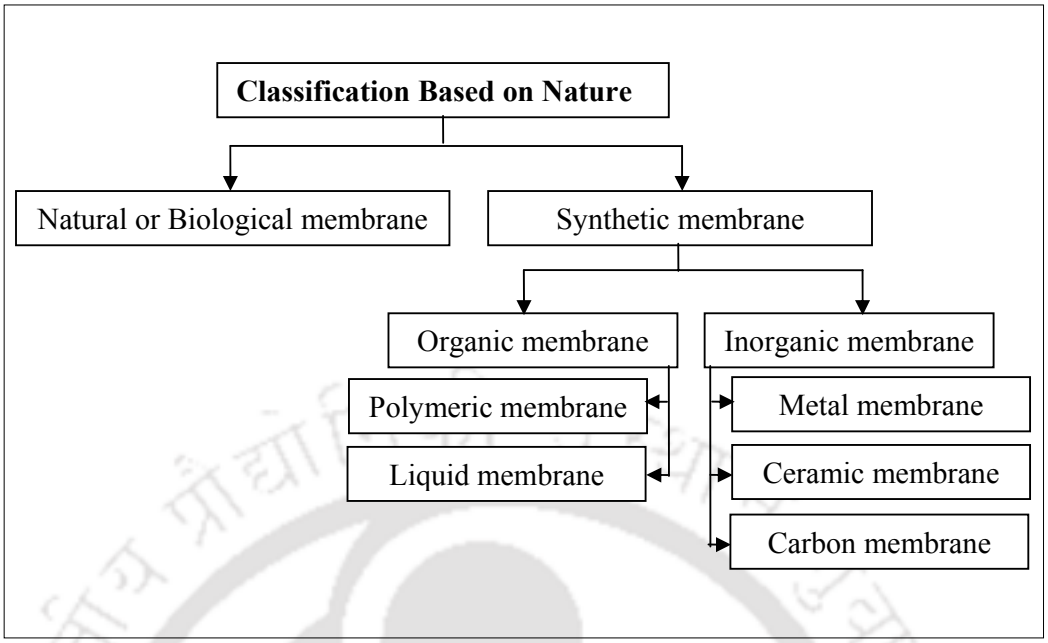

Fig. 1.3 Classification based on the nature of the membranes.

Earlier stages of the membranes are made up of natural materials obtained from the bladders of pigs, cattle or fish as well as from the sausage casings of animal gut (Noble and Stern 1995; Baker 2004). Today these have been replaced with the synthetic membranes. Synthetic membranes are classified into two major groups, namely organic and inorganic. For the past 60 years, many polymeric membranes have been commercialized and successfully employed in industries for separation and purification applications due to their higher selectivity (Hsieh 1996; Baker 2004). However most of the recent research works have been focused on development of inorganic membranes attributed to their advantages, such as high thermal, chemical and mechanical stability (Burggraaf and Cot 1996; Tsuru 2001). Although it has many advantages over polymeric membranes, the implementation of inorganic membranes in industries is still limited due to certain difficulties associated with the modules, which are given in Table 1.3 (Caro *et al.,* 2000; Tsuru 2001).

Table 1.3 The arguments (favor and against) of the inorganic membranes

Arguments favor on inorganic membranes	Arguments against inorganic membranes
• Long-term stability at high temperature	• High capital cost
• Resistance to harsh environment	• Brittleness
• Resistance to high pressure	• Low membrane surface per module volume
• Inertness to microbiological degradation	• Difficulty in achieving high selectivities in large scale microporous membranes
• Easy cleanability after fouling	• Generally low permeability of the highly selective (dense) membranes at medium temperature
• Easy catalytic activation	• Difficult membrane-to-module sealing at high temperature

Membranes which are made up of inorganic materials like ceramics, glass, metals, etc., are called as inorganic membranes. In general, ceramic membrane find more application, in liquid phase separation, in which most of the membranes are fabricated using inorganic oxides, such as alumina, titania and zirconia (Burggraaf and Cot 1996; Tsuru 2001).

1.3.1 Types of inorganic membranes

In general, inorganic membranes are broadly classified into two categories, i.e., dense and porous membranes, based on the absence or presence of the pores in the membrane structure. However, the actual classification is based on the transport mechanism of the species through the membrane. If the separation mechanism is mainly controlled by sieving the species (molecules, ions etc.,) then it is called as porous membranes. If the membrane follows general solution-diffusion type

mechanism for the transport of species, then the membranes are referred as dense membranes. The separation mechanism is attributed to the affinity (selective adsorption and diffusion) of molecules with membrane materials and it plays an important and dominant role when the pore size is relatively small.

1.3.1.1 Dense membranes

Two major types of dense inorganic membranes, metal and solid electrolyte, have been studied and developed extensively for gas separation. Dense metal membranes made of palladium and its alloys have been suggested for hydrogen separation and purification applications (Hsieh 1996). Other metal membranes fabricated using tantalum, vanadium and niobium posses better selectivity for hydrogen. Solid electrolyte membranes are made of mixed conducting oxides (doped zirconia and thoria) that are selective to certain ionic species. These are widely applied for oxygen separation. Recently, liquid immobilised membranes (LIMs), which consist of a porous support filled with a liquid or molten salt which is semipermeable, are also regarded as dense membranes (Hsieh 1996). In general, dense membranes are widely applied for the separation and purification of gas systems. Hardly ever, they are used for liquid systems. Schematic of dense membrane is presented in Fig. 1.4(a).

1.3.1.2 Porous membranes

Porous inorganic membranes are prepared with several layers of porous materials. These layers have gradations of pore diameters and each layer is applied and stabilized so as to act as the support for the next finer layer. In general, microfiltration, ultrafiltration and nanofiltration membranes are porous in nature and employed in various industrial liquid phase applications to concentrate or purify dilute (aqueous) solutions (Noble and Stern 1995). The microstructure of the membranes

(shape, size, porosity, tortuosity etc.,) will strongly depend on the method of fabrication (Burggraaf and Cot 1996). Different pore morphologies of inorganic membranes are shown in Fig. 1.4. The simplest form is the symmetric pore morphology that consists of a single, uniformly structured wall of a certain material (also called as stand-alone membranes). Membranes containing indistinguishable separating layer and porous support of homogeneous structure in the direction of the membrane thickness are called as symmetric or isotropic membranes (Fig. 1.4(b)). The main challenge of these membranes is to withstand the processing conditions and especially pressure gradients. Very thin membranes do not exhibit good mechanical strength and a thick membrane creates more transport resistance and this results in decreased flux through the membrane. The above challenges have been overcome by the use of asymmetric membranes (Burggraaf and Cot 1996; Hsieh 1996; Mulder 1997). Asymmetric membranes consist of a thin top selective layer that is supported on a porous support with large pores (low flow resistance) having sufficient mechanical strength (Fig. 1.4(c)). A composite membrane is a special type of asymmetric membrane, which consists of a porous support and a selective layer with or without one or more intermediate layers of gradually decreasing pore size (Fig. 1.4(d)). The distinction between asymmetric and composite membrane is that the graded pore structure of asymmetric membranes are made from the same material across its thickness whereas in the composite membrane the graded pore layers are made with distinctively different materials (Burggraaf and Cot 1996; Hsieh 1996).

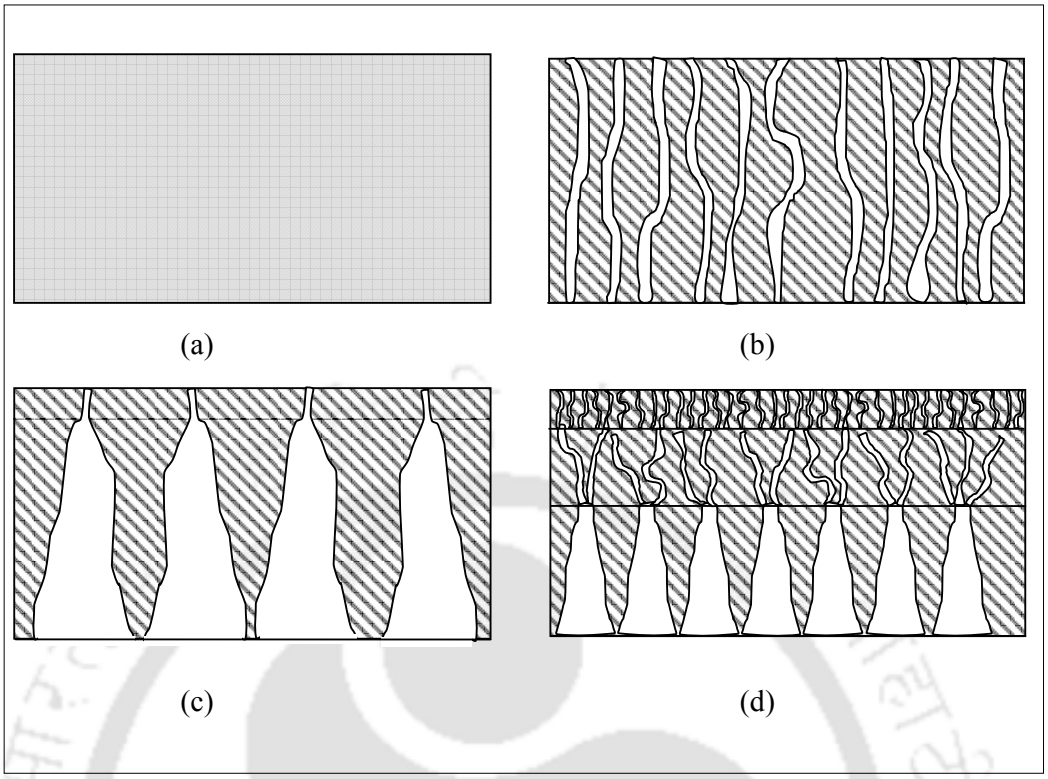

Fig. 1.4 Schematic of pore shapes. (a) Dense membrane, (b) symmetric membrane with cylindrical shaped pore, (c) asymmetric membranes with conical shaped pore and (d) composite membrane with interconnected pores (redrawn from Burggraaf and Cot 1996).

Typical pore structure of a composite membrane (two layered) is schematically represented in Fig. 1.4 (d), which consists of a porous support system, with a few millimeters thickness and pore size in the range of 0.5-10 μm, which provides mechanical strength to the membrane; an intermediate layer, with 10-100 μm thickness and pore size in the range of 0.05-0.5 μm, which acts as transition phase and prevents the top layer from penetrating into the porous structure of the support; and finally a top layer, with 1-10 μm thickness and pore size in the range of 2-50 nm, which plays the main role in membrane filtration processes.

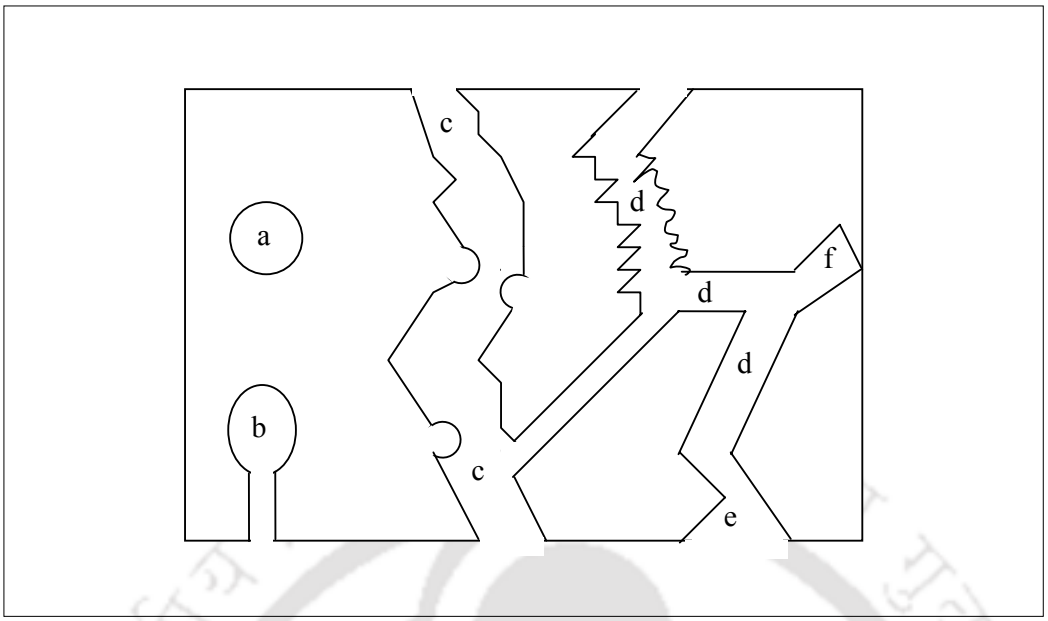

Fig. 1.5 Schematic representation of possible pore types in a porous membrane. a-isolated pore; b,f-dead end pore; c,d-tortuous and/or rough pores; e-conical pore (redrawn from Burggraaf and Cot 1996).

The generic reasons for one or more layers are to decrease the average pore size, surface roughness and void defect density of the membrane support (Burggraaf and Cot 1996). In general, composite membranes must have interconnected pores of tortuous pore networks with many constrictions and dead-end pores. Different types of pores present in a porous membrane are presented in Fig. 1.5. Porosity, pore size distribution, pore shape, roughness, interconnectivity and orientation are the important parameters which influence transport properties and the economic performance. These parameters are indirectly related to the particle size distribution and shape of the starting raw materials (Burggraaf and Cot 1996). In general, a heterogeneous packing provides higher porous and permeable membrane supports with a lesser strength and surface smoothness. The contrary applies for the homogeneous packing.

Preparation of composite or multilayer ceramic membranes has been receiving more attention in the membrane technology due to their higher permeability and selectivity. A good composite ceramic membrane requires a macroporous membrane support with one or more thin defect free separation layers. The macroporous asymmetric membrane support minimizes the hydraulic resistance to the permeate flow resulting in a higher permeability and the thin separation layer resulting in a higher selectivity (Burggraaf and Cot 1996; Hsieh 1996; Mulder 1997; Tsuru 2001).

भारतीय प्रौद्योगिकी संस्थान गुवाहाटी
Indian Institute of Technology Guwahati

Chapter 2

LITERATURE REVIEW AND OBJECTIVE

2.1 INTRODUCTION

In this Chapter, firstly a detailed literature review on the fabrication of inorganic composite membranes is presented. Eventually, various steps involved for the fabrication of membrane supports and selective layers, advantages and disadvantages of each fabrication processes and various parameters that have influence on the membrane formation are presented. The Chapter also deals with the literature review on oil-water separation, bovine serum albumin (BSA) separation and electrolytes separation from their aqueous solutions using membranes. Finally the motivation towards the objective based on the broader literature review, impact of the thesis work to the research community and its organization are presented.

2.2 CERAMIC SUPPORT PREPARATION

From Chapter 1, it is evident that the preparation of a composite ceramic membrane starts with the fabrication of an appropriate support. Generally, the ceramic supports are formed by shaping a powder in the desired shape followed with the consolidation of the green body by sintering. Generally, fabrication of any ceramic membrane support involves the following four main stages:

1. Selection of appropriate inorganic raw materials or precursors
2. Preparation of the powder/paste for membrane fabrication
3. Membrane fabrication or shaping
4. Heat treatment (sintering/firing)

Choice of the raw materials decides the sintering temperature, pore characteristics (porosity, pore size and tortuosity) and cost (economy) of the membrane supports (Burggraaf and Cot 1996). Based on the fabrication methodology of the membrane supports the raw materials are prepared in the form of powder, paste or colloid. The choice of the shaping process decides the geometry of the final product. Circular or tubular shaped membrane supports are common in practice. However, monoliths (honey-comb) and hollow fiber modules are also recently fabricated and utilized for industrial application to process huge feed volumes (Burggraaf and Cot 1996).

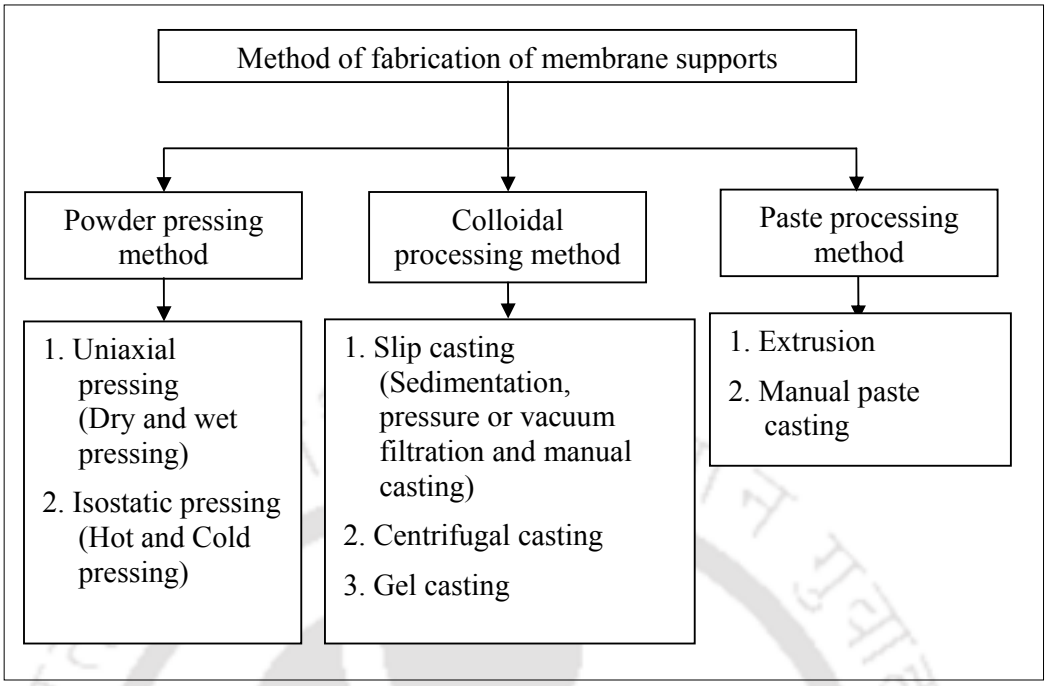

Fig. 2.1 Different methods used for the fabrication of ceramic membrane supports.

Many fabrication methods have been practiced by the researchers for their specific requirement. Eventhough it is very difficult to classify the ceramic support fabrication methods, the majority of the fabricated supports (commercial and home-made membrane supports) would fall under anyone of the following methods represented in Fig. 2.1.

2.2.1 Powder pressing method

Uniaxial pressing method is inexpensive and suitable for high volume production of simple geometrical shapes. The powder is compacted in a rigid die by applying pressure in a single axial direction through a rigid punch or piston. Uniaxial pressing is classified into two types, namely, dry pressing and wet pressing. Wet pressing involves the addition of binders to the ceramic raw materials for shaping and dry pressing involves only the dry powders (without any binder). During fabrication, care

must be taken to avoid the crack formation in the membrane supports, which can be caused by air entrapment, die wear and uneven pressure distribution.

In isostatic pressing, the pressure is applied from multiple directions to achieve greater uniformity of compaction and increased shape capability compared to uniaxial pressing. Isostatic pressing methods are classified into cold and hot isostatic pressing. In the cold isostatic pressing, the isostatic pressure is created by applying an external pressure onto the fluid (water or oil) and this pressure is uniformly applied to ceramic powder to form a required shape. In the case of hot isostatic pressing, the isostatic pressure is created by heating the encapsulated fluid (generally argon gas) to the working temperature and this isostatic pressure is applied to the ceramic powder to form the desired shape.

Many circular shaped membrane supports were fabricated using high purity α-alumina of various particle sizes in mechanical press at high pressures without additives (Jayaraman *et al.,* 1995; Kim and Lin 1999). Over the years, the dry pressing method was replaced with the wet pressing method by the addition of binders, especially organic binders such as poly vinyl alcohol (PVA), poly acrylic acid (PAA), poly ethylene glycol (PEG), methyl cellulose etc., which usually increases the green strength (handling strength), uniformity at the applied pressure and the pore network properties of the support (Palacio *et al.,* 1998; Vercauteren *et al.,* 1998; Falamaki *et al.,* 2004a; Falamaki *et al.,* 2004b; Chang *et al.,* 2005; Wang *et al.,* 2006; Dong *et al.,* 2008). The binder is chosen in such a way that it must be completely burned off during sintering without leaving any ashes on the membrane support. The pore growth in the membrane supports is a function of the initial powder particle size and compaction pressure (Falamaki *et al.,* 2004a). The investigation focused on the evolution of typical membrane characteristics, such as permeability

and tortuosity, of α-alumina and zircon ($ZrSiO_4$) membrane supports and it revealed that the porosity, shrinkage and mean pore size mainly depends on the sintering temperature (Falamaki *et al.,* 2004a). Enhancing the particle size of the raw materials increases the pore size of the membrane along with the compaction pressure required to form the support goes high. (Falamaki *et al.,* 2004a; Falamaki *et al.,* 2004b; Kim and Lin 1999). Only a significant change in the porosity of the membrane supports with an increase in the sintering temperature, however, it is greatly decreased with increased compaction pressure and decreased raw material particle size (De Vos and Verweij 1998; Kim and Lin 1999; Chang *et al.,* 2005; Wang *et al.,* 2006; Dong *et al.,* 2008). However, there is a limitation for compaction pressure and particle size of the raw materials. Increased sintering temperature results in densification of the support that always decreases the permeability and increases the mechanical strength of the support. Most of the research concluded that the optimum sintering temperature of a membrane support is the temperature when the membrane posses maximum permeability along with a reasonable mechanical strength value (De Vos and Verweij 1998; Falamaki *et al.,* 2004a; Bouzerara *et al.,* 2006; Wang *et al.,* 2006).

Few works have been reported on the fabrication of membrane supports by isostatic pressing method (Luyten *et al.,* 1997; De Vos and Verweij 1998; Vercauteren *et al.,* 1998; Gu *et al.,* 2003; Fukushima *et al.,* 2009). Sometimes the support is fabricated by uniaxial pressing followed by isostatic pressing (Luyten *et al.,* 1997; De Vos and Verweij 1998). These investigations revealed that the isostatic pressing results in dense membrane supports with high mechanical strength than uniaxial pressing. Tubular shaped membrane supports could also be fabricated by isostatic pressing methods (Luyten *et al.,* 1997; De Vos and Verweij 1998).

Typical sintering temperature (1200 to 1800°C) of alumina, titania and zirconia membrane supports inevitably increases the production cost. Many research works have been focused to reduce the sintering temperature (Zeng and Gao 1999; Chakradhar *et al.,* 2006; Wang *et al.,* 2006; Dong *et al.,* 2008). Zeng and Gao (1999) pointed out that the reduced particle size of α-Al_2O_3 (<20 nm) resulted in low sintering temperature (below 1000°C). Several low temperature sintering technologies (such as liquid phase assisted sintering) involve the doping of raw powders with transition metal oxide and high reactivity nanometric size powders (Luyten *et al.,* 1997; Sathiyakumar *et al.,* 2002; Wang *et al.,* 2006; Dong *et al.,* 2008; Fukushima *et al.,* 2009). Instead of organic binders, some inorganic sintering aids have been used to decrease the sintering temperature as well as to enhance the pore property, porosity and strength of the membrane support. In many research works, calcium carbonate is used as an inorganic sintering aid to increase the porosity of the membrane support. Magnesium carbonate, sodium carbonate and calcium magnesium carbonate have also been used as porosifiers (Palacio *et al.,* 1998; Bouzerara *et al.,* 2006; Fukushima *et al.,* 2009). The decomposition of $CaCO_3$ produces largest pores at lower temperature (<1000°C). However, higher temperature (>1300°C) led to reduced pore size due to the liquid phase sintering mechanism, which produces low melting calcium-aluminate and calcium-aluminate-silicate species (Falamaki *et al.,* 2004b). In addition, it also reduces the tortuosity and roughness that results in more rounded shaped pores. Their work confirmed that, with proper choice of the process parameters (such as sintering temperature and amount of porosifier), it is possible to fabricate rounded pore shape membrane supports with higher permeability. Wang *et al.,* (2006) fabricated ceramic supports using α-alumina with titania (rutile) as sintering aid and their observations

revealed that the addition of rutile powder to alumina drastically reduces the porosity, pore size and the corrosion resistance of the membrane support.

Several research works have been focused on the other way of reducing the cost of the ceramic support by the use of low cost raw materials (Palacio *et al.,* 1998; Bouzerara *et al.,* 2006; Dong *et al.,* 2008). In order to reduce the fabrication cost, mullite ceramic supports have been synthesized from various inexpensive natural mineral materials, especially from kaolin. Other starting materials are sometimes added to increase the concentration of mullite phase (Palacio *et al.,* 1998; Bouzerara *et al.,* 2006; Chakradhar *et al.,* 2006; Dong *et al.,* 2008; Bi *et al.,* 2011). The addition of wollastonite to the ceramic mixtures reduces the sintering time and temperature as well as increases the strength of the membrane supports (Chakradhar *et al.,* 2006; Bi *et al.,* 2011).

In general, most of the membrane supports are fabricated with high purity α-alumina powder as a starting material and sintered at high temperature, which increases the cost of the membranes (Luyten *et al.,* 1997; De Vos and Verweij 1998; Dong and Lin 1998; Vercauteren *et al.,* 1998; Kim and Lin 1999; Falamaki *et al.,* 2004a; Falamaki *et al.,* 2004b; Wang *et al.,* 2006). Kaolin based mullite ceramic supports have been found to be one of the best alternate for α-alumina, due to its outstanding properties, such as low thermal conductivity and expansion, excellent creep resistance and excellent thermal, chemical and mechanical stability. In addition, it will retain porosity at elevated temperatures. Although few reports were found for low cost kaolin supports, however, a complete investigation on its properties are not yet available as compared to the research carried out with commercialized high cost alumina, zirconia and titania membrane supports.

2.2.2 Colloidal processing method

Based on the consolidation mechanism, the colloidal processing methods are classified in to three major classifications, namely slip, centrifugal and gel casting. In slip casting, ceramic membranes of several pore diameters have been fabricated by pouring a stable slip (suspension of clay or ceramic material in water) in porous mould; especially gypsum mould or in nonporous surfaces, such as petridishes or glass plates. Based on the fabrication and solvent removal mechanism, the slip casting is termed as sedimentation (Darcovich *et al.,* 2001; Wang *et al.,* 2001; Weir *et al.,* 2001), pressure or vacuum filtration (Garrido and Aglietti 2001; Shqau *et al.,* 2006; Maleksaeedi *et al.,* 2008; Mottern *et al.,* 2008) and simply slip casting, which refers to casting the slip in porous moulds, (Hyun and Kang 1994; Huang and Chen 1995; Erdem *et al.,* 2006).

The first and foremost hard challenging task in the slip casting process is the preparation of stable colloidal suspension by controlling various interaction forces, such as Van Der Waals, steric, electrostatic and interparticle forces. The particle size and its concentration in the slip determine the pore characteristics of the membrane supports. In general, the pore size distribution of the membranes depends on the state of aggregation of the particles (see Fig. 2.2), which could be controlled with the addition of surfactants or dispersing agents and acids or bases. Generally, stable slips are obtained by controlling the pH at a particular value (Hyun and Kang 1994; Huang and Chen 1995; Darcovich *et al.,* 2001; Erdem *et al.,* 2006). In general, the colloidal suspensions are in dispersed and flocculated (weakly or strongly flocculated) states, as shown schematically in Fig. 2.2.

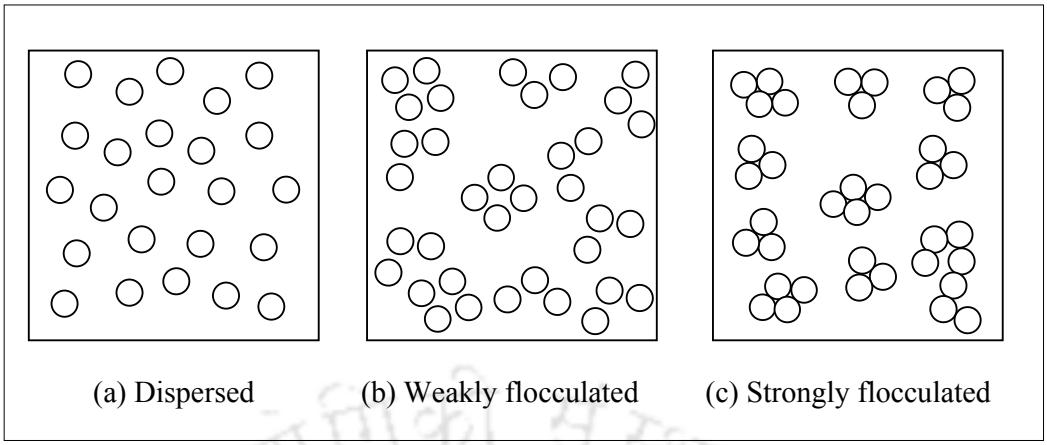

Fig. 2.2 Schematic illustration of different forms of colloidal suspension.

In general, ammonium polymethylacrylic acid electrolyte ($NH_4^+PMA^-$, commercially referred as Darvan C) is used as a dispersing agent (Darcovich *et al.,* 2001; Steenkamp *et al.,* 2002; Hyun and Kang 1994; Erdem *et al.,* 2006), starch as pore forming agent (Erdem *et al.,* 2006) and pH was adjusted with acids or bases (Darcovich *et al.,* 2001; Chowdhury *et al.,* 2005; Shqau *et al.,* 2006). Also, PVA is used as binder and colloid stabilizer (Huang and Chen 1995) and sometimes inorganic ceramic materials, such as kaolin, $CaCO_3$, SiO_2, alumina and yittria, have been used as sintering aids (Moreno *et al.,* 1999; Jun-hui *et al.,* 2002).

Various methodologies, such as stirring, grinding (in ball mills), sonicating and degassing, have been practiced by the researchers to obtain a homogeneous slip solution (Huang and Chen 1995; Steenkamp *et al.,* 2002; Shqau *et al.,* 2006). The particle size and surface charge of the starting raw material decides the stability of the slip solution. Many investigations reported in literature were focused on the high purity α-alumina of different particle sizes by varying the concentrations of the slips (Huang and Chen 1995; Steenkamp *et al.,* 2002; Shqau *et al.,* 2006). In general, this technique is widely used for the fabrication of UF and NF membranes, however, some

macroporous supports have been fabricated by the flocculated slips (Huang and Chen 1995; Darcovich *et al.,* 2001; Erdem *et al.,* 2006). Generally, the narrow particle size results in narrow pore size distribution and these membranes have higher selectivity. However the permeation and separation results reported by Darcovich *et al.,* (2001) revealed that superior performance were obtained from the functionally gradient pore size membrane supports than the narrow pore size dense membrane supports.

Centrifugal casting method is used to prepare tubular membrane supports from the slip solution subjected to a high centrifugal force. The largest particles present in the suspension move firstly to the mould wall followed by the smaller particles. The quality of the outer surface of the tubular support depends on the surface quality of the mould, whereas the inner surface of the support depends on the suspension quality, especially the quantity of the smallest particles present in the suspension (Burggraaf and Cot 1996; Steenkamp *et al.,* 2002). Speed of the centrifuge and the particle size distribution of the slip solution are the main parameters that affect the mean pore size of the membrane supports.

Gel casting is based on the theory of in-situ polymerization of monomers on ceramic slurry, which forms a strong and cross-linked polymer-solvent gel after poured into a mould (Liu *et al.,* 2001; Prabakaran *et al.,* 2002). The acrylate monomer in organic solvent was used in gel casting and was replaced with the acrylamide monomer in water due to the anticipation of environmental problems and additional costs concerned with the removal of the organic solvents. Generally, two monomers have been used; the main monomer (acrylamide) has a single double bond and forms a linear polymer upon polymerization and the second monomer is the crosslinking monomer (N,N-methylenebisacrylamide (MBAM)) which has at least two double bonds. When both are polymerized together, a cross linked polymer-solvent gel is

formed (Meng *et al.,* 2000; Liu *et al.,* 2001; Jun-hui *et al.,* 2002; Prabakaran *et al.,* 2002). The highest health hazard rating (1-low, 2-moderate, 3-high and 4-extreme) of the monomers (acrylamide-4, MBAM-2) limits its commercialization. Some special fabrication methods, such as electro-deposition (Mohammadi and Pak 2003), have also been employed for the fabrication of the membrane supports by the colloidal processing method.

2.2.3 Paste processing method

Paste processing is one of the widely used traditional technique for the fabrication of ceramic membranes. Membrane supports are fabricated by extrusion and manual pasting method, in which extruded supports are most widely used for industrial application. In extrusion method, the homogeneous paste is forced through the opening of a die with the help of an endless screw, especially auger or extruder, (in industry) or a piston (in the laboratory). Ceramic membranes are fabricated with various specifications (for example, the number of channels, diameter of channels, external diameter of the tubes etc.,) by changing the geometry of the die. Generally, tubular and multi-channel membrane supports have been prepared by this method (Burggraaf and Cot 1996; Tsuru 2001). The high surface to volume ratio of the modules provides good opportunity to process large feed rates. Due to this reason, the membranes have enhanced implementation in industries. Most important parameters that determine the membrane properties (mean pore size and porosity) are particle size of the ceramic or clay powder, nature and proportion of organic additives, pugging and ageing of the paste, extrusion pressure and velocity.

Unlike other fabrication methods, so far discussed, the majority of the membrane supports fabricated by extrusion method are made up of clays (Khider *et al.,* 2004; Saffaj *et al.,* 2004a; Mohammadi *et al.,* 2005; Dong *et al.,* 2006; Bouzerara *et al.,*

2006; Kazemimoghadam and Mohammadi 2007; Khemakhem *et al.,* 2007; Jedidi *et al.,* 2009). This is attributed to the rheological properties (plastic behavior) of the clay. Clay readily forms paste and can be easily extruded to the desired shape without much extrusion pressure. Processing of inorganic ceramics by mixing with binders, plasticizers, lubricants etc., as additives, will give the required plastic properties that provide excellent shape forming capabilities without losing its cohesion. In general, cellulose derivatives (methyl cellulose, carboxymethyl cellulose, hydroxyethyl cellulose, etc.) are used as binders, organic polymers (PVA, PAA, PEG, etc.) are used as plasticizers or lubricants and starch derivative, especially corn starch, is used as pore forming agent (Benito *et al.,* 2005; Bouzerara *et al.,* 2006; Wang *et al.,* 2007a; Qi *et al.,* 2010). Numerous research works have focused on the development of kaolin based supports by mixing with other sintering aids, such as alumina, quartz, ball clay, feldspath, calcium carbonate, magnesium carbonate, sodium carbonate, talc, titania (rutile), flyash, to enhance the porosity and mechanical strength of the membrane support (Almondoz *et al.,* 2004; Benito *et al.,* 2005; Mohamaddi *et al.,* 2005; Dong *et al.,* 2006; Bouzerara *et al.,* 2006).

In manual pasting method, the membrane supports are fabricated manually on a flat porous (gypsum) or nonporous surfaces. The pressure is applied manually to form the required shape. It is the simplest and the oldest technique compared to any other fabrication method and doesn't require any instrument for fabrication. However, controlling the microstructure is a hard challenge and requires skills to achieve membrane supports without defects and to produce optimum reproducible results. Anil Kumar and coworkers (Potdar *et al.,* 2002; Neelakandan *et al.,* 2003; Sachdeva and Kumar 2008) fabricated kaolin supports using low cost ceramic clay mixtures and applied for various liquid separation applications. Similar type of ceramic clay

mixtures were also used by other researchers for the fabrication of ceramic membrane supports (Almondoz *et al.*, 2004; Belouatek *et al.*, 2005; Nandi *et al.*, 2008).

The advantages and disadvantages of the various support fabrication techniques are summarized in Table 2.1. A list of the commercial membranes used in the membrane application is given in Appendix-I. Although various commercial ceramic membranes are available today, there are few reports on the preparation of ceramic membrane supports, which presumptively resulted from strictly commercial secret. The main membrane transport properties depend on the pore structure parameters of membrane support such as open porosity, pore shape, pore size and its distribution. These are mainly influenced by the raw powders and sintering conditions. In summary, most of the ceramic supports are routinely prepared from high purity expensive powders as starting materials, accompanying with the combustion of organic pore-forming agents.

2.3 SELECTIVE LAYER PREPARATION

Several routes have been proposed and addressed for the preparation of the selective layer of a composite membrane, such as, dip-coating, physical vapor deposition (PVD), chemical vapor deposition (CVD), electrochemical deposition (anodic oxidation), electroless plating and spray pyrolysis of metal-organics (Lee *et al.*, 1995). Among these methods, dip-coating have been widely used for membrane preparation. In general, low viscosity sols and lower withdrawal velocity of the support from the colloidal solution yield defect free membranes. Sol-gel technology is widely used due to its simplicity, doesn't require any high cost sophisticated equipments, ease of control parameters (as compared to other techniques) and less energy consumption.

Table 2.1 Advantages and disadvantages of various support fabrication methods

Method	Advantages	Disadvantages
Uniaxial pressing	• Simple and cost effective • Ease of fabrication • High production rate	• Fabrication is restricted to flat shaped membranes (disc, rectangular or square shaped)
	• Controlling parameters are very less	• Possibility of defect formation is more due to air entrapment • Die wear and uneven pressure distribution
Isostatic pressing	• Fabrication of tubular supports and other configurations are possible	• Dense products were obtained (not suitable for liquid phase membrane application due to nonporous nature)
	• Possibility of defect is less due to uniform pressure distribution	• Complication in the press operation
	• Greater uniformity of compaction • Increased shape capability	• Energy consumption is more than uniaxial pressing
Slip casting	• High quality tubes are fabricated by this method	• Very slow and more expensive process
	• All complicated shapes (for example: star, disc and tubular shaped) of membranes can be fabricated by this method.	• Difficult to maintain controlling parameters of the colloidal sol • Chemicals requirements are high to produce stable colloidal sol
	• No instruments are required for fabrication	• Environmental, safety and health hazards involved in using the precursors of the colloidal sol
Extrusion	• Tubular membranes are produced in higher production rates	• Higher fabrication cost, high energy consumption (due to the higher operating cost of the extruder)
	• High quality membranes are fabricated using low cost clays	• Difficulty in maintaining the rheology of the paste (especially during pugging and ageing)

The inherent advantages of the sol-gel method is that it produces extremely active products with high surface area, controllable and facile incorporation of other compounds, such as promoters or stabilizers, fine-tuning of the products pore structure and direct casting of the selective layer over the membrane support (Agrafiotis and Tsetsekou 2002). In addition, it produces high purity products with narrow pore size distribution and requires low sintering temperature. Hence, the sol-gel technique has been extensively used for the preparation of selective layers, such as alumina, titania, zirconia and silica, which are common in practice (Leenars and Burgraff 1985; Uhlhorn *et al.,* 1992; Chang *et al.,* 1994; Kuzniatsova *et al.,* 2008).

A sol is a colloidal suspension of very fine solid particles in a liquid. It is prepared by hydrolysis and condensation of the corresponding metal alkoxides or inorganic salts. The precursors used in the sol-gel process consist of a metal or metalloid element surrounded by various ligands, which are easily transformed into chemically reactive forms of oxoalkoxides on hydrolysis. In fact, the stable form of sols that could be gelled can obtained from oxoalkoxides rather than from hydrated oxides (Brinker and Scherer 1990; Caro *et al.,* 2000). In the drying process of the coated sol, gelation took place and the thermal treatment crosslinks the gel particles to produce the desired product. In general, thin, crack free membrane layers are usually obtained with a stable colloidal sol consisting of either dense spherical particles or polymeric macromolecules as shown schematically in Fig. 2.3.

The main parameters that determine or control the formation of the selective layer during dip coating process are

1. Source of raw materials (used for the preparation of the sol)
2. Sol peptizing agent (type and amount)

3. Concentration of the dipping sol
4. Dipping time
5. Properties of the support (roughness, pore size, surface charge and porosity)
6. Calcination temperature

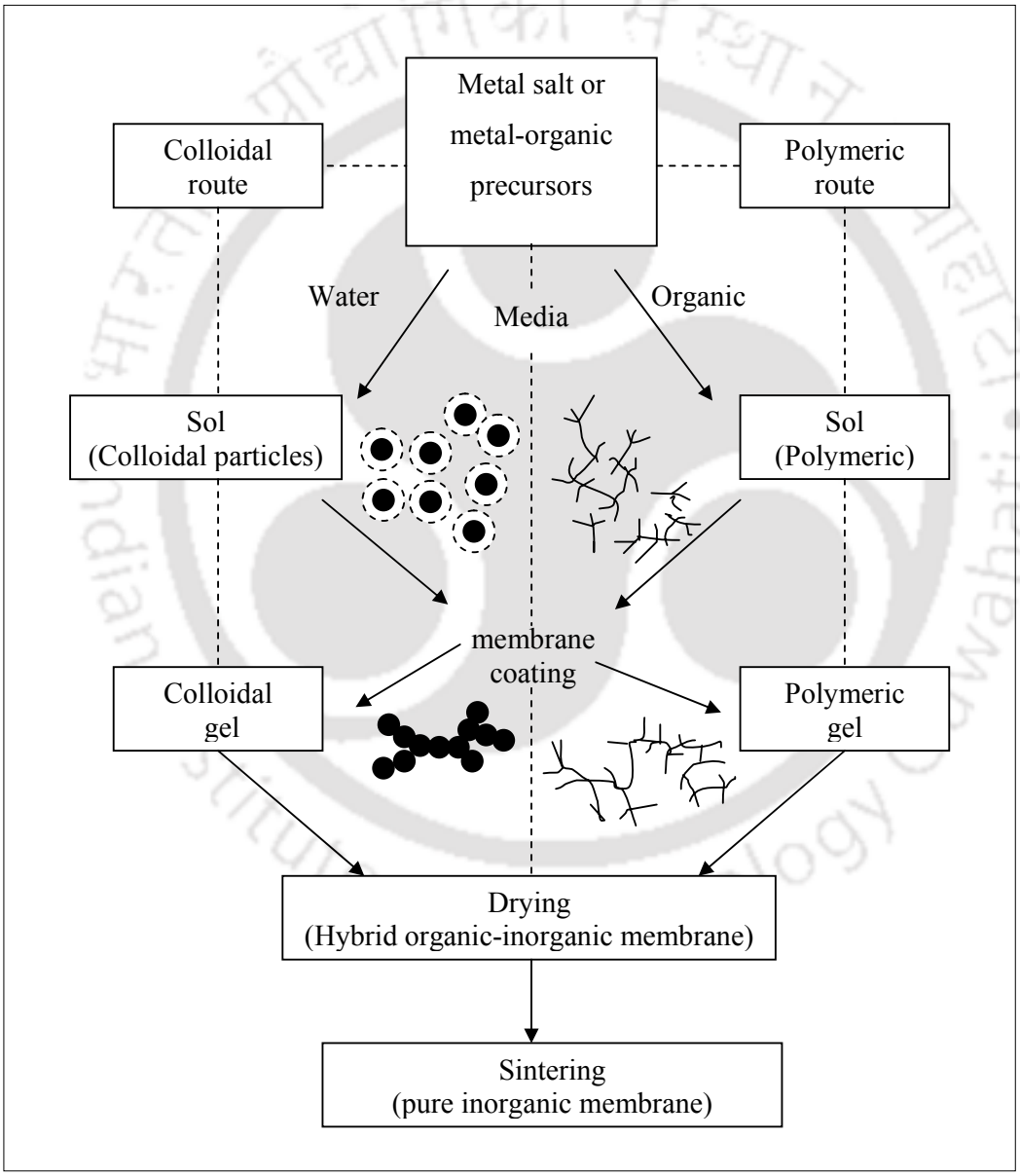

Fig. 2.3 Schematic of inorganic membrane preparation by sol-gel method.

2.3.1 Synthesis of γ-Al_2O_3 powder for membrane fabrication

Transparent porous alumina was first prepared by Yoldas from an alumina sol using aluminium alkoxide precursors (Yoldas 1975a; Yoldas 1975b), henceforth, alumina membranes have received a great deal of attention. He revealed that the gelling point of the sol mainly depends on the sol concentration and the peptizing agent. The effect of sol dispersion medium (methanol, ethanol, water, propylene glycol and triethylene glycol) on the pore morphology reveals that alumina with higher surface area and smaller pore diameter (55 Å) is obtained by using water as a dispersion medium. The partial replacement of water with alcohol results in smaller pore size due to capillary activeness, which accelerates the gel formation. The partial replacement of water with glycerol results in a larger pore size.

Leenars *et al.*, (1984), prepared a γ-Al_2O_3 membrane by dip coating process, which is basically a slip casting process, on a porous support with a colloidal solution of boehmite (γ-AlOOH). While, lower density gel layer is formed (using smaller boehmite particles) in the dipcoating process, whereas higher density gel layer is formed (using higher boehmite particles) in slip casting process. Leenars and Burgraff (1985), further investigated the formation of γ-Al_2O_3 membrane and its thickness with the variation in the dip coating process variables, such as, pore size of the support, sol concentration, peptizing agent and dipping time. They found that gel layer is formed irrespective of the peptizing agent (HCl, HNO_3 and $HClO_4$), when the pore size of the support is smaller (0.12 μm) whereas for the larger pore size supports (0.8 μm), the gel layer is formed only when HCl is used as a peptizing agent due to the higher boehmite particle size (due to the agglomeration of boehmite particles). Their investigation also revealed that the boehmite sol of higher concentration (>0.5 M) results in thick gel layer formation due to the agglomeration of boehmite particles. No

layers were formed at lower boehmite sol concentration (0.1 M). However, a gel layer could be formed at lower sol concentrations (0.1 M) by increasing the dipping time. They found that the ratio of the boehmite particle size (directly or indirectly related to sol concentration, peptizing agent, aging and dipping time) to the pore size of the support decides the gel layer formation. They also found that enhancement in the thickness of the gel layer increased with the square root of the dipping time.

In general, the higher concentration of sol or longer dipping time leads to agglomerated boehmite particles and also it forms a thick selective layer that might increases the possibility of defects in membranes. Generally, lower concentration of properly dispersed sol has been used with shorter dipping time to avoid the defects. Multiple dipping procedures have also been used to form a thin defect free γ-Al_2O_3 membrane (Uhlhorn *et al.,* 1992; Lafarga *et al.,* 1998).

Generally, the stable dipping sol has been prepared by the addition of acid to the boehmite, which breaks up the agglomerates by partial dissolution and charge stabilization of the particles (commonly called as peptization). Strongly ionized acids (HCl, HNO_3, $HClO_4$) non-complexing with Al^{3+} provides sufficient dissolution and charging. The nature of the particle size of the sol solution with the addition of the acid during peptization is shown in Fig. 2.4.

The effect of peptizing agent on the mean pore size of the γ-Al_2O_3 membranes was examined using various organic (CH_3COOH) and inorganic (HCl, HNO_3 and $HClO_4$) peptizants by several researchers (Leenars and Burgraff 1985; Albani and Arciprete 1992; Huang *et al.,* 1997). The detailed investigation revealed that the acids in the order of $HClO_4 > HNO_3 > HCl$ are found to be more effective in decreasing the size of the boehmite particles. The thickness of the layer increases with an increase in the size of the boehmite particles, which could be observed by an increase in the turbidity

of the sol (Leenars and Burgraff 1985). Albani and Arciprete (1992) reported that the inorganic peptizants (HCl, HNO_3 and $HClO_4$) yielded a γ-Al_2O_3 layer of smaller pore size (39 Å) than the organic peptizant (CH_3COOH, pore size = 54 Å). Huang *et al.*, (1997) found that stable sol could be obtained at a suitable concentration ($H^+/A1^{3+}$ molar ratio = 0.07:1) of peptizant acid. At a lower peptizant concentration, the sols becomes unstable and form precipitates. They have also found that HC1, HNO_3, CH_3COOH are suitable peptizant agents for forming stable boehmite sol and H_2SO_4 cannot be used as a peptizant because it will not peptize the boehmite particles. Peptizing the sol in closed containers at 75 to 95°C under stirring conditions transforms the agglomerated boehmite into regular rectangular plate-like morphology that forms a gel layer.

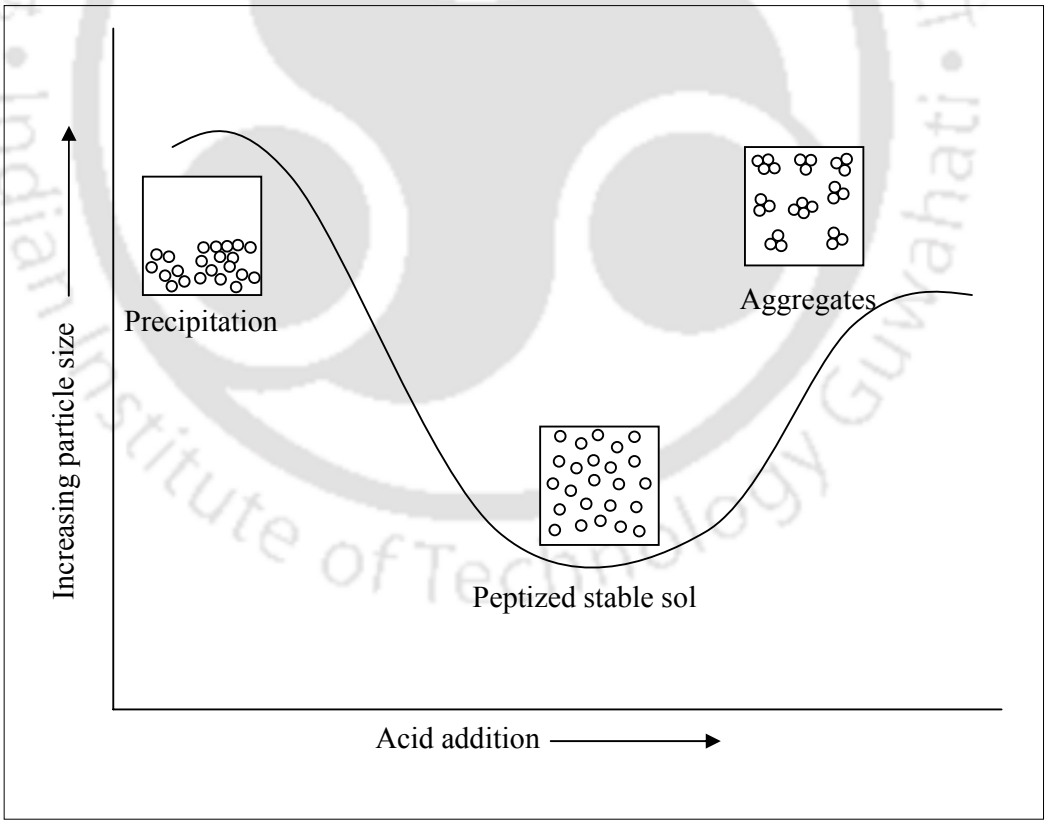

Fig. 2.4 Effect of acid on the size of the particle present in the sol.

Research emphasizing continuous variations of the Yoldas method have reduced the mean pore radii of γ-Al_2O_3 membranes from about 96 Å to about 10 Å (Anderson *et al.,* 1988; Hsieh *et al.,* 1988; Albani and Arciprete 1992; Sheng *et al.,* 1992; Uhlhorn *et al.,* 1992; Alanmi-Younssi *et al.,* 1994; Larbot *et al.,* 1994; Chang *et al.,* 1994; Kuzniatsova *et al.,* 2008). In general, most of the γ-$A1_2O_3$ membranes were prepared by particulate sol method using the alkoxide precursors, such as aluminium tri sec-butoxide, aluminium sec-butoxide and aluminium iso propoxide. The temperature of the hydrolysis reaction was usually maintained above 80°C (range of 80-90°C) to avoid the formation of gibbsite (bayerite, doyleite and nordstrandite) and especially bayerite (β-$Al(OH)_3$). These hydroxides cannot form gel and hinder the gel layer formation (Anderson *et al.,* 1988; Huang *et al.,* 1997; Lafarga *et al.,* 1998; Van Gestel *et al.,* 2002; Agrafiotis and Tsetsekou 2002; Li *et al.,* 2006; Ahmad *et al.,* 2008; Kuzniatsova *et al.,* 2008). However, few researchers reported that the bayerite formed by hydrolysis of aluminium alkoxide at temperatures <80°C could be converted to boehmite by heating to its boiling point immediately after hydrolysis, which can be peptized (Sheng *et al.,* 1992; Huang *et al.,* 1997). However, the preparation of γ-Al_2O_3 layer from boehmite has been encouraged by the researchers and still boehmite is considered as a direct parent for highly pure γ-Al_2O_3. This is attributed to certain advantages of boehmite over gibbsite (Huang *et al.,* 1997; Panias and Krestou 2007). Boehmite is an energy saving precursor material for the production of γ-Al_2O_3. Although boehmite dehydrates at a higher temperature (490°C) than gibbsite (310°C), the enthalpy of the dehydration reaction of boehmite (72 kJ/mol Al_2O_3) is low when compared to that of gibbsite (187 kJ/mol Al_2O_3) (Panias and Krestou 2007). The aforementioned advantages of boehmite have forced the researchers to develop various new procedures for the preparation of boehmite, especially boehmite with low

crystallinity. Because the high crystalline boehmite usually produces lower surface area γ-Al_2O_3 that is not preferred for membrane applications (Panias and Krestou 2007).

In many cases, these precursors are very sensitive to water as well as alcohols (2-propanol or 2-butanol). This creates difficulty in controlling the hydrolysis reaction, which is a hard challenge for the researchers (Uhlhorn *et al.,* 1989; Albani and Arciprete 1992; Ahmad *et al.,* 2008; Zhang *et al.,* 2008). Many research works have been focused on decreasing the mean pore size of γ-Al_2O_3 by certain modifications in the hydrolysis step, especially varying the ratios of water/alkoxide, acid/alkoxide and alcohol/alkoxide (Uhlhorn *et al.,* 1989; Larbot *et al.,* 1994; Huang *et al.,* 1997).

The effect of calcination temperature on the microstructural characteristics of alumina was investigated by several researchers (Lin *et al.,* 1991; Chang *et al.,* 1994; Alami-Younssi 1994; De Lange *et al.,* 1995; Lafarga *et al.,* 1998; Van Gestel *et al.,* 2002). Upon controlled calcination, boehmite undergoes topotactic transformation into various metastable states of aluminas (γ-, η-, δ- and θ-alumina) to a stable α-alumina (Lin *et al.,* 1991; De Lange *et al.,* 1995; Ersoy and Gunay 2004a). It was observed that the temperatures at which transitions have been observed are somewhat variant and are dependent upon the starting materials and thermal treatment. However, the transition follows the same sequence from γ- to α-alumina. The investigation reveals that, with an increase in sintering temperature, aluminium monohydroxide (boehmite, up to 400°C) is transformed to γ-Al_2O_3 (400 to 800°C) and then to other transitional aluminas (θ-Al_2O_3 at 900°C via η- and δ-Al_2O_3 and α-Al_2O_3 at 1000°C). The phase transformation of the alumina results in decreased surface area and increased pore size. The wide investigation by the researchers revealed that the boehmite coated

membrane supports sintered at 600°C yielded γ-Al_2O_3 that is free from other polymorphs (such as η-, δ- and θ-Al_2O_3 phases).

Some researchers used different sintering techniques to enhance the pore characteristics of the γ-Al_2O_3 membrane. Chang *et al.,* (1994) performed the heat treatment under two different conditions: dried air and steam/air (1:1) atmospheres. The pore sizes of the alumina membranes after firing under the steam/air atmosphere are larger than those under dried air. Their studies revealed that the steam enhances the process of pore structure change of the γ-Al_2O_3 membrane at high temperatures. Larbot *et al.,* (1994) used flash firing technique to obtain the γ-Al_2O_3 membrane. During heat treatment, there may a possibility of formation of the defects (cracks and pinholes), which should be usually avoided by addition of organic additives and controlled (very slow) rate heating and cooling of the membranes.

In general, poly-vinylalcohol (PVA), has been employed as an organic additive for the production of defect free γ-Al_2O_3 membranes by the dip coating method. It adjusts the viscosity of the sol and controls the drying rate, which reduces the residual stresses created during heat treatment process (Uhlhorn *et al.,* 1989; Lin *et al.,* 1991; Huang *et al.,* 1997; Luyten *et al.,* 1997; Van Gestel *et al.,* 2002; Agrafiotis and Tsetsekou 2002; Ahmad *et al.,* 2008). Furthermore, the addition of PVA (molecular weight, 72000 g/mol) did not result in a significant change in the microstructure of γ-Al_2O_3 layer after sintering (Uhlhorn *et al.,* 1989). Larbot *et al.,* (1994) prepared γ-Al_2O_3 membranes (thickness = 0.5 to1 μm) without any inorganic binders by flash firing method. However, this method is suitable only if the thickness of γ-Al_2O_3 layer is small (< 2 μm). This heat treatment cannot be useful for membranes prepared by dip coating process because dip coating process forms higher thickness membranes (~20-50 μm).

In many research works, the pore size of the γ-Al_2O_3 membrane was estimated by BET (Brunauer-Emmett-Teller) pore size distribution analysis and the pore size reported was the mean pore size of the unsupported membranes (unsupported or nonsupported membranes refers to the γ-Al_2O_3 membranes prepared by pouring the dipping sol solutions in the petridishes and the dried membranes are heat treated by the same heat treatment procedure as that of the γ-Al_2O_3 membranes). The work done by De Lange *et al.,* (1995) revealed that the supported membranes showed a slightly higher pore radius (2.5 nm) than the unsupported membranes (2.2 nm), which is attributed to the support constraints. However, this is not a significant variation.

Generally, α-alumina membrane supports with very low mean pore diameter (0.2 μm) have been used for the preparation of γ-Al_2O_3 membrane. Few research works have focused on the coating of γ-Al_2O_3 layer on cordierite and kaolin supports (Santos *et al.,* 1997; Agrafiotis and Tsetsekou 2002; Ersoy and Gunay 2004b; Benito *et al.,* 2005). Even though the alumina and kaolin supports had similar pore diameter (0.76 μm for kaolin and 0.67 μm for alumina), the quality of the membranes deposited upon alumina was much better and this was attributed to the narrower pore structure of alumina when compared to that of kaolin (Santos *et al.,* 1997). However, Benito *et al.,* (2005) revealed that the γ-Al_2O_3 layer deposited on cordierite or alumina supports have similar pore structural characteristics.

In summary, the wide literature survey reveals that aluminium alkoxide precursors have been widely used for the preparation of boehmite sol. However, these metal alkoxide precursors have some disadvantages such as being expensive, flammable and toxic (Li *et al.,* 2006) and very sensitive to water and alcohols due to which hydrolysis reaction cannot be controlled (Uhlhorn *et al.,* 1989; Larbot *et al.,* 1994; Huang *et al.,* 1997). Therefore, some researchers search towards an alternate route to

fabricate γ-Al_2O_3 membranes using inexpensive inorganic salt precursors, such as aluminium nitrate (Varma *et al.,* 1994; Music *et al.,* 1998; Chuah *et al.,* 2000; Hochepied and Nortier 2002), aluminium chloride (Furuta *et al.,* 1994; Zeng *et al.,* 1998; Hwang *et al.,* 2001; Pacewska *et al.,* 2005; Li *et al.,* 2006; Seok *et al.,* 2006; Liu *et al.,* 2008) and aluminium sulphate (Unuma *et al.,* 1998; Mishra *et al.,* 2000; Castillo *et al.,* 2005; Xu *et al.,* 2006). The existence of anions (NO_3^-, Cl^-, SO_4^{2-}) in the hydrosol would affect the boehmite sol properties. Therefore, the preparation of the boehmite hydrosol without these undesirable anions is the hard challenge in this process. Precipitation of boehmite from these inorganic aluminum salts ($AlCl_3$, $Al_2(SO_4)_3$ and $Al(NO_3)_3$) solutions under similar reaction conditions revealed that the hydrolysis of $Al_2(SO_4)_3$ occurs at lower temperature and the transformation of boehmite to γ-Al_2O_3 occurs at a higher temperature than the $AlCl_3$ and $Al(NO_3)_3$ solutions (Mishra *et al.,* 2002; Castillo *et al.,* 2005). More homogeneous surfaces can be produced using aluminium chloride than the aluminium sulfate attributed to delayed crystallization, which is due to the presence of residual sulfates (Castillo *et al.,* 2005). Maintaining the pH at 8.0 during the hydrolysis reactions yielded boehmite (without the formation of gibbsite), which can be easily gelled during membrane preparation (Hwang *et al.,* 2001; Padmaja *et al.,* 2004; Castillo *et al.,* 2005). Few research works have been reported on the fabrication of γ-Al_2O_3 membrane using stable boehmite sol prepared from low cost aluminium chloride precursor (Furuta *et al.,* 1994; Hwang *et al.,* 2001; Li *et al.,* 2006).

The formation of boehmite to γ-Al_2O_3 follows sequence of reactions (during hydrolysis and calcination). The sequence of reactions involved for the formation of γ-Al_2O_3 using aluminum chloride as the starting precursor follows different schemes based on the experimental conditions and the possible schemes are given below.

2.3.2 Possible schemes of chemical reactions involved during hydrolysis, condensation and calcination

Scheme 1

$$AlCl_3 + 3NH_4OH \xrightarrow{50-80^{o}C} \gamma - AlO(OH) + 3NH_4Cl + H_2O \quad (2.1)$$

$$\gamma - AlO(OH) \xrightarrow{400-600^{o}C} \gamma - Al_2O_3 + H_2O \quad (2.2)$$

$$\gamma - Al_2O_3 \xrightarrow{700-800^{o}C} \delta - Al_2O_3 \xrightarrow{800-900^{o}C} \theta - Al_2O_3 \xrightarrow{1100^{o}C} \alpha - Al_2O_3 \quad (2.3)$$

Scheme 2

$$AlCl_3 + 3NH_4OH \longrightarrow Al(OH)_3 + 3NH_4Cl \quad (2.4)$$

$$2Al(OH)_3 \xrightarrow{100-400^{o}C} \gamma - AlO(OH) + H_2O \quad (2.5)$$

$$\gamma - AlO(OH) \xrightarrow{400-600^{o}C} \gamma - Al_2O_3 \xrightarrow{800-1000^{o}C} \alpha - Al_2O_3 \quad (2.6)$$

Scheme 3

$$AlCl_3 + 3NH_4OH \longrightarrow Al(OH)_3 + 3NH_4Cl \quad (2.7)$$

$$Al(OH)_3 \xrightarrow{250-400^{o}C} \chi - Al_2O_3 \xrightarrow{500-600^{o}C} \kappa - Al_2O_3 \xrightarrow{1000^{o}C} \alpha - Al_2O_3 \quad (2.8)$$

From the above schemes it is clear that the scheme 1 and 2 will produce γ-Al_2O_3 and are highly preferred for the preparation of γ-Al_2O_3 membranes whereas the scheme 3 cannot be used for the preparation of γ-Al_2O_3 membranes.

2.4 LIQUID PHASE SEPARATION

Membranes have been used for various liquid phase separation applications (Tsuru *et al.,* 2001; Mohammadi *et al.,* 2004; Belouatek *et al.,* 2005; Hwang *et al.,* 2006; Tung *et al.,* 2007). This thesis focuses on three different liquid phase separation applications that have prominent research interests. These correspond to the reduction of oil content from oil-water solution, BSA concentration and purification from aqueous solutions and electrolytes separation from aqueous solutions. The reason for choosing the above application and its necessity, challenges involved in achieving the separation or purification, factors influencing its efficiency and optimum conditions to achieve greater efficiency are discussed in the following sub-sections.

2.4.1 Separation of oil from oil-water solution

In general, large volumes of oily wastewater with oil concentrations ranging between 50 and 1000 ppm have been produced from food processing, petroleum refineries, petrochemical, metallurgical and transportation industries (Arnot *et al.,* 2000; Cumming *et al.,* 2000; Mohammadi *et al.,* 2004; Ezzati *et al.,* 2005; Razi *et al.,* 2009; Chen *et al.,* 2009). Almost all industries produce oil-water wastes from the machineries in which oil is used as a lubricant. The disposal of large volume of oily wastewater paces a significant burden on the environment and this ecologically hazardous oily wastewater should be treated before being discharged. Based on the environment regulation of the country, the existing tolerance limits of total oil and grease concentrations in wastewater is about 10 to 50 ppm (Hua *et al.,* 2007; Mallada and Menendez 2008; Nandi *et al.,* 2009). The Central Pollution Control Board (CPCB) of India fixed the norms of discharge wastewater as 10 ppm for most of the industries and 20 ppm for edible oil and vanaspathi industry (http://cpcb.nic.in/Industry_Specific_Standards.php). Various traditional methods

such as gravity settling (API separator), skimming, dissolved air flotation, coalescence and centrifuging, etc., have been applied for treating the unstable oil/water emulsion (Srijaroonrat *et al.,* 1999; Cumming *et al.,* 2000; Hua *et al.,* 2007; Zhou *et al.,* 2010). Each conventional technology has their own advantages and disadvantages as mentioned in the literature (Razi *et al.,* 2009).

Many technological solutions have been reported for the treatment of oily wastewaters using membrane for the feed oil concentrations of 500 to 3000 ppm. Higher oil concentration of the feed contains unstable oil droplets having sizes greater than 50 μm that could be treated easily (Srijaroonrat *et al.,* 1999; Mohammadi *et al.,* 2004; Ebrahimi *et al.,* 2009). However, the oil emulsion containing oil droplets less than 20 μm size exists in feed with oil concentrations below 100 ppm is so stable and it can't be treated effectively by traditional methods (Srijaroonrat *et al.,* 1999; Pan *et al.,* 2007; Razi *et al.,* 2009; Zhou *et al.,* 2010). In such cases, membrane technology has been found to be more effective than the conventional methods. Both MF (pore size = 0.1 and 10 μm) and UF (pore size <0.1 μm) polymeric or ceramic membranes have been used for concentrating/treating oil emulsions, as they are highly efficient for removing oil, do not require chemical additives and are more economical than conventional separation techniques. However, ceramic membranes are preferred over delicate polymeric membranes because they have better tolerance to higher processing temperature, high oil content, foulants, and strong cleaning agents (Mohammadi *et al.,* 2004; Lobo *et al.,* 2006; Bader 2007; Cui *et al.,* 2008; Razi *et al.,* 2009).

Most of the investigations on the separation of oil from oil-water solution were conducted using alumina, zirconia, titania and zeolite or ZrO_2/α-Al_2O_3, TiO_2/α-Al_2O_3, TiO_2/ TiO_2 membranes (Yang *et al.,* 1998; Srijaroonrat *et al.,* 2009; Lobo *et al.,* 2006; Cui *et al.,* 2008; Ebrahimi *et al.,* 2009; Ebrahimi *et al.,* 2010). The studies revealed

that the performance of oil-water separation is directly related to the properties of membrane materials, such as surface tension or surface energy, surface charge and ion sorption in aqueous solution and the adsorption behavior of the oil with the membrane surfaces. In general, fouling is greater in hydrophobic membranes than in the hydrophilic membranes. This is due to the effect of concentration polarization (CP). The CP effect can be minimized by operating at a transmembrane pressure lower than the capillary pressure. Recent research works have focused on the utilization of low cost membranes, such as kaolin and carbon membranes. Various researchers investigated the potential of these membranes for the separation of oil from oil-water solution (Mohammadi *et al.,* 2004; Pan *et al.,* 2007; Razi *et al.,* 2009; Nandi *et al.,* 2009).

2.4.2 Concentration of bovine serum albumin (BSA) from aqueous solution

Separation of bovine serum albumin (BSA) is a topic of profound significance in bioscience and biotechnology. BSA separation is regarded as a very important downstream processing operation that requires membranes having high permeability and selectivity for cost effective and efficient separation (Hwang *et al.,* 2006; Tung *et al.,* 2007; Fakhfakh *et al.,* 2010). Generally, it is difficult to separate BSA by size sieving because BSA is a globular prolate ellipsoid of dimensions 140×40×40 nm with an iso electric point (IEP) of 4.9 (Zeman and Zydney 1996; Persson *et al.,* 2003; Lin *et al.,* 2008). Since it is a charged protein, the effective separation can be achieved by regulating the pH of the solution (Saksena and Zydney 1997; Ghosh and Cui 1998; Persson *et al.,* 2003). Several researchers examined the separation of BSA using polymeric and ceramic membranes and found that the IEP plays a vital role in the flux and rejection of BSA (Randon *et al.,* 1995; Saksena and Zydney 1997; Ghosh and Cui 1998; Pujar and Zydney 1998; Persson *et al.,* 2003; Shah *et al.,* 2007; Ke *et al.,* 2009).

Many articles examined the basis of electrostatic interactions between charged proteins and charged membranes and reported that the pH values and ionic strengths have profound effects on BSA separation (Saksena and Zydney 1997; Ghosh and Cui 1998; Pujar and Zydney 1998; Persson *et al.,* 2003; Shah *et al.,* 2007; Ke *et al.,* 2009). Numerous researches have been carried out on polymeric membranes, especially on polyethersulfone or polysulfone membranes, due to their higher selectivity (Feins and Sirkar 2005; Wilharm and Rodgers 1996; Iratani *et al.,* 1995; Persson *et al.,* 2003; Rao and Zydney 2006; Hwang *et al.,* 2006; Tung *et al.,* 2007; Lin *et al.,* 2008). Most of the literatures are interested on the fouling mechanism of the membranes (mostly polymeric) for various BSA concentrations, especially in the dead end filtration module (Iratani *et al.,* 1995; Su *et al.,* 1999; Maruyama *et al.,* 2001; Iratani *et al.,* 2002; Feins and Sirkar 2005; Rao and Zydney 2006; Lin *et al.,* 2008). In general, the dead-end stirred cell devices are commonly used in laboratories to characterize the separation behavior of the ultrafiltration membranes. The membrane flux and separation data have been used for scale-up of membranes process. Typically, the operating conditions (pressure and temperature) are inherently different for continuous or semi-continuous industrial processes. Few research works have been reported on comparison of dead-end filtration and cross flow filtration to optimize the laboratory data to industrial application (Youm *et al.,* 1996; Shukla *et al.,* 2000; Becht *et al.,* 2008). In general, the tendency of the membranes for fouling is more and obvious for BSA separation; it is very difficult to determine the actual rejection obtained by the membranes especially for the case of dead-end filtration. Due to the difficulties associated with the measurement of BSA concentration on the membrane surface during ultrafiltration, various theoretical models, such as gel polarization, osmotic pressure, boundary layer and cake filtration models, have been proposed to

find the actual rejection of the membrane (Iritani *et al.,* 2002; Noordman *et al.,* 2002; Afonso *et al.,* 2009). Although, significant amount of research have been attempted to find the real rejection, the osmotic pressure model holds good for separation of dilute solutions to understand the rejection mechanism completely (Noordman *et al.,* 2002; Afonso *et al.,* 2009). Numerous efforts have been made to increase the rejection and permeate flux by optimizing operating parameters, such as pressure, flow rate, temperature, pH and feed concentration (Maruyama *et al.,* 2001; Persson *et al.,* 2003; Hwang *et al.,* 2006; Ke *et al.,* 2009). The overall investigation reveals that the protein-protein and protein-membrane interactions are very important in achieving higher rejection and permeate flux. This could be optimized by controlling the process parameters (Ghosh and Cui 1998; Pujar and Zydney 1998; Su et al., 1999; Persson *et al.,* 2003; Hwang *et al.,* 2006; Ke *et al.,* 2009). Eventhough significant research efforts have been carried out for BSA separation using membranes, only few works have been reported for the separation of BSA using ceramic membranes. Amongst these, most of the investigations are conducted on commercially available membranes (Randon *et al.,* 1995; Su *et al.,* 1999; Erdem *et al.,* 2002; Erdem *et al.,* 2006; Ding *et al.,* 2006; Ke *et al.,* 2009; Fakhfakh *et al.,* 2010).

2.4.3 Separation of electrolytes from aqueous solution

Currently, UF/NF membranes have been widely employed in many industries for the removal of ionic salts, which form an electrolyte solution with water, due to the advantage of the lower operating pressures than that of the reverse osmosis process (Bowen and Mukthar 1996). Lower operating pressures increase the membrane life time, consume less energy (economically efficient) and also increase the throughput that facilitate the treatment of large volumes of electrolytes.

In general, the solute flux through an UF membrane is the sum of convective (due to applied pressure across the membrane) and a diffusive flux (due to concentration difference on both sides of the membrane). The factors influence the flux and retention could be explained with various separation mechanisms of the electrolytes, such as sieving, electrostatic interactions between the membrane and the ions or between the ions mutually and differences in diffusivity and solubility or a combination of both. Several models such as irreversible thermodynamic, pore sieving, space charge, fixed charge, electrostatic and steric-hindrance, donnan-steric pore and dielectric exclusion models have been established to express the separation performance of UF membranes for neutral and charged solutes in aqueous solutions for better understanding of separation mechanism (Levenstein *et al.,* 1996; Maryasova and Semin 1998; Peeters *et al.,* 1998; *et al.,* 2000; Labbez *et al.,* 2002; Wang *et al.,* 2002; Shang *et al.,* 2006; Tu *et al.,* 2010). Moreover, these models are used in the prediction of rejection behavior of a given membrane for a particular electrolyte solution. This is very useful during scale-up of laboratory results to industrial processes (Peeters *et al.,* 1998; Labbez *et al.,* 2002; Tu *et al.,* 2010).

So far, various polymeric (polyamide, polysulfone, regenerated cellulose, etc.) and inorganic (Al_2O_3, SiO_2, TiO_2, ZrO_2, HfO_2, SnO_2, etc.,) materials have been tested and used for manufacturing commercial and laboratory membranes for the separation of electrolyte solutions (Palmeri *et al.,* 2000; Elmarraki *et al.,* 2001; Bandini *et al.,* 2005; Chung *et al.,* 2005; Vazquez *et al.,* 2005; Mazzoni *et al.,* 2009; Tu *et al.,* 2010). Rejection of charged molecules, especially simple ions, is influenced by the inherent charge of the membranes. The retention measurement with model salt solutions of various compositions gives an overview about the efficiency of the process. The retention of single salt solutions mainly depends on the distribution of the co-ions

between membrane and solution that can be influenced by the interaction between the ions and membrane material for both charged and uncharged membranes (Peeters *et al.,* 1998; Xu and Lebrun 1999; Koter 2006). Ceramic ultrafiltration membranes with pore size higher than 2 nm indicated good filtration capability of electrolyte solutions due to the strong interactions developed between the surface groups of ceramic material that are responsible for the rejection of the electrolytes (Elmarraki *et al.,* 2001). The amphoteric behavior is an interesting property of membrane material that makes the membrane negatively or positively or neutrally charged by adjusting the pH of the solution. It is found to be useful in the efficient separation of electrolyte solution (Xu and Lebrun 1999; Elmarraki *et al.,* 2001; Tu *et al.,* 2010).

Most of the research works were focused on the separation of common electrolyte solutions, such as NaCl, $CaCl_2$, Na_2SO_4, $CaSO_4$, $MgCl_2$, KCl, Na_2SO_4 and $MgSO_4$ using polymeric and ceramic membranes (Bowen and Mukthar 1996; Chung *et al.,* 2005; Peeters *et al.,* 1998; Xu and Lebrun 1999; Palmeri *et al.,* 2000; Elmarraki *et al.,* 2001; Labbez *et al.,* 2002; Chung *et al.,* 2005). In addition, the effect of operating conditions such as salt concentration, applied pressure, pH and type (valence of the ion) of the solute (Xu and Lebrun 1999; Labbez *et al.,* 2002; Mazzoni *et al.,* 2009) was investigated using these membranes. Although significant literature have been found for the separation of electrolyte solution using ceramic membranes (Peeters *et al.,* 1998; Palmeri *et al.,* 2000; Elmarraki *et al.,* 2001; Wang *et al.,* 2002; Vazquez *et al.,* 2005; Zhao *et al.,* 2005), most of them are commercial membranes. However, few researchers have used home made γ-Al_2O_3 composite membranes prepared by the sol-gel process using expensive aluminium alkoxide precursors (Alami-Younssi *et al.,* 1995; Peeters *et al.,* 1998; De Lint and Benes 2005).

Treatment of $AlCl_3$ and $MgCl_2$ effluent produced from various sources, such as, the effluents from Friedel craft acylation reaction, waste water effluents (in which those are used as coagulating or flocculating agents) and ore mining and refining effluents. This must be treated before disposal to reduce the hazardous impact on the environment (Stringer and Johnston 2001; Kogel *et al.,* 2006; Sheldon *et al.,* 2007; Hodge and Popovici 1994; Tan *et al.,* 2000). Most of the research investigation was focused to develop the theoretical models using commercial or home made membranes. Few researchers investigated for the real (intrinsic) rejection of charged membranes (Xu and Lebrun 1999; Labbez *et al.,* 2002; Wang *et al.,* 2002; Chung *et al.,* 2005; Shang *et al.,* 2005; Shukla and Kumar 2005; Zhao *et al.,* 2005). The real rejection of the charged membrane depends on the concentration of feed on the membrane surface. Due to concentration polarization, the concentration of the solute on membrane surface is higher than the bulk solution, which enhances or hiders the solute permeation. Hence various models have been developed to evaluate the realistic scenario. The thermodynamic irreversible Spiegler-Kedem black box model holds good for single electrolyte solution (Levenstein *et al.,* 1996; Xu and Lebrun 1999; Koter 2006). This model approach is simple and describes the filtration characteristics of membranes in contact with ionic solutes very well. Also, the obtained results have been found to be good agreement with the Nernst-Planck equation for the case of single salt solutions (Peeters *et al.,* 1998; Xu and Lebrun 1999; Koter 2006).

2.5 THESIS OBJECTIVE

The main objective of the thesis is to develop a low cost clay composite membrane capable for liquid phase separation applications. The objective of the thesis is majorly categorized into three folds, namely (i) develop a ceramic porous support using low

cost raw materials (clays) and optimize its properties with the sintering temperature, (ii) formation of selective layers by dip-coating method using a stable sol prepared from inexpensive precursors (inorganic salts) and (iii) evaluate the potential of the membrane for diverse liquid phase applications.

In the first phase, the purpose is to prepare the membrane support using low cost clays, such as kaolin, ballclay, quartz, pyrophyllite, feldspar and calcium carbonate, by simple uniaxial pressing method. A detailed characterization is carried out to obtain the optimum ceramic support based on sintering temperature (850 to1000°C) Also, the variation in the pore characteristics by incorporating TiO_2 to the low cost raw materials during support fabrication is investigated. Eventually, membrane separation capability is evaluated for the separation of oil from oil-water solution.

Later, the second objective is achieved by the formation of γ-Al_2O_3 layer on the membrane support. The γ-Al_2O_3 layer is prepared with a boehmite sol using aluminium chloride instead of commonly used expensive aluminium alkoxide precursor (boehmite sol prepared by modified Yoldas method using aluminium alkoxide precursors that is generally followed by other researchers).

The third and important part of the objective is to examine the potential of the membrane for its separation capability in the diverse field of industrially important applications, such as BSA protein and electrolyte ($AlCl_3$ and $MgCl_2$) separation applications.

2.6 IMPACT OF PROPOSED RESEARCH

The first achievement of this work is the fabrication of a stable ceramic support by reducing the cost, in three ways, that is using low cost raw materials (kaolin, ballclay, quartz, pyrophyllite, feldspar and calcium carbonate), low sintering temperature

(950°C) and simple fabrication technique (uniaxial pressing method). Uniaxial fabrication of membrane supports with mixed low cost raw materials is a new attempt and so far not practiced by other researchers with raw materials of similar type and composition. Moreover the support itself acts as a standalone microfiltration membrane that possess some separation capabilities due to the narrow pore size distribution with an average pore size in the range of microfiltration application.

The second achievement is the development of γ-Al_2O_3-clay composite membrane using the stable boehmite sol prepared from inexpensive aluminium chloride precursor and this approach is also a new attempt in the field of ceramic membrane technology.

2.7 THESIS ORGANIZATION

The first concern of the research is the fabrication of a stable membrane support. Chapter 3 deals with the detailed fabrication procedure of the support and its characterization using various techniques such as particle size distribution (PSD), thermogravimetric analysis (TGA), X-ray diffraction (XRD) and scanning electron micrograph (SEM) analysis along with the measurement of the porosity, flexural strength, corrosion resistance, water permeability and solvent permeability. Prior to that, a brief analysis of clay powders (which is used as the raw material for membrane support fabrication) is discussed. In addition, optimization of the membrane supports based on sintering temperatures is also presented in this chapter.

The Chapter 4 of the thesis addresses the effect of addition of TiO_2 powder along with other raw materials used for the preparation of the support (support-I) in Chapter 3. The performance of the fabricated TiO_2 supports (3G and 6G support) and support-I for separation of oil and BSA from its solution are investigated and compared.

Detailed cost estimation is made and presented for the three fabricated membrane supports.

Chapter 5 deals with the synthesis of γ-Al_2O_3 selective layer over the support-I (γ-Al_2O_3-clay composite membrane) by dip coating technique using boehmite sol derived from inexpensive aluminium chloride salt. The membrane is characterized with various techniques to ensure the γ-Al_2O_3 phase and to verify any defects in the membrane and the projected cost for the preparation of the membrane is also estimated.

Chapter 6 deals with the detailed investigation of the separation of BSA protein and $AlCl_3$ and $MgCl_2$ electrolytes from aqueous solution using γ-Al_2O_3-clay composite ultrafiltration membrane by varying the process parameters such as pH, applied pressure and feed concentration. In addition, the intrinsic rejections of BSA and electrolyte solution are estimated using the Spiegler-Kedem model.

In Chapter 7, the overall conclusions obtained from this thesis work and suggestions for future work are presented.

Chapter 3

FABRICATION OF MEMBRANE SUPPORTS FROM LOW COST RAW MATERIALS AND ITS OPTIMIZATION BASED ON SINTERING TEMPERATURE

3.1 INTRODUCTION

The main aim of this Chapter is to fabricate a macroporous membrane support having better permeability, porosity and mechanical strength using low cost clays as starting raw materials. As mentioned earlier that the cost of the membrane supports mainly depends on the starting raw materials, sintering temperature and the method of fabrication. Therefore a new low cost starting materials (clay mixtures) is used for the fabrication of membrane supports by simple uniaxial compaction technique and sintered at comparatively low temperature (850 to1000°C) than that of commercial membrane supports (>1200°C) is the main theme of this Chapter. The membrane supports sintered at different temperatures are characterized with various techniques to find the optimum one that would be an alternate for high cost commercial α-alumina, zirconia and titania membrane supports.

3.2 MATERIALS AND METHODS

The raw materials, i.e. the clay powders kaolin, ball clay, feldspar, pyrophyllite, quartz and calcium carbonate, used in this work were collected from Kanpur, India. Calcium carbonate ($CaCO_3$), sulfuric acid (H_2SO_4), hydrochloric acid (HCl), sodium hydroxide (NaOH) and poly vinylalcohol (PVA; mol. wt. = 72,000) were procured from Merck India Ltd. Water used in this work was collected from Millipore system (Elix-3). All the other chemicals used in this work were procured from Merck India Ltd unless otherwise stated.

3.2.1 Fabrication of the ceramic membrane support

The composition of the clay powders used for the fabrication of membrane supports along with its significance is given in Table 3.1 and the fabrication procedure is schematically represented in Fig. 3.1. The clay powders were mixed in a stainless steel ball mill (dimension 140×140×360 mm, 50 numbers of S.S balls having 12.7 mm diameter) with 4 ml (2 wt.%) of aqueous poly vinylalcohol (PVA) solution for 1200 s at 40 rpm. The resulting powder was sieved in a 40 mesh standard screen. A requisite (~30 gm) amount of screened powder was uniaxially pressed at a pressure of 50 MPa with the help of stainless steel mould, designed for single-ended pressing, to form a circular disc shaped green support having 63 mm diameter and 4.5 mm thickness. The fabricated green supports were first dried at ambient condition for 24 h and then dried in hot air oven at 200°C for 24 h. The above controlled drying process ensures maximum removal of moisture and also eliminates any thermal stresses during moisture removal.

Table 3.1 Composition of clay powders used for the preparation of membrane support

Raw Materials	Composition (wt.%)	Significance
Kaolin ($Al_2(Si_2O_5)(OH)_4$)	14.45	Low plasticity and high refractory property
Ball Clay ($3SiO_2Al_2O_3$)	17.58	Provides plasticity and strength to the green support
Feldspar ((Na, Ca) ($AlSi_3O_8$))	05.60	Acts as a flux to form glassy phase at low temperature
Quartz (SiO_2)	26.59	Increases mechanical and thermal stability
Calcium carbonate ($CaCO_3$)	17.14	Pore forming agent
Pyrophyllite ($Al_2(Si_2O_5)_2(OH)_2$)	14.73	To reduce crazing

The binder, PVA enhances the handling strength of the green support before drying. The dried supports were placed vertically in the grooves of an insulation bricks to ensure uniform sintering. Then, the supports were sintered at 850, 900, 950 and 1000°C for 6 h with a heating and cooling rate of 2°C/min in a muffle furnace at air atmosphere. The rate of heating in the furnace was kept low to minimize the possibility of bending due to radiation shock waves. The cooling rate was kept low (2°C/min) to reduce the cooling stresses as well as to achieve the homogeneity of the microstructure. It also improves the porosity of the support due to the formation of large grain size at lower cooling rate (Rittidech and Tunkasiri 2009). The mould used for the fabrication of the membrane support and the support at various stages are presented in Fig. 3.2.

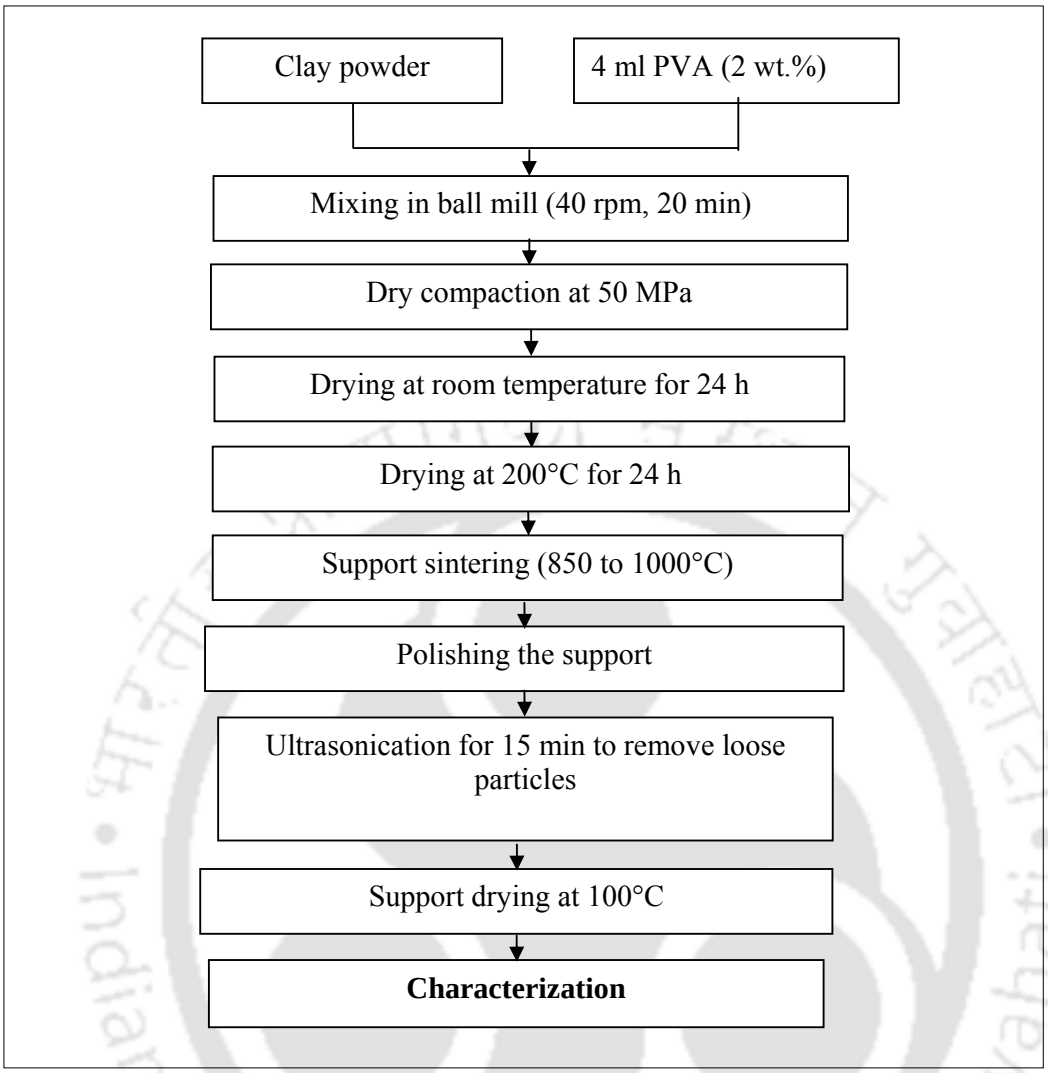

Fig. 3.1 Schematic representation of membrane support fabrication.

A minimum of four supports was prepared for each sintering temperature. After sintering, the change in the support diameter and thickness was measured. The rigid and porous sintered supports were polished and shaped to 42 mm diameter and 4 mm thickness with silicon carbide abrasive papers (C-120, C-220 and C-320) to get a uniform smooth surface. The polished membrane supports were kept in 250 ml beaker containing 200 ml of Millipore water and sonicated for 15 minutes in an ultrasonic bath (Elma, India, model: TranssonicT 460) to remove the loose particles adhered on

the surface of the support during polishing. The fabricated supports were kept in a vacuum desiccator to avoid the possibility of impurities adhere on the surface.

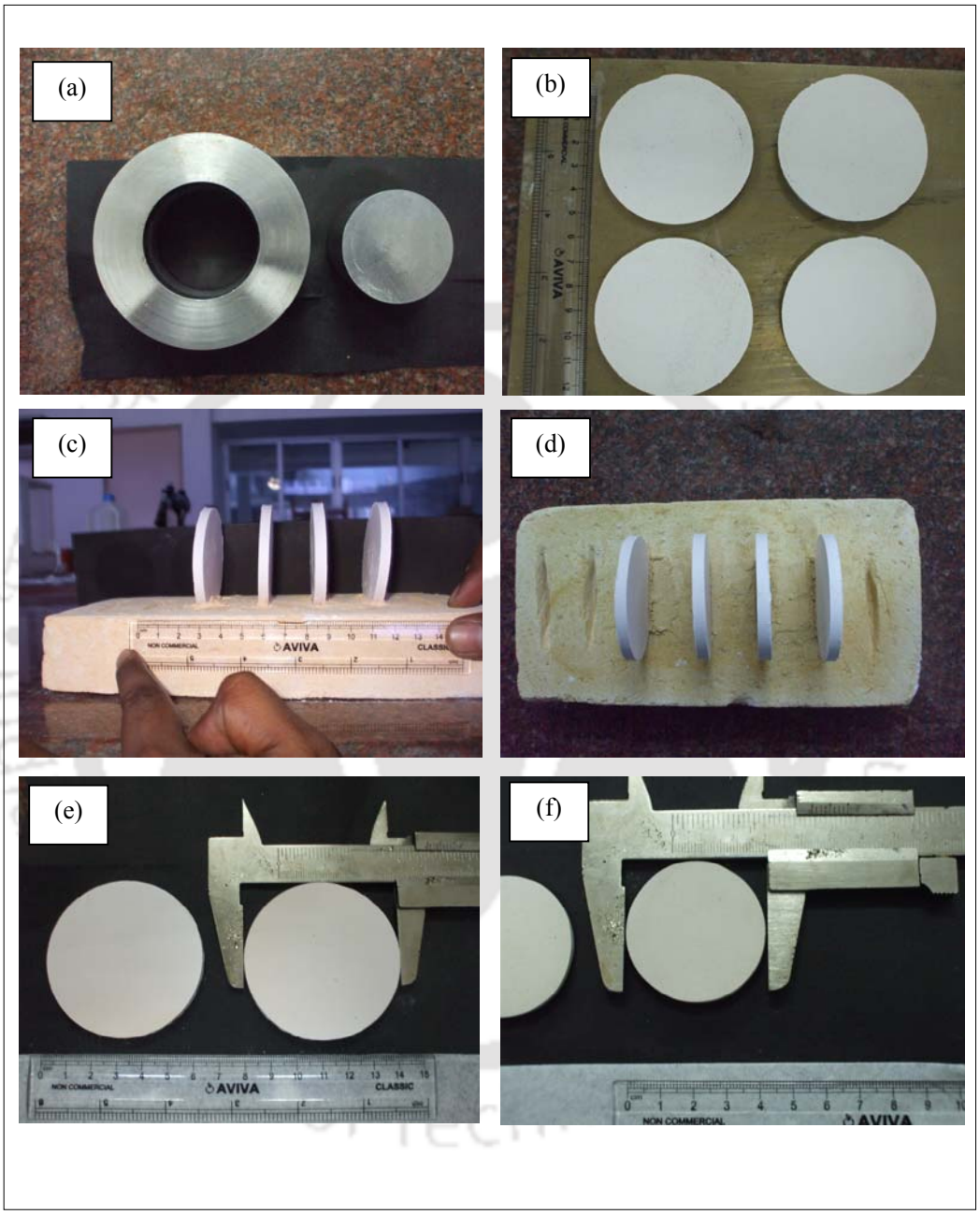

Fig. 3.2 Photographs of the membrane support at various stages. (a) Stainless steel mould, (b) green membrane supports, (c) and (d) membrane supports placed in insulation bricks, (e) sintered membrane support and (f) shaped membrane support.

3.2.2 Characterization methods

Thermal degradation behavior of the raw materials was characterized through Mettler Toledo thermo gravimetric analyzer (TGA/SDTA 851® model) under nitrogen atmosphere at a heating rate of 10°C/min from 25 to 970°C in a 150 μL platinum crucible. The particle size distribution analysis of the raw materials was carried out in a particle sizing machine Malvern Mastersizer 2000 (APA 5005® model, hydro MU) in wet dispersion mode by circulating the heterogeneous feed at constant flow rate (pump speed = 2700 rpm) with an ultrasound to avoid the agglomeration of the clay powders during analysis. The X-ray diffraction (XRD) profile of the sintered ceramic supports was carried out on a Bruker AXS instrument using Cu Kα (λ = 1.5406 Å) radiation operating at 40 kV and 40 mA. The patterns were acquired for 2θ range between 5 and 75° with a scan speed of 0.05°/s. Scanning electron microscope (SEM) analysis was carried out using variable pressure digital scanning electron microscope (LEO 1430VP® model) with an energy dispersive X-ray spectroscopy (EDX). Porosity of the support was calculated by Archimedes' principle using water as an immersing medium. Corrosion resistant of the fabricated supports was characterized in terms of mass loss before and after corrosion using 20 wt.% of H_2SO_4, HCl and NaOH solutions individually. Three point flexural strength measurements were performed on 60mm × 5mm × 5mm rectangular bars using Universal Testing Machine (M/s Deepak Polyplast, Model: DUTT-101, Mumbai). Span length of 50 mm and crosshead speed of 0.5 mm/min were used. Permeation tests were conducted in home made dead-end filtration setup made up of stainless steel 316. Four samples of each sintering temperature were tested for all the experiments and the average value was reported.

3.3 RESULTS AND DISCUSSIONS

3.3.1 Characterization of clay powders

Particle size of the clays determines the pore size and sintering temperature of the ceramic support. Pore growth in the ceramic supports is a function of initial powder particle size and compaction pressure (Luyten *et al.,* 1997; Vercauteren *et al.,* 1998; Biesheuvel and Verweij 1999; Falamaki *et al.,* 2004a; Fukushima *et al.,* 2009). Finer (nanosized) particles require relatively low temperature for sintering but results in a large transport resistance because of too small effective pore size. On the other hand, courser particles require relatively high sintering temperature and results in a small transport resistance because of the macropores but the mechanical strength is reduced (Gu *et al.,* 2003; Wang *et al.,* 2007b). The particle size distribution of the clay powders is shown in Fig. 3.3. All the analysis is done two times for the laser obscuration limit greater than 10% and the averaged value of the results is presented in Table 3.2. The volume or mass moment mean, D[4,3] and the surface area moment mean, D[3,2] are calculated using the following formula

$$D[4,3] = \frac{\sum d^4}{\sum d^3} \tag{3.1}$$

$$D[3,2] = \frac{\sum d^3}{\sum d^2} \tag{3.2}$$

where, d is the diameter of the particle (μm). The advantage of this method of calculation (equation 3.1 and 3.2) is that the formulae do not contain the number of particles and therefore the calculations of the means and distributions do not require knowledge of the number of particles involved. D[4,3] is usually reported in a prominent manner.

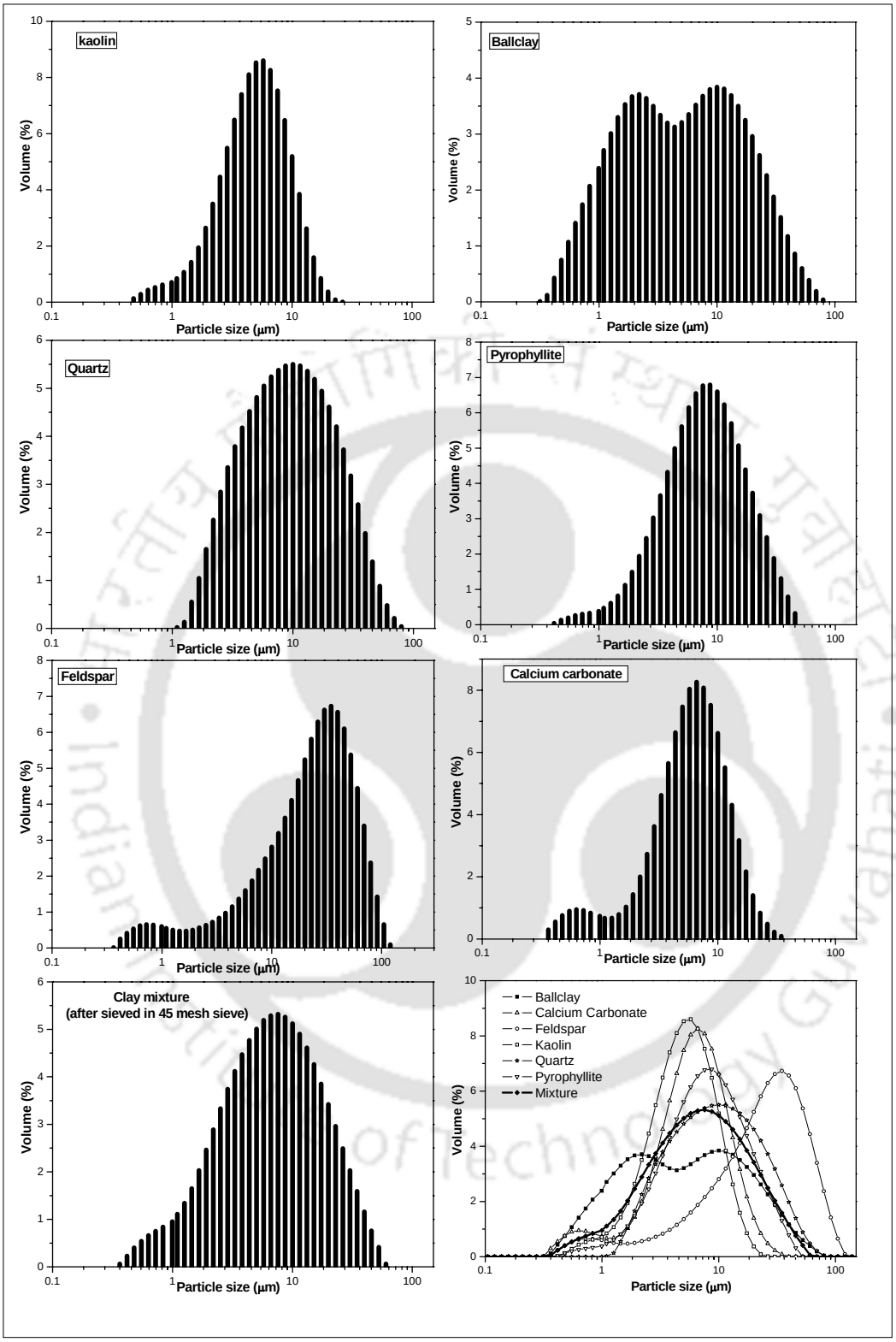

Fig. 3.3 Particle size distribution of the clay powders used for preparation of membrane supports.

Table 3.2 Particle size distribution of various clay powders used in the preparation of membrane support

Clay Powder	Particle size			Span	Specific surface area (m^2/g)	D[3,2] (µm)	D[4,3] (µm)
	D(V,0.1) (µm)	D(V,0.5) (µm)	D(V,0.9) (µm)				
Kaolin	1.852	04.656	9.814	1.710	1.750	3.419	05.354
Feldspar	3.855	22.925	56.284	2.287	0.315	6.898	27.082
Quartz	2.680	08.650	27.107	2.824	0.994	6.034	12.242
$CaCO_3$	2.083	06.460	14.299	1.891	1.610	3.735	07.557
Ballclay	0.954	05.039	24.749	4.722	0.923	2.499	09.659
Pyrophyllite	2.805	08.428	22.786	2.371	0.379	5.581	10.926
Mixture	1.840	07.326	24.450	3.125	0.516	4.094	10.639

D[3,2] = surface area moment mean or the Sauter Mean Diameter (SMD).

D[4,3] = volume or mass moment mean or the De Broucker mean.

D[v,0.5] = volume median diameter sometimes shown as D_{50} or $D_{0.5}$.

The diameter of the clay particles calculated using volume weighted mean formula is found to be in the range of 5 to 10 µm. Clays having particle size of this range would quite useful for the preparation of macroporous ceramic supports. Similar particle size distributions of the clays were discussed and applied for the fabrication of macroporous membrane support (Almondoz *et al.,* 2004; Belouatek *et al.,* 2005; Bouzerara *et al.,* 2006). The surface area of the raw materials are in the sequence of feldspar < pyrophyllite < ballclay < quartz < calcium carbonate < kaolin, which is also considered while choosing the composition of the raw materials for support preparation. This gives a rough idea about the composition of the raw materials to be taken for the fabrication of support.

Span is also another useful parameter in determining the usability of the clay mixture that can be calculated using the formula.

$$\text{Span} = \frac{D_{90} - D_{10}}{D_{50}} \qquad (3.3)$$

A large span value may be due to one or more of the following: (a) very high D_{90} and very small D_{10} (b) moderate D_{90} and D_{10} but very small D_{50}. A very high span value with a very high D_{90} is undesirable in the preparation of ceramic supports due to higher percentage of coarser particles (Wang *et al.,* 2007b). Span values obtained from the analysis are found to be in the similar range (1.8 to 3) for all the clay powders used in this work, which indicates similar width of the size distributions. This provides a good mixing and uniform distribution between the particles that might result in good microfiltration membrane support.

Scanning electron microscope images of the clays along with the EDX is presented in Fig. 3.4. The EDX analysis (qualitative analysis) of kaolin, ball clay and pyrophyllite indicates that the clay powders contain oxides of aluminium and silicon. However, no other peaks are obtained even using spot EDS at higher magnification, suggesting that it is free from other impurities or has only a trace amount of impurities (<5 wt.%) that cannot be detected by SEM. The quartz showed only the oxides of silicon that indicates its purity and the Ca elemental peak obtained for feldspar indicates that the feldspar is of plagioclase type, which is triclinic in nature. The commercially purchased calcium carbonate shows only the peaks of Ca and O, which confirms its purity. The Si/Al ratio obtained with the EDX analysis of the different clays is apparently closer to the theoretical value of those clays (Castellano *et al.,* 2010).

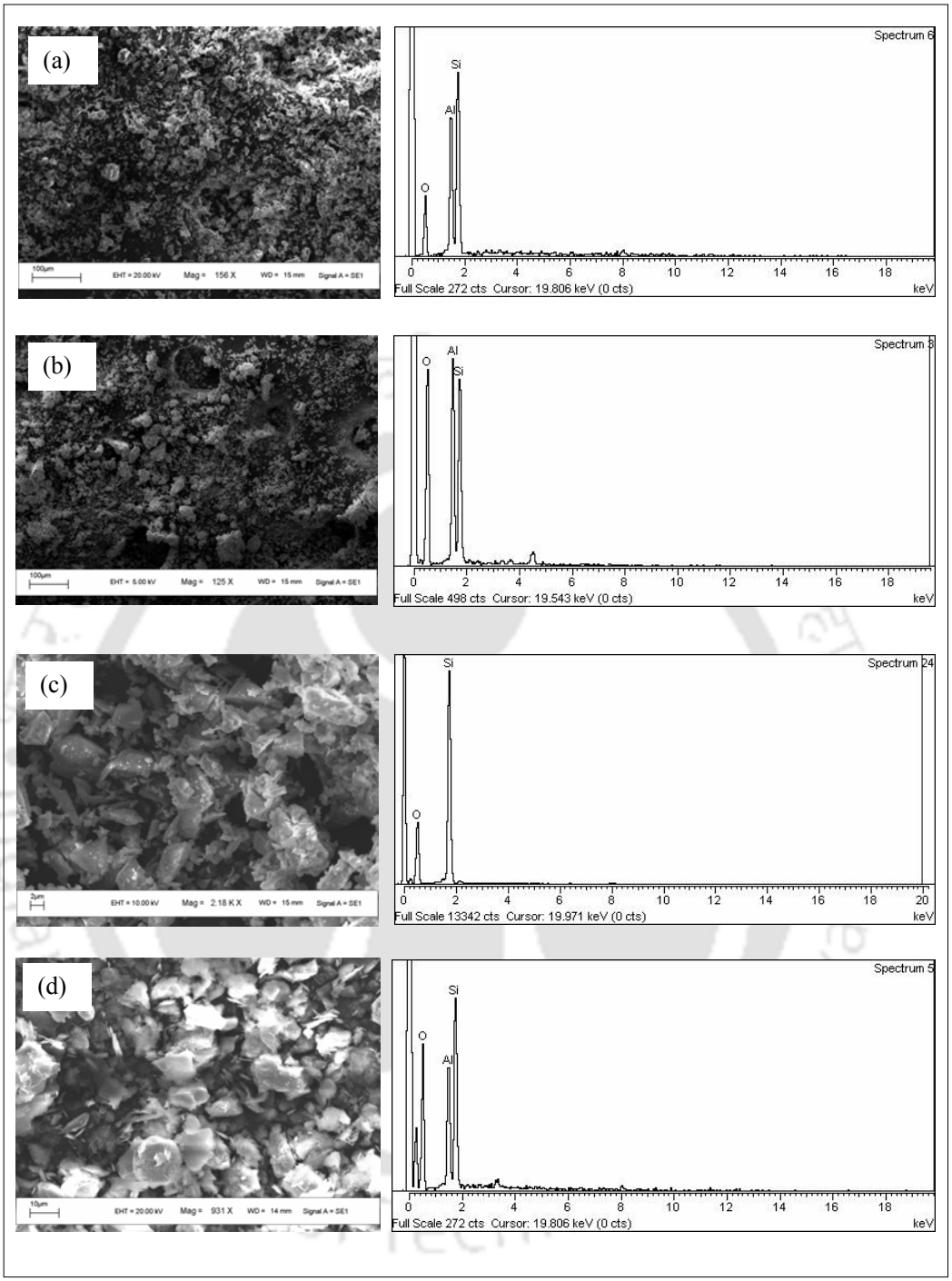

Fig. 3.4(a-d) SEM and EDX analysis of the clay powders used in support fabrication. (a) Kaolin, (b) Ball clay, (c) Quartz, (d) Pyrophyllite.

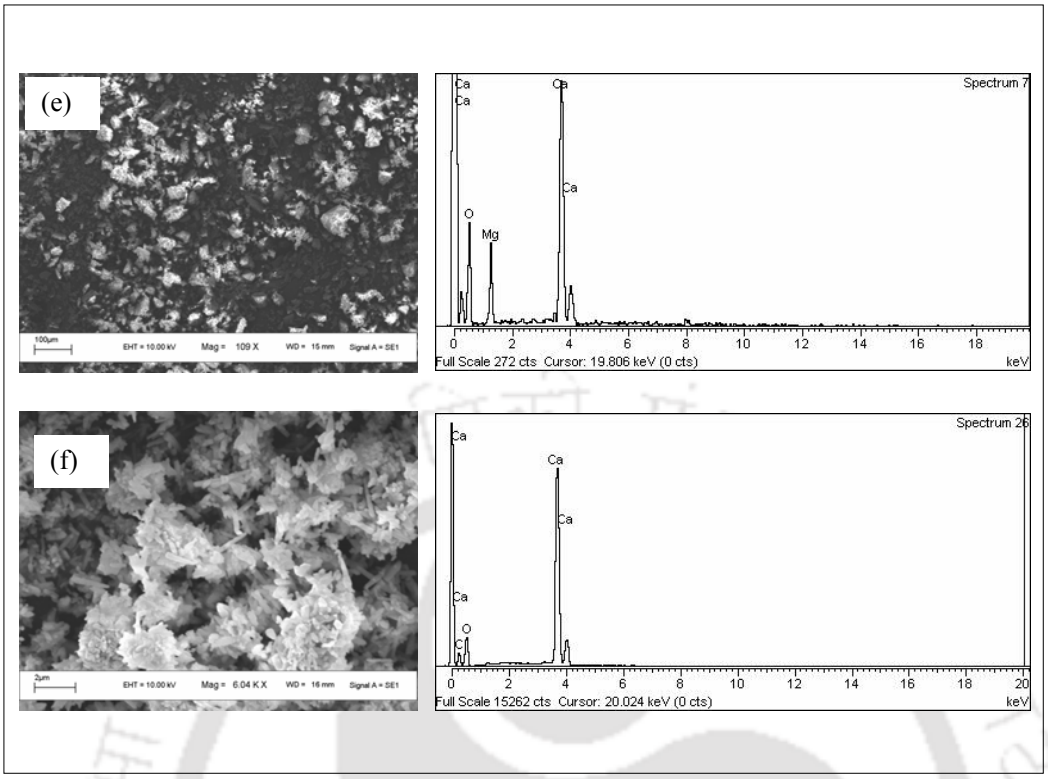

Fig. 3.4(e-f) SEM and EDX analysis of the clay powders used in support fabrication. (e) Feldspar and (f) $CaCO_3$

Similarly, all the clay powders were analyzed with XRD and the obtained patterns are very well matching with the standard Joint Committee on Powder Diffraction Standards (JCPDS) files. The XRD patterns of the clay powders are presented in Fig. 3.5. The XRD peaks of the kaolin match well with the reflections of standard JCPDS card number 14-164 and the other additional reflections match with the JCPDS card number 10-446. This indicates that kaolin also contains dickite, which is the same composition as kaolinite with different crystal structure (Mohammadi *et al.,* 2005; Shameri and Rong 2009; Castellano *et al.,* 2010). The main crystalline phases observed in the ball clay corresponds to kaolin (2θ = 12.25 and 24.85°) and quartz. The 2θ reflections (2θ = 20.85 and 26.65°) of quartz match well with the JCPDS card number 46-1045, which corresponds to the pure quartz phase (Gonzalez *et al.,* 2007).

Similarly the 2θ reflections of the pyrophyllite and feldspar clays match with the standard JCPDS card number 12-203 and 09-456, respectively (Sugiyama *et al.*, 1993; Hojamberdiev *et al.*, 2011).

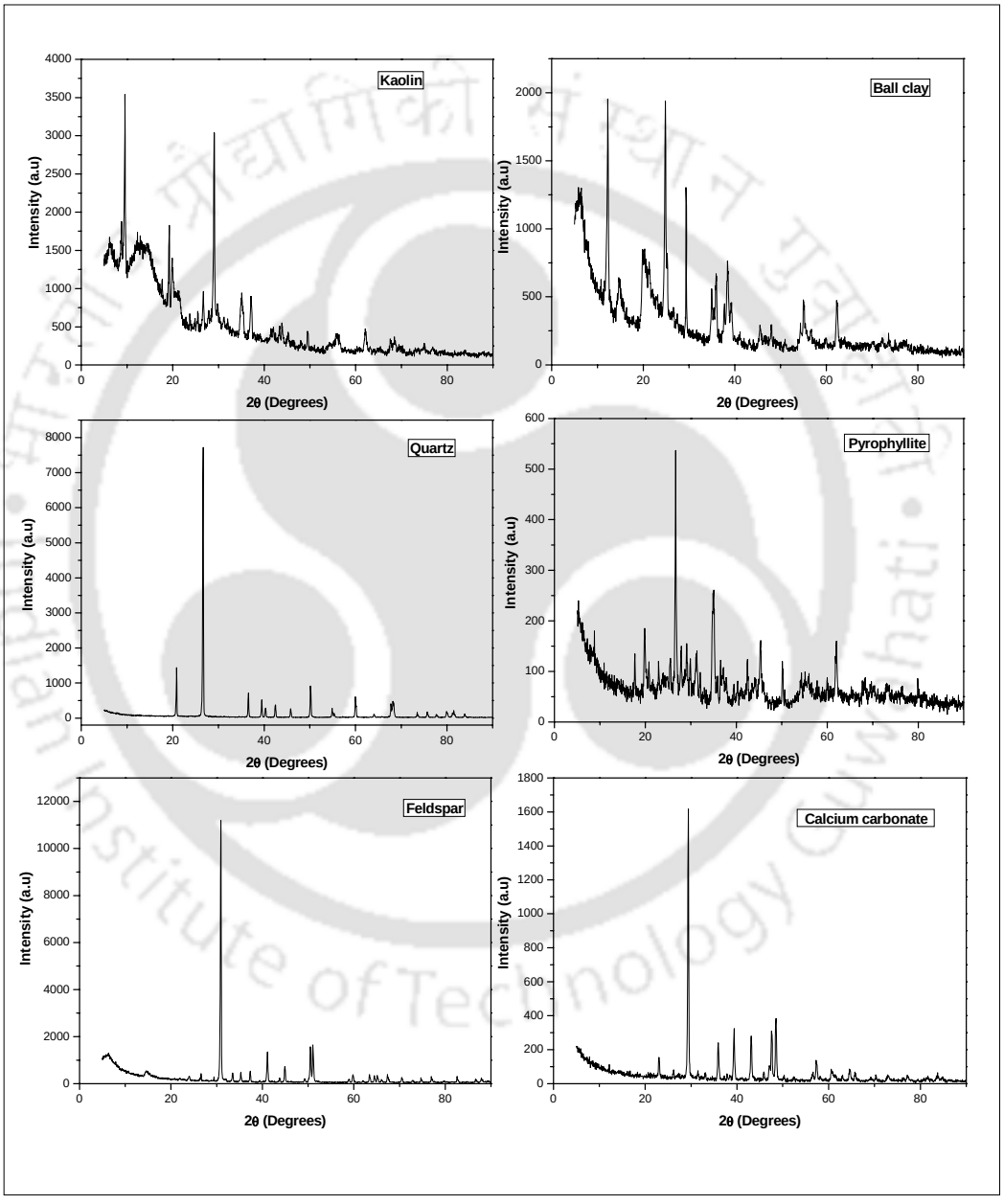

Fig. 3.5 XRD Patterns of the clays used for the preparation of membrane supports.

Sintering temperature is one of the important parameter for controlling the porosity, pore size and mechanical stability of the membrane supports. Thermal analysis of individual clays was done to identify the minimum sintering temperature for a stable support and the obtained results are plotted in Fig. 3.6. The weight loss at temperature less than 150°C is mainly due to the removal of physisorbed water and at higher temperature (500 to 800°C), the loss corresponds to the dehyroxylation of surface hydroxyl group or removal of structural water. Thermal decomposition (540 to 760°C) of $CaCO_3$ results in major weight loss and forms CaO and CO_2. The porosity of the membrane support mainly depends on the path taken by the evolved CO_2 gas. Due to the increased release of OH groups attached to Al and Si and subsequent conversion of kaolin to metakaolin ball clay show a relatively higher weight loss (14.15%) than that of kaolin (5.58%) and pyrophyllite (4.46%).

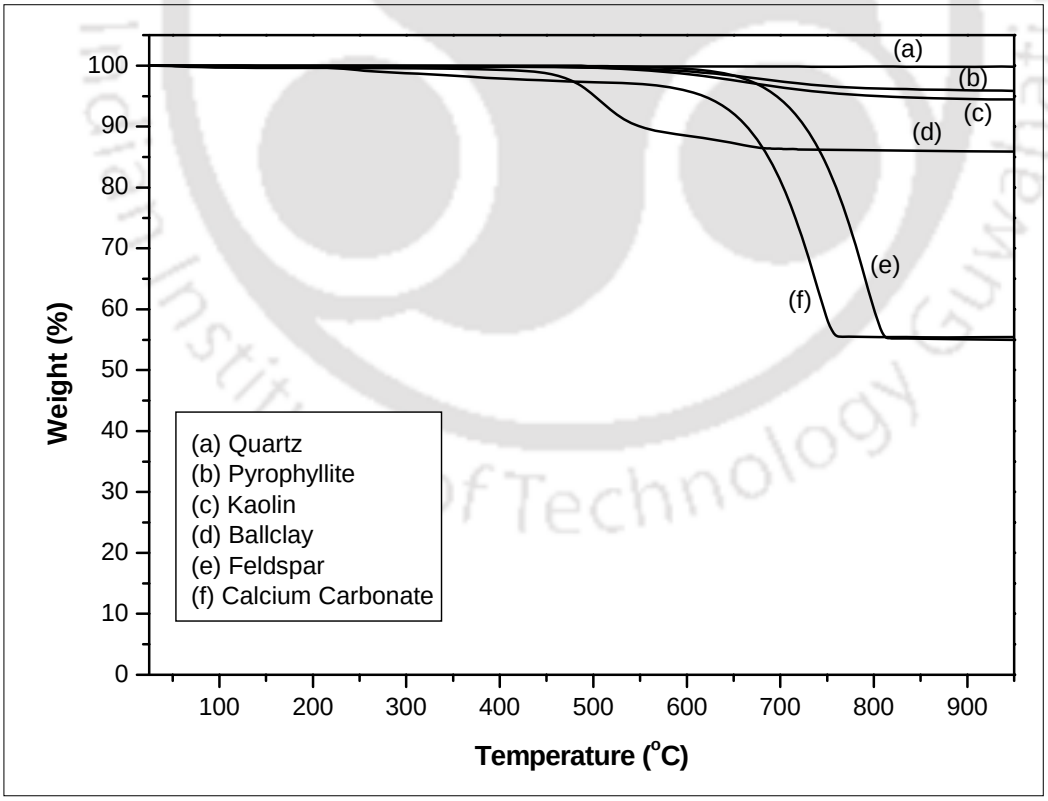

Fig. 3.6 Thermogravimetric analysis (TGA) of the clay powders.

The typical weight loss obtained for feldspar is difficult to explain, however, the possible reason might be the degradation of calcium feldspar to form CaO and CO_2 that causes greater weight loss. Similar type of results was reported for K-feldspar and K_2CO_3 (Miao *et al.*, 2005).

It is also observed that, after 820°C, only a negligible weight loss has been found for the clays suggests that the green support has to be sintered to a minimum of 850°C to get a stable membrane support having higher thermal and mechanical stability. Furthermore, the binder burnout mechanism has also been studied for the given composition of clays (with and without binder) as depicted in Fig. 3.7.

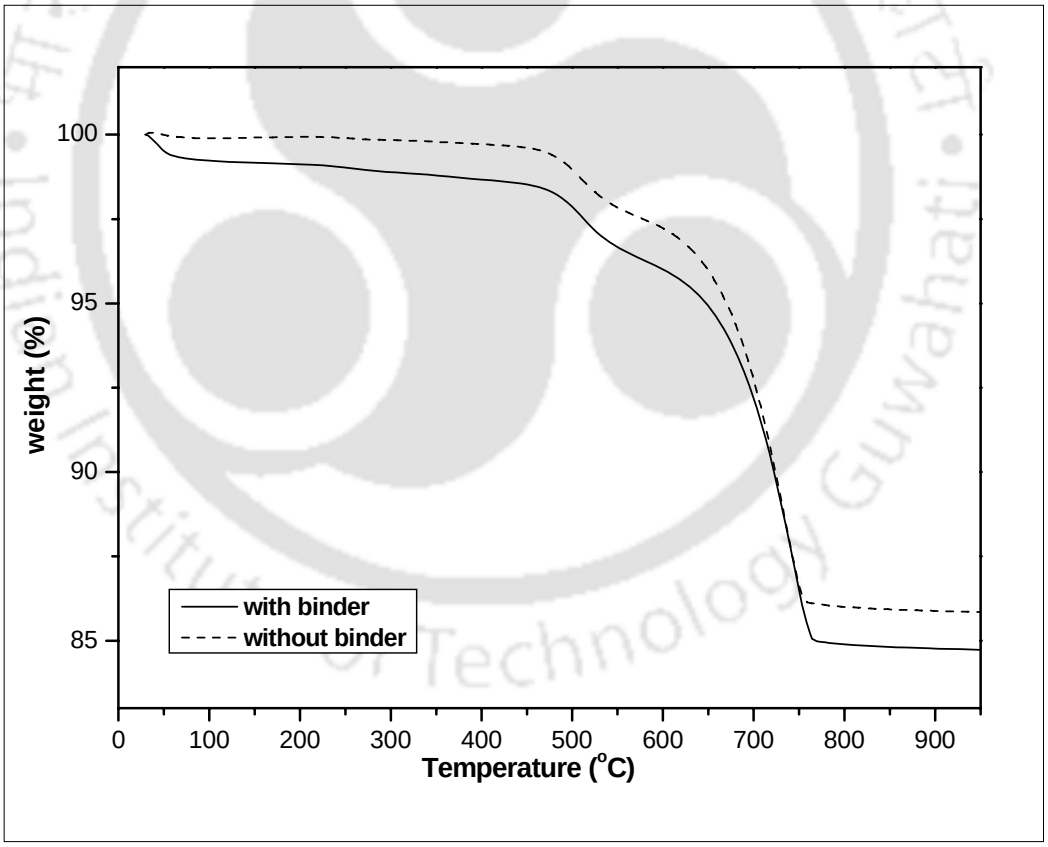

Fig. 3.7 Thermogravimetric curves of the clay mixture with and without binder.

During sintering, the binder initially spreads on the clays as a thin layer and then burnout uniformly. The degradation of the organic binder occurs in two steps; elimination of the side-groups at temperature between 200 and 350°C and the decomposition of the main chain of PVA between 450 and 650°C. The binder is completely removed at 720°C. The PVA chain enhances the thermal stability of the ceramic support (Falamaki *et al.,* 2004a; Guo *et al.,* 2007; Dong *et al.,* 2008).

3.3.2 Characterization of the fabricated membrane supports

3.3.2.1 XRD analysis

The crystallization or phase transformation behavior of the membrane supports was identified by XRD analysis as shown in Fig. 3.8. Sintering produces a series of chemical reactions and phase transformations that leads to the formation of new phases, which results in the appearance or disappearance and shifts in the XRD peak positions. There may be an existence of amorphous silica evidenced by a background noise in the XRD pattern for 850°C sintered support (Gualtieri *et al.,* 1995). Complete crystalline phase is identified for the supports sintered at 900, 950 and 1000°C. The main observed phases of the sintered support are quartz (SiO_2), mullite ($3Al_2O_3.2SiO_2$), anorthite ($CaO.Al_2O_3.2SiO_2$) and wollastonite ($CaSiO_3$). The phase transformation of kaolin to mullite via metakaolinite is occurred in the temperature ranges between 800 and 1000°C, which is due to the decomposition of kaolin structure (Palacio *et al.,* 1998; Bouzerara *et al.,* 2006; Guo *et al.,* 2007). This transformation is clearly seen from the Fig. 3.8(b).

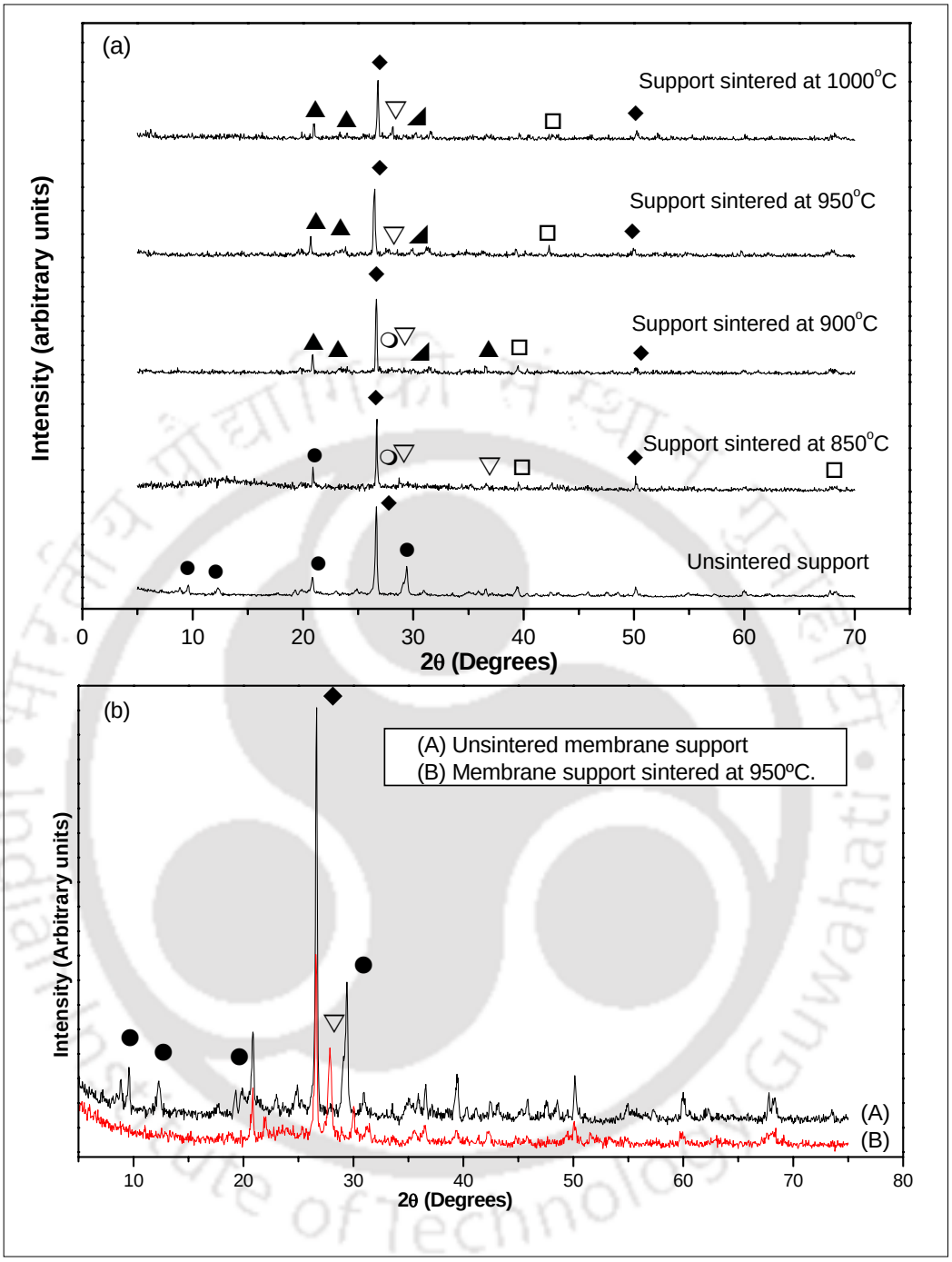

Fig. 3.8 XRD pattern of the sintered membrane support at different temperatures. ◆ Quartz; ● Kaolin; ◢ Wollastonite; ▲ Mullite; ▽ Anorthite; ◘ Calcium Oxide; ❍ Feldspar.

Crystallite size of the membrane supports before and after sintering is calculated using Scherer's formula

$$d_{XRD} = \frac{K\lambda}{\beta \cos\theta} \qquad (3.4)$$

where, K is the shape constant (0.9), λ is the wave length (1.5406 Å) of CuKα radiation, β is the full width at half maximum and θ is the diffraction angle (degree). A decrease in crystallite size is found at higher temperature (1000°C) indicates a higher degree of particle interlocking which may lead to densification of the support. For all the sintered supports, quartz is found to be the major phase and its decreased peak intensity during sintering indicates the newly formed silicates and mullite.

3.3.2.2 Volume shrinkage and porosity analysis

The shrinkage of the membrane supports was determined using the initial and final volume of the supports before and after sintering. As the sintering temperature increases the shrinkage of the support also increases as shown in Fig. 3.9. A maximum shrinkage of 5.5% is obtained for 1000°C sintered support. It is evident that the shrinkage of the support sintered at 900°C is found to be more (~ 4.5%) than the 850˚C sintered support due to the removal of binder and phase transformation of kaolin to mullite at the temperatures between 850 and 900°C. Increased shrinkage is found for 850 to 900°C. The shrinkage is less pronounced for the sintering temperatures 900 and 950°C. Again, an increase in the shrinkage for 1000°C sintered support indicates the internal rearrangement (densification process) of the support which may lead to blind pores (Whittemore and Sipe 1974; Falamaki *et al.,* 2004a).

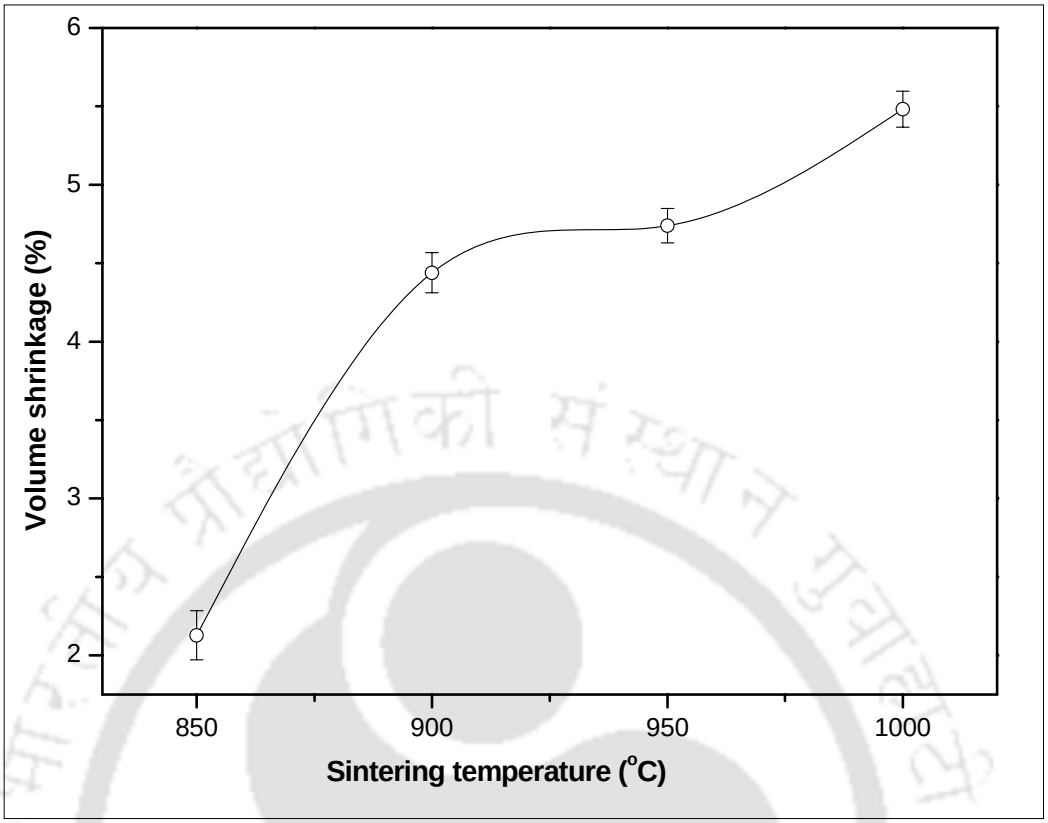

Fig. 3.9 Volume shrinkage versus sintering temperature of the membrane support.

Porosity of the membrane supports sintered at different temperature is calculated using the Archimedes' principle (Laux *et al.,* 2005).

$$\varepsilon = \frac{m_W - m_D}{m_W - m_A} \qquad (3.5)$$

where m_D is the mass of the dry support, m_W is the mass of the support with pores filled with water (pores are filled with water under vacuum), m_A is the mass of the water saturated support measured in water (A refers to Archimedes) and ε is the porosity.

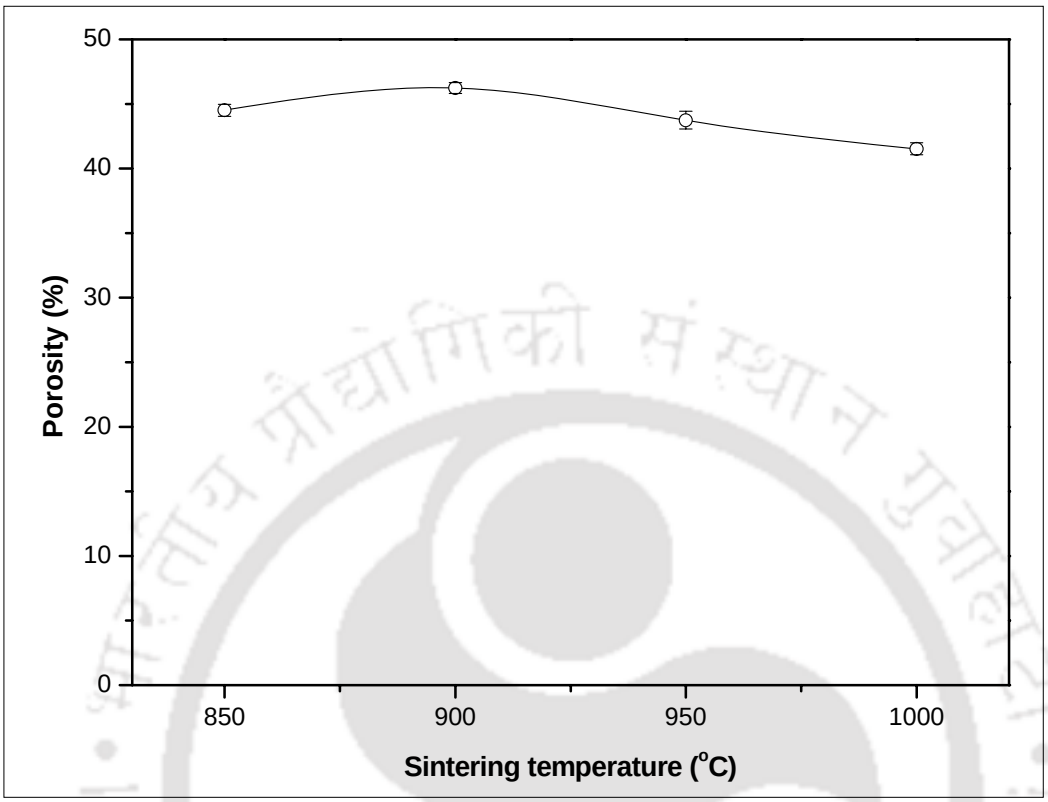

Fig. 3.10 Porosity versus sintering temperature of the ceramic support.

Fig. 3.10 depicts the porosity of the membrane supports as a function of the sintering temperature. It is seen that the porosity versus sintering temperature curves follow a 'convex' trend with maximum at 900°C within the studied temperatures. The decrease in porosity from 900 to 1000°C is an indication of the densification of the support. The porosities of the sintered support lies in the range of 41 to 46% and the support sintered at 900°C have the maximum porosity of 46%. Falamaki *et al.*, (2004a) have also reported the similar trends of porosity and shrinkage for alumina and zircon supports.

3.3.2.3 Flexural and corrosion resistance analysis

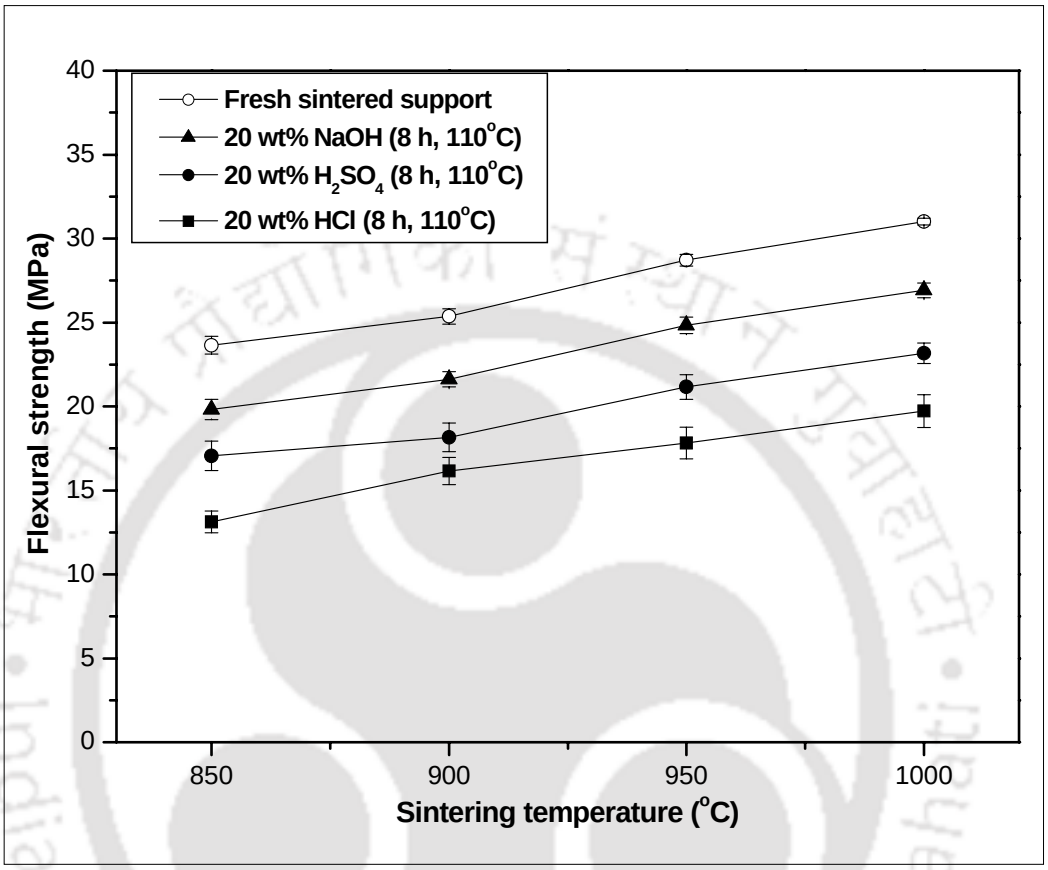

Fig. 3.11 Flexural strength as a function of sintering temperature of the membrane support.

Figure 3.11 shows the flexural strength (three points bending) of the supports sintered at different temperatures calculated by the following equation

$$\sigma_{fl} = \frac{3F_p L}{2bt^2} \qquad (3.6)$$

where σ_{fl} is the flexural strength (MPa), F_p is the load at the fracture point, L is the span length, b is the width of the sample and t is the thickness of the sample.

Flexural strength increases (25 to 32 MPa) with increase in the sintering temperatures (850 to 1000°C). It is clearly seen from the Fig. 3.11 that the flexural strength increases linearly with the sintering temperature. The increase in the flexural strength is due to the densification of the support. Similar trends were also reported for supports fabricated from other types of inorganic clays (Falamaki *et al.,* 2004a; Wang *et al.,* 2006).

Corrosion tests were performed using 20 wt.% of HCl, H_2SO_4 and NaOH solutions individually at room temperature and 110°C to check the chemical stability of the membrane supports. For this, the membrane supports (Ø = 63 mm and thickness = 4 mm) are placed in the corrosive environments (100 ml) for 30 days at room temperature (without stirring) and also for 8 h in boiling state at 110°C. Corrosion resistance of the fabricated membrane supports is analyzed in terms of mass loss and flexural strength. The weight loss due to the corrosion of acids and alkali is shown in Fig. 3.12 and it is found to be decreasing in the order of HCl > H_2SO_4 > NaOH. Similar types of results have also reported for other inorganic supports (Wang *et al.,* 2006; Dong *et al.,* 2007). The flexural strength of the corroded support is also calculated and depicted in Fig. 3.11.

The average percentage loss of flexural strength of the supports after the corrosion test in boiling liquids (NaOH, H_2SO_4 and HCl) at 110°C for 8 h is found to be 14, 27 and 38%, respectively. Dong *et al.,* (2007) have also reported similar type of results for cordierite and alumina support. The obtained results revealed that the fabricated support shows greater corrosion resistance in both acidic and basic media than that of cordierite and alumina support (Dong *et al.,* 2007). Hence it can be utilized for membrane applications.

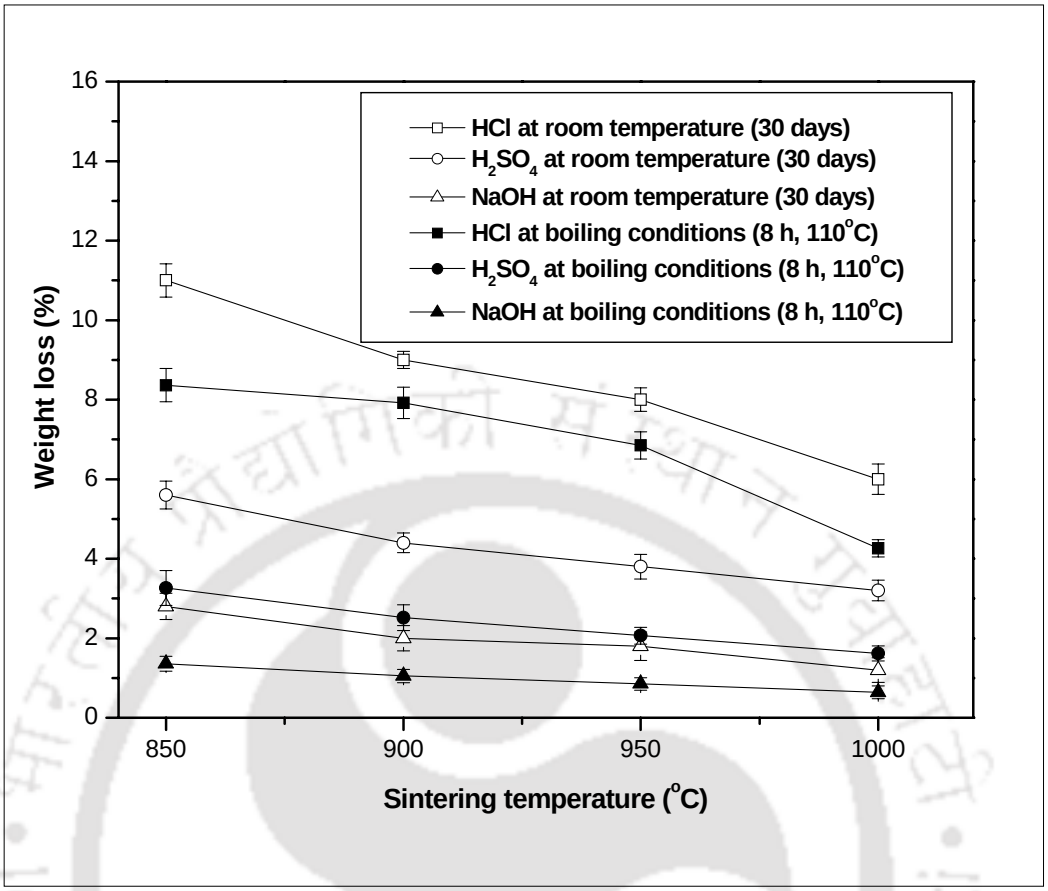

Fig. 3.12 Corrosion resistance of the sintered supports in acid and alkali media.

3.3.2.4 SEM analysis

Surface morphology of the sintered membrane supports analyzed by SEM is shown in Fig. 3.13. The pore size distribution and average pore diameter of the sintered support are estimated from the SEM micrographs using ImageJ software (open source software provided by National Institute of Health (NIH), weblink: http://rsbweb.nih.gov/ij/download.html) for pores (~100 pores per micrograph) having circularity greater than 0.8. To minimize the errors of image analysis, eight SEM micrographs (randomly selected sections of 4 supports) are analyzed for each sintered temperature.

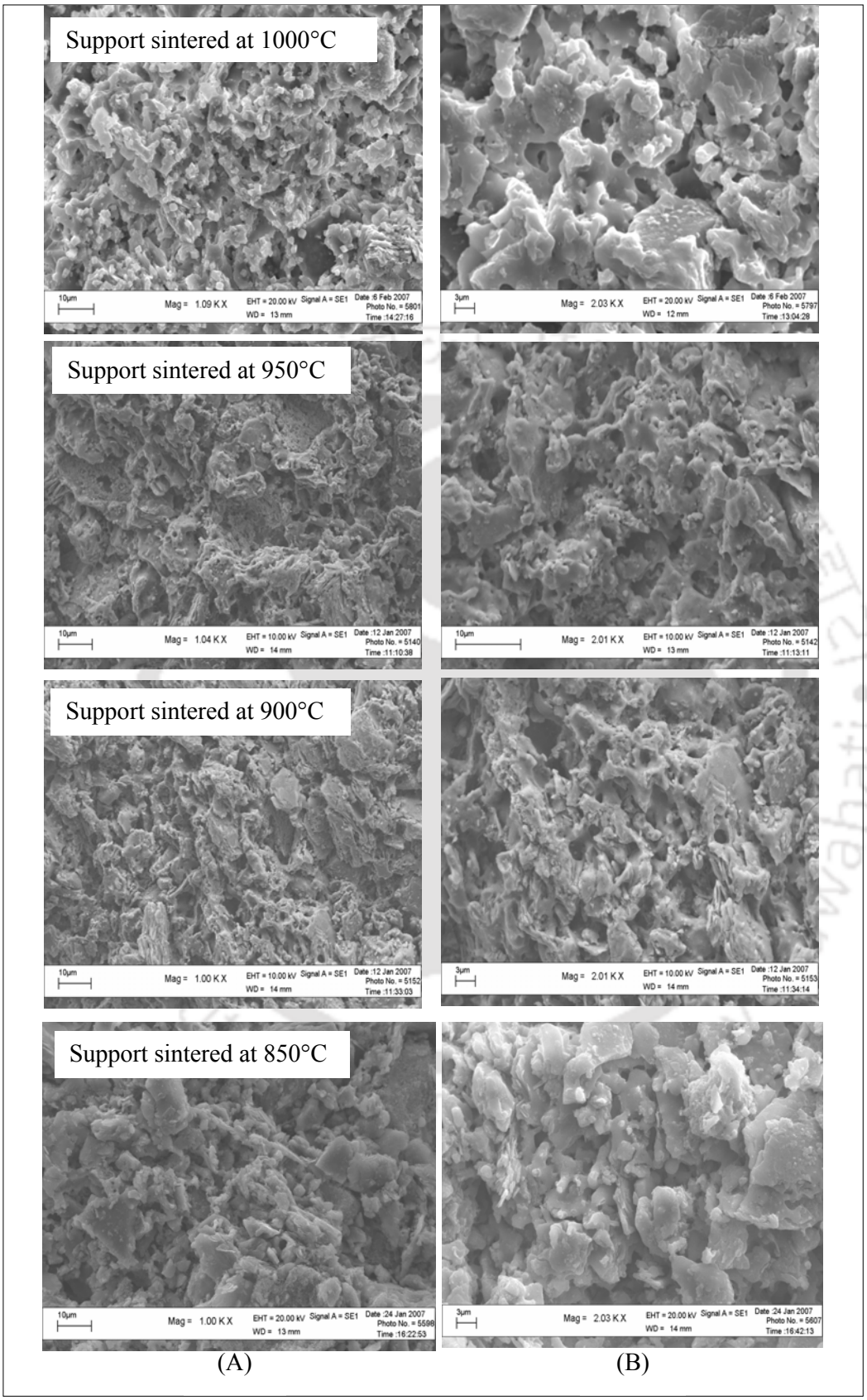

Fig. 3.13 SEM micrographs of the sintered membrane supports at two different magnifications. (A) 1.00 KX and (B) 2.00 KX.

The average pore size, D_{avg} of the membrane supports is calculated by the following equation

$$D_{avg} = \frac{\sum_{i=i}^{n} n_i d_i}{\sum_{i=1}^{n} n_i} \qquad (3.7)$$

where, D_{avg} is the average pore diameter (μm), n is the number of pores and d_i is the diameter of the i^{th} pore (μm).

It is clearly seen from the Fig. 3.13 that the compact structure of the 850°C sintered support is transformed into an open structure at 900 and 950°C. The support sintered at 1000°C seems to have a densified structure. The average pore diameter is found to be 0.87, 0.96, 1.01 and 1.10 μm for the supports sintered at 850, 900, 950 and 1000°C, respectively. The pore diameter distribution of the sintered supports is plotted against sintering temperature as shown in Fig.3.14. The supports sintered at 950 and 1000°C shows a unimodal distribution having maximum number of pores (90-95%) between 0.2 and 1.2 μm. The supports sintered at 850 and 900°C shows a bimodal distribution having maximum number of pores in two regions, 60 to 70% of pores between 0.2 and 1.4 μm and 20 to 30% of pores between 1.4 and 2.4 μm.

Based on the porosity and image analysis, it is observed that with increase in sintering temperature, pore diameter increases while porosity decreases. This is because of adjacent pores tend to fuse together to form bigger pores at an elevated sintering temperature. Some of the pores may even disappear during sintering resulting in shrinkage of the membrane support. It is reported in literature that the membrane thickness has important influence on the pore size distribution. The mean pore size of the supports decreases and the pore size distribution becomes narrower with the

increase of membrane thickness (Wang *et al.*, 1999). By virtue of these reasons, the support thickness is fixed when the effect of sintering temperature was studied.

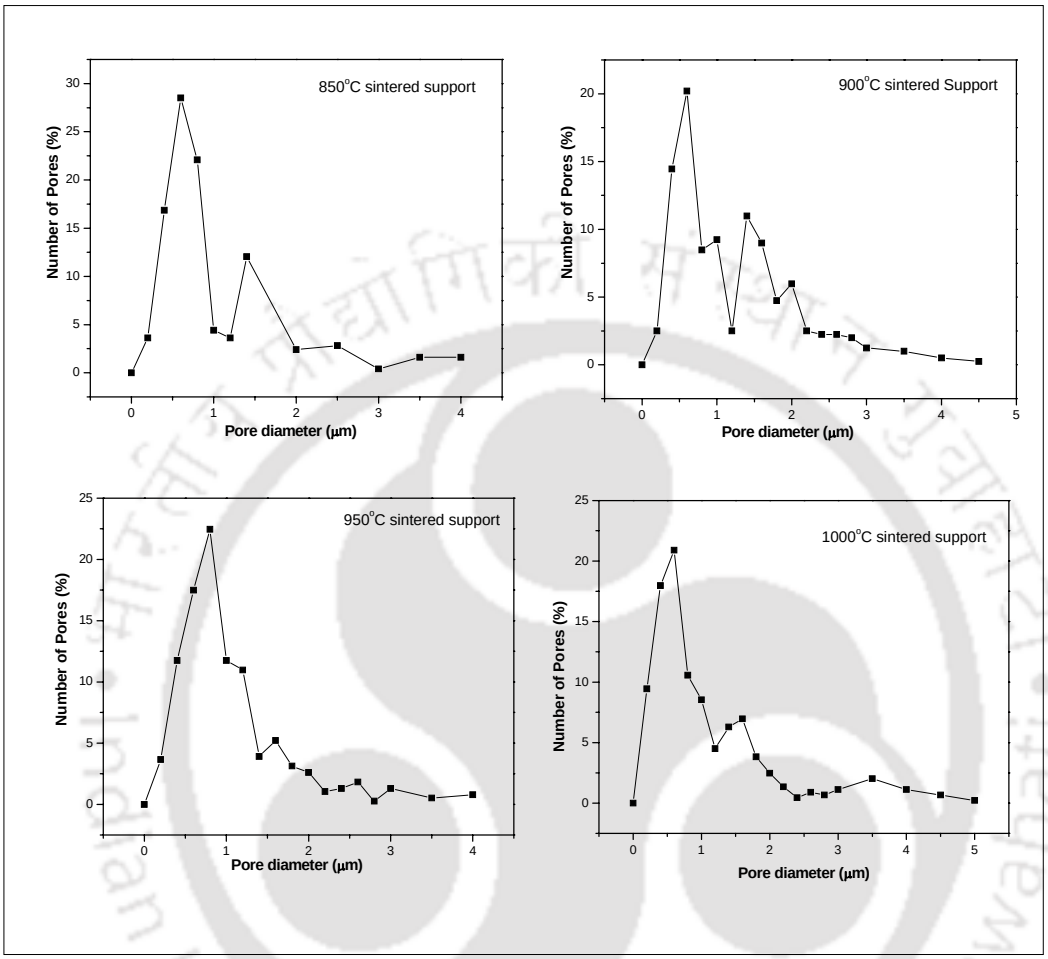

Fig. 3.14 Effect of sintering temperature on pore size distribution.

Mapping analysis of the SEM as shown in Fig. 3.15 confirms the uniform distribution of the silica-aluminates throughout the membrane supports. The elements identified by the EDX are Al and Si, which is in the form of oxides (Al_2O_3 and SiO_2), Ca in the form of calcium oxide as well as wollastonite and anorthite.

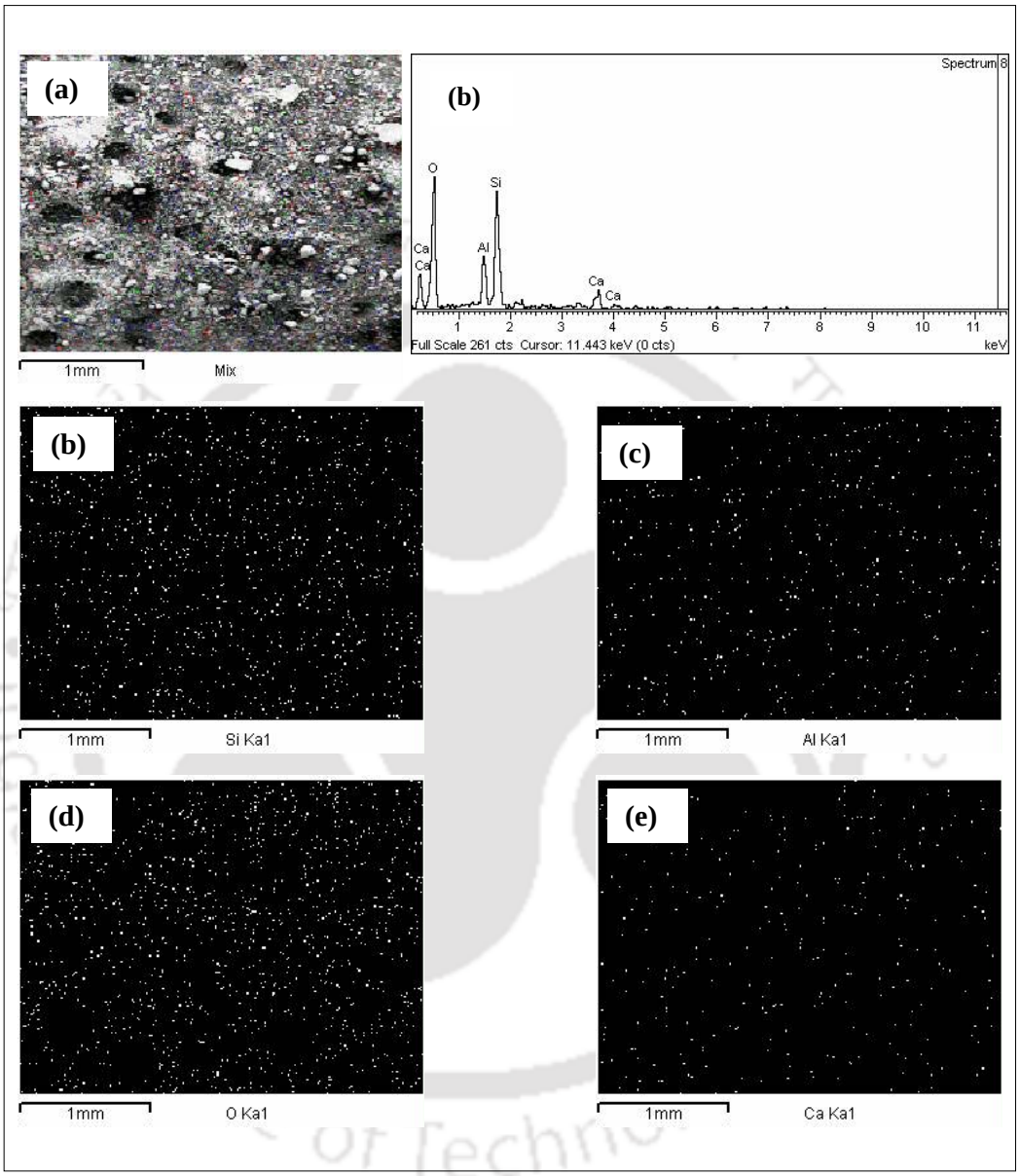

Fig. 3.15 SEM mapping analysis of the sintered support. (a) Zone at which EDX and mapping analysis done, (b), (c), (d) and (e) represents the mapping results of Si, Al, O and Ca, respectively.

3.3.2.5 Pure water permeation experiments

Pure water and organic solvent permeation studies were carried out in a dead-end flow setup made up of stainless steel 316. The schematic and photographs of the permeation setup along with its specifications are depicted in Fig. 3.16 and 3.17, respectively.

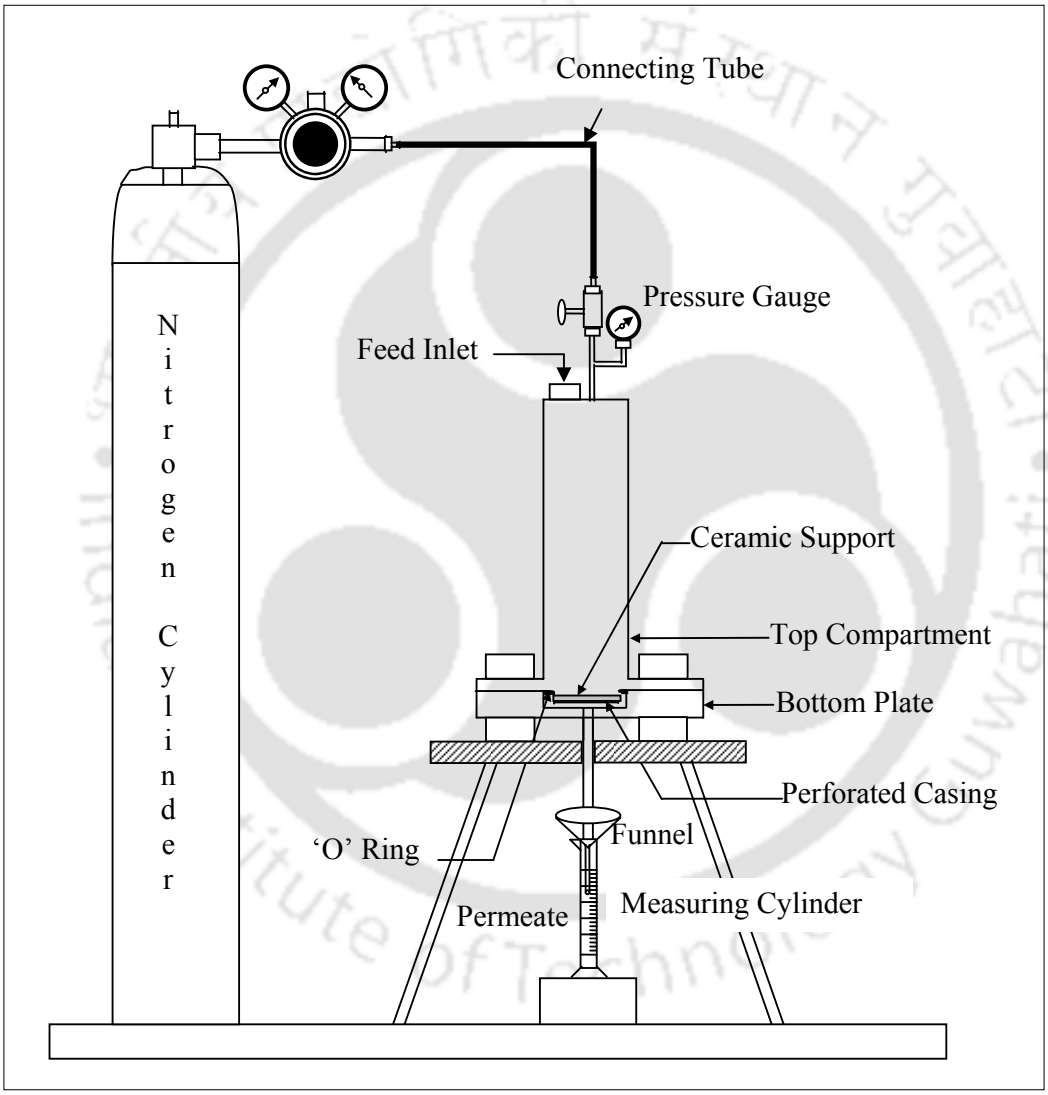

Fig. 3.16 Schematic of batch permeation experiment setup

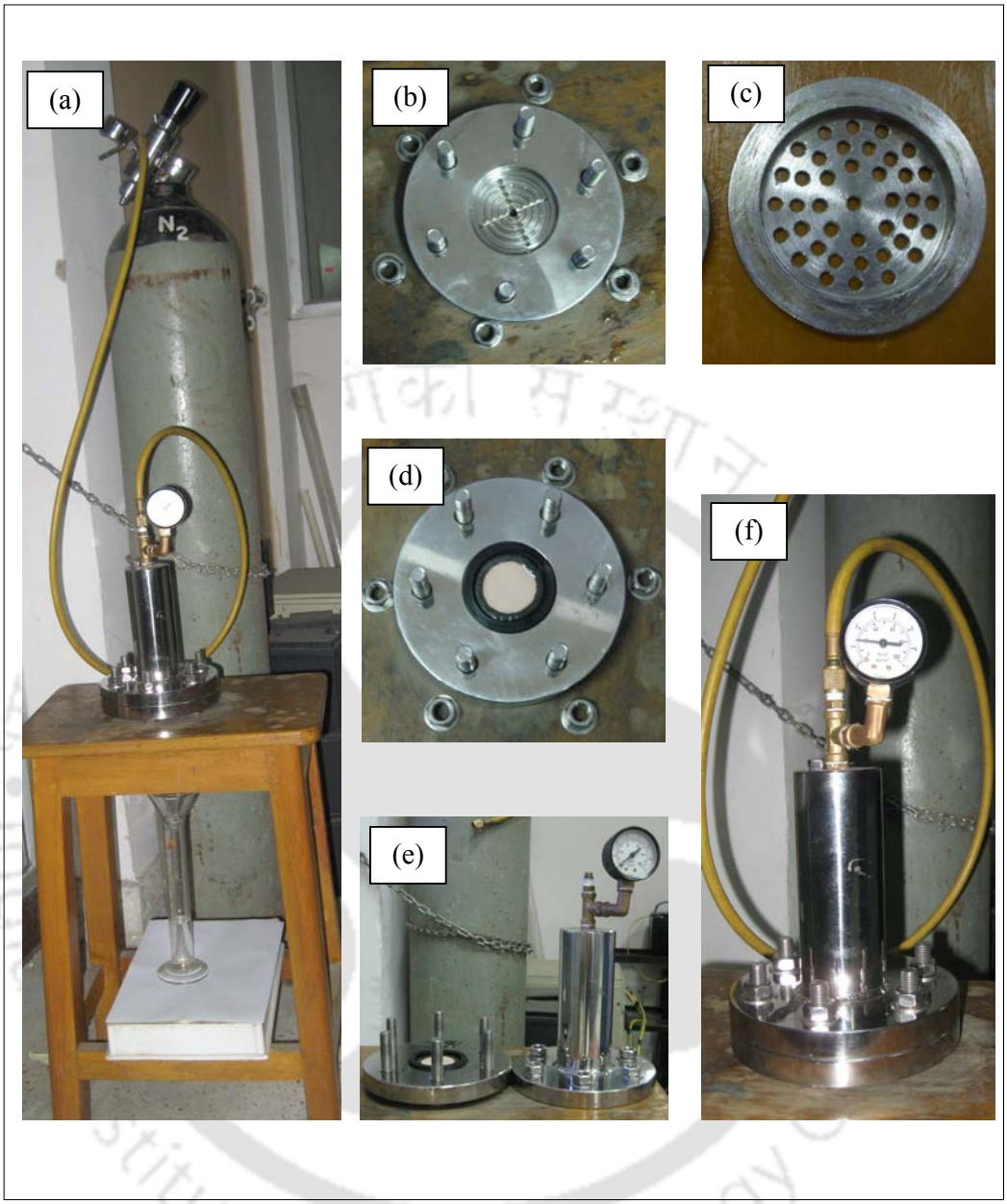

Fig. 3.17 Photographs of home-made permeation setup. (a) Permeation cell connected to nitrogen cylinder (b) bottom compartment (c) casing (d) membrane support sealed in the casing and gasket is kept over the casing (e) bottom and top compartment and (f) permeation cell under operating condition.

The setup consists of two parts, a cylindrical top part and a base plate with a provision to keep a support. The membrane support is rested on a perforated disk (casing) and placed in the bottom compartment. Neoprene "O" ring or gasket is compressed against the membrane support to prevent leakage. The upper compartment of the batch cell is pressurized using N_2 gas by setting a desired pressure through the regulator attached with the nitrogen cylinder. Prior to permeation studies, pure water is passed thorough the fresh supports at higher pressure to remove any loose particles (particles which are not removed during ultrasonication) present in the pore path. All the experiments were carried out by filling 250 ml of water in the top compartment. After discarding the first 50 ml of water at a fixed pressure, the time required to collect next 50 ml was noted down to calculate the water flux at that applied pressure using the following equation

$$J_w = \frac{Q}{A\Delta T} \qquad (3.8)$$

where, J_w is the pure water flux (m/s), Q is the volume of water permeated (m^3), A is the effective membrane area (m^2) and ΔT is the sampling time (s). Four supports from two different batches were analyzed for each sintering temperature.

Typical result of water flux on the sintered (850, 900, 950 and 1000°C) membrane supports is shown in Fig. 3.18. Water flux increases with increase in sintering temperature (up to 950°C) due to increase in the average pore diameter. Decreased water flux for 1000°C sintered support is due to the reduced porosity. Higher sintering temperature (1000°C) eliminates pore connectivity to a large extent that leads to dead-end pores. The linear dependence of water flux on pressure drop across a support indicates Poiseuille flow through the pores.

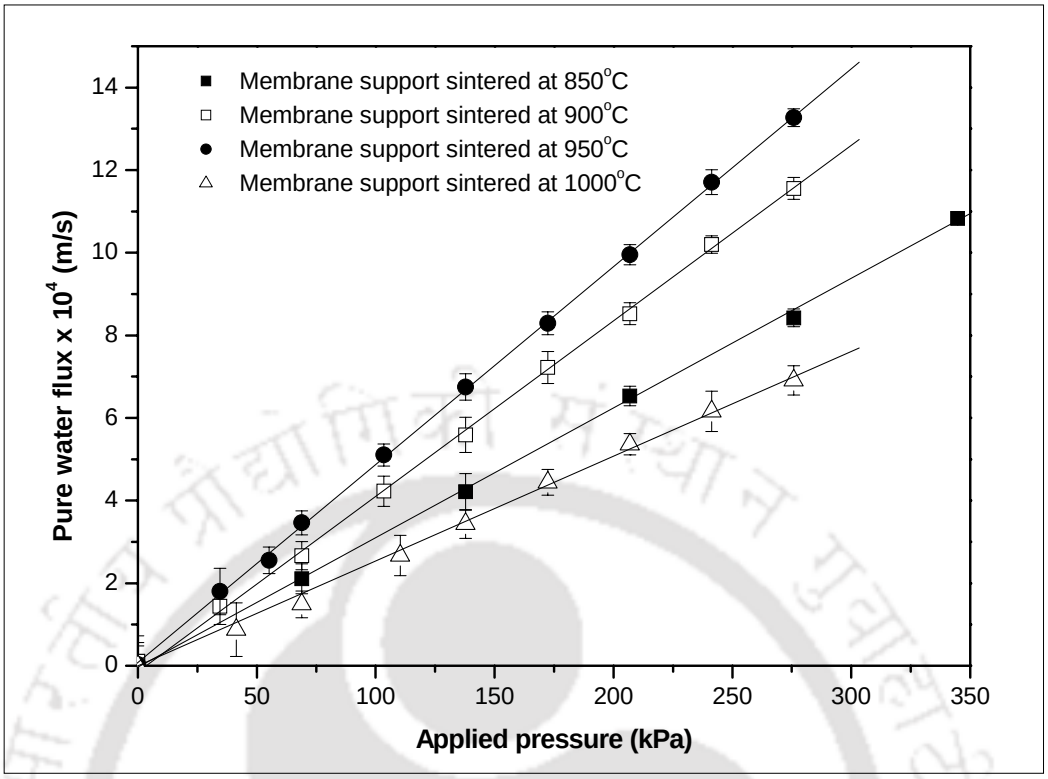

Fig. 3.18 Pure water flux on the membrane supports as a function of applied pressure.

The average pore radius of the membrane support is estimated by using the deduced form of Hagen-Poiseuille (H-P) equation by assuming the pores are cylindrical.

$$r_m = \sqrt{\frac{8\mu\Delta x J}{\varepsilon \Delta P}} \qquad (3.9)$$

where r_m is the mean pore radius (μm), μ is the viscosity (kPa s), Δx is the thickness (μm), J is the permeate flux rate (μm/s), ε is the porosity, ΔP is the transmembrane pressure (kPa), $\frac{J}{\Delta P}$ is the permeability (μm/s kPa), determined from the slope of the linear relationship between the pure water flux (J) and transmembrane pressure (ΔP).

It is observed from the Fig. 3.19 that the average pore size calculated from water permeation data using H-P equation is higher than the SEM image analysis. The possible reason may be that the small nanosized pores cannot be obtained from the SEM image of the membrane support due to instrument limitations that might have also contributed in the permeation. The mean pore diameter obtained by the H-P equation is an average along the total permeation pathway through which a solute travels (free from dead-end pores) whereas the mean pore diameter obtained by SEM is an average of the surface pores on the membrane supports.

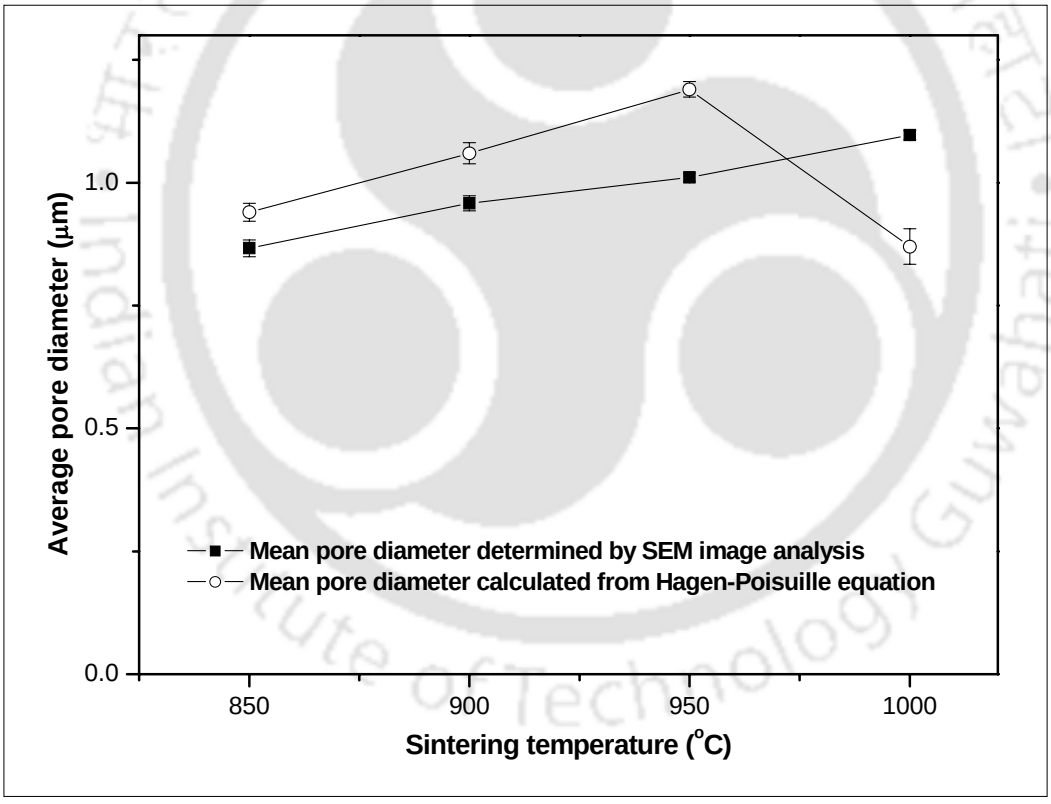

Fig. 3.19 Mean pore size versus sintering temperature of the membrane supports.

Eventhough the pore diameter of the 1000°C sintered support calculated by the SEM analysis is higher than the other sintered supports, the water permeability experiments confirm that the membrane support has the possibility of more dead-end pores due to the densification of the membrane support at higher temperature. Based on the detailed analysis of the support, the membrane support sintered at 950°C is selected as an optimum support because of its high flexural strength (28 MPa), average pore diameter (0.98 µm) and good porosity (44%).

3.3.2.6 Solvent permeation experiments

Pure organic solvent permeation studies were performed with ethanol, butanol, acetone, toluene and *n*-hexane for the ceramic support sintered at 950°C and the solvent flux results are plotted in Fig. 3.20.

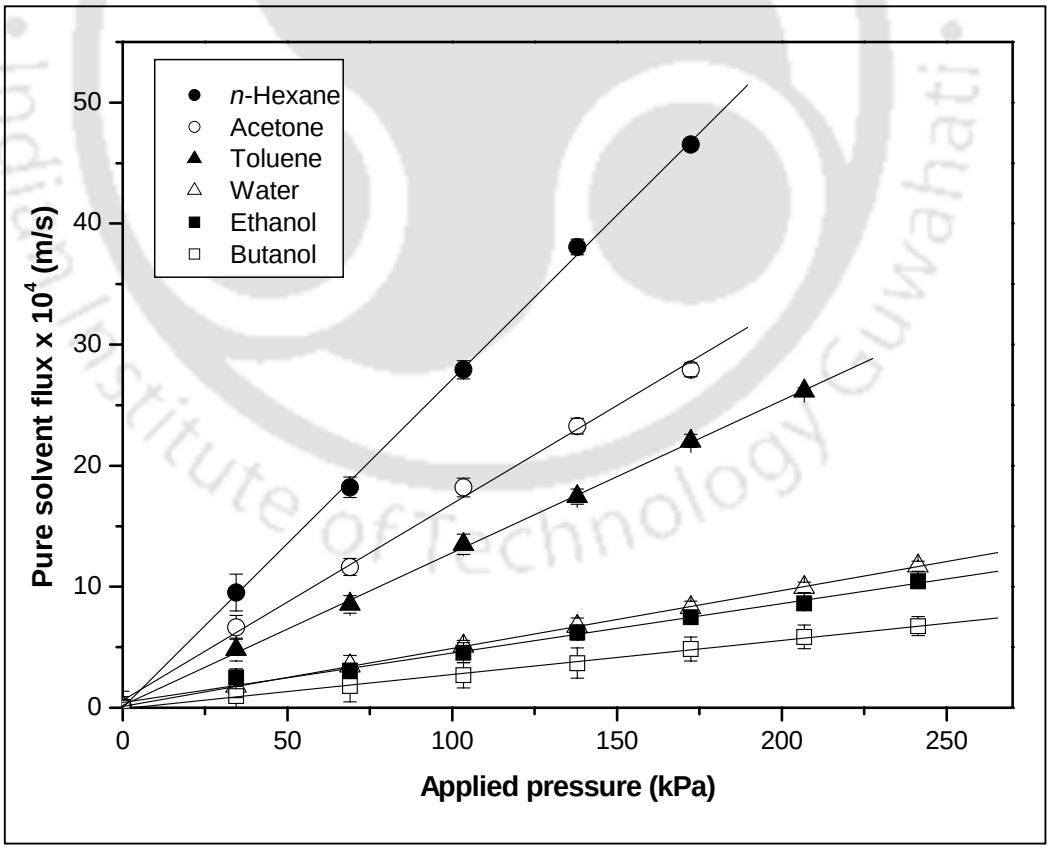

Fig. 3.20 Solvent flux of the optimized membrane support (sintered at 950°C).

Permeation experiments were started with butanol and ended with *n*-hexane. While changing the solvents from one to other, the cell was loaded and flushed with the next solvent (~ 100 ml). In all the cases, the solvent flux increases linearly with the applied pressure which indicates that pressure difference is the only driving force for the permeation of solvents. When the transport mechanism obeys the viscous flow model, the flux versus pressure plot should be expressed as a straight line which coincides with the origin, irrespective of the types of feed solution (Darcy's law). It can be seen from Fig. 3.20 that the solvent flux increases with decreasing viscosity of the solvent indicating that the viscosity is a main factor which controls the transport of solvent through the support.

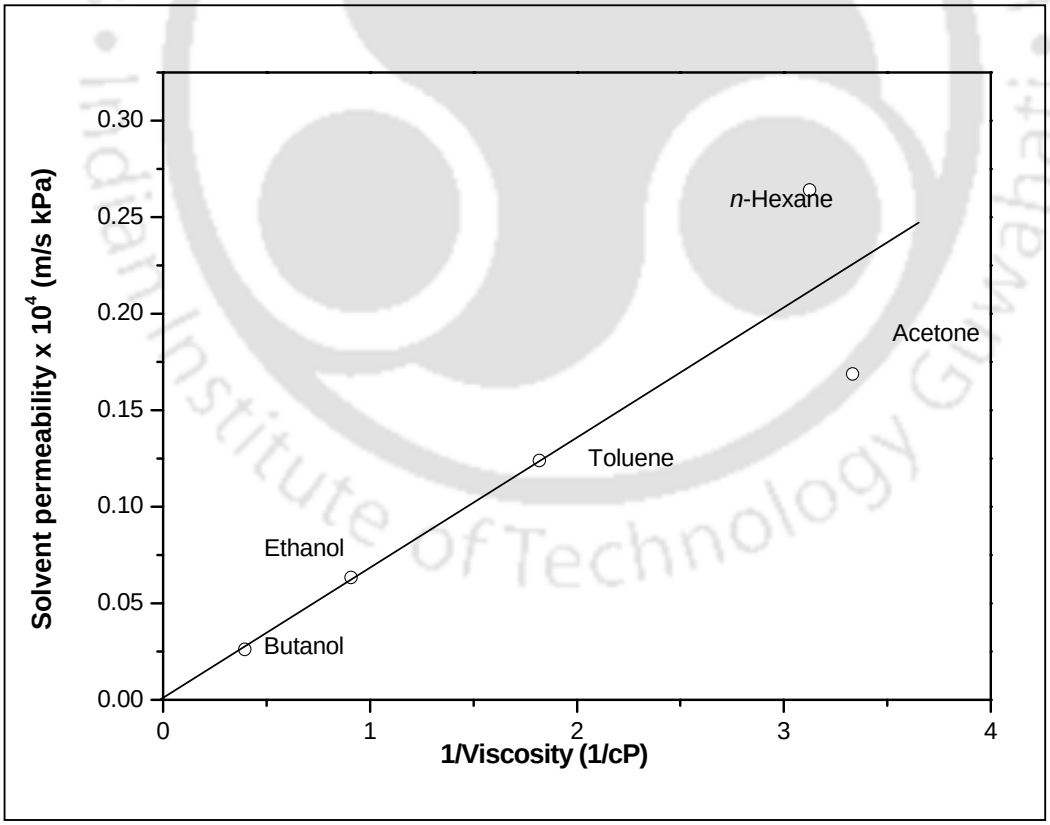

Fig. 3.21 Variation of solvent permeability of 950°C sintered membrane support.

Figure 3.21 validates the above comments showing a good correlation between the solvent permeability and the inverse of the solvent viscosity. It is observed that the non-polar solvents (*n*-hexane, toluene) show higher permeability than the polar solvents. The permeability of *n*-hexane is ten times greater than butanol while the permeability of water is two times greater than butanol. It confirms that the ceramic supports reported in this work are hydrophobic in nature. If the viscosity of the solvent is only the controlling factor then the flux of *n*-hexane and acetone would be identical because of identical viscosities. However, it is evident from the Fig. 3.20 and 3.21 that the flux of *n*-hexane and acetone are dramatically different. This implies that the support-solvent interactions also influence the solvent permeability in addition to viscosity (Bhanushali *et al.,* 2001; Chowdhury *et al.,* 2003). It is reported in the literature (Machado *et al.,* 1999) that the solvent interactions can be expected to vary with changes in solvent properties such as surface tension, di-electric constant and molecular size.

In general, the polarity of the solvent also plays an important role i.e increasing the polarity of the solvent decreases the solvent flux for hydrophobic membranes because polarity of organic solvents is strongly related with surface tension (Machado *et al.,* 1999). Hexane has a lower surface tension (17.9 mN/m) than acetone (23.3 mN/m) that causes it to penetrate faster through the hydrophobic support. Bhanushali *et al.,* (2001) have also shown that the surface tension of solvents is inversely proportional to flux for hydrophobic membranes. Based on these results, it is clear that the solvent flux of the hydrophobic support is mainly influenced by applied pressure, solvent viscosity and interactions of the solvent with support. Similar observations were also reported in the literature for α-alumina and other types of hydrophobic membrane (Machado *et al.,* 1999; Bhanushali *et al.,* 2001; Guizard *et al.,* 2002; Chowdhury *et*

al., 2003). The weight of the dry support before and after each solvent permeation studies has been checked and no weight loss is observed after the permeation studies. This implies that the support is very stable in all the studied solvents.

3.4 COST ANALYSIS

Although ceramic membranes have good chemical, mechanical and thermal properties over polymeric membranes, their usage in industrial application is limited due to its high cost. Cost of conventional polymeric membrane is around 20-200 $/m^2 (Bhide and Stern 1991). Generally, the cost of the ceramic membrane is 3-5 times higher than the polymeric membranes (Garmash *et al.,* 1995). The cost of the ceramic membranes is projected around 500-1000 $/m^2 (Cheryan 1998; Koros and Mahajan 2000). The high cost of ceramic membranes is compensated by its higher permeability and longer lifetime, which reduces the operating and maintenance cost.

The cost of the fabricated membrane support is estimated based on the raw materials used in this work. The projected cost of the fabricated membrane support is presented in Table 3.3. The estimated cost is found to be Rs. 480/m^2 (10 $/m^2). Including the pumping cost, maintenance cost, cleaning and replacement cost, labour cost etc., for the above support, the cost of the inorganic membrane may reach a value, which would be closer to the value of polymeric membrane (Cheryan 1998). The reported value of the membrane cost is conceptual in nature and may vary significantly depending on the above cost factors. However, permeability and mechanical strength data obtained in this work indicates a long time performance, which in turn may reduce the above cost factors. The result of cost evaluation indicates that the fabricated support is of low cost than that of alumina and zirconia supports based on the raw materials cost and sintering temperature used in this work.

Table 3.3 Cost analysis of the fabricated support based on unit cost of raw materials

Raw material	**Unit price (Rs./kg)**	**Amount of raw materials used for the fabrication of one membrane support (kg)**	**Cost estimated for the fabrication of one membrane support (Rs.)**
Kaolin	6.00	4.335×10^{-3}	0.02601
Ball Clay	3.00	5.274×10^{-3}	0.015822
Feldspar	4.00	1.68×10^{-3}	0.00672
Quartz	10.00	7.977×10^{-3}	0.07977
Pyrophyllite	5.00	4.419×10^{-3}	0.022095
Calcium carbonate	240.00	5.142×10^{-3}	1.23408
Raw materials cost for one membrane support fabrication			1.3844
Cost of one ceramic membrane support of 4 mm thickness and 63 mm diameter (rounded value)			**1.50/support**
Estimated raw materials cost per unit area of the fabricated membrane support			**480/m^2**

3.5 SUMMARY

Porous ceramic membrane supports have been successfully prepared by uniaxial compaction method using low cost clays as raw materials. The support is sintered at different temperature (850 to1000°C) and analyzed with various characterization techniques to find an optimum membrane support. Initial analysis on the clays for the particle size distribution suggests that the particle diameter between 5 and 10 μm, which is suitable for macroporous membrane supports. The XRD and SEM analysis of the clays confirms that the clays are matching with the corresponding JCPDS files and mostly containing silica and alumina as well as trace amounts of other exchange ions, for example Ca. Thermal characterization confirms that the binder is completely removed at 720°C suggesting that the support must be sintered above this temperature

to get a binder free support and negligible weight above 820°C suggests that the minimum temperature for a good support might be 850°C. The porosity of the membrane supports sintered at different temperatures is ranging between 41 and 46%. The percentage shrinkage of the support is found to be 5.5% for the studied temperature. Thermal and XRD analysis inferred various reactions and phase transformations undergone during sintering and quartz is found to be the major phase in all the sintered supports. The pore size distribution based on image analysis showed a good unimodal distribution for 950 and 1000°C and bimodal distribution for 850 and 900°C sintered supports. The result of SEM analysis reveals that the average pore diameter of the supports increases with increase in the sintering temperature. All the supports showed good mechanical strength (> 20 MPa) and chemical stability (< 12% weight loss in acidic media and < 3% weight loss in basic media) for both acidic and basic media. The support sintered at 950°C is concluded as an optimum support for membrane applications due to its good mechanical strength (28 MPa) and uniform pore size distribution having an average pore diameter of 0.98 μm with a porosity of 44%. The conducted solvent permeation studies on the optimized support (950°C) showed that the support is hydrophobic in nature. Despite the use of simple fabrication method, lower sintering temperature and inexpensive raw materials, the excellent properties of the membrane supports substantiates that it could be effectively used for the development of composite membranes for industrial applications.

Chapter 4

EFFECT OF TiO_2 ADDITION ON THE PROPERTIES OF OPTIMIZED MEMBRANE SUPPORT AND ITS PERFORMANCE EVALUATION FOR THE SEPARATION OF OIL AND BOVINE SERUM ALBUMIN (BSA) FROM ITS SOLUTION

4.1 INTRODUCTION

The main objective of the work reported in this Chapter is to study the changes in the properties of the membrane supports (pore size, porosity, mechanical strength and pure water permeability) by the addition of titanium dioxide (TiO_2). The fabricated membrane supports are characterized with various analytical techniques and testing methods as reported in Chapter 3. In general, macroporous membrane supports are applied for various separation applications such as the separation of salt, dye, heavy metals, oil emulsion, protein etc., (Saffaj *et al.,* 2004b; Belouatek *et al.,* 2005; Ezzati *et al.,* 2005; Ding *et al.,* 2006; Erdem *et al.,* 2006; Saffaj *et al.,* 2006; Becht *et al.,* 2008). Few literature are available on the membrane separation for oil droplets from oil-in-water emulsion, however, separation of oil droplets having size less than 20 μm (oil concentrations below 100 ppm) is still a challenging task. So the fabricated

membrane supports are tested for the separation of oil at low concentration. Also an attempt is been made for the separation of bovine serum albumin (BSA) protein from its aqueous solution. For the better understanding of the rejection mechanism, a brief study on fouling of the membrane supports for oil-water system is also been carried out and discussed in this Chapter.

4.2 MATERIALS AND METHODS

The raw materials (kaolin, ball clay, feldspar, pyrophyllite and quartz) were collected from Kanpur, India. Calcium carbonate, titanium dioxide, HCl, NaOH, BSA and Poly vinyl alcohol (PVA, M.W. 72000) were procured from Merck India Ltd. Crude oil was collected from Guwahati Refinery, Indian Oil Corporation Limited (IOCL), India and oil-in-water emulsions were prepared without any further treatment of crude oil. Water used in this work was collected from Millipore system.

4.2.1 Fabrication of membrane supports

The composition of the clay powders used for the fabrication of the three membrane supports is given in Table 4.1. The fabrication procedure is schematically represented in Chapter 3 (Fig. 3.1). 3g and 6g of TiO_2 were added by removing an equal amount of $CaCO_3$ from porous membrane support composition (fabricated in Chapter 3) to form the new membrane supports. The membrane supports were fabricated by uniaxial pressing method and sintered at 950°C. The initial optimized membrane support (as detailed in Chapter 3) was named as support-I and the other two membrane supports prepared with 3g and 6g TiO_2 loading were named as 3G and 6G supports, respectively.

Table 4.1 Raw materials composition of the membrane supports

Raw materials	Support-I (wt %)	3G support (wt %)	6G support (wt %)
Kaolin	14.5	14.5	14.5
Ball Clay	17.6	17.6	17.6
Feldspar	05.6	05.6	05.6
Quartz	26.6	26.6	26.6
Pyrophyllite	14.7	14.7	14.7
Calcium carbonate	17.0	14.0	11.0
Titanium dioxide	------	03.0	06.0

4.2.2 Preparation of feed solutions for microfiltration experiments

Five different concentrations (50, 75, 100, 150 and 200 ppm) of oil-in-water emulsions were prepared using a sonication bath (Make: Elmasonic; Model: S30H). Stable oil-in-water emulsions were obtained by operating the sonication bath for 15-25 h at a temperature of 25°C and no surfactant was added due to the natural surfactants present in the crude oil that itself yield a highly stable emulsion. The completion of the emulsification process can be evidenced by the disappearance of the oily layer on the water surface. However, the stability of the emulsion was further confirmed by measuring the oil droplet size distribution and its absorbance wavelength (236 nm) at regular intervals using UV-visible spectrophotometer (Perkin-Elmer, model: Lambda 35, USA). The prepared emulsions were stable for 7-8 days. After that, a thin oil film on the water surface was formed indicating that the oil droplets were coalesced and formed unstable emulsion. Therefore, all separation performance experiments were carried out within 1 or 2 days and analyzed immediately to avoid any experimental errors. The standard deviation of the absorbance of each prepared samples varies within ± 0.102.

BSA samples were prepared by dissolving the appropriate amount of BSA in Millipore water. The pH of the freshly prepared solution was found to be 7.0. The prepared BSA solution was utilized within 6 h to minimize the aggregation or denaturation of protein during storage.

4.2.3 Characterization procedures

The membrane supports and clays were characterized under the same conditions as already reported in Chapter 3 (section 3.2.2). Nitrogen adsorption/desorption isotherms of the membrane supports were measured by the BET method at -196°C using Beckmen-Coulter surface area analyzer (SA^{TM} 3100 model). Prior to the N_2 adsorption/desorption analysis, the membrane supports (Diameter = 3 mm. and thickenss = 2 mm) were degassed at 150°C for 3 h. Rejection performances of the membrane supports for oil-in-water emulsion and BSA were carried out with the dead-end filtration setup (see Fig. 3.17, Chapter 3). The concentration of oil and BSA was determined using a standard calibration graph of absorbance versus concentration prepared with a UV-visible spectrophotometer (Perkin-Elmer, model:Lambda 35, USA) at the wavelength of 236 and 280 nm, respectively. The pH of the solution was measured using a calibrated pH meter (Eutech instruments, model: pH 510). The surface tension of the oil-water emulsion was estimated at 25°C with a GBX 3S tensiometer, with an accuracy of 0.01 mN/m. A platinum du Nuoy ring was used as the probe and standardized with Millipore water. The reported values were the average of at least three measurements and represent the equilibrium surface tension values. Three membrane supports of each composition were tested for all the permeation and separation experiments and the average value was reported.

4.3 RESULTS AND DISCUSSIONS

4.3.1 Characterization of raw materials

The particle size distribution of the commercial TiO_2 is analyzed and the result is depicted in Fig. 4.1. The volume average mean diameter of the TiO_2 is 1.826 μm. This indicates that the particle size of TiO_2 is smaller than that of other clays used in the fabrication of the membrane supports. Although the average particle size of TiO_2 is smaller, the similar span value (2.049) suggests that the uniform mixing can be achieved (Sarkar *et al.,* 2005; Aimable *et al.,* 2010). The particle size distribution of the three different membrane support clay mixtures is found to be in the range of 0.3 to 90 μm with an average particle size varying between 7.5-8.6 μm. This indicates uniform mixing of raw materials to accomplish a good macroporous membrane support.

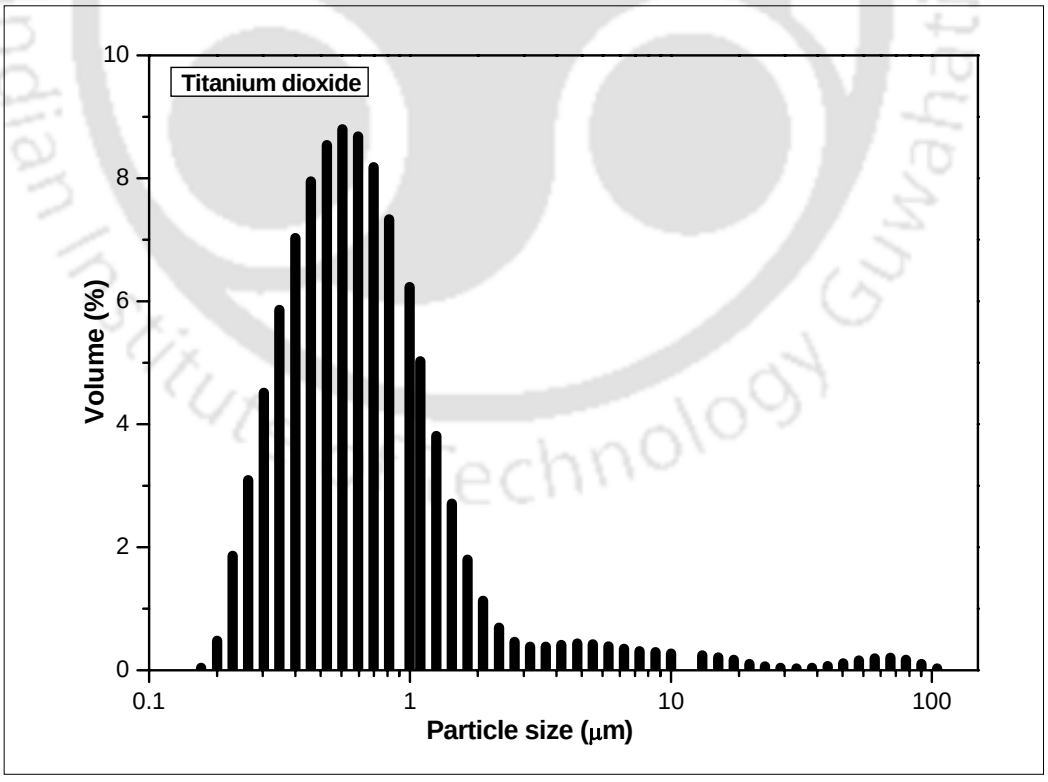

Fig. 4.1 Particle size distribution (PSD) of TiO_2 Powder.

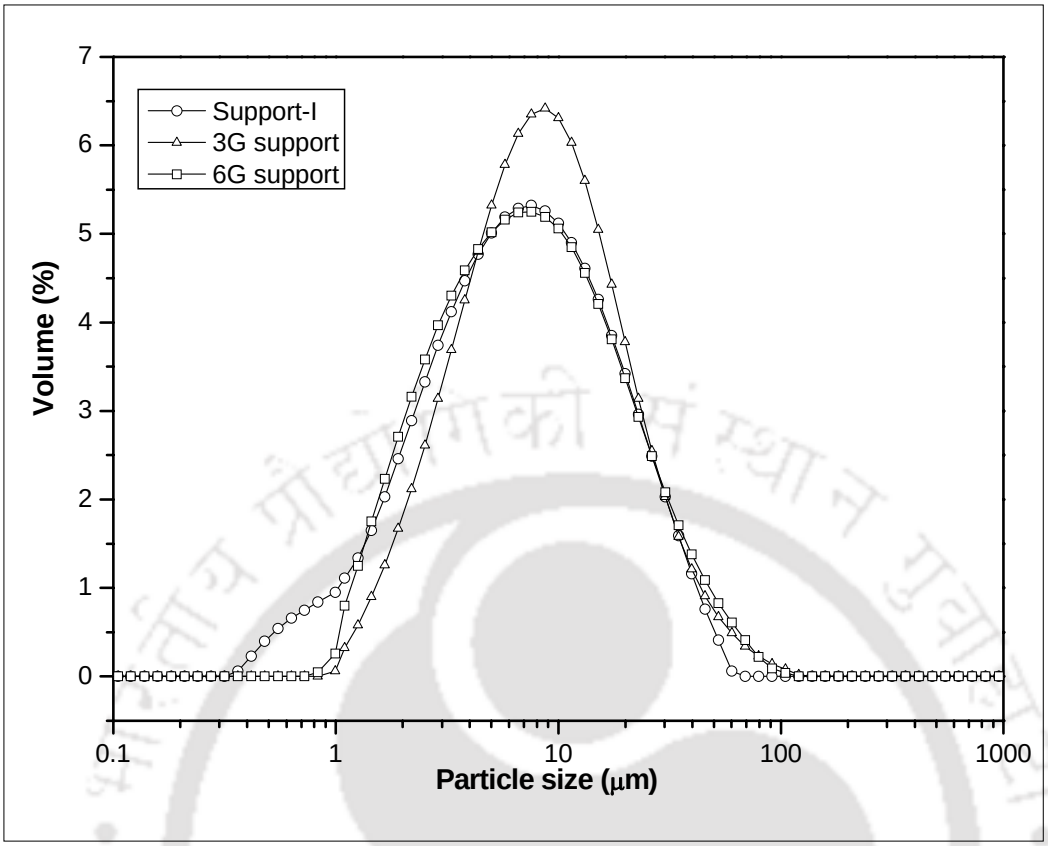

Fig. 4.2 Particle size distribution of the three different membrane support mixtures used for the membrane support fabrication.

From Fig. 4.2, it is clear that the addition of TiO_2 significantly shifts the particle size distribution towards right, which means that the particle size is higher than the support-I and the removal of calcium carbonate may have detrimental effect on the pore characteristics of the membrane supports.

Since the commercial TiO_2 is calcined at higher temperature, no weight loss could be occurred during the thermogravimetric analysis and the binder burnout mechanism follows the same trend for the three membrane supports. The binder is completely burnt off at 720°C for all the membrane supports as shown in Fig. 4.3.

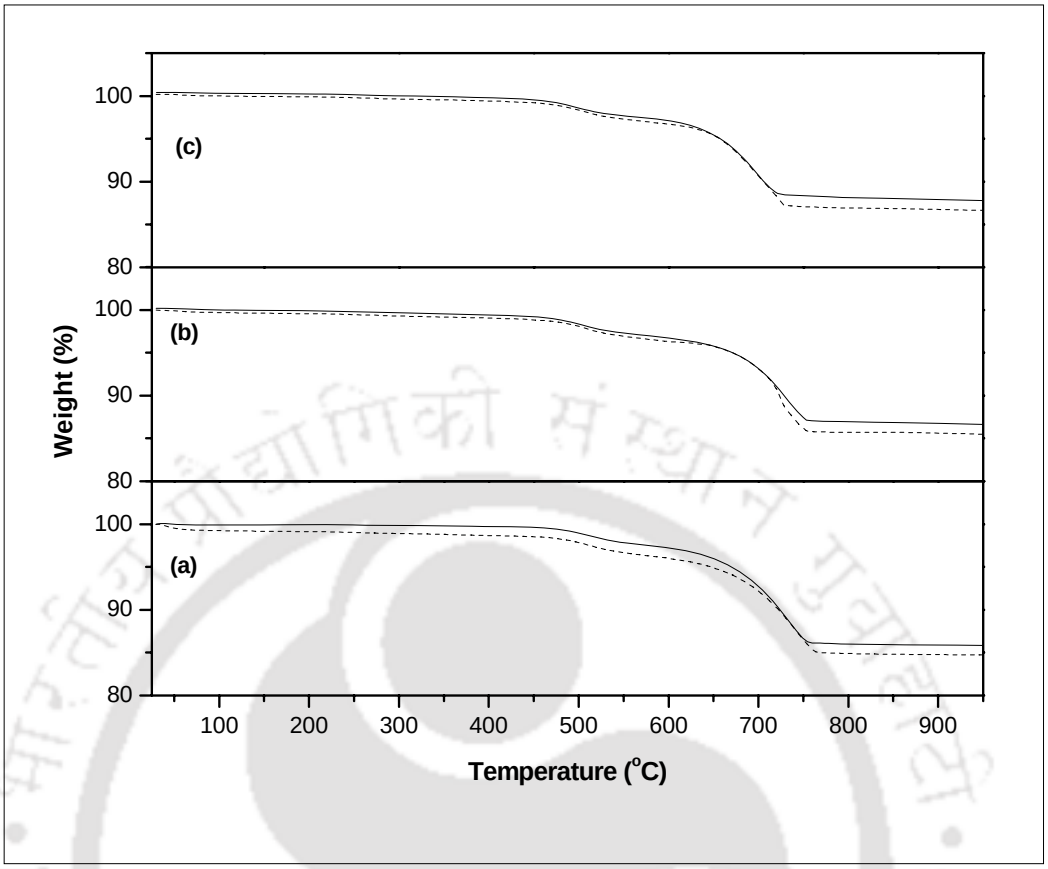

Fig. 4.3 Thermogravimetric analysis of the membrane supports with and without binder. (a) Support-I; (b) 3G support; (c) 6G support (Dashed line denotes with binder, solid line denotes without binder).

4.3.2 Characterization of the membrane supports

4.3.2.1 XRD analysis

XRD patterns of membrane supports before and after sintering are presented in Fig. 4.4. Although many phase transformation occurs during tsintering of membrane supports, the main phase transformation of the prepared membrane supports is the conversion of kaolin to mullite, which is evidenced by the disappearance of the peaks at 2θ value of 8.8, 9.6 and 12.6 degrees.

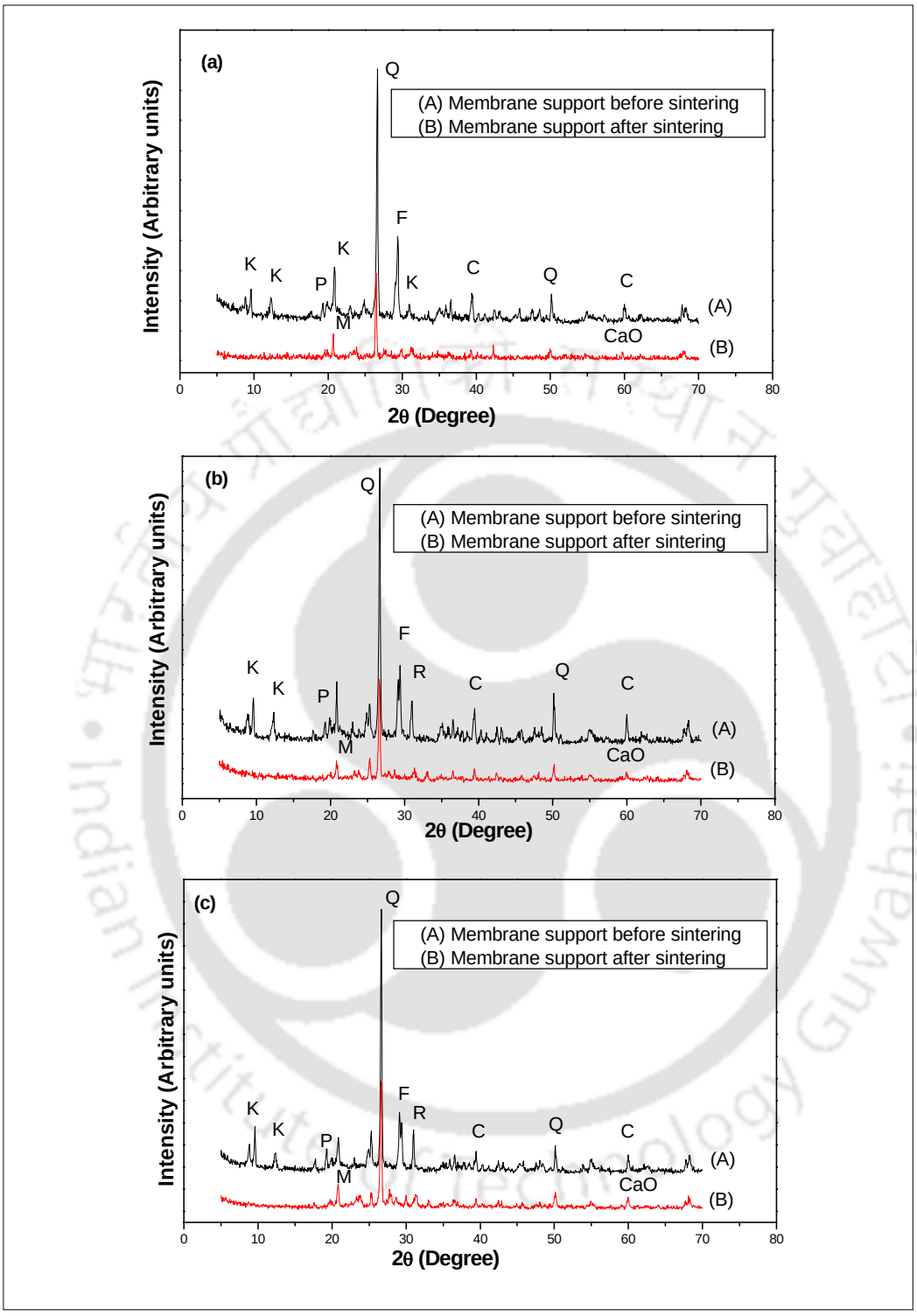

Fig. 4.4 XRD patterns of the membrane supports before and after sintering. (a) Support-I, (b) 3G support and (c) 6G support. C-Calcium carbonate; CaO-Calcium oxide; F- Feldspar; K-Kaolin, M-Mullite; P-Pyrophyllite; Q-Quartz; R-Rutile.

A rutile phase of TiO_2 is observed for the 3G and 6G supports before and after sintering. The background noise in the XRD pattern of the sintered supports suggests that there may be an existence of amorphous silica (Gualtieri *et al.,* 1995; Cultrone *et al.,* 2001). This amorphous silica reacts with the CaO to form new phases such as wollastonite ($CaSiO_3$) and anorthite ($CaO.Al_2O_3.2SiO_2$). This is also identified in the XRD analysis. Quartz remains as the most abundant phase for all the three membrane supports. Few unidentified weak peaks are also observed after sintering, which is attributed to other calcium aluminates or silicate.

Crystallite size of the membrane supports before and after sintering is calculated using Scherrer's formula and the results are presented in Table 4.2. The decrease in the crystallite size is found to be 8, 20 and 23% for the support-I, 3G and 6G supports, respectively. The results suggests that there may be a decrease in pore size and pore size distribution of 3G and 6G supports in comparison to support-I. Due to this reason, permeability is significantly influenced.

Table 4.2 Crystallite size obtained from the XRD analysis of the membrane supports

Membrane support	**Sintering condition**	**Full width at half maximum**	**2θ (Degree)**	**crystallite size (nm)**
Support-I	Before sintering	0.174	26.64	46.86
	After sintering	0.189	26.47	43.16
3G support	Before sintering	0.195	26.64	41.97
	After sintering	0.244	26.61	33.49
6G support	Before sintering	0.182	26.64	44.96
	After sintering	0.235	26.61	34.73

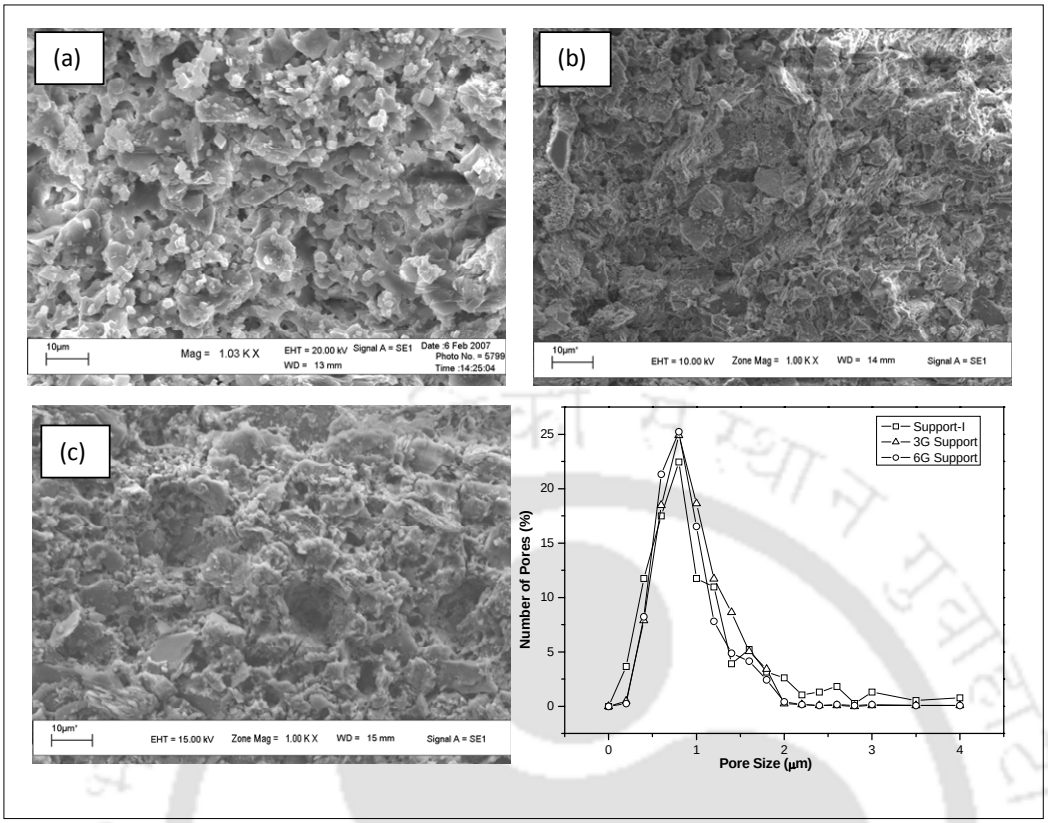

Fig. 4.5 Microstructure and pore size distribution analysis of the membrane supports. (a) Support-I; (b) 3G support; (c) 6G support; (d) Pore size distribution of the supports estimated using ImageJ open software.

4.3.2.2 SEM analysis

Surface morphology of the sintered membrane supports is presented in Fig. 4.5. The pore size distribution and average pore diameter of the sintered membrane support are estimated from SEM micrographs (see Fig. 4.5) using ImageJ software (open source software provided by National Institute of Health (NIH), weblink: http://rsbweb.nih.gov/ij/download.html) for pores having circularity greater than 0.8. The average pore diameter of the support-I, 3G and 6G supports is found to be 1.01, 1.06 and 0.97 μm, respectively.

4.3.2.3 Porosity and flexural strength analysis

Porosity of the membrane supports is calculated using the Archimedes' principle and is found to be 44, 38 and 36% for the support-I, 3G and 6G supports, respectively. The decrease in the porosity of the 3G and 6G supports is due to the decrease in the amount of the porosifier (i.e. $CaCO_3$). Similar results were reported in the literature for the increase in porosity with an increase in the amount of the porosifier (Falamaki *et al.,* 2004b; Bouzerara *et al.,* 2006; Boudaira *et al.,* 2009). Flexural strength for the support-I, 3G and 6G supports is found to be 28, 31 and 33 MPa, respectively. The increase in the flexural strength of the 3G and 6G supports might be due to the reduction in the pore size. Linear correspondence of the flexural strength for the three supports and a reduction in the porosity of the 3G and 6G supports validates the above point.

4.3.2.4 Water permeation experiments

Water permeation studies were carried out using a home-made filtration setup to estimate the mean pore size of the three membrane supports. Water flux of the membrane supports with applied pressure is presented in Fig. 4.6. The linear dependence of water flux on the pressure drop across membrane supports indicates Poiseuille flow through the pores and the average pore diameter calculated from the water permeation data using Hagen-Poiseuille equation is found to be 0.98, 0.93 and 0.83 μm for the support-I, 3G and 6G supports, respectively.

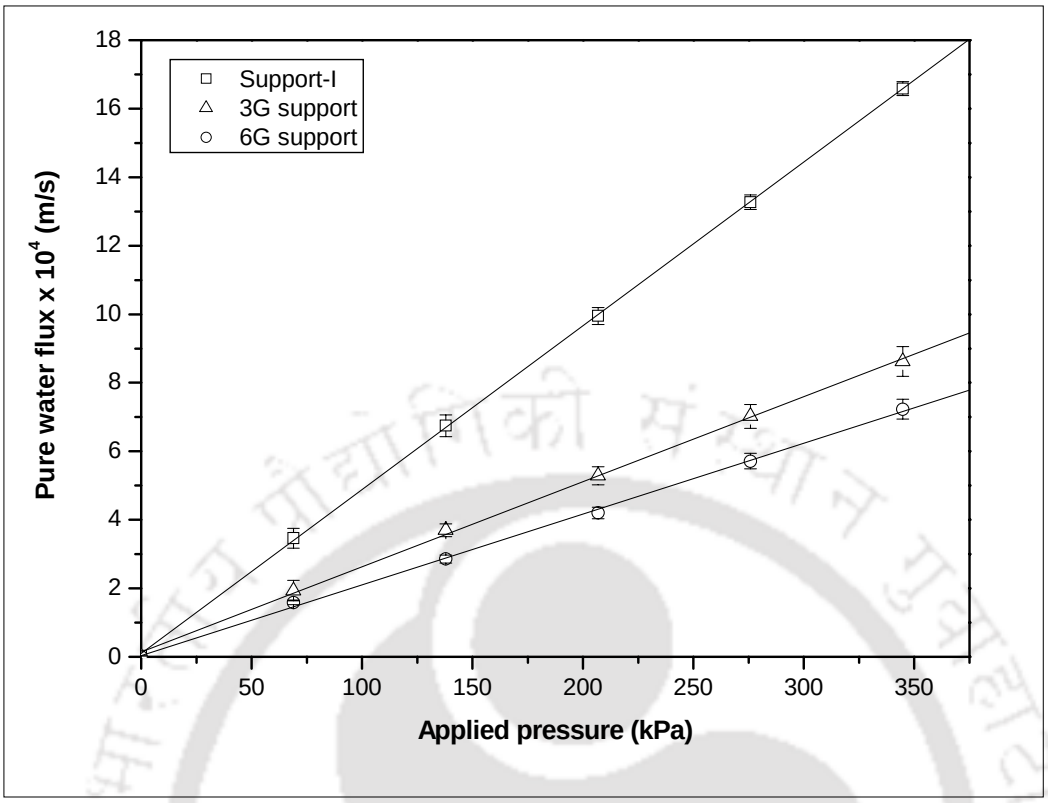

Fig. 4.6 Pure water flux of the membrane supports

4.3.2.5 Solvent permeation experiments

Polar (alcohols) and non-polar (alkanes) aliphatic solvents are chosen to study the nature of the membrane supports (hydrophobic/hydrophilic) as well as the resistance of the prepared membrane supports in these solvents. Solvent permeation experiments are performed in the following sequence: starting with methanol, ethanol, propanol, butanol, acetone, toluene, pentane, hexane and ended with heptane. While changing the solvents from one to other, the cell is loaded and flushed with 50 ml of the next solvent. The physical properties of the solvents used in this work are presented in Table 4.3.

Table 4.3 Physical properties of the solvents used in the permeation experiments

Solvent	Molar volume (cm^3/mol)	Viscosity (cP)	Density (g/cm^3)	Surface energy mN/m	Kinetic diameter (nm)	Molar volume /Viscosity (cm^3/mol cP)
Methanol	40.7	0.59	0.7917	22.6	0.38	69.0
Ethanol	58.5	1.20	0.7893	22.3	0.44	48.8
Propanol	76.9	2.25	0.7854	23.8	0.48	34.3
Butanol	91.5	2.95	0.810	24.6	0.50	31.0
Water	18.0	1.02	0.998	72.0	0.27	17.7
Acetone	74.0	0.30	0.792	23.3	0.63	247.0
Toluene	25.4	0.56	0.8669	28.0	0.59	184.4
Pentane	116.2	0.234	0.626	16.0	0.43	496.0
Hexane	131.6	0.32	0.659	17.9	0.45	411.3
Heptane	146.2	0.40	0.684	19.7	0.47	366.0

For all membrane supports, the flux increases linearly with the applied pressure for all solvents (Fig. 4.7 (a-c)) indicating that the pressure difference is the only driving force for the permeation of solvents. The linear fit for the flux versus applied pressure plot is greater than 0.9, irrespective of the types of the solvents. This reveals that the transport mechanism obeys the viscous flow model given by Darcy (Burggraaf and Cot 1996; Mulder 1997). From Fig. 4.7(a-c), one can clearly seen that the solvent flux increases with decreasing viscosity of the solvent indicating that the viscosity is a main factor that controls the transport of solvent through the membrane supports. Permeability of the three membrane supports are presented in Fig. 4.7 (d).

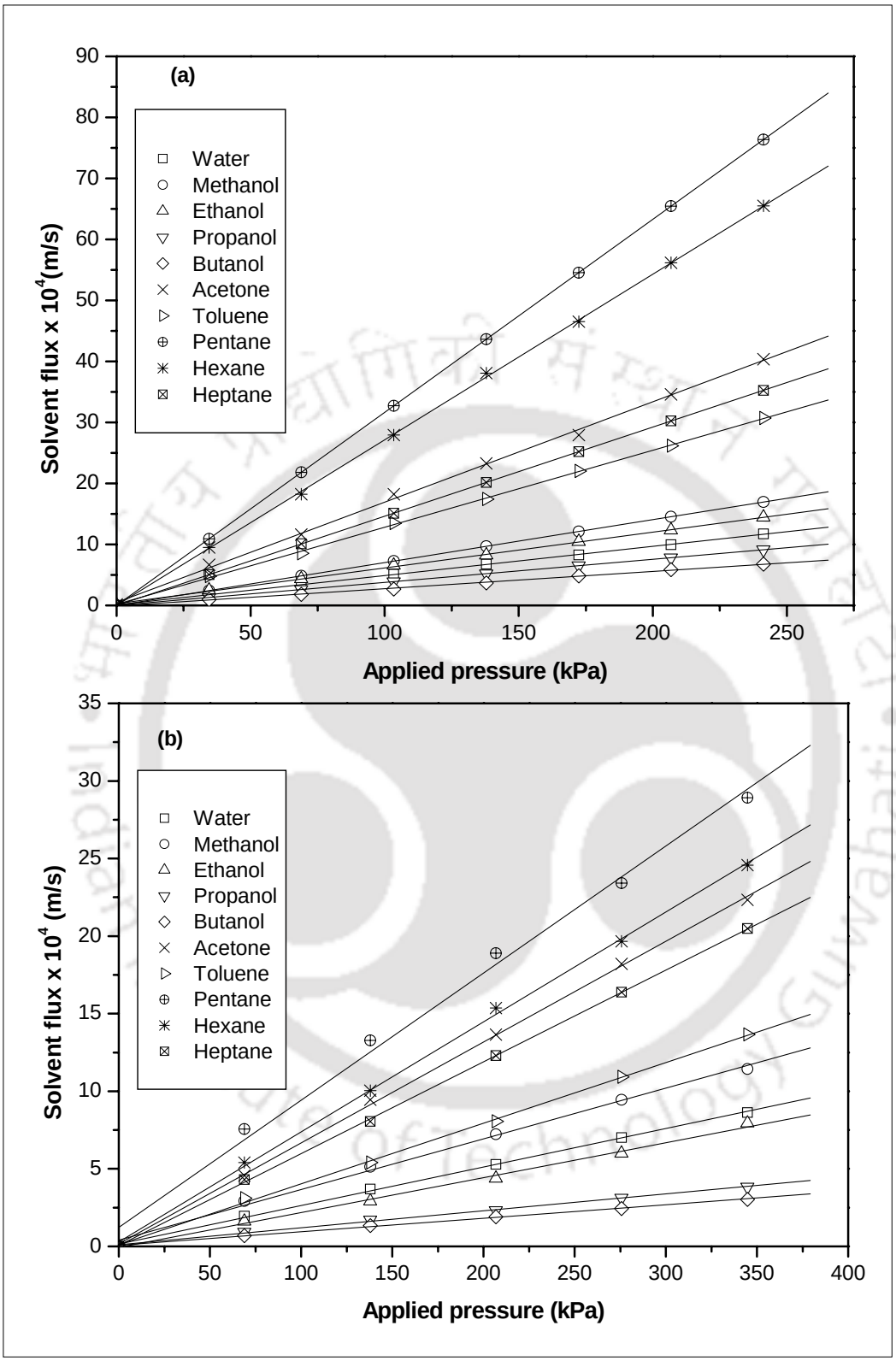

Fig. 4.7(a-b) Solvent flux of various solvents through the membrane supports.

(a) Support-I and (b) 3G support.

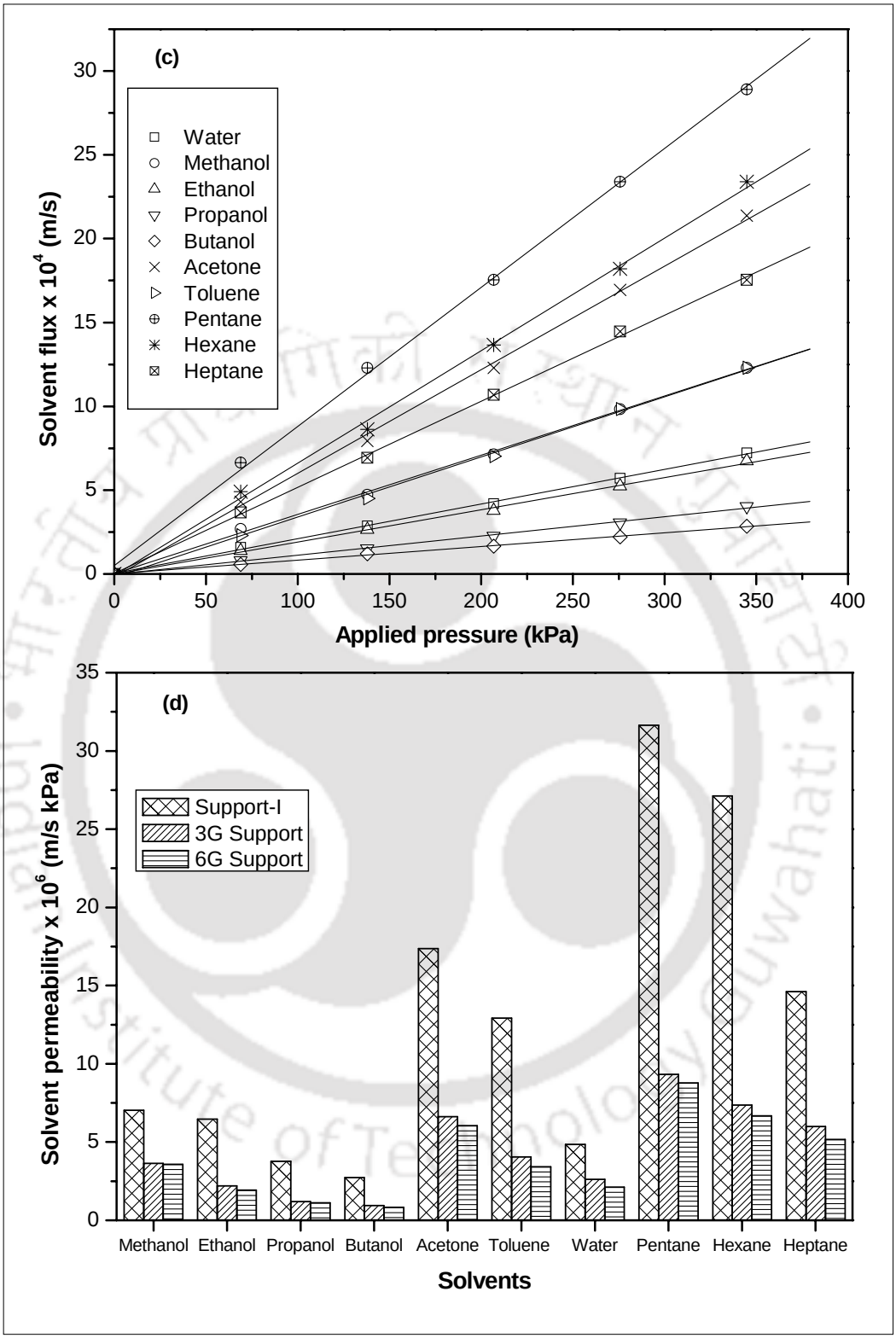

Fig. 4.7(c-d) Solvent flux of 6G support (4.7(c)) and permeability of the membrane supports for various solvents (4.7(d)).

A good correlation between the solvent permeability and the inverse of the solvent viscosity (except for acetone and toluene) validates the above comments (see Fig. 4.8). It is observed that nonpolar solvents (hexane, toluene) show higher permeability than polar solvents that confirms the membrane supports are hydrophobic in nature. If the viscosity of the solvent is the only controlling factor then the flux of hexane and acetone as well as methanol and toluene would be identical because of the identical viscosities. This implies that the support-solvent interactions must have significant influence on solvent permeability in addition to the viscosity (Bhanushali *et al.,* 2001; Chen *et al.,* 2010).

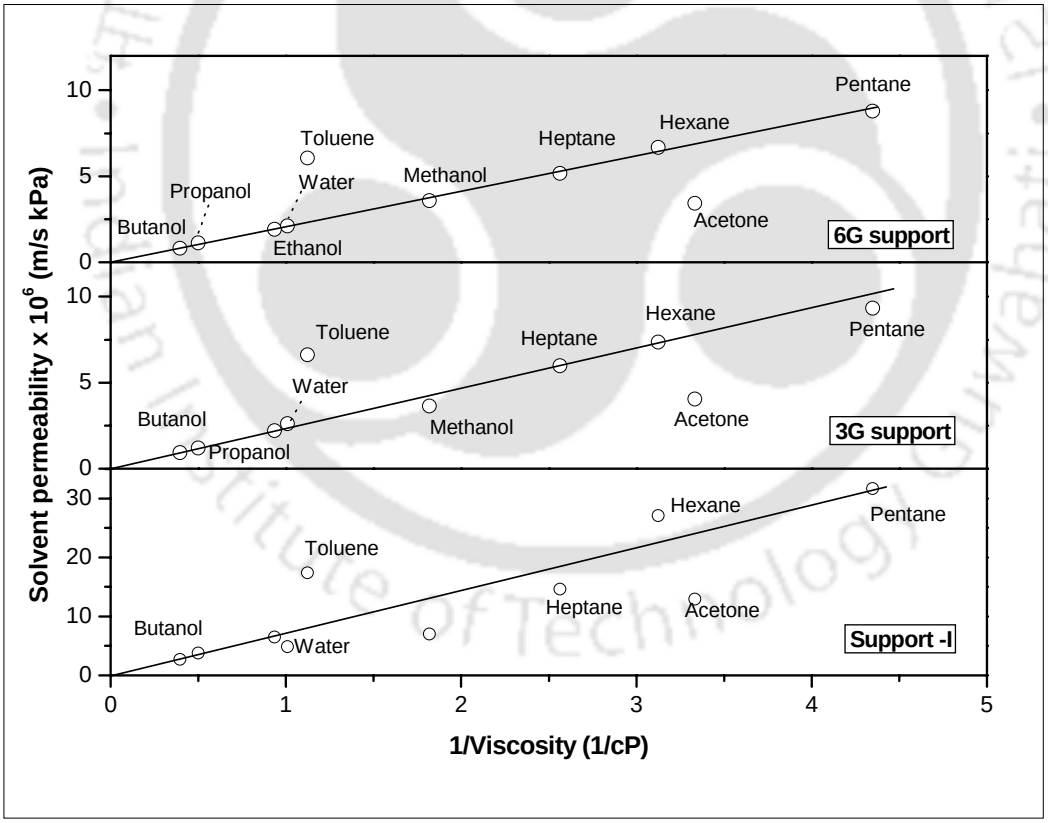

Fig. 4.8 Variation of the solvent permeabilities to its viscosity of the three different membrane supports.

In general, solvent interactions can be expected to vary with changes in solvent properties such as surface tension, and molecular size (Machado *et al.,* 1999; Bhanushali *et al.,* 2001; Chen *et al.,* 2010). In addition to the above parameters, polarity of the solvent also plays a vital role because it is strongly related with surface tension (Machado *et al.,* 1999). Increased solvent polarity results in decreased flux for hydrophobic membranes (Bhanushali *et al.,* 2001). Based on these results, it is clear that the solvent flux of hydrophobic membrane supports is mainly influenced by applied pressure, solvent viscosity and interactions of the solvents with membrane supports. Similar observations were also reported in literature for α-alumina and other types of hydrophobic membranes (Machado *et al.,* 1999; Guizard *et al.,* 2002; Chowdhury *et al.,* 2003; Chen *et al.,* 2010).

4.3.3 Separation of oil droplets from oil-in-water emulsion

Performance of the membrane supports for the separation of oil-in-water emulsion was tested with the permeation cell filled with 100 ml of the feed solution. At a fixed pressure, the first 20 ml of the collected permeate was discarded and the time required to collect the next 10 ml of permeate was noted down to calculate the permeate flux at that pressure. The observed rejection of the membrane support was calculated by the following equation

$$R = \frac{C_f - C_p}{C_f} \times 100 \qquad (4.1)$$

where, R is the observed rejection (%), C_f is the concentration of the feed solution (ppm) and C_p is the concentration of the permeate solution (ppm). After each experimental run, the membrane supports were cleaned with a detergent solution to obtain the same water flux of the membrane supports. The variation in pure water flux

of the membrane supports before and after cleaning was found to be negligible (< ±2%).

The performance of the membrane supports for rejecting the oil-in-water emulsion was performed at five different concentrations (50, 75, 100, 150 and 200 ppm) and applied pressure ranging between 69 and 345 kPa. The oil droplet size distribution of the feed solution having different concentration is obtained using particle size analyzer is presented in Fig. 4.9. The oil droplet diameter is ranging between 0.05 and 4 μm with a volume median diameter ($d_{0.5}$) ranging between 0.716 and 0.743 μm for oil concentrations of 50, 75 and 100 ppm solutions. A volume median diameter ($d_{0.5}$) ranging between 1.183 and 1.211 μm is observed for 150 and 200 ppm solutions. The volume median diameter of the oil droplet is higher than the pore diameter of the membrane supports suggesting a greater possibility for the rejection of oil droplets.

The rejection and permeate flux of the membrane supports for oil-in-water emulsion system are shown in Figs. 4.10-4.12. In general, the permeability depends on diameter of the pores and characteristics of the membrane supports. Therefore, larger support pore sizes provided higher permeabilities. The rejection increases with an increase in the concentration and decreases with an increase in the applied pressure. The increased rejection obtained at higher concentration for all the membrane supports is due to the increase in oil droplet size and droplet density. All the supports showed 90-99% rejection and the maximum rejection of the oil-in-water is in the following sequence: 6G support > 3G support > support-I. The rejection pattern with applied pressure follows similar trend for all the membrane supports. However, one can see the flux is more affected if the concentration of oil-in-water emulsion is increased.

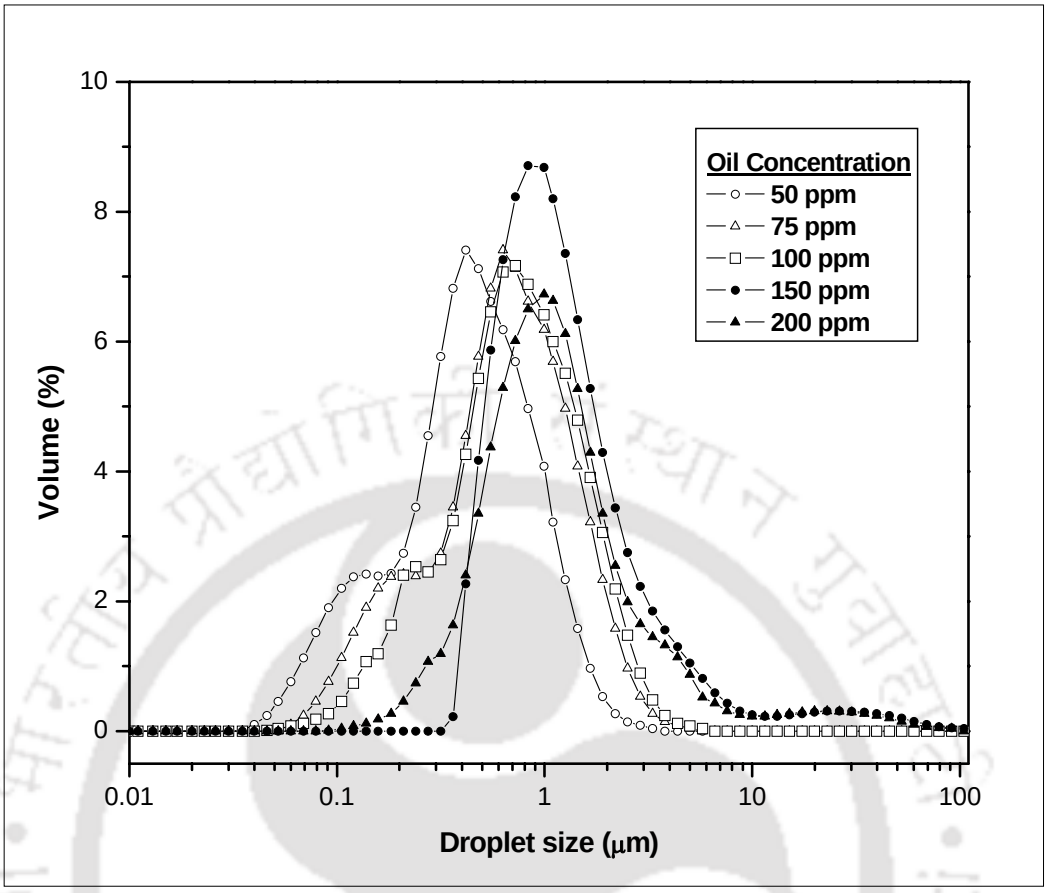

Fig. 4.9 Droplet size distribution of the oil-in-water emulsion.

Figs. 4.10-4.12 clearly indicate that the higher feed oil concentrations corresponds to greater flux reduction and rejection. Higher concentration of oil leads to coalescence of the oil droplets forming a bigger droplet that result in a higher rejection. The coalesced oil adheres on the surface of the membrane supports which causes fouling and this results in reduced flux. Similar types of results were reported in literature (Srijaroonrat *et al.,* 1999; Arnot *et al.,* 2000; Mohammadi *et al.,* 2004; Nandi *et al.,* 2009; Chakrabarty *et al.,* 2008).

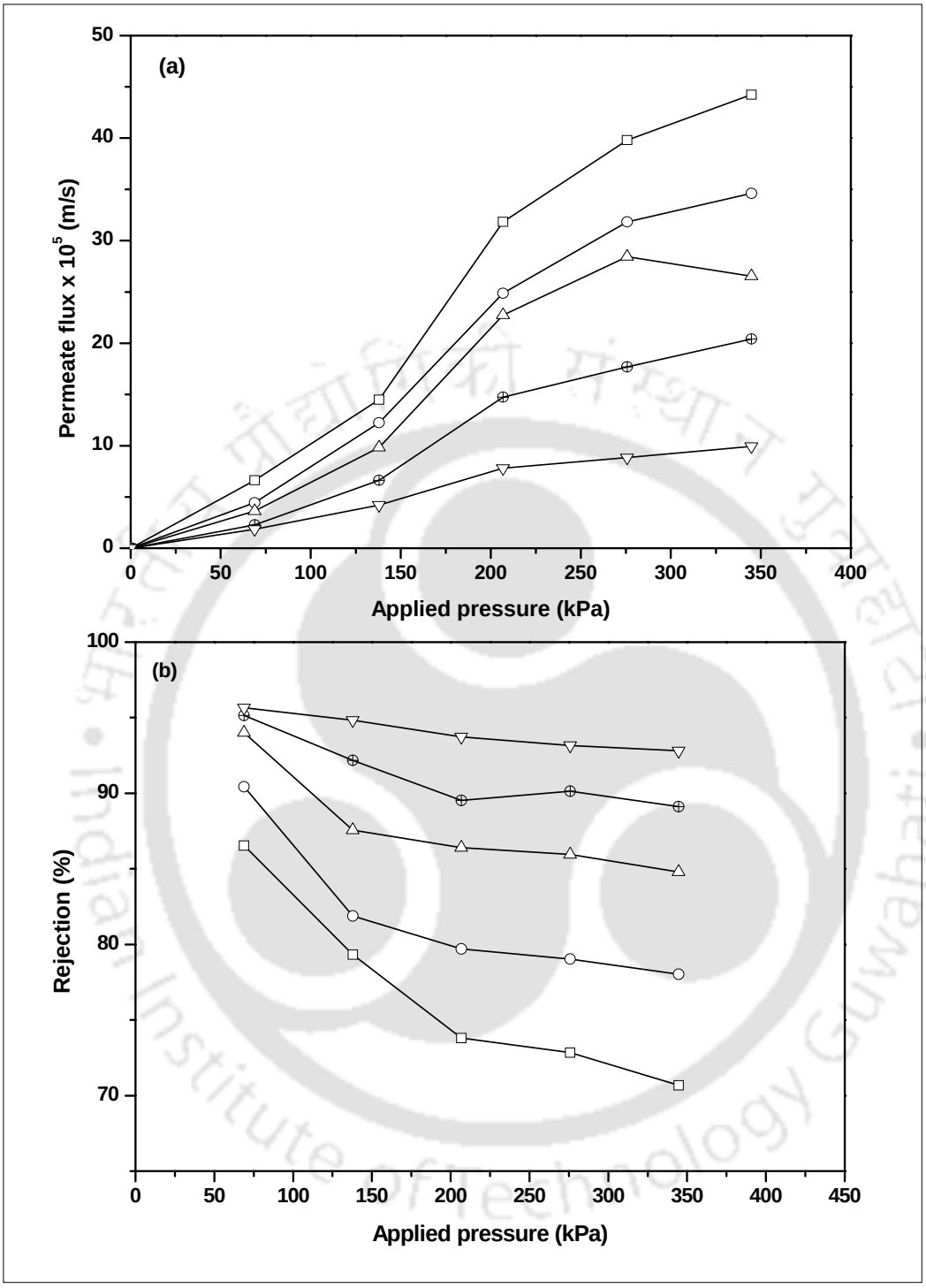

Fig. 4.10 Permeate flux and rejection performance of support-I for oil-in-water emulsion system. (a) Permeate flux and (b) Rejection.

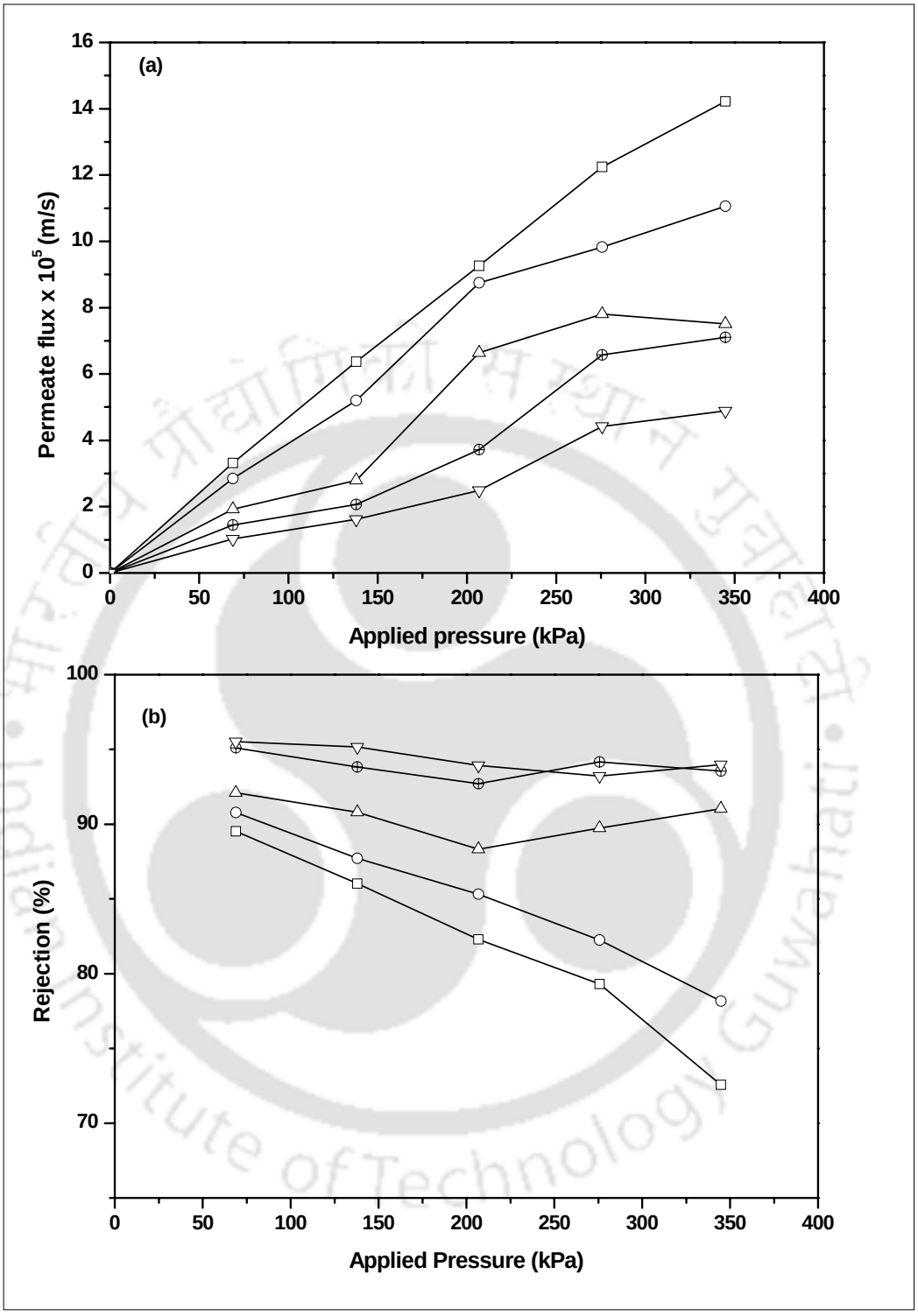

Fig. 4.11 Permeate flux and rejection performance of 3G support for oil-in-water emulsion system. (a) Permeate flux and (b) Rejection.

—□— 50 ppm, —○— 75ppm, —△— 100 ppm, —⊕— 150 ppm, —▽— 200 ppm

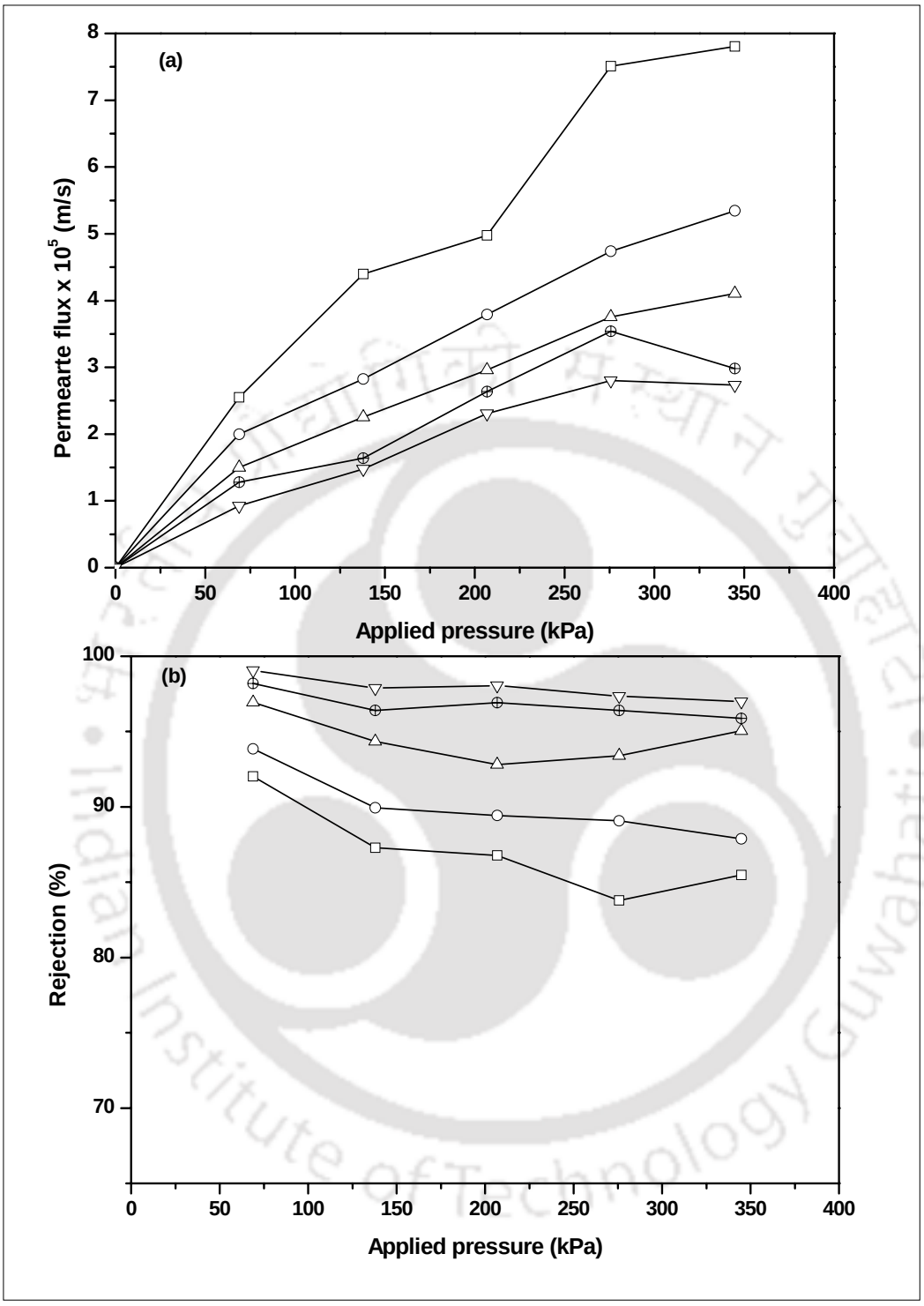

Fig. 4.12 Permeate flux and rejection performance of 6G support for oil-in-water emulsion system. (a) Permeate flux and (b) Rejection.

At higher pressures, the oil droplet will deform and pass through the small pores and results in decreased rejection. Sometimes the rejection of oil is found to be higher at higher pressures. This may be due to the formation of large oil droplets. The reduction in the flux is due to the pore blocking mechanism of oil with the membrane supports. To understand the pore blocking mechanism, studies were carried out for the oil concentrations of 100 and 200 ppm at 69 kPa for all the membrane supports and the permeate is collected continuously for 30 min .

In general, the resistance to permeate flow in microfiltration occurs due to two major factors. The first factor is due to the pores partially occupied by small particles/molecules, which is related to membrane properties. The second one is due to the formation of a fouling layer on the membrane surface, which is related to the operating conditions such as transmembrane pressure difference and feed concentration (Srijaroonrat *et al.,* 1999; Cumming *et al.,* 2000; Pan *et al.,* 2007). The membrane fouling in dead-end filtration at a constant pressure has been generally explained by the Hermia's model. The reformatted form of Hermia's model is given by the following formula (Arnot *et al.,* 2000; Pan *et al.,* 2007).

$$J = J_0[1 + k(2-n)(AJ_0)^{2-n} t]^{1/(n-2)} \qquad (4.2)$$

where, J_0 and J represents the permeate flux at time t = 0 and t = t, respectively. The parameter, n, represents different fouling mechanisms. The values of n corresponds to 1.5, 1.0 and 0 in the above equation represents the standard pore fouling, the intermediate pore fouling and the cake filtration models, respectively. The obtained experimental permeate flux was fitted with the above models (linearized form).

The plots of flux versus time are presented in Fig. 4.13 and the obtained parameter values are given in Table 4.4.

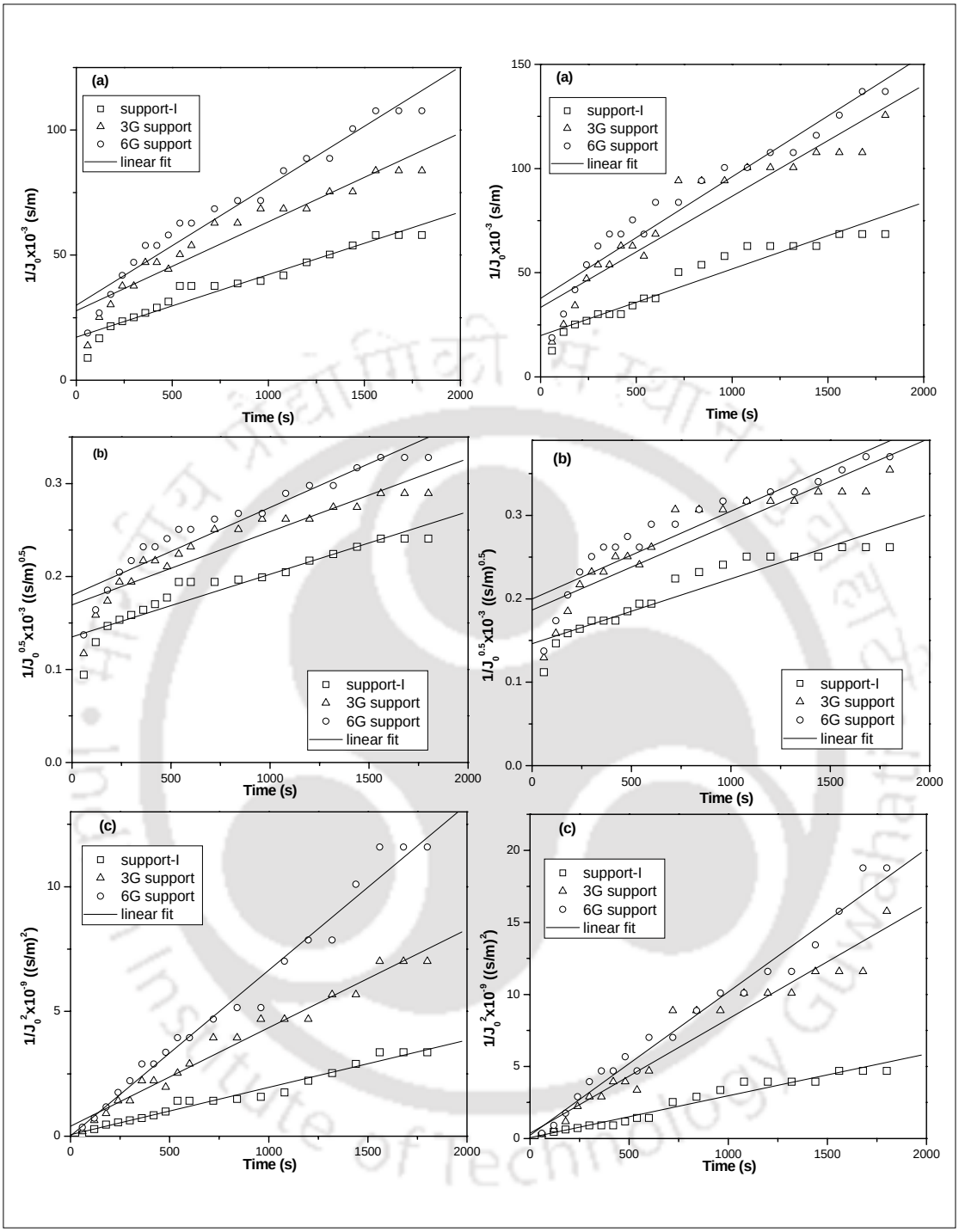

Fig. 4.13 Linear plot of flux versus time for different pore blocking models. (a) Intermediate pore fouling (b) Standard pore fouling and (c) Cake filtration. (left- 100 ppm and right – 200 ppm of initial oil concentration).

Table 4.4 Parameters of the pore fouling models fitted with linear regression for the oil-in-water feed concentration of 200 ppm at 69 kPa. (The values in the parenthesis indicate the parameter values at 100 ppm)

Model	Parameter Value	support-I	3G support	6G support
Intermediate pore fouling model	Slope (K_i) (1/m)	31.96 (25.04)	53.38 (35.57)	58.39 (47.71)
	Intercept ($1/J_0$) (s/m)	1.98×10^4 (1.72×10^4)	3.33×10^4 (2.77×10^4)	3.77×10^4 (2.99×10^4)
	R^2	0.9262 (0.9402)	0.8876 (0.9147)	0.9335 (0.9565)
Standard pore fouling model	Slope (K_s) $(1/m.s)^{0.5}$	0.078 (0.067)	0.103 (0.079)	0.105 (0.094)
	Intercept $(1/J_0^{0.5})$ $(s/m)^{0.5}$	146.12 (135.07)	186.54 (169.46)	199.72 (179.81)
	R^2	0.8883 (0.8769)	0.8248 (0.8441)	0.8586 (0.9027)
Cake filtration model	Slope (K_c) (s/m^2)	2.91×10^6 (1.89×10^6)	7.94×10^6 (3.94×10^6)	9.94×10^6 (6.64×10^6)
	Intercept $(1/J_0^2)$ $(s/m)^2$	0.058×10^9 (0.062×10^9)	0.360×10^9 (0.401×10^9)	0.230×10^9 (0.110×10^9)
	R^2	0.9561 (0.9723)	0.9378 (0.9756)	0.9769 (0.9802)

The regression coefficients of the experimental data (see Table 4.4) indicate that the cake filtration is the dominating mechanism for fouling. However, it is very difficult to identify the region at which it switches from one dominant fouling mechanism to another.

In general, hydrophobic membrane supports have a greater tendency to foul than that of hydrophilic membrane supports (Srijaroonrat *et al.,* 1999; Mohammadi *et al.,* 2004; Zhou *et al.,* 2010). Since, all prepared membrane supports are hydrophobic in nature, they have a greater tendency to foul. However, one can reduce the fouling by operating at a pressure lesser than the capillary pressure of oil droplets (Srijaroonrat *et al.,* 1999).

The surface tension of the oil-in-water emulsion is obtained using tensiometer (ranging between 54.25 and 57.25 mN/m) and the estimated capillary pressure of oil droplets is ranging between 110 and 130 kPa. The above results indicate that the employment of applied pressure greater than 130 kPa is probably unwise for separation of oil-in-water emulsion in the dead-end experiments and this may lead to poor flux due to pore blocking.

The permeability and percentage rejection of the prepared membrane supports compared with other commercial and laboratory made membranes are presented in Table 4.5. From Table 4.5, it is clear that the fabricated membrane supports have the potential of removing the oil from oil-water solution and the obtained results are comparable with other membranes.

4.3.4 Separation of BSA from its aqueous solution

The BSA separation performance of the membrane supports was carried out for the concentrations ranging between 100 and 3000 ppm at 207 kPa. The effect of pressure on the separation of BSA was performed at the feed concentration of 500 ppm by applying pressure ranging between 69 and 345 kPa. The rejection performance of BSA with respect to applied pressure and concentration on the membrane supports are presented in Fig. 4.14 and 4.15, respectively.

Table 4.5 Comparison of permeability and rejection of other membranes with the fabricated membrane supports

Membrane/ support Material	Mean pore size	Feed Concentration (ppm)	Permeability (m/s kPa)	Rejection (%)	Reference
γ-Al_2O_3/ α-Al_2O_3	10 nm	5000	5×10^{-8}	99.8	Yang *et al.*, (1998)
α-Al_2O_3/ α-Al_2O_3	0.2 µm	5000	6.1×10^{-8}	99.9	Yang *et al.*, (1998)
α-Al_2O_3/ α-Al_2O_3	1.0 µm	5000	7.5×10^{-8}	94.3	Yang *et al.*, (1998)
ZrO_2/ α-Al_2O_3	0.2 µm	5000	25.8×10^{-8}	99.8	Yang *et al.*, (1998)
Poly(vinylidene)flouride (PVDF)	0.10 µm 0.34 µm 0.52 µm	10000	9.06×10^{-8} 14.5×10^{-8} 6.58×10^{-8}	77.0	Kong and Li (1999)
ZrO_2	50 nm	1000	68.9×10^{-8}	-----	Srijaroonrat *et al.*, (1999)
ZrO_2	100 nm	1000	97.9×10^{-8}	------	Srijaroonrat *et al.*, (1999)
α-Al_2O_3	500 nm	1000	80.8×10^{-8}	------	Srijaroonrat *et al.*, (1999)
NaA zeolite/ α-Al_2O_3	1.2 µm	100	16.7×10^{-8}	98.8	Cui *et al.*, (2008)
NaA zeolite/ α-Al_2O_3	0.4 µm	100	1.38×10^{-8}	99.4	Cui *et al.*, (2008)
α-Al_2O_3	2.1 µm	100	13.9×10^{-8}	55.0	Cui *et al.*, (2008)
Al_2O_3	0.16 µm	600 to 11000	1.42×10^{-8}	98.0	Cui *et al.*, (2008)
α-Al_2O_3	0.1 µm	150	88.6×10^{-8}	61.4	Ebrahimi *et al.*, (2010)
TiO_2/TiO_2	1000 Da	565	17.7×10^{-8}	99.5	Ebrahimi *et al.*, (2010)
Support-I	0.98 µm	50	96.2×10^{-8}	86.5	Present work
3G support	0.93 µm	50	48.1×10^{-8}	89.5	Present work
6G support	0.83 µm	50	37.0×10^{-8}	92.0	Present work

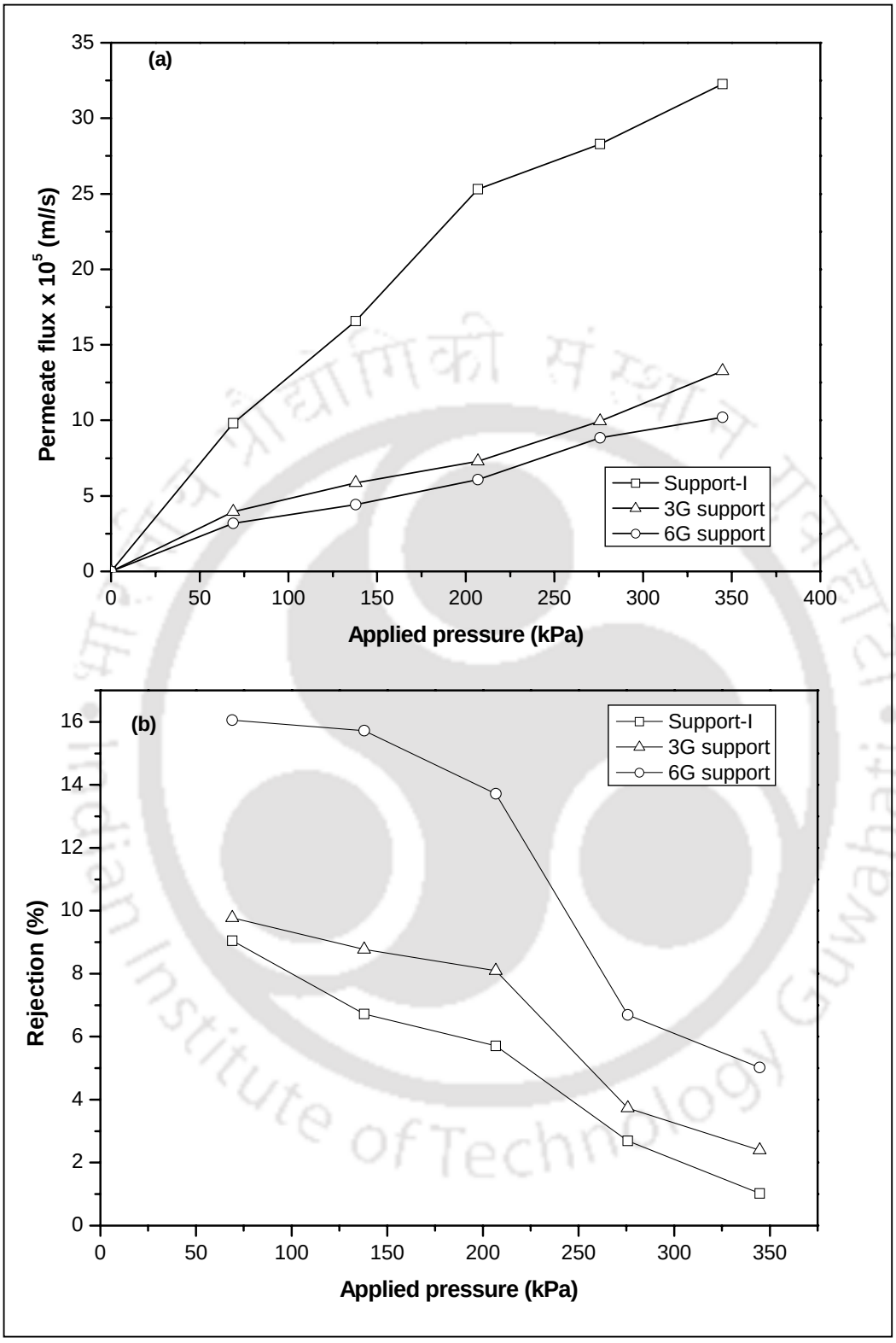

Fig. 4.14 Effect of applied pressure on BSA separation through the membrane supports. (a) Permeate flux and (b) Rejection. (Concentration = 500 ppm; pH = 6.98).

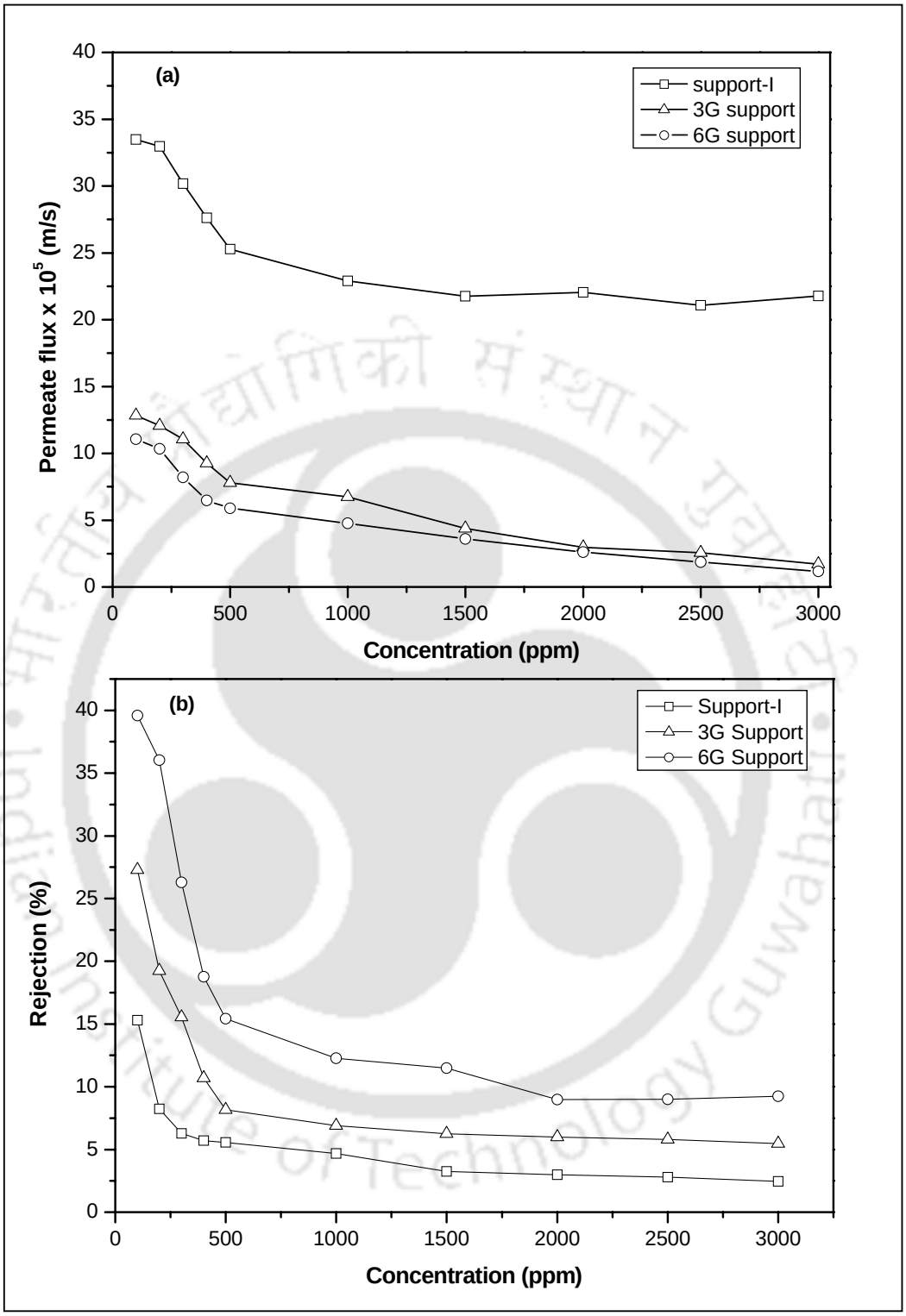

Fig. 4.15 Effect of Concentration on BSA separation through the membrane supports. (a) Permeate flux and (b) Rejection. (Concentration = 500 ppm; pH = 6.98).

The observed rejection is found to reduce with an increase in BSA concentration. Also, rejection remained almost constant for concentrations above 500 ppm for all membrane supports. BSA is a globular prolate ellipsoid of dimensions 140×40×40 nm and has a molecular weight of 67 kDa. The approximate size of the BSA is calculated using the equation given in literatures (Ding *et al.,* 2006; Becht *et al.,* 2008) and is found to be 11 nm in diameter. Since the diameter of BSA is lower than the average diameter of the pore, the observed rejection is very low and doesn't show any further rejection above 500 ppm of BSA solution.

The observed rejection is found to be decreased with an increase in the applied pressure. However, a considerable amount of BSA rejection is obtained for all membrane supports. This may be due to the presence of nanopores. To confirm this, BET isotherm was carried out for each membrane support and the pore size distribution is reported in Fig. 4.16. It clearly indicates the presence of nanopores in the membrane support, which might have an effect on BSA rejection. All membrane supports illustrate a type-II adsorption/desorption curve having H1 hysteresis suggesting the presence of nanopores and open porosity with a cylindrical geometry (Uhlhorn *et al.,* 1992; Leite *et al.,* 2003). It is to be noted that there is no change in pore geometry (means that the pores present in all the membrane support are cylindrical) of the membrane supports (see Fig. 4.16) due to the addition/removal of TiO_2/$CaCO_3$. A higher rejection of BSA solution is obtained for the 3G and 6G support than the support-I. The possible reason for this is that the presence of more number of nanosized pores present in the 3G and 6G supports than the support-I.

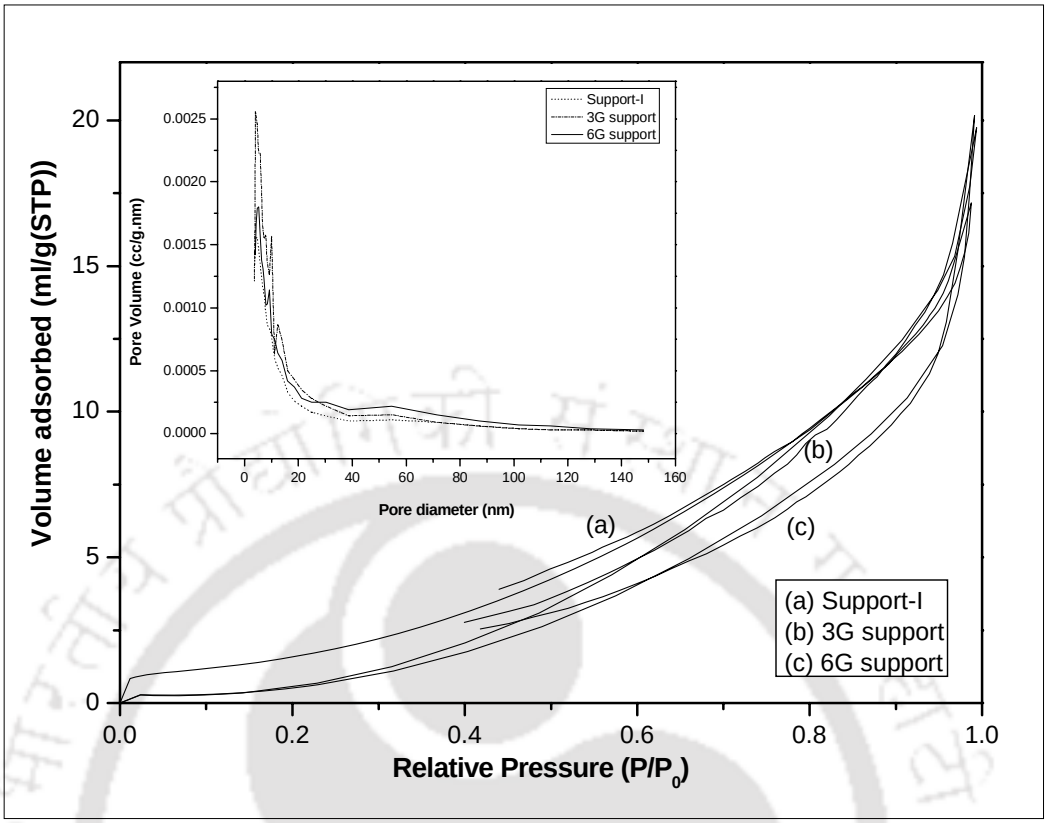

Fig. 4.16 Nitrogen adsorption/desorption isotherms of the sintered supports. (Inset shows the pore size distribution of the supports).

4.4 COST ANALYSIS

In general, the high cost of ceramic membranes is compensated by their higher permeability and longer lifetime, which reduces the operating and maintenance cost. Cost analysis is of the membrane supports including the fabrication and sintering cost along with the raw materials cost is estimated and presented in Table 4.6. The estimated cost is ranging between 13 and 17 $\$/m^2$.

Table 4.6 Cost analysis of the fabricated support based on unit cost of raw materials

Raw materials used for the fabrication of membrane supports	**Unit price (Rs./kg)**	**Amount of raw materials required for the fabrication of one membrane support (diameter = 63 mm and thickness = 4 mm) (g)**		
		Support-I	3G support	6G support
Kaolin	6.00	4.335	4.335	4.335
Ball Clay	3.00	5.274	5.274	5.274
Feldspar	4.00	1.680	1.680	1.680
Quartz	10.00	7.977	7.977	7.977
Pyrophyllite	5.00	5.142	4.242	3.342
Calcium carbonate	240.00	4.419	4.419	4.419
Titanium dioxide	520.00	-----	0.900	1.800
Raw materials cost per membrane support (Rs.)		1.5	1.8	2.0
Raw materials cost per unit area of the membrane support (Rs./m^2)		480	580	640
Raw materials cost per unit area of the membrane support ($./$m^2$)		10.00	12.08	13.33
Total fabrication cost (including pressing and sintering cost) of the membrane support ($./$m^2$)		**13.53**	**15.61**	**16.86**

The reported value of the membrane cost is conceptual in nature and may vary significantly depending on the above cost factors. The result of cost evaluation

indicates that the fabricated support is inexpensive than that of alumina and zirconia supports based on the raw materials cost and sintering temperature used in this work.

4.5 SUMMARY

This work indicates that the porosity and pore size of the support decreases with the removal of calcium carbonate and the addition of TiO_2 increases the mechanical strength of the membrane supports. The porosity of the support-I, 3G and 6G supports was found to be 44, 38 and 36% with an average pore diameter of 0.98, 0.93 and 0.83 μm, respectively. Flexural strength of the membrane support increases with the addition of TiO_2 and a maximum flexural strength of 33 MPa was obtained for 6G support. Solvent permeation experiments confirmed that all the membrane supports were hydrophobic in nature. All the membrane supports showed higher rejection at lower pressure and higher feed concentration. However, to reduce fouling, it is advisable to operate the membrane support with lower concentration and at an applied pressure less than 130 kPa. The attempted bovine serum albumin (BSA) separation using the prepared membrane supports gave a maximum observed rejection of 40% for lower concentrations (100 ppm). The obtained result suggests that the membrane support could be used for microfiltration application. These results suggest that changing the composition of the raw materials would not reduce the pore size of the membrane support for ultrafiltration or nanofiltration applications. Moreover, the addition of TiO_2 also enhances the cost of the membrane supports. Instead of changing the composition, one can obtain a membrane for UF and NF applications by forming a selective layer over the support by any one of the coating techniques. Therefore, support-I can be utilized for the fabrication of composite membrane, but not the 3G and 6G supports

.

भारतीय प्रौद्योगिकी संस्थान गुवाहाटी
Indian Institute of Technology Guwahati

Chapter 5

PREPARATION AND CHARACTERIZATION OF γ-Al_2O_3-CLAY COMPOSITE ULTRAFILTRATION MEMBRANE FROM BOEHMITE NANOMATERIAL BY DIP-COATING TECHNIQUE

5.1 INTRODUCTION

In this Chapter, the preparation of γ-Al_2O_3 selective layer on the membrane support-I by dip-coating technique using boehmite sol is discussed. In order to reduce the fabrication cost of γ-Al_2O_3-clay composite membrane, inexpensive aluminium chloride salt is used as a starting material for the preparation of boehmite sol instead of expensive aluminium alkoxide precursors. Boehmite powder and the sol are investigated by means of TGA, XRD, SEM, FTIR, N_2 adsorption-desorption isotherm and DLS analysis to obtain its characteristics and to confirm the conversion of boehmite to γ-Al_2O_3. In addition, the fabricated γ-Al_2O_3-clay composite membrane is characterized by liquid displacement technique to find the pore size distribution of the membrane. Pure water flux and the fabrication cost of the prepared membrane are also estimated for its possibility in industrial application.

5.2 MATERIALS AND METHODS

Aluminium chloride ($AlCl_3.6H_2O$, 99.5% pure), calcium carbonate ($CaCO_3$), nitric acid (HNO_3), hydrochloric acid (HCl), aqueous ammonia solution (30 wt.%) and sodium hydroxide (NaOH) were procured from Merck India Ltd. Water used in this work was collected from Millipore system.

5.2.1. Synthesis of γ-Al_2O_3-clay composite membrane

Boehmite sol was synthesized from aluminium chloride by controlled precipitation followed by peptization using dilute nitric acid at pH 3-3.5. Aqueous ammonia solution (30 wt.%) was added drop by drop to the aluminium chloride (4 wt.%) solution at room temperature under constant stirring until the pH of the precipitate reaches 8.0. A white boehmite precipitate formed was filtered and washed repeatedly with Millipore water to remove the excess chlorides present in the precipitate. Boehmite powders were obtained by the controlled precipitation method was transferred into a beaker and the stable sol was obtained by peptizing it with the addition of 0.3 wt % HNO_3 at the pH of 3.5. The binder, PVA (0.5 wt.%) was mixed with the sol and refluxed at 85°C for 24 h to get a stable and a clear or slightly translucent dipping sol. The PVA is used for the adjustment of the sol viscosity (as a thickener) as well as it protects the thin alumina layer from cracking during calcination. It generally burns off during calcination without leaving ash. Finally, the γ-Al_2O_3-clay composite membrane was prepared by dipping the membrane support (support-I) into the above prepared sol for one minute. Prior to this, one side of the clay support (support-I) was wrapped with polytetrafluoroethylene (PTFE) sealing wrap and the coating was applied only on the other side. Before dipping into the boehmite sol, the polished support-I were heated at 200°C for 2-3 h and then cooled in a desiccator. After dipping, the dip-coated clay support was dried overnight at room

temperature followed by heating at 50°C for 24 h to remove maximum moisture. Finally, the boehmite coated membrane support was calcined at 600°C for 3 h with a controlled heating rate (0.5°C/min) to obtain a γ-Al_2O_3-clay composite membrane

5.2.2 Characterization of boehmite and γ-Al_2O_3 particles

For characterization purpose, γ-Al_2O_3 powder was prepared by pouring the boehmite sol (without adding PVA) on a glass plate and then dried overnight at 50°C. Then, this as-dried sample (boehmite) was calcined to γ-Al_2O_3 at the same conditions as followed for γ-Al_2O_3-clay composite membrane. Thermo-gravimetric analyses of boehmite was conducted in a TGA instrument of Mettler Toledo thermo gravimetric analyzer (TGA/SDTA 851® model) under air atmosphere at a heating rate of 10°C/min from 25 to 900°C. To identify phases and their crystallinity of as-synthesized (boehmite) and calcined sample (γ-Al_2O_3), X-ray powder diffraction (XRD) pattern was recorded in a Bruker AXS instrument using Ni filtered Cu Kα radiation (λ = 1.5406 Å) operating at 40 kV and 40 mA. Diffraction intensities were measured by scanning from 10 to 80° (2θ) with a step size of 0.05°/s. The FTIR spectrum of the γ-Al_2O_3 powder was obtained on a Nicolet Impact-410 Fourier transform infrared spectrometer (Nicolet Impact-410). The transformation temperature of boehmite to γ-Al_2O_3 was determined from the DTG curve. The BET (Brunauer–Emmet–Teller) specific surface area, pore volume and pore size distribution of the γ-Al_2O_3 powder was determined by N_2 adsorption-desorption isotherm at -196°C measured in a surface area analyzer (make: Beckman-Coulter; model: SA 3100). The pore size distribution was determined by a BJH (Barett-Joyner-Halenda) model from the adsorption branch of the nitrogen isotherms. The pore volume was calculated from the amount of nitrogen adsorbed at a relative pressure, P/P_0 of 0.99, where it was assumed that all the pores were filled. The particle size

distribution of dipping boehmite sol was examined by dynamic light scattering equipment (make: Horiba; model LB-550V) with a He–Ne laser source. Scanning electron microscopy (make: LEO; model: 1430VP) was used to determine the surface morphology of clay support as well as γ-Al_2O_3-clay composite membrane. The top layer thickness of the alumina thin films was determined from SEM image of the cross-section of the composite membrane. Pure water permeation test was conducted in home made dead-end filtration setup made up of stainless steel 316. Pore size distribution of the γ-Al_2O_3-clay composite membrane was determined by liquid displacement technique using water as a wetting liquid and butanol as a non-wetting liquid.

5.3 RESULTS AND DISCUSSIONS

5.3.1 Thermogravimetric analysis

Thermogravimetric (TG) and differential thermo gravimetric (DTG) curves of boehmite is depicted in Fig. 5.1. The boehmite appears to undergo three stages of decomposition during heating. The first stage of decomposition (<120°C) is the liberation of physically adhered water present in the pores. The second stage of weight loss between 120 and 320°C can be assigned to the removal of the crystal water in the sample. The final step (>320°C) corresponds to dehydroxylation of boehmite to γ-Al_2O_3 (Mani *et al.,* 1994; Hwang *et al.,* 2001; Padmaja *et al.,* 2004; Li *et al.,* 2006). As can be seen from DTG curve, an endothermic peak at around 100°C corresponds to the removal of water molecules adsorbed on the gel. The second endothermic peak at about 277°C corresponds to the loss of crystal water from this sample. The third endothermic peak around 390°C is ascribed to boehmite

decomposition to produce γ-Al_2O_3 involving elimination of OH groups (Mani *et al.,* 1994; Li *et al.,* 2006).

5.3.2 XRD analysis

XRD patterns of the boehmite and γ-Al_2O_3 powder are depicted in Figs. 5.2. All the reflections of diffraction peaks (Fig. 5.2(a)) matches well with the JCPDS PDF No. 21-1307, which corresponds to boehmite with an orthorhombic unit cell (Liu *et al.,* 2008; Zhang *et al.,* 2008). The XRD patterns of calcined samples (Fig. 5.2(b)) matches very well with the JCPDS PDF No. 10-0425 that confirms the formation of γ-Al_2O_3 phase. The strongest intensity of the diffraction peaks (400 and 440) confirms the presence of γ-Al_2O_3 nanocrystallites in the walls of the framework (Liu *et al.,* 2008).

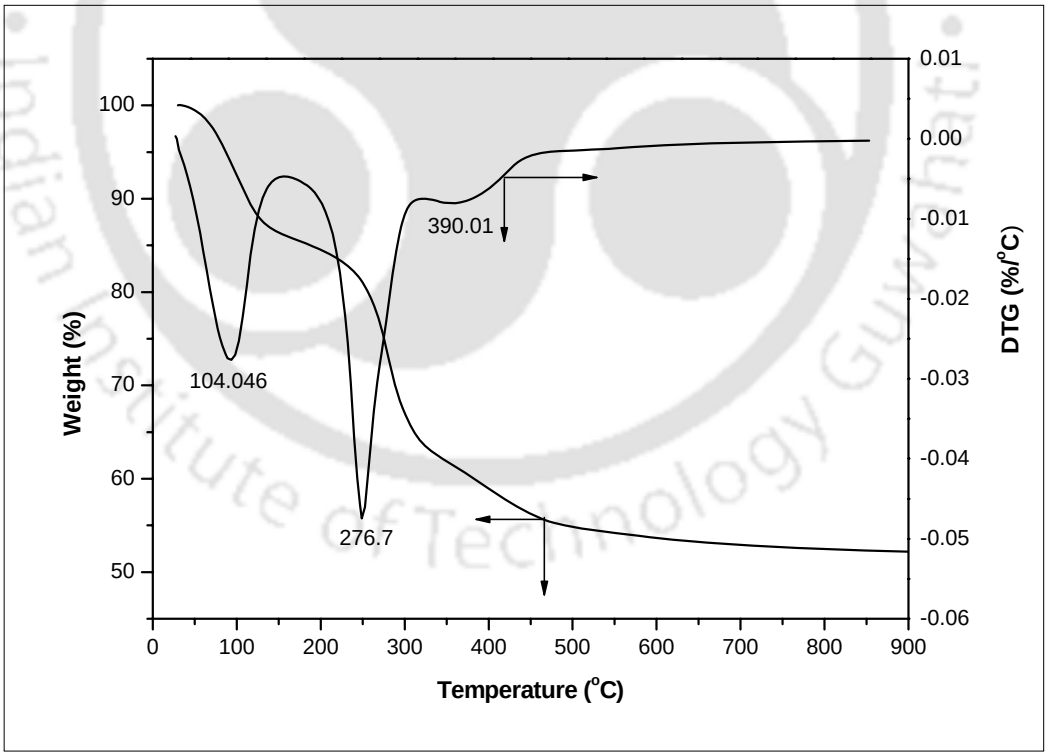

Fig. 5.1 Thermogravimetric (TG) and differential thermogravimetric (DTG) profile of boehmite sol.

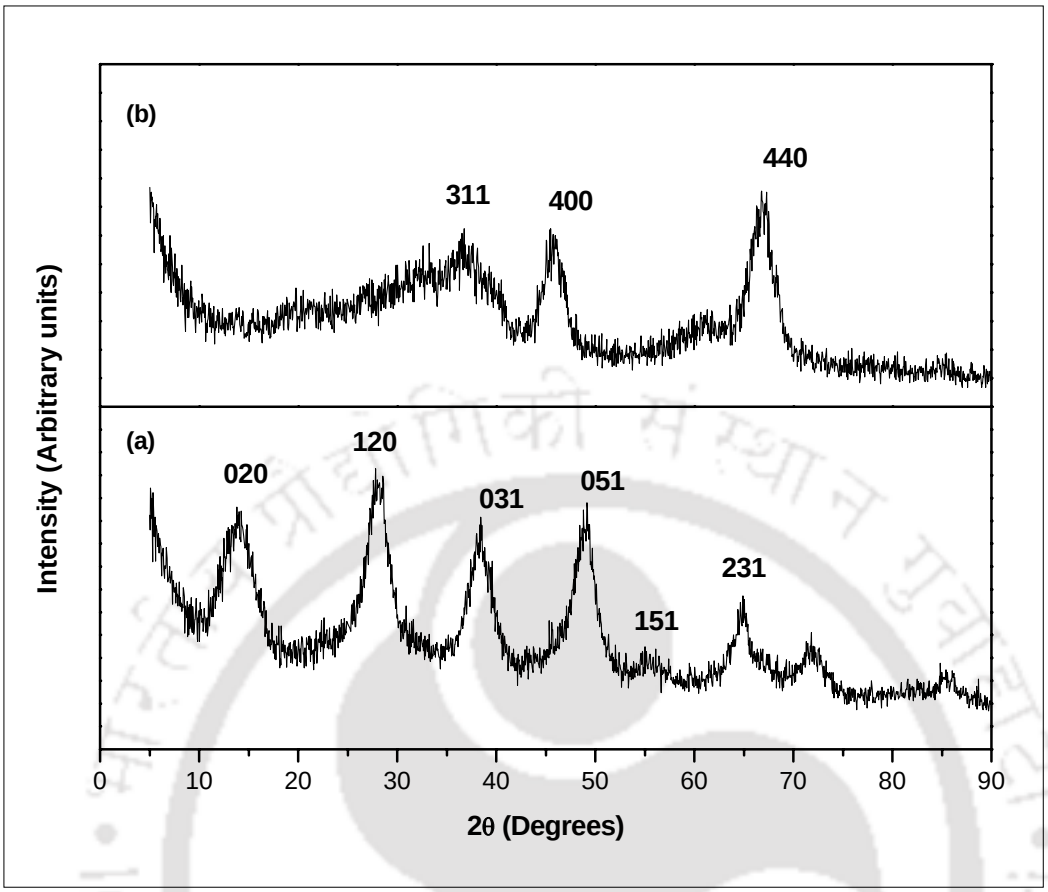

Fig. 5.2 XRD pattern (a) boehmite sol and (b) γ-Al_2O_3.

The crystallite size of the boehmite and γ-Al_2O_3 is calculated using Scherer equation from the broadening of the (020) diffraction peak (Fig. 5.2(a)) and (400) diffraction peak (Fig. 5.2(b)), respectively, and it is found to be 2.4 nm and 3.3 nm, respectively. The calculated crystallite size values confirm the presence of γ-Al_2O_3 phase and matches with the reported literature (Padmaja et al., 2004; Li et al., 2006).

5.3.3 FTIR analysis

Figure 5.3(a) shows the FTIR spectrum of boehmite. The bands at 744, 628 and 1075 cm^{-1} can be assigned to the defined characteristics of boehmite (Frost *et al.*, 1999). It is observed an intense band at 1075 cm^{-1} and a shoulder at 1171 cm^{-1}, which are assigned to the symmetric and asymmetric bending modes of Al-O-H, respectively

(Colomban 1988). The intense band at 1634 cm^{-1} and broad band centered at 3414 cm^{-1} are assigned to the bending and stretching modes of adsorbed water molecule (Colomban 1988). The OH torsional mode expected around 750 cm^{-1} could not be observed because it overlaps with the Al-O stretching vibrations. The weak band at 2098 cm^{-1} observed for boehmite is assigned to a combination band, which disappears in the spectra of the calcined samples (see Fig. 5.3(b)). In aluminium oxides, aluminium can have different types of coordination with oxygen. If the coordination is octahedral (AlO_6), the Al-O stretching and bending modes are expected in the region 500-750 cm^{-1} and 330-450 cm^{-1}, respectively. However, a tetrahedral coordination (AlO_4) is expected to give stretching modes in the narrow range of 750-870 cm^{-1} and bending modes between 250 and 320 cm^{-1}.

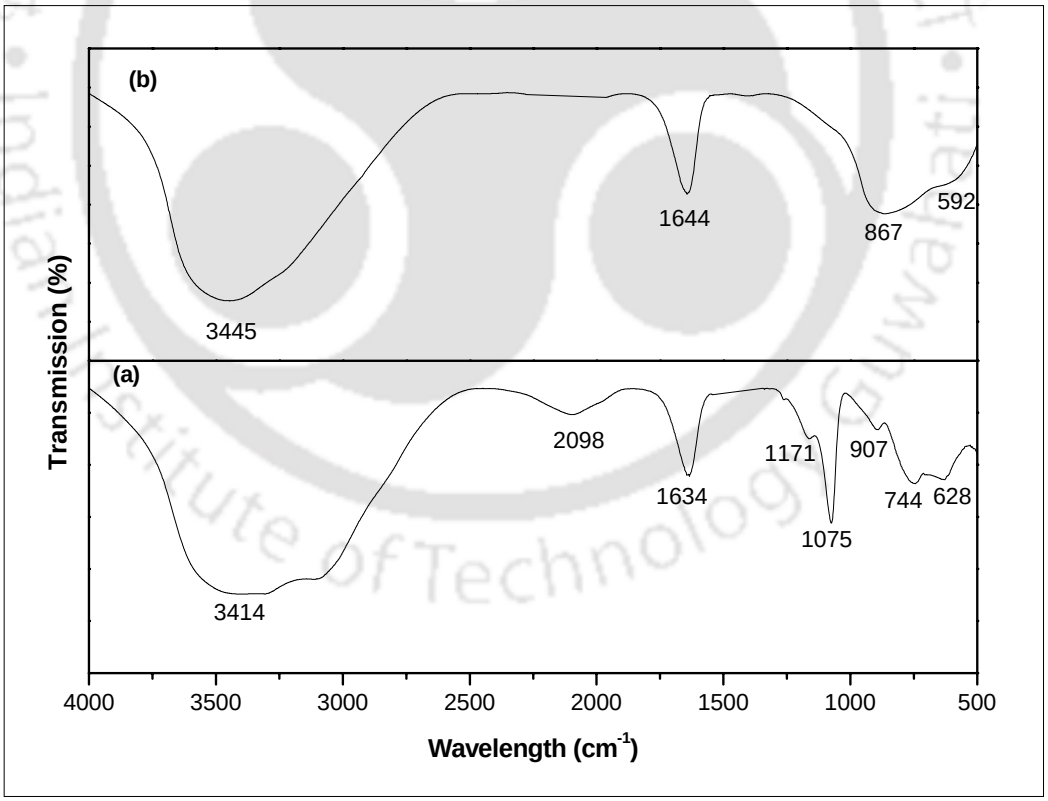

Fig. 5.3 FTIR spectra of (a) boehmite sol and (b) γ-Al_2O_3.

For boehmite (Fig. 5.3(a)), the bands observed at 744 and 628 cm^{-1} are assigned to the stretching modes of AlO_6 (McMillan and Piriou 1982). Fig. 5.3(b) depicts the FTIR spectra of the γ-Al_2O_3. Upon controlled calcinations at 600°C, the IR bands observed at ~1075 and 2098 cm^{-1} for boehmite sample disappears suggesting the complete dehydration or dehydroxylation of boehmite and its conversion to γ-Al_2O_3. Broad bands observed around 3445 and 1644 cm^{-1} are due to the water absorbed during pelletization. The peak at 592 cm^{-1} is assigned to AlO_6 and the shoulder observed at 867 cm^{-1} is assigned to AlO_4. From these results, we conclude that γ-Al_2O_3 (calcined samples) contain tetrahedral and octahedral Al-O, where as boehmite is purely octahedral in nature (Cross 1964).

5.3.4 N_2 adsorption/desorption analysis

N_2 adsorption-desorption isotherm of γ-Al_2O_3 powder is shown in Fig. 5.4. The γ-Al_2O_3 particles give an isotherm of type IV with an H2 hysteresis loop according to the IUPAC classification. This kind of hysteresis loop is an indication of a network of interconnected pores with narrower parts. Pore size distribution of γ-Al_2O_3 was computed from the adsorption isotherm by the BJH method (Jones and Barron 2007) as shown in Fig.5.5. This plot confirms that the pore size of γ-Al_2O_3 is in the mesoporous range. It also shows a unimodal narrow pore size distribution with pores in the range of 3.6-10 nm in diameter. Moreover, 85% of the pores are smaller than 6.0 nm for γ-Al_2O_3. BET surface area and pore volume of γ-Al_2O_3 are calculated to be 216.89 m^2/g and 0.30 ml/g, respectively, which are strongly higher than the values reported in literature (Buelna and Lin 1999; Kandri *et al.*, 1999).

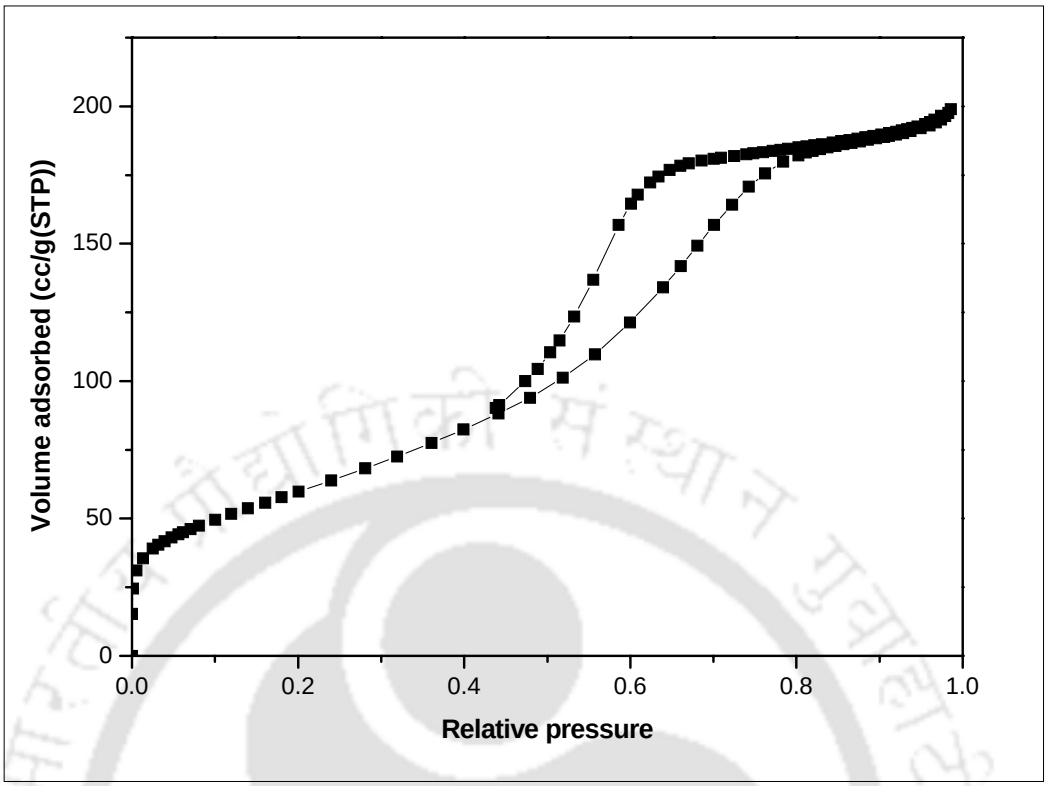

Fig. 5.4 N_2 adsorption-desorption isotherm of γ-Al_2O_3 particles.

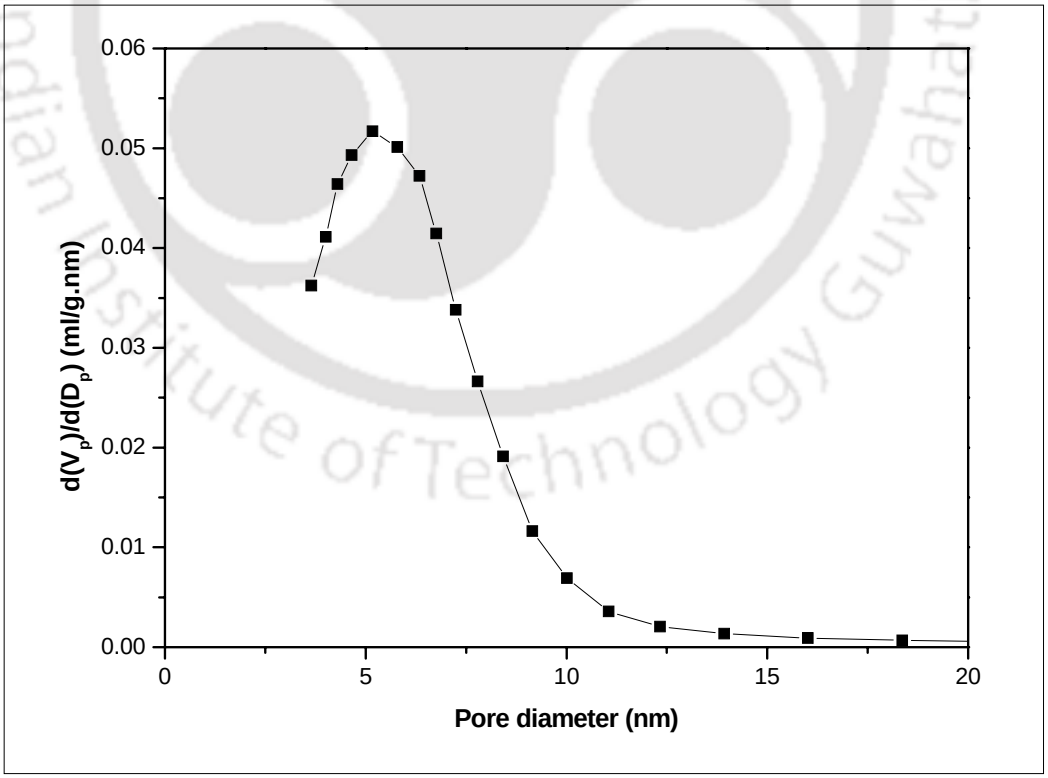

Fig. 5.5 BJH pore size distribution of γ-Al_2O_3 particles.

Particle size distribution of the boehmite sol obtained from DLS is depicted in Fig. 5.6. Dipping sols with large particle size will necessarily have large interstitial spaces, and, because of site exclusion, will not cover the surface uniformly leaving patches of exposed untreated surface. The obtained narrow particle size distribution of the boehmite sol with a mean particle size of 30.9 nm suggests that a uniform coating can be applied on the surface of the support using this stable sol.

5.3.5 SEM analysis

Figures 5.7(a) and (b) show the top surface and cross section of the clay support obtained from SEM micrographs. The macroporous structure and connectivity between the pores of the support is clearly visible in Fig. 5.7. The average pore size of the support estimated using ImageJ analysis is found to be 1.01 μm.

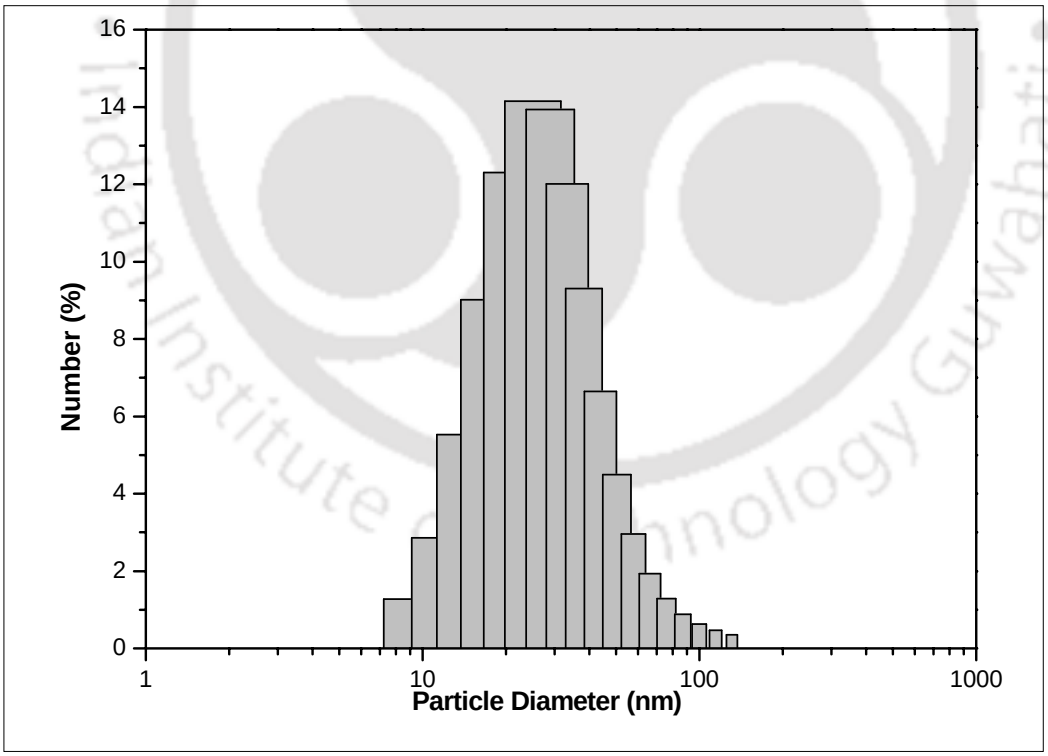

Fig. 5.6 Particle size distribution of boehmite sol.

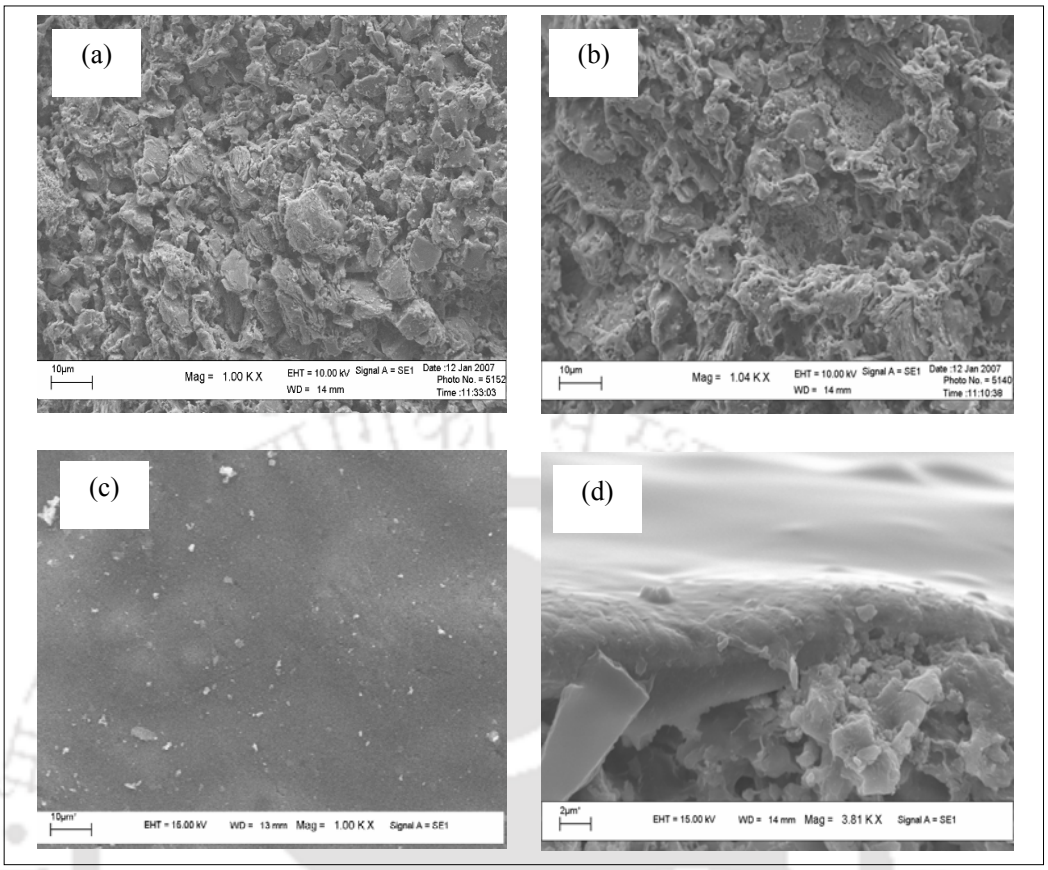

Fig. 5.7 SEM images of clay support ((a) top surface and (b) cross section) and γ-Al_2O_3-clay composite membrane ((c) top surface and (d) cross section).

SEM images of the top and cross sectional view of γ-Al_2O_3 composite membrane is presented in Fig. 5.7(c-d). After coating, reduction in the pore sizes is clearly visible when compared with pore sizes of clay support. The top layer (γ-Al_2O_3) has a finer structure because of smaller particle size of the sol. Fig. 5.7(d) also clearly demonstrates a uniform interphase between the γ-Al_2O_3 layer and the macroporous clay support, suggesting that the γ-Al_2O_3 layer has good adhesion to the support. Furthermore, it is found that no infiltration of sol particles occurred during the dip-coating process. Thickness of the coated γ-Al_2O_3 layer is measured using the cross-section of SEM image of the composite membrane and is found to be ~2.6 μm. Two distinct layers are also clearly seen from the SEM image.

5.3.6 Pore size distribution estimated by liquid displacement technique

Pore size distribution of γ-Al_2O_3-clay composite membrane was determined using water as a wetting liquid and butanol as a non-wetting liquid. This method essentially measures the differential pressure needed to overcome the resistance offered to the displacement of a wetting liquid (water) by a non-wetting liquid (butanol). The differential pressure is given by the Laplace equation

$$\Delta P = \frac{2\gamma \cos\theta}{r} \qquad (5.1)$$

where r is the radius of capillary shaped pore (nm), γ is the interfacial tension between the two fluids (mN/m) and θ is the contact angle between the fluids and the γ-Al_2O_3 membrane (degrees). The contact angle and surface tension of water-butanol system are taken from literature (Jakobs and Koros 1997).

The pore size distribution of the composite membrane is determined employing liquid displacement technique. Here, water was selected as a wetting liquid and butanol used as a non-wetting liquid. First, butanol flux was measured through a dry membrane as a function of pressure and a straight line was obtained as shown in Fig. 5.8. Then the membrane was wetted with water and again butanol flow rate was determined as a function of applied pressure. Up to a certain pressure, there was no flow due to the resistance offered by wetting liquid (water). It was observed at a certain minimal pressure of 276 kPa, butanol flow started where it was assumed that largest pore was empty. Then at a certain higher pressure of ~ 700 kPa, the butanol flow of the dry membrane was equal to wet membrane i.e. all the pores were available for butanol flow. By using the equation (5.1) with the knowledge of these pressures, the pore size range for the membrane was calculated and found in the range of 5.4-13.6 nm.

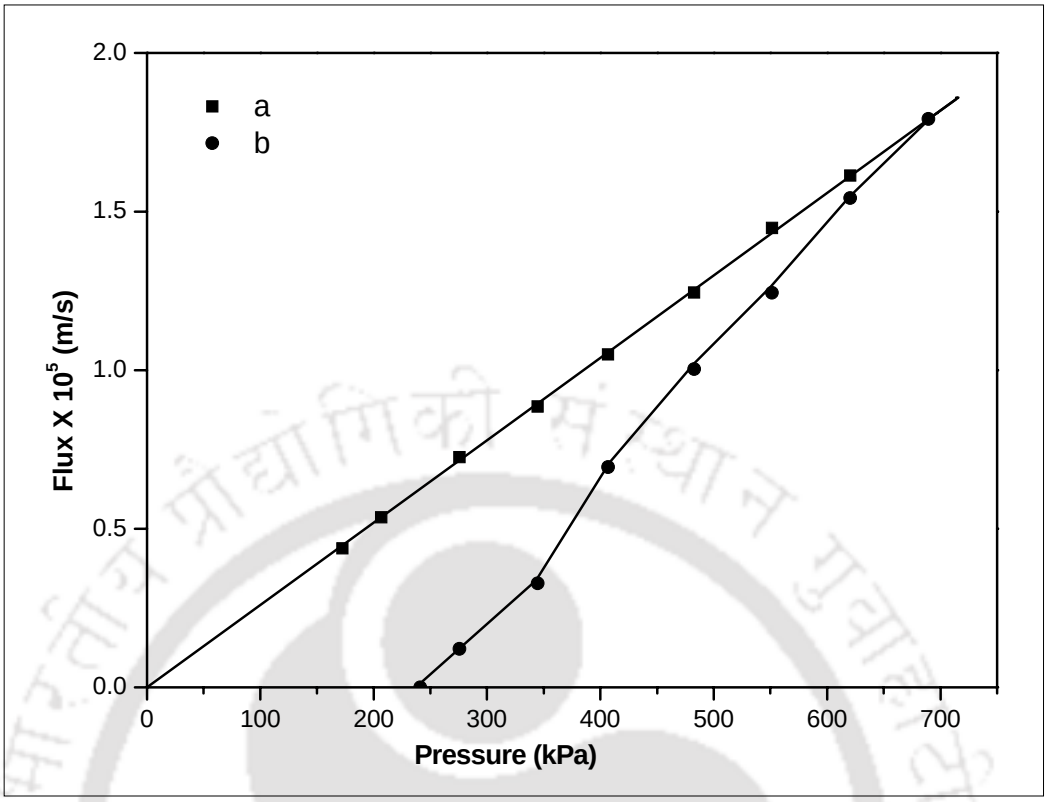

Fig. 5.8 Flux-pressure curve for pore size distribution of γ-Al_2O_3-clay composite membrane. (a: Butanol flux, b: Butanol flux when the membrane pores are filled with water).

The same data is plotted in a different manner in order to define a flow averaged pore size (Fig. 5.9). The experimental data obtained by butanol-water flux is divided by the butanol flux obtained at the same pressure to get the flux ratio. This flux ratio is plotted against the pore radius as shown in Fig. 5.9. The curve in the graph gives a cumulative fraction of the hydrodynamic flux that flows through pores of a desired size and all smaller pores (Jakobs and Koros 1997). Fifty percent of the flow of the binary mixture is passing through pores of roughly 5 nm (Fig. 5.9) and smaller and hence this is the flow weighted average pore size. To evaluate the hydraulic permeability of the membrane support and composite membrane, the pure water flux was measured at different applied pressures using batch permeation setup.

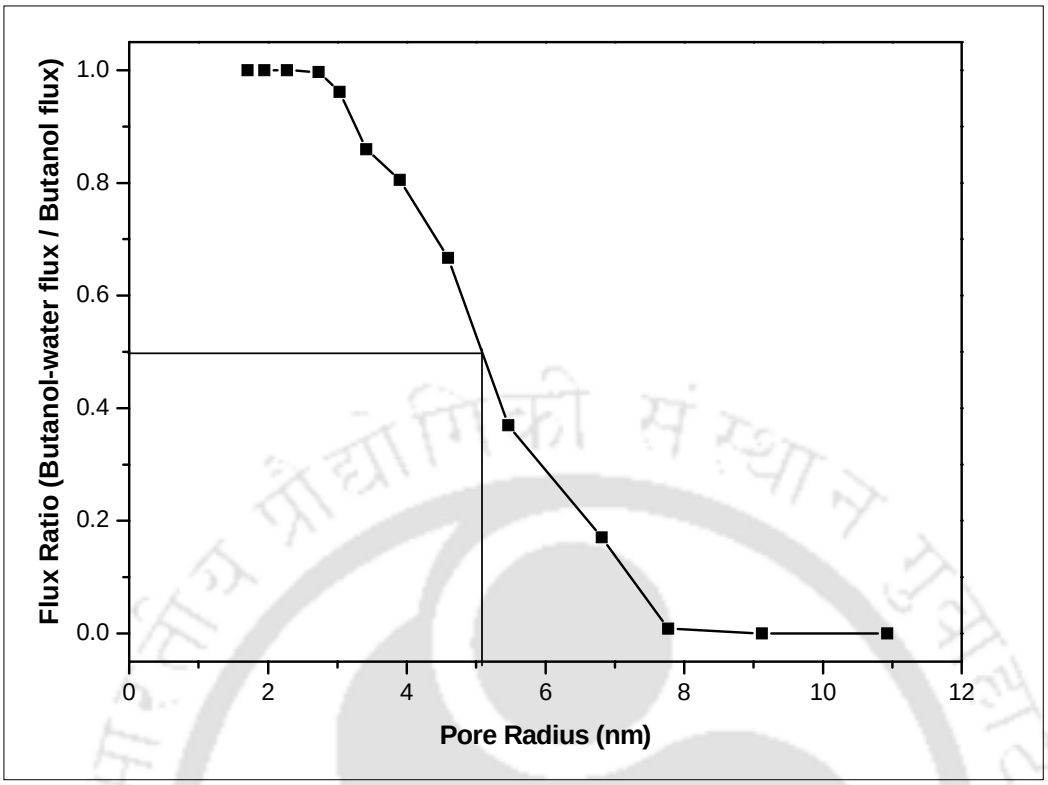

Fig. 5.9 Flow weighted average pore size distribution of γ-Al_2O_3-clay composite membrane.

5.3.7 Water permeation experiment

The permeation cell was initially filled with 250 ml of water and the required pressure was applied. For water flux determinations at each pressure, 50 ml of permeate was allowed to pass and the time required for collections of the next 25 ml permeate was noted down. The reported values of water flux were average of three readings. The hydraulic permeability was evaluated from the slope obtained from the experimental data of the pure water flux versus applied pressure.

$$L_p = \frac{J_w}{\Delta P} \qquad (5.2)$$

where, L_p is the hydraulic permeability (m/s kPa), J_w is the pure water flux (m/s) and ΔP is the applied differential pressure (kPa). Figure 5.10 shows the pure water flux of the support-I and γ-Al_2O_3-clay composite membrane. It is found that the water flux of the composite membrane is much lower than that of the clay support which indicates the decrease in pore size resulting in decreased hydraulic permeability of γ-Al_2O_3-clay composite membrane. The hydraulic permeability of the support-I and the composite membrane is found to be 4.838×10^{-6} and 2.357×10^{-7} m/s kPa, respectively.

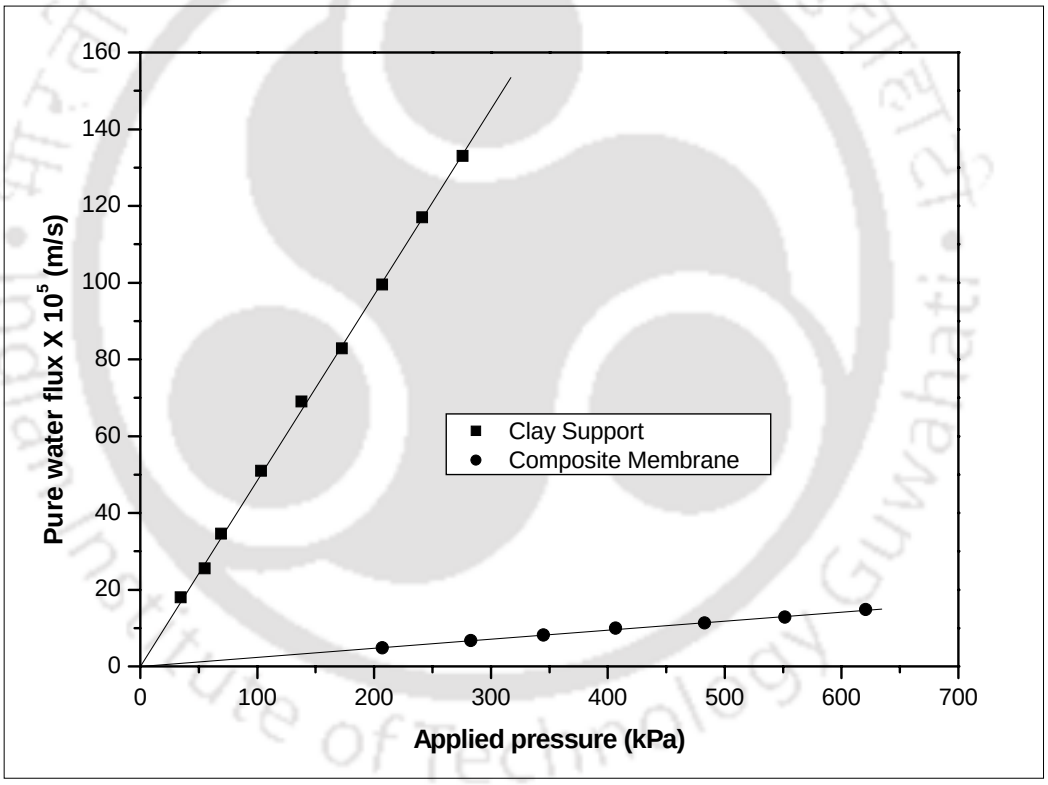

Fig. 5.10 Pure water flux of clay support and γ-Al_2O_3-clay composite membrane as a function of pressure.

5.4 COST ANALYSIS

A detailed cost analysis is made and presented in Table 5.1. The cost of the prepared γ-Al_2O_3-clay composite membrane is estimated to be 26.04 \$/m^2.

Table 5.1 Cost analysis of γ-Al_2O_3-clay composite membrane

Details	**Price (\$)**
Fabrication cost for the ceramic support	
Raw materials cost for ceramic support prepared from low cost clays	\$ 10/m^2
Compaction or Pressing cost (based on particle size and compaction pressure)	\$ 2 (Brookes 2008)
Sintering cost for the support (950˚C for 6 h)	\$ 1.53
Total cost required for the fabrication of a ceramic support	**\$ 13.53/m^2**
Preparation cost for γ-Al_2O_3 layer	
Raw materials cost (4 g Aluminium chloride + other chemicals) for the preparation of the boehmite sol	\$ 0.1022
Raw materials cost for the preparation of one membrane (42 mm diameter and 2.6 μm thickness membrane)	\$ 0.01022
Cost required for the preparation of γ-Al_2O_3 layer	\$ 7.38/m^2
Cost required for reflux condenser operation	\$ 2.62
Cost required for sintering (600˚C for 3 h)	\$ 2.51
Total cost required for the preparation of γ-Al_2O_3 layer on clay support (rounded value)	**\$ 12.51/m^2**
Total cost required for the preparation of γ-Al_2O_3-clay composite membrane	**\$ 26.04/m^2**

5.5 SUMMARY

A γ-Al_2O_3-clay composite ultrafiltration membrane has been successfully developed with a boehmite sol derived from inexpensive aluminium chloride salt. The particle size distribution of the boehmite sol used for coating is very narrow with a mean

particle size of 30.9 nm. The prepared composite membrane has the pore size in the range of 5.4-13.6 nm and the pure water permeability of the membrane is found to be 2.357×10^{-7} m/s kPa. The estimated cost of the prepared membrane is 26.04$/$m^2$, which would be relatively lower than other commercial membranes in the market.

Chapter 6

SEPARATION OF BSA PROTEIN AND ELECTROLYTES FROM AQUEOUS SOLUTION USING γ-Al_2O_3-CLAY COMPOSITE ULTRAFILTRATION MEMBRANE

6.1 INTRODUCTION

In this Chapter, the separation potential of the fabricated low cost γ-Al_2O_3-clay composite membrane is investigated for BSA and electrolytes ($MgCl_2$ and $AlCl_3$) from its aqueous solution. This Chapter is divided into two sections; the influence of pH, feed concentration and applied pressure on BSA separation is investigated in the first section and in the second section, the separation performance is investigated for the two electrolyte solutions ($AlCl_3$ and $MgCl_2$) by varying the pH, applied pressure and feed concentration. In addition, an investigation is carried out on the real rejection of BSA and electrolytes through the membrane using Spiegler-Kedem model.

6.2 MATERIALS AND METHODS

Magnesium chloride, aluminium chloride, hydrochloric acid and sodium hydroxide were procured from Merck India Ltd. Sodium dodecyl sulfate (SDS) was purchased from Loba Chemie, Mumbai. Bovine serum albumin (BSA; mol. wt: 67000 Da) was obtained from Spectro Chem. Pvt. Ltd., Mumbai. Water used in this work was collected from Millipore system.

6.2.1 Experimental procedure for BSA separation

BSA feed solution (500 ppm) was prepared by dissolving 0.5g of BSA in 1000 ml volumetric flask using Millipore water and stirred continuously for 1 h. Influence of pH on BSA separation experiments was conducted at different pH values ranging between 3 and 8 at a fixed applied pressure of 207 kPa. The pH of the solution was adjusted with NaOH or HCl. The effect of applied pressure on the permeate flux and retention behavior of BSA was studied with a feed concentration of 500 ppm at pH 3. The influence of feed concentration was also investigated in the range between 100 and 500 ppm at a constant pressure of 207 kPa. For all these experiments, the permeation cell was filled with 100 ml of protein solution. After discarding the first 20 ml of the protein solution at a fixed pressure, the time required to collect the next 10 ml of permeate was noted down to calculate the permeate flux at that pressure. BSA concentration in the permeate solution was determined spectrophotometrically at 280 nm with a UV-visible spectrophotometer (Make: Perkin-Elmer; model: Lambda 35). The prepared BSA solution was utilized within 6 h to minimize the aggregation or denaturation of proteins during storage. After each experiment, the membrane was initially rinsed with Millipore water and then it was washed with a mixture of NaOH and sodium dodecyl sulfate (SDS) solution for 30 min in order to regenerate the membrane. Finally, the membrane was rinsed again with Millipore water until it

reaches neutrality (i.e., the pH of the rinsed water equals the pH of pure water). Complete recovery of the membrane was checked by measuring the membrane hydraulic permeability equals to the actual hydraulic permeability or within the limits of ±2% of actual permeability. Single composite membrane has been used for these studies to eliminate any issues that can arise from membrane to membrane variability. However, the variation in the permeability of multiple membranes (prepared at different times using the same procedure) was also been checked and the variation was found to be ± 6%.

6.2.2 Experimental procedure for electrolyte separation

The separation capability of the membrane was investigated for single salt solution of $MgCl_2$ and $AlCl_3$ as a function pH, salt concentration, applied pressure and nature of cation present in the solution. The pH was studied in the range of 3-8 at a constant pressure of 207 kPa with a feed concentration of 3000 ppm. The pH of the salt solution was adjusted by adding dilute NaOH and HCl solution. The effect of pressure on the separation of electrolytes was studied in the ranges between 138 and 550 kPa at pH 3 for the feed concentration of 3000 ppm and the effect of concentration was investigated for the range of 1000 to 5000 ppm at pH of 3 for an applied pressure of 207 kPa. The electrolyte solutions were prepared using Millipore water. The membrane can adsorb the electrolyte salts during the separation experiments. It is important to determine the extent of adsorption of electrolytes in order to avoid the errors in calculating the observed rejection. This experiment was carried out in two methods at a pressure of 207 kPa by the following procedure (Neelakandan *et al.,* 2003). In the first method, a fresh membrane was taken and carried out the experiment with 250 ml of salt solution (1000 ppm). Each run 20 ml of permeate was collected for the determination of the rejection. Similar runs were performed on the same

membrane, till the rejection becomes constant. In the second method of experiment, fresh membrane was soaked in higher concentration (2000 ppm) of salt solution for 6 h and then carried out the separation experiments with 1000 ppm solution as described in the first method. These trial run experiments reveals that, when the membrane is fresh (without soaking in higher concentration), the rejection remains positive (higher for first run) and becomes constant after third run i.e. after passage of 40 ml of permeate. When the membrane is soaked in higher concentration, it was found that the first reading shows negative rejection but the rejection becomes positive from the second reading and constant after the passage of 40 ml of permeate. Based on this information, for each run, the cell was filled with 250 ml of electrolyte solution and the first 45 ml of permeate passed through the membrane was discarded. Permeate flux was calculated by measuring the time interval corresponding to next 25 ml permeate volume. The concentrations of the salts in the feed and permeate were determined by a calibrated conductivity meter (Model: VSI-04, India) with 0.1 μmho accuracy. The calibration was carried out using 0.1N KCl solution. After each experiment, the membrane was flushed with Millipore water at higher pressures to regain its original water permeability.

6.3 SPIEGLER–KEDEM MODEL

6.3.1 Theory

The transport of the solute through a membrane by pressure driven membrane processes can be described by irreversible thermodynamics, where the membrane is considered as a black box. The solute flux through the membrane can be described as the sum of a convective (due to applied pressure gradient across a membrane) and diffusive (due to concentration difference) flux. In ultrafiltration (UF) and nanofiltration (NF), the rejection factor is defined as

$$R_{obs} = 1 - \frac{C_P}{C_f} \quad (6.1)$$

$$R_{int} = 1 - \frac{C_p}{C_m} \quad (6.2)$$

where, C_p is the concentration of solute in the permeate, C_f is the bulk concentration of feed, C_m is the concentration on the surface of the membrane, R_{obs} is the observed rejection and R_{int} is the intrinsic (real) rejection. R_{int} is an inherent property of the membrane whereas R_{obs} depends strongly on the operating conditions. Therefore, it is desirable to report the separation performance of a membrane interms of R_{int} even though the determination of C_m is difficult. The C_m can be determined by either of the two following techniques (Shukla and Kumar 2005).

(i) Direct measurement of C_m through interoferometric method

(ii) Optical shadow measurements

Apart from the above two techniques, C_m can also be determined by solving transport equations in the polarization layer. Accuracy of the estimated C_m depends upon the validity of the hydrodynamic model used.

In the second technique, the following equations are used for determination of C_m. The membrane surface concentration is calculated using the osmotic pressure model (Clifton 1982; Shukla and Kumar 2005).

$$J_v = L_P(\Delta P - \sigma\Delta\pi) \quad (6.3)$$

where, J_v is the permeate flux, L_P is the pure water permeability, ΔP is the applied pressure difference, σ is the membrane reflection coefficient and $\Delta\pi$ is the osmotic pressure difference.

The osmotic pressure difference is calculated using the van't Hoff equation for electrolytes.

$$\Delta\pi = \nu RT\Delta C \qquad (6.4a)$$

where, ν is the number of moles of ions given by each mole of the electrolyte in the solution, R is the universal gas constant, T is the absolute temperature and ΔC $(=C_m - C_p)$ is the difference in the concentration of the solute at the membrane surface (upstream side) and in the permeate

The osmotic pressure can't be determined by the linear Van't Hoff for BSA solution because of its high concentrations. Therefore, the osmotic pressure can be related to the solute concentration of the membrane by a polynomial equation as given below (Bhattacharjee and Bhattacharya 1992; Afonso *et al.,* 2009; Darcovich *et al.,* 2009; Sarkar and De 2011).

$$\Delta\pi = a_0 C_m + a_1 C_m^2 + a_2 C_m^3 + a_3 C_m^4 \qquad (6.4b)$$

where, a_0, a_1, a_2 and a_3 are the virial coefficients, which becomes important for high solute concentrations. Based on their experimental data, the best polynomial fit of third or fourth order yields the virial coefficients. However, a polynomial expression for the osmotic pressure as a function of concentration used in this work is taken from the literature data (Sarkar and De 2011) up to third virial coefficient.

$$\Delta\pi = 134.70369C_m - 0.40688C_m^2 + 0.00225C_m^3 \qquad (6.4b)$$

The above correlation of osmotic pressure is valid in the range of 0-500 ppm concentration of BSA. However, similar correlations given by other authors (Afonso *et al.,* 2009; Darcovich *et al.,* 2009) (for BSA concentration of 0-500 ppm) also gave similar results of relection coefficient (σ) with a percentage error less than 0.6%.

The reflection coefficient related to the intrinsic rejection of the membrane by the following equation (Spiegler and Kedem 1996).

$$R_{int} = \frac{\sigma(1-F)}{1-\sigma F} \qquad (6.5)$$

where, F is given by the expression

$$F = \frac{\exp(-(1-\sigma)J_v)}{P_m} \qquad (6.6)$$

where, P_m is the solute permeability of the membrane. According to equation 6.5 and 6.6, the rejection increases with increasing the water flux (J_v). The reflection coefficient, σ is a characteristic of the convective transport of the solute. If $\sigma = 1$ means that the convective solute transport does not take place at all. This is the case for ideal reverse osmosis (RO) membranes where the membranes have no pores available for the convective transport. For the UF and NF membranes having pores, the σ value will be less than 1 if the solutes are small enough to enter the membrane pores. The parameter C_m, σ and P_m are determined using equation (6.3) to (6.6) following an iterative technique schematically represented in Fig. 6.1 (Ghose *et al.,* 2000; Shukla and Kumar 2005). In this technique, the C_m is calculated using equations (6.3) and (6.4a or 6.4b) by assuming a σ value. The P_m values and its

standard deviation for various experimental data are then calculated using equations (6.5) and (6.6).

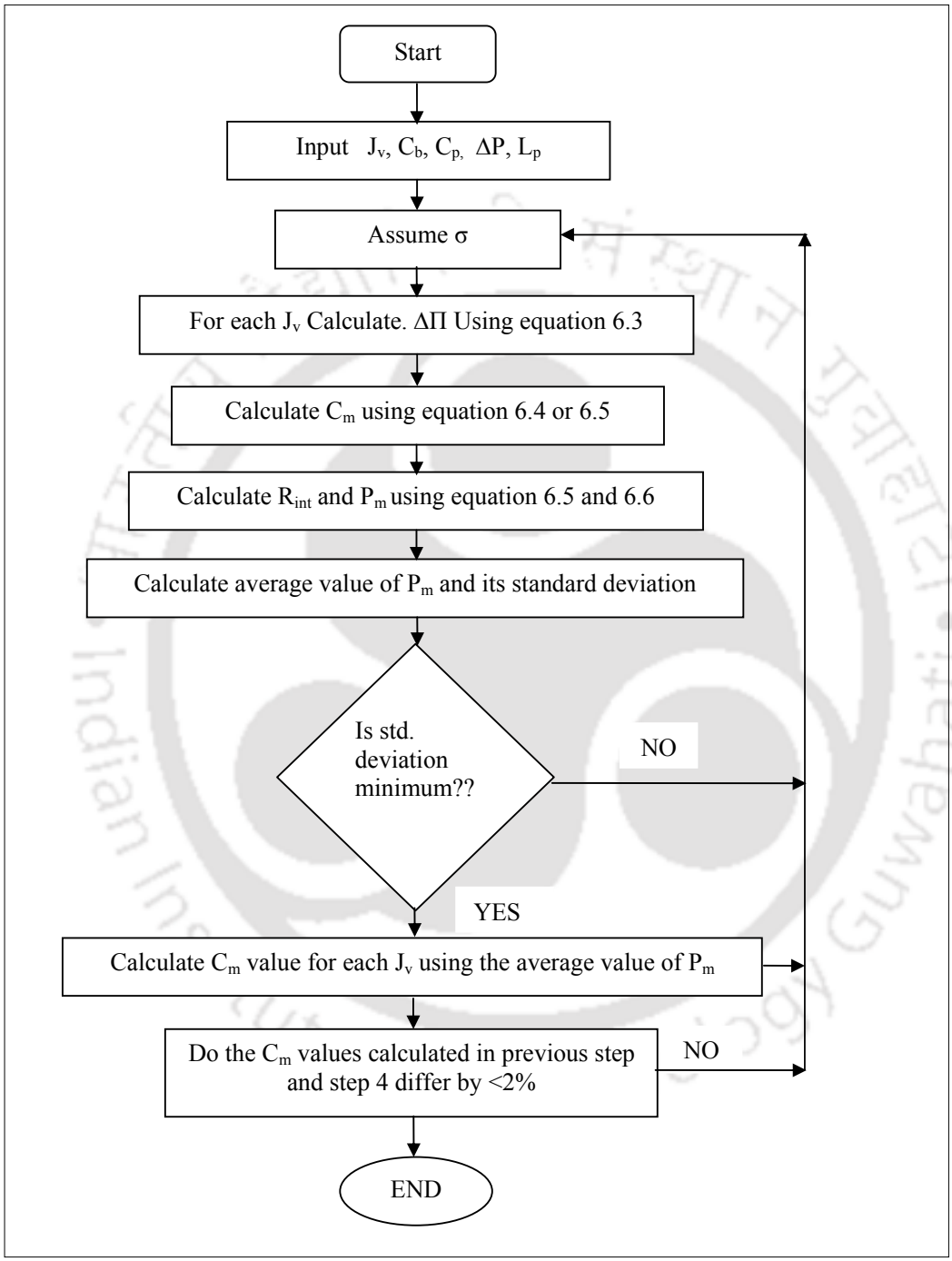

Fig. 6.1 Flowchart showing the algorithm used to find C_m and the intrinsic rejection.

The standard deviation of the P_m values is minimized by adjusting the σ value and the obtained σ value obtained is used to calculate the surface concentration (C_m) of the membrane. If the value of surface concentration of the membrane (C_m) calculated from equation 6.2 and 6.4 satisfies the convergence criterion (less than 2 %) then the program ends and gives the optimized value of σ and P_m. The obtained C_m value is used for the calculation of intrinsic rejection.

6.4 RESULTS AND DISCUSSIONS

6.4.1 Separation of BSA protein solution

Filtration studies of different proteins using charged membranes demonstrated that the membrane charge, pore size, applied pressure, solution pH and concentration have marked effect on the protein rejection (Reed 1998). The separation potential of the fabricated γ-Al_2O_3-clay composite membrane was studied using BSA protein solution and the influence of the operating condition such as applied pressure, pH and feed concentration was also investigated to understand the separation mechanism.

6.4.1.1 Effect of pH on BSA separation

The electrical charge of the protein as well as the membrane can be altered by changing the pH of the solution that creates either an electrostatic attraction or repulsion between the membrane and BSA. The solution pH can also alter the conformation (size and shape of the molecule) of BSA, which can affect the rejection and permeation of the membrane (Pujar and Zydney 1998; Giacomelli *et al.,* 1999). BSA can exist in three different conformations depending upon pH of the solution, namely, normal form (pH 5 to 8), fast form (pH 3-4) and expanded form (pH <3). In general, the separation ability of the membranes increases as the conformation (size) of the feed solute increases. The size increasing trend of the BSA molecule follows

the sequence of normal form < fast form < expanded form (Giacomelli *et al.,* 1999; Freeman *et al.,* 2004).

Fig. 6.2 illustrates the variation of BSA flux and rejection with pH for a feed concentration of 500 ppm at 207 kPa. It is observed from Fig. 6.2 that the permeate flux increases with increase in the pH of the solution, which is due to the electrostatic interaction between BSA and the γ-Al_2O_3-clay composite membrane. It is already reported in the literature that the isoelectric point (IEP) of the γ-Al_2O_3 membrane is 8-9 and hence is electrically positive for pH values lower than 8-9 and negative for pH values greater than 8-9 (Rios *et al.,* 1996; Zeman and Zydney 1996; Pujar and Zydney 1998; Persson *et al.,* 2003; Lin *et al.,* 2008). So the prepared composite membrane is positively charged at the studied pH in this work. When the solution pH is less than 4.9 (ie., pH < IEP), both BSA and membrane are positively charged, which causes an increase in the electrostatic repulsion between the membrane and BSA, resulting in lower permeate flux. At pH = IEP (ie., pH = 4.9), BSA is uncharged while the membrane remains positively charged. An increase in the permeate flux is due to the reduction in the electrostatic repulsion between BSA and membrane and the permeation mainly depends on the sieving mechanism. When pH is greater than 4.9 (ie., pH > IEP), BSA carries a negative charge, which increases the electrostatic attraction between the BSA and membrane, resulting in higher permeation flux (Casa *et al.,* 2007). However, another mechanism by which changes in pH could affect the observed flux is by changing the packing characteristics of the retained protein layer at the membrane surface (Iritani *et al.,* 1995).

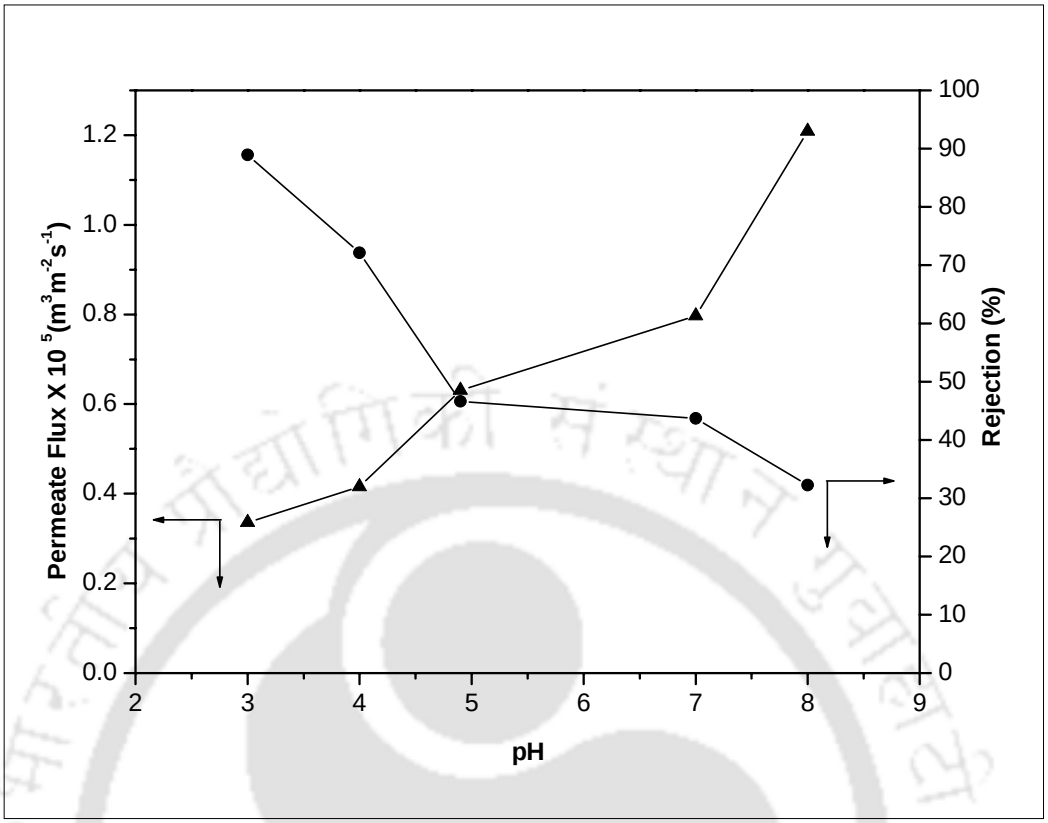

Fig. 6.2 Permeate flux and retention of BSA as a function of pH. (Feed concentration = 500 ppm and pressure = 207 kPa).

The rejection performance of the membrane follows a decreasing trend with increase in the pH. At pH 3, the rejection of BSA is as high as 89% and at pH 8 (above IEP) observed rejection is 32%. At pH < IEP (4.9), both size exclusion as well as the electrical repulsion factor exists as both the membrane and BSA are positively charged. In particular, the repulsive interactions could obstruct the transmission of the protein through the pore and consequently higher rejection is observed at pH 3 (Giacomelli *et al.,* 1999; Casa *et al.,* 2007). Also at pH 3, BSA is in the expanded form, due to the conformational changes of the BSA molecule attached perpendicular to the γ-Al_2O_3 membrane surface by weak end-on orientation, which reduces the transmission of BSA and leads to higher rejection. The uncharged BSA showed a

47% rejection at pH 4.9 indicating that the sieving is expected to outweigh electrostatic interaction. At pH > 4.9, BSA is negatively charged and the positively charged membrane didn't hinder BSA transport through the membrane, leading to lower rejection. The BSA molecule binds parallel to the membrane by a flat configuration similar to side-on orientation and the rejection depends on the sieving mechanism as well as electrostatic attraction between the BSA and membrane (Giacomelli *et al.,* 1999; Urano and Fukuzaki 2000).

6.4.1.2 Effect of pressure on BSA separation

Figure 6.3 shows the flux and retention behavior of BSA with applied pressure. Concentration and pH of the BSA solution used in this study are 500 ppm and 3, respectively.

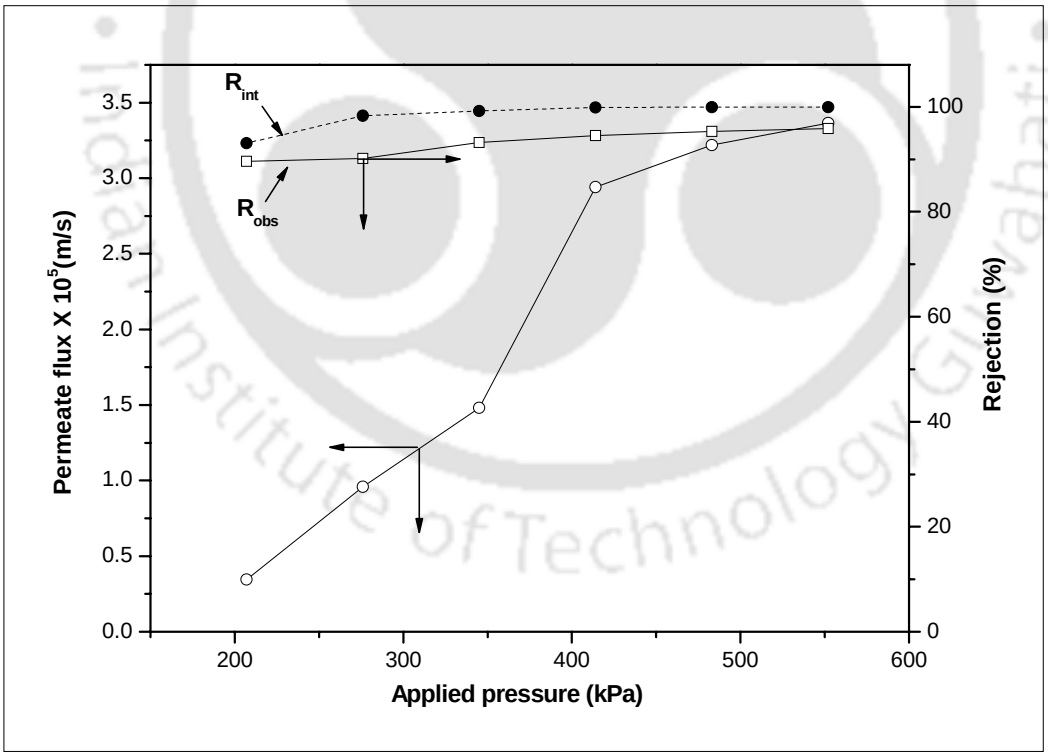

Fig. 6.3 Variation of permeate flux and observed rejection of BSA protein solution with applied pressure. (Feed concentration = 500 ppm; pH = 3).

The flux and rejection of BSA increase when the applied pressure increases. The increase in the BSA rejection is due to the concentration polarization effect. It can be seen from the Fig. 6.3 that at low pressures (207 to 406 kPa), the flux increases linearly with increasing pressure with a greater slope. Above 406 kPa, the rate of flux enhancement is low (nearly constant and pressure independent) due to concentration polarization effects (Ghosh and Cui 1998). At high pressure, protein is transported to the membrane surface by convection and in addition to this, solute migration takes place due to interaction between protein and the charged surface resulting in adsorption of protein onto the membrane surface. With a surface deposit, a membrane has resistance much larger than that of the clean membrane. Thus the membrane gives additional resistance at higher pressure. The permeability of the deposit is determined by the balance between the compressive pressure associated with filtration and the electrostatic repulsion between proteins in the deposit. The electrostatic repulsion between adsorbed layer and bulk protein solution increases the observed rejection at higher pressure.

The maximum rejection obtained is 95% at the applied pressure of 552 kPa. The intrinsic rejection of the BSA is found to be higher than the observed rejection and follows similar trend as that of the observed rejection (see Fig. 6.3). The reflection coefficient (σ) and solute permeability (P_m) value for BSA solute is found to be 0.9637 and 3.0704×10^{-7} m/s, respectively.

6.4.1.3 Effect of feed concentration on BSA separation

An increase in the feed concentration results in a decrease in the permeate flux and increase in the retention as shown in Fig. 6.4. When the feed concentration increases, the surface concentration of the BSA molecules also increases and causes additional resistance.

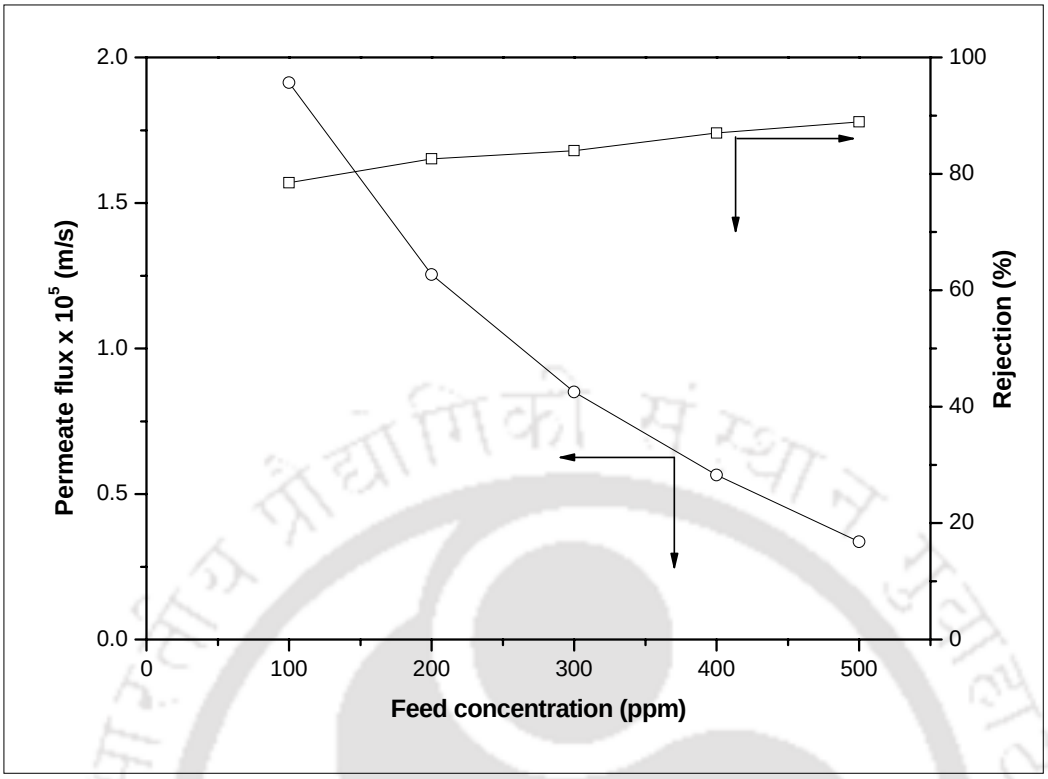

Fig. 6.4 Variation of permeate flux and observed rejection of BSA protein solution with feed concentration. (pressure = 207 kPa; pH =3).

The decline in protein transmission is probably due to the retention of protein in the deposit. The reason for the rapid decline in flux and increase in retention is that the protein agglomerates are formed more rapidly when the concentration of proteins in the solution is high (Persson *et al.*, 2003).

The permeability and rejection of BSA in the present study is compared with other membranes (see Table 6.1) and the result reveals that the fabricated γ-Al_2O_3-clay composite membrane is suitable for BSA separation application. The prepared membrane showed higher rejection compared other polymeric and ceramic membranes. The permeability of the prepared γ-Al_2O_3 membrane is comparable with similar type of membrane on alumina support reported by Thomas *et al.*, (1991).

Table 6.1 Reported permeability and rejection values of BSA on various membranes

Membrane Material	Mean pore size	Feed concentration (ppm)	Permeability (m/s kPa)	Rejection (%)	Reference
γ-Al_2O_3	5.5 nm	500 (pH=7.4)	10.0×10^{-8}	90	Thomas *et al.*, (1991)
Polysulfone (PS)	50 kDa	500 (pH=5.2)	12.0×10^{-8}	79	Ghosh and Cui (1998)
Polyethersulfone (PES)	0.16 µm	400 (pH=3.0)	44.5×10^{-8}	83	Persson *et al.*, (2003)
Nylon	0.2 µm	400 (pH=3.0) 1000 (pH=3.0)	58.3×10^{-8} 55.5×10^{-8}	93 91	Persson *et al.*, (2003)
Polyethersulfone (PES)	50 kDa 100 kDa	500 (pH=4.0) 500 (pH=4.0)	22.0×10^{-8} 35.0×10^{-8}	87 59	Tung *et al.*, (2007)
Polyethersulfone (PES)	50 kDa	500 (pH=5.0)	88.8×10^{-8}	88	Becht et al., (2008)
Polyacrylonitrile (PAN)	0.1 µm	500 (pH=5.0)	90.2×10^{-8}	79	Barroso *et al.*, (2011)
γ-Al_2O_3 membrane	5.1 nm	500 (pH=3)	6.09×10^{-8}	95	Present Work

6.4.2 Separation of electrolyte solutions

$AlCl_3$ and $MgCl_2$ salts are released as effluents from various chemical processes and industries (Stringer and Johnston 2001; Kogel *et al.,* 2006; Sheldon *et al.,* 2007; Hodge and Popovici 1994; Tan *et al.,* 2000). The recovery of these electrolytes is necessary from both environment and economic points of view.

6.4.2.1 Effect of pH of salt solution

The surface charge of the material which depends on the pH of the solution is an important parameter realizing the efficiency of a membrane separation process, especially when removing ionic species. In view of this, the rejection is measured over the ranges of pH (2.5-8) for a constant $MgCl_2$ concentration (3000 ppm) and transmembrane pressure (207 kPa). Figure 6.5 depicts the observed rejection of $MgCl_2$ as a function of pH. The result indicates that the rejection strongly depends on the operating pH value and the highest rejection (75%) is found at pH 2.5.

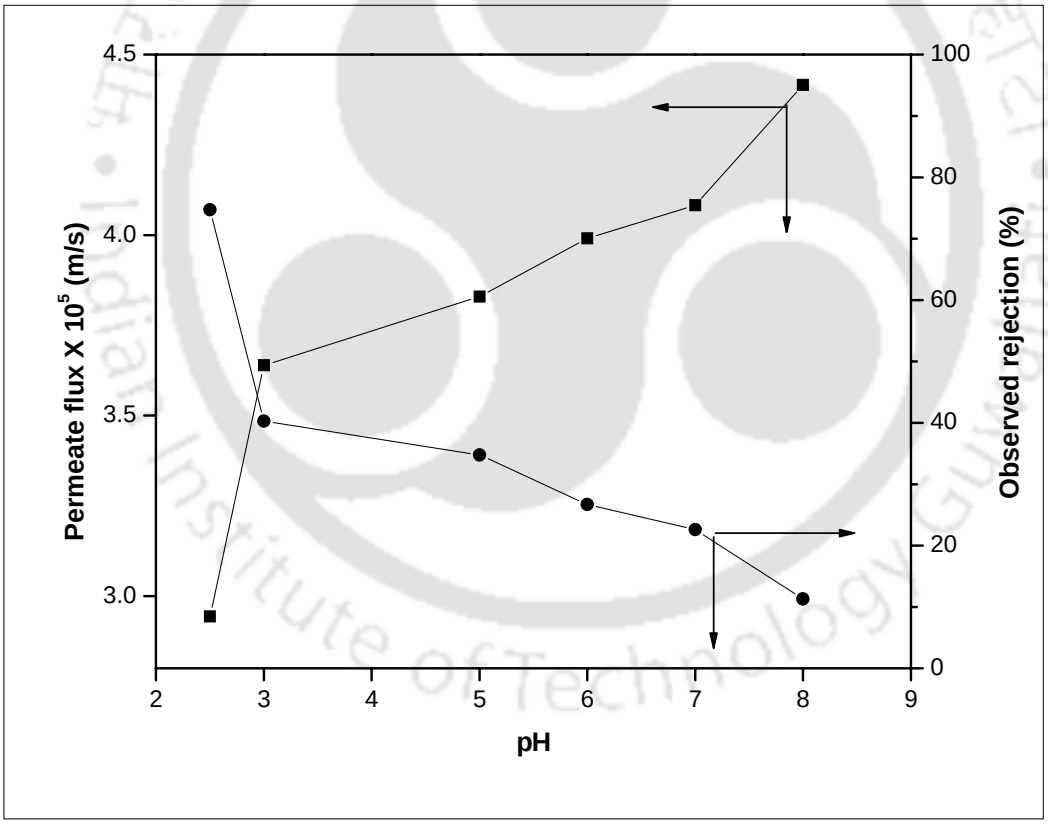

Fig. 6.5 Permeate flux and retention of $MgCl_2$ solution as a function of pH. (Feed concentration = 3000 ppm and applied pressure = 207 kPa).

It is already reported in the literature (Parks 1965; Rios *et al.,* 1996) that the isoelectric point (IEP) of the γ-Al_2O_3 membrane is 8-9 and hence it is electrically positive for the pH values lower than 8-9 and negative for pH values greater than 8-9. So the prepared composite membrane is positively charged at the studied pH during the filtration experiments. With increasing pH of the feed solution from 2.5 to 8, the observed rejection of $MgCl_2$ shows a decreasing trend. This can be explained by the variation of interaction between membrane surface and Mg^{2+} ion at different pH.

When a charged membrane is in contact with an electrolyte solution, the concentration of co-ions (ions with the same charge as the membrane) near the surface of the membrane will be lower than that in solution, whereas the counter-ions, which have the opposite charge, have a higher concentration in the membrane than in the solution. Because of this concentration difference, a potential difference is generated at the interface between the membrane and the solution to maintain electrochemical equilibrium between solution and membrane. By this potential, which is called the Donnan potential, co-ions are repelled by the membrane (Chung *et al.,* 2005). When pH of the solution increases from 2.5 to 8, the surface potential (charge) of the membrane decreases since the IEP of membrane is 8-9. Therefore the repulsion between Mg^{2+} and positively charged membrane decreases and consequently reduces the rejection of Mg^{2+}. Since the cation and anion cannot act independently, Cl^- is also rejected to maintain electroneutrality. When the magnitude of the surface potential decreases, the permeate flux increases due to the decreased electroviscous effect (i.e. decrease in the apparent viscosity of the fluid permeating through the membrane pores) which can be seen from Fig. 6.5 (Nazzal and Wiesner 1994; Huisman *et al.,* 1998). Electroviscous considerations imply a maximum in permeate flux at the IEP of the membrane (Huisman *et al.,* 1998).

6.4.2.2 Effect of type of salts and pressure

In Fig. 6.6, the permeate flux of $AlCl_3$ and $MgCl_2$ salts are plotted against the applied pressure for a fixed concentration of 3000 ppm and pH of 3. The solution permeability for both the salts is lower than that of the pure water with increasing pressure. It reveals that an additional resistance is created by the presence of Al^{3+} and Mg^{2+} salts that reduces the flow. It can be seen from Fig. 6.6 that the permeate flux increases with applied pressure. This can be explained by considering salt transport through the membrane as a result of diffusion and convection, which are respectively due to concentration and pressure gradient across the membrane.

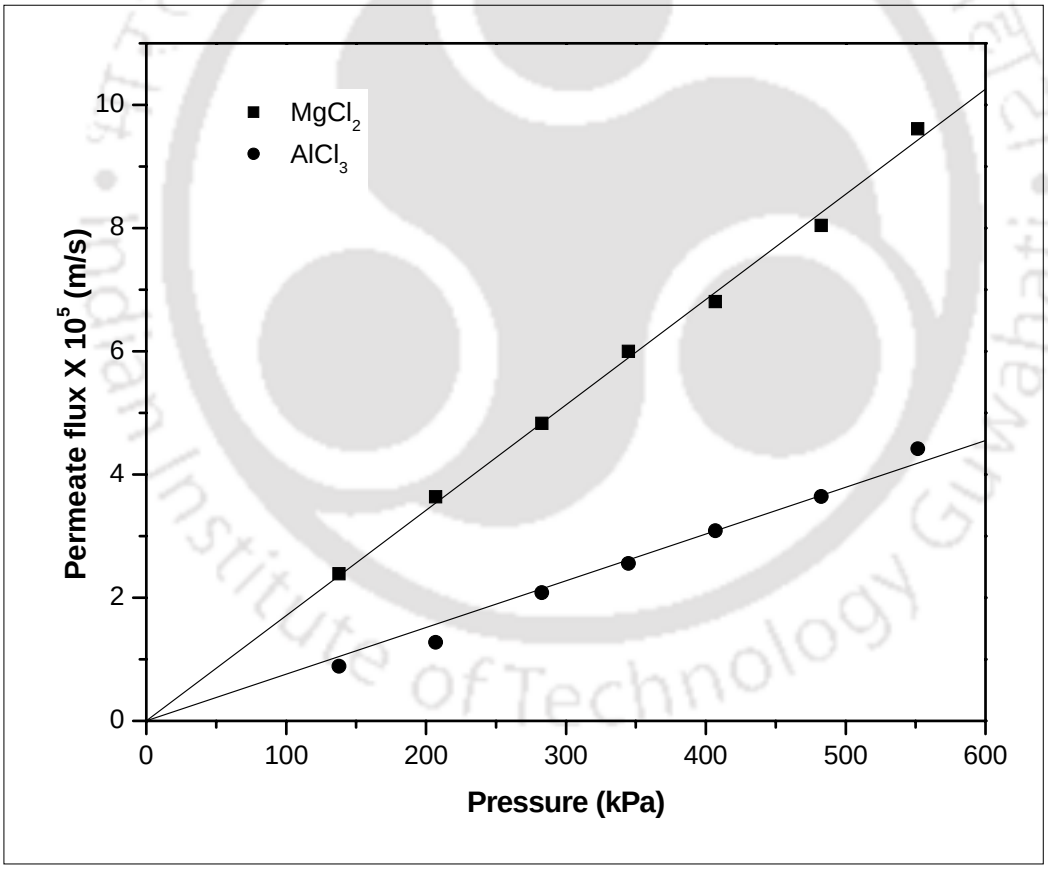

Fig. 6.6 Variation of permeate flux with applied pressure for $MgCl_2$ and $AlCl_3$ solution. (Feed concentration = 3000 ppm and pH = 3).

At lower applied pressure, diffusion contributes and convection dominates the overall process at higher applied pressure. The permeate flux of $MgCl_2$ is higher than the $AlCl_3$ salt solution which depends upon the electrostatic interaction between the electrolyte and surface charge of the membrane giving additional resistance for flow through membrane. The effect of pressure on the rejection of Mg^{2+} and Al^{3+} ions is also shown in Fig. 6.7. The membrane shows the following rejection sequence: $R(AlCl_3)>R(MgCl_2)$ i.e. rejection increases when the valence of associated cation increases. This is in accordance with Donnan exclusion model. Donnan exclusion effect will be more if cation charge is high. Since the membrane is positively charged, Al^{3+} ion is excluded more than the Mg^{2+}, which enhances the rejection of $AlCl_3$ salt from its aqueous solution. Additionally, the diffusion coefficient of $AlCl_3$ is also lower than $MgCl_2$ salt. As expected, a lower diffusion contribution to the salt transport through the membrane yields a higher retention and similar type of rejection trend was reported for positively charged polymeric membranes (Peeters *et al.,* 1998; Xu and Lebrun 1999; Wang *et al.,* 2002; Chung *et al.,* 2005; Shang *et al.,* 2005). The observed rejection for both the salts decreases with increase in the pressure as has been reported in literature (Shukla and. Kumar 2005). With increasing pressure, there is more accumulation of solute particles on the membrane surface that causes severe concentration polarization and also increases the permeate concentration due to increasing convective flux. Thus observed rejection is less as it is calculated using equation (6.1) which is based on bulk feed concentration. With this observation, the Spiegler-Kedem model has been used to determine the intrinsic (real) rejection, which calculates the solute concentration at the membrane surface by taking the account of concentration polarization effects.

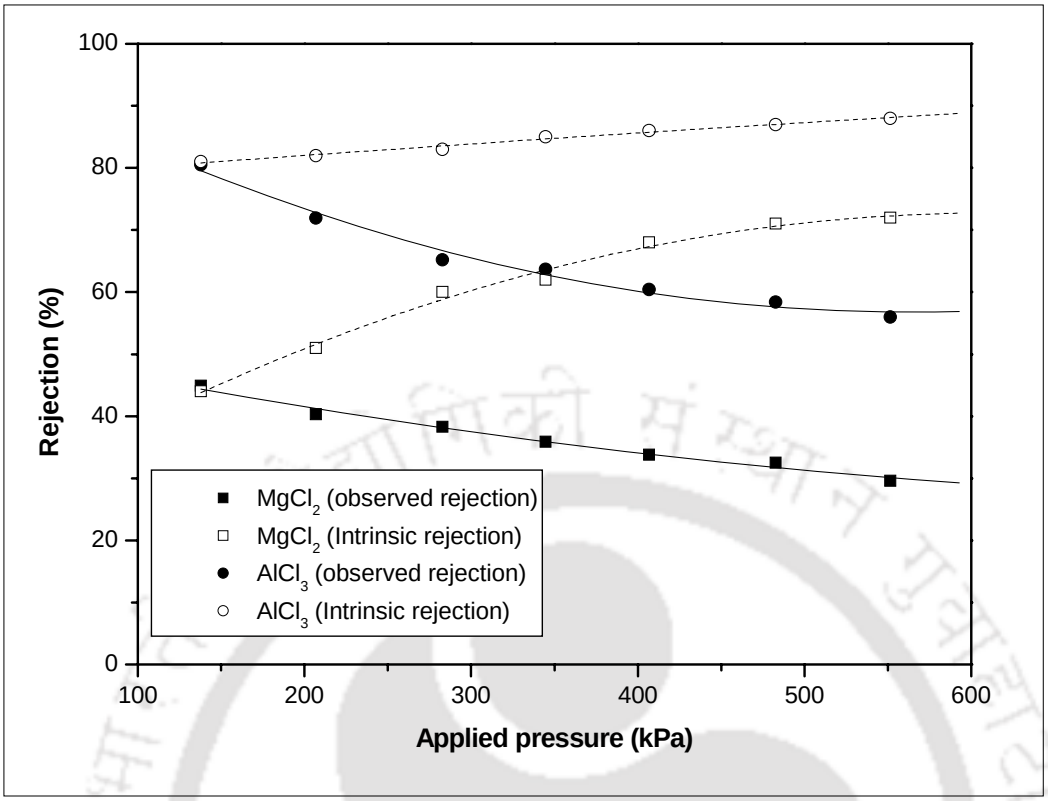

Fig. 6.7 Rejection of $MgCl_2$ and $AlCl_3$ as a function of applied pressure. (Feed concentration = 3000 ppm and pH = 3).

The model result shows that the concentration at the membrane surface is 2-3 times higher than the bulk concentration for both the solutes. As can be seen from Fig. 6.7, the intrinsic (real) rejection increases with the applied pressure, which is a common trend followed by electrolytes through charged membranes (Pugazhenthi and Kumar 2005; Shukla and Kumar 2005). The maximum rejection of $MgCl_2$ and $AlCl_3$ salt solution is found to be 72 % and 88 %, respectively.

The values of reflection coefficient (σ) and the solute permeability (P_m) have been calculated from experimental data of the observed rejection and the permeate flux using equations (6.2)-(6.6). The σ value for $MgCl_2$ and $AlCl_3$ solute is found to be 0.77 and 0.94, respectively. The solute permeability (P_m) value for $MgCl_2$ and $AlCl_3$

solute is found to be 8.442×10^{-6} and 2.51×10^{-6} m/s, respectively. It is well established that the values of P_m and σ depend on the salt concentration, type of salts and the type of membrane (Hilal *et al.,* 2005). The value of P_m is higher for $MgCl_2$ than $AlCl_3$, which is due to the high amount of salt passing through the membrane. So the σ value is lower for $MgCl_2$ salt separation due to the decreasing of the salt rejection.

The relationship between permeate flux and intrinsic rejection is generally described by Kimura-Sourirajan model (Kimura and Sourirajan 1967; Levenstein *et al.,* 1996).

$$J = P_m \left(\frac{R_{int}}{1-R_{int}} \right) \qquad (6.7)$$

where, J and P_m are the permeate flux (m/s) and solute permeability of the membrane (m/s), respectively. In this model, the maximum intrinsic rejection can reach 100% when permeate flux tends to be infinite; and the minimum rejection equals to zero when the permeate flux tends to zero. It can be seen from the Fig. 6.6 and 6.7 that the intrinsic rejection increases with increasing permeate flux. The strong dependency of separation on the permeate flux was also observed for negatively charged membrane, neutral membrane (Tsuru *et al.,* 1999) and positively charged membrane (Xu and Lebrun 1999). The obtained experimental result also confirms that it is true for γ-Al_2O_3 composite membrane, which is positively charged at the studied pH.

6.4.2.3 Effect of salt concentration

Figure 6.8 depicts the effect of salt concentration on rejection and permeate flux for a fixed applied pressure (207 kPa) and pH (3). It is observed that the permeate flux decreases with the increase in salt concentration because of the concentration polarization and partial plugging of pores of the membrane at higher concentration. At

the studied pH, the membrane is positively charged. So $AlCl_3$ is much better retained than $MgCl_2$. It is seen that the observed rejection decreases with increase in salt concentration. The higher value of observed rejection is obtained for both salts at lower feed concentration of 1000 ppm. At higher salt concentration, the membrane charge will be shielded to a large extent, resulting in a lower effective charge and consequently a decrease in rejection is observed. The decrease in retention with increasing salt concentration is typical of charged membranes, for which Donnan exclusion plays an important role (Chung *et al.,* 2005). The effect of Donnan exclusion reduces with increasing electrolyte concentrations.

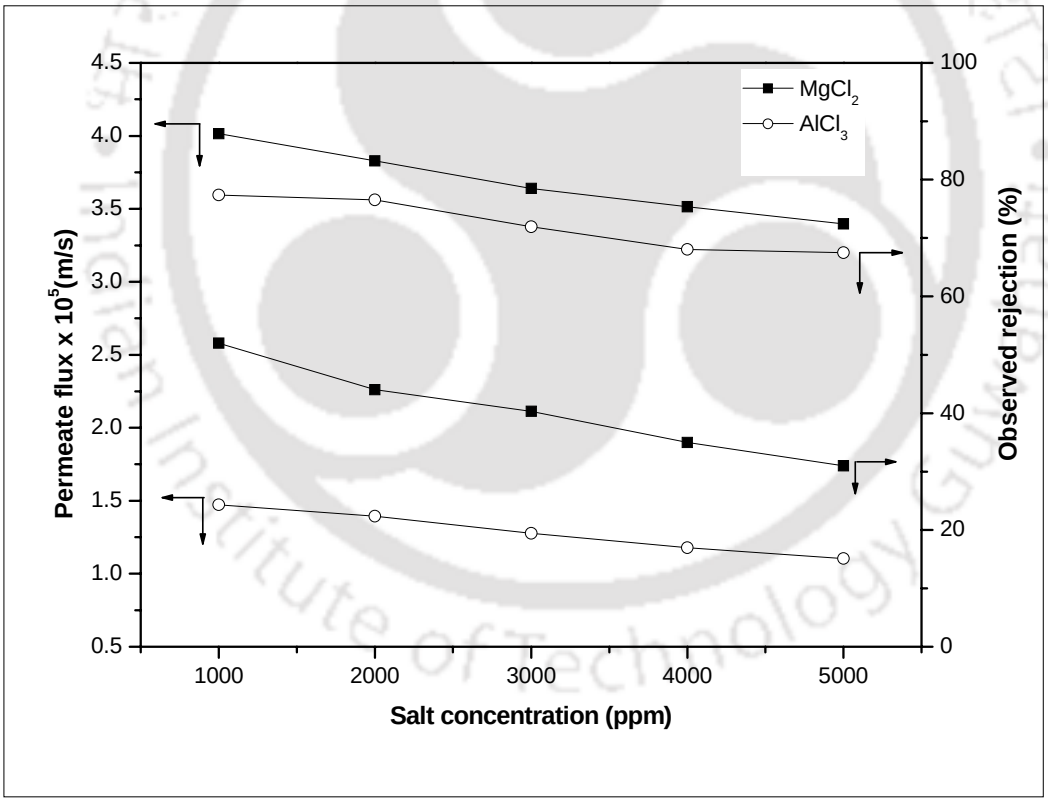

Fig. 6.8 Variation of rejection and permeate flux of $MgCl_2$ and $AlCl_3$ salt solution as a function of feed concentration. (Applied pressure = 207 kPa and pH of salt solution = 3).

With increase in salt concentration, surface concentration also increases leading to severe concentration polarization that enhances solute permeation by diffusion. Consequently, the permeate concentration also increases. In case of $AlCl_3$ (Fig. 6.8), only a small decrease in rejection is observed with increasing salt concentration, which indicates that the charge effect stays nearly constant for these concentrations. This means that either the effect of membrane charge is so small or the charge effect is still important but does not further decrease at higher concentrations.

6.4.3 Comparison of the performance of this membrane with other membranes

The rejection (72% for $MgCl_2$ and 88% for $AlCl_3$) reported in this work at 550 kPa with salt concentration of 3000 ppm is comparable or even higher than those reported in the literature (Rios *et al.,* 1996; Afonso *et al.,* 2001; Hilal *et al.,* 2005; Shukla and Kumar 2005; Skluzacek *et al.,* 2006; Wu *et al*., 2006). Shukla and Kumar (2005) have obtained the enhanced rejection for $AlCl_3$ (90% for both Z_2 and Z_3 with permeate flux of ~1.75×10^{-6} m/s) using chemically modified zeolite-clay composite membranes than the unmodified membrane (84 % for Z_1 with permeate flux of ~ 4.25×10^{-6} m/s) at 420 kPa for salt concentration of 500 ppm. In another work (Wu *et al.,* 2006), a negatively charged polyamide (PA) composite membrane showed 96.5% (permeate flux of 5.3×10^{-6} m/s) and 92.4% (permeate flux of 4.2×10^{-6} m/s) rejection, respectively for $MgCl_2$ and $AlCl_3$ at 1600 kPa for salt concentration of 2000 ppm. However, the rejection of $MgCl_2$ using commercial membranes, N30F (Hilal *et al.,* 2005) and Desal G-20 (Afonso *et al.,* 2001) was about 6% (permeate flux of ~0.9×10^{-5} m/s at 900 kPa for the salt concentration of 5000 ppm) and 70% (permeate flux of ~2.0×10^{-5} m/s at 1300 kPa with the salt concentration of 20 ppm), respectively. The iron modified silica membrane (Skluzacek *et al.,* 2006) and γ-Al_2O_3 ceramic membrane (having pore size of 1 nm) supported on macroporous α-alumina (Rios *et al.,* 1996) showed

10% (permeate flux of ~ 6.9×10^{-5} m/s at 1725 kPa and salt concentration of 6000 ppm) and 96% (permeate flux of ~0.7×10^{-5} m/s at 1000 kPa and salt concentration of 2000 ppm) $MgCl_2$ rejection, respectively.

As compared to the results reported in the literature, the permeate flux of the membrane reported in this work (9.6×10^{-5} m/s for $MgCl_2$ and 4.4×10^{-5} m/s for $AlCl_3$) is one order higher even at lower applied pressure of 550 kPa. In addition, the net separation, which is permeate flux times the difference in concentration of solute in the retentate and permeate is also high. The above comparison study confirms that that the membrane reported in this work is comparable or even better than the commercial membranes and other inorganic membranes reported in the literature.

6.5 COST ESTIMATION

Cost estimation for the separation of BSA and electrolyte solution with the fabricated γ-Al_2O_3-clay composite for large scale operation has made based on the obtained experimental results (Cheryan 1998; Singh and Cheryan 1998). The total cost of the membrane system including the equipment cost (muffle furnace ($1020), permeation setup ($170) and compressor ($150)), piping and instrumentation cost (~ 40% of equipment cost) is found to be $1836. For instance, the prepared γ-Al_2O_3-clay composite membrane is operated at a pressure of 406 kPa and feed concentration of 500 ppm with pH = 3; then the obtained permeate flux is 3×10^{-5} m/s. Therefore, total amount of BSA treated in a year (8 h operation per day) is 400 L/year. For treating 400 L/year, the energy cost required for operating compressor (1 hp and 8 h/day) for the batch permeation setup is estimated as $160/year. The depreciation value of the ceramic membrane is calculated using a 7-year straight line depreciation method and found to be $ 0.021/year. The life time of the ceramic membranes is generally around 3-5 years. However, considering the worst case, the membrane life time is taken as 2

years and the membrane replacement cost is around $ 0.036/year. Membrane cleaning cost, maintenance cost (@ 3 % of total cost of membrane system) and labor cost (2% of total cost of membrane system) are also estimated and presented in Table 6.2. Similarly, the cost is estimated for the separation of electrolyte solutions. Since the same equipments have been used for the separation studies of electrolyte solution, the estimated cost remains the same. However the change in the permeate flux values indicates that the amount of feed treated per year will vary depends on the process under similar operating conditions (see Table 6.2). The detailed cost analysis reveals that the prepared composite membrane is cost effective and could be used as an alternate for the expensive ceramic membranes.

Table 6.2 Estimated cost analysis for BSA and electrolytes separation

Amount of BSA and electrolytes processed per year	
BSA	410 L/year
$MgCl_2$	310 L/year
$AlCl_3$	110 L/year
Details	**Estimated cost**
Total direct (fixed) cost	$ 1836
Operating cost	$ 160/year
Membrane cost	$ 26.04/m^2
Depreciation	$ 0.021/year
Membrane replacement cost	$ 0.036/year
Maintenance cost	$ 55/year
Labor cost	$ 36.72/year

6.6 SUMMARY

Separation characteristic of the membrane is successfully checked by performing filtration studies of BSA and electrolytes. The obtained results confirm that the permeate flux and rejection are strongly affected by the applied pressure, solution pH and feed concentration for both BSA and electrolyte solutions. The maximum rejection of BSA can be obtained at lower solution pH (3), higher feed concentration (500 ppm) and at higher applied pressure (552 kPa). The rejections to inorganic electrolytes ($MgCl_2$ and $AlCl_3$) declined with the growth of electrolyte concentrations accordance to Donnan theory. The intrinsic rejections are found to increase with an increase in the applied pressure, a trend typical of the separation of electrolytes through the charged membranes. The maximum rejection of $MgCl_2$ and $AlCl_3$ is found to be 72% and 88%, respectively for salt concentration of 3000 ppm. The obtained results clearly indicate that the prepared γ-Al_2O_3-clay composite membrane has a good potential for the separation of BSA and electrolyte solution. It could be utilized as a low cost alternative for high cost alumina, zirconia and titania composite membranes.

Chapter 7

CONCLUSIONS AND FUTURE SCOPES

This Chapter summarizes the conclusions and future scope of the research work. The main theme of this thesis is to fabricate a low cost composite membrane for liquid phase separation applications. During the study, several interesting issues have been explored that are broadly associated with material and surface science. These observations are concluded in the following section.

7.1 CONCLUSIONS

- Porous ceramic support (support-I) was successfully prepared by uniaxial compaction method using low cost raw materials and optimized with sintering temperature.
- The support sintered at 950°C was found to be the optimum support for membrane applications due to its good mechanical strength (28 MPa), better pore diameter (0.98 μm) and porosity (44%).

- The effect of addition of TiO_2 powder for the fabrication of two different membrane supports (3G and 6G supports) was investigated for the liquid phase separation of oil and BSA and the results were compared with the support-I.
- Higher rejection (90-99%) was obtained for all the supports to achieve the separation of oil from its solution. A maximum rejection of 40% was obtained for BSA from its solution.
- No significant changes in the rejection were observed by the addition of TiO_2. Also it enhances the cost of the membrane supports. Therefore, support-I was utilized for the development of a selective layer on it to increase the separation potential of the BSA from its aqueous solution.
- A γ-Al_2O_3-clay composite membrane was effectively developed using a boehmite sol derived from inexpensive aluminium chloride salt. The pore size of the fabricated composite membrane was in the range of 5.4-13.6 nm. Also, the γ-Al_2O_3-clay composite membrane showed comparatively higher pure water permeability (2.357×10^{-7} m/s.kPa).
- The fabricated composite membrane was investigated for the separation of BSA and electrolytes ($AlCl_3$ and $MgCl_2$) from aqueous solutions. Higher rejection (99% for BSA, 72% for $MgCl_2$ and 88% for $AlCl_3$) and permeate flux (3.4×10^{-5} m/s for BSA, 9.6×10^{-5} m/s for $MgCl_2$ and 4.4×10^{-5} m/s for $AlCl_3$) were obtained for both BSA and electrolytes. This confirmed that the composite membrane was comparable or even better than other commercial membranes and has the potential for liquid phase separation applications.

- The estimated cost of the fabricated membrane (26.04 $/m^2) would be relatively lower than other commercial membranes. Therefore, it could be utilized as a low cost alternative for high cost alumina, zirconia and titania membranes.

7.2 FUTURE SCOPES

Based on the findings of this thesis work, some recommendations for future research in this field are presented as follows:

- The effect of stirring (dead-end filtration setup equipped with stirrer) for the separation of BSA and electrolytes using γ-Al_2O_3-clay composite membrane can be studied.
- The membrane can also be operated in cross flow mode using a cross flow experimental setup to explore the separation performance of BSA and electrolytes. These results can be compared with the performance of dead-end filtration that would give more insight on the separation mechanism.
- The work can be extended by varying the support raw materials, selective layers, and coating techniques. The membranes can also be utilized for other separation and purification applications such as separation of dyes, treatment of tannery effluents and concentration of juices.
- Developing other membrane configuration (example: tubular) using the suggested low cost raw materials of given compositions must be useful for industrial application

Appendix I

LIST OF COMMERCIAL MEMBRANE SUPPORTS PRODUCERS

Support material	Commercial producer	Details of the membrane support	Reference
Titania	TAMI	Tubular support: Pore size = 1.7 µm Porosity = 32%	Wang *et al.*, 2008
α-alumina	PALL	Tubular support O.D=10 mm Length = 80 mm Pore size = 1.0 µm Porosity = 40%	Li *et al.*, 2008
α-alumina	Membralox membrane (T 1.70), Pall Exekia	Tubular composite membrane with three concentric layers of α-alumina: Layer 1 T = 1.5 mm, Pore diameter = 12µm Layer 2 T = 0.04 mm, Pore diameter = 0.8 µm Layer 3 T = 0.02 mm, Pore diameter = 0.2µm	Haag *et al.*, 2006

Support material	Commercial producer	Details of the membrane support	Reference
α-alumina	Whatman Anopore Filters	Circular Disc support: Diameter = 47 mm T = 50 μm Pore size = 0.2 μm	Zhang *et al.*, 2006
α-alumina	Netzsch	Multichannel support (19 Channels) Permeation area = 0.2 m^2 Pore size = 10 nm	Basso *et al*, 2006
α-alumina	NOK Co. (Japan).	Tubular support: O.D=2.7 mm L = 50 mm Pore size = 0.1 μm Porosity = 40%	Nomura *et al.*, 2006
Tubular AZT (a mixture of alumina, zirconia, and titania)	CeRAM Inside, TAMI North America, St. Laurent, Quebec, Canada)	Tubular ceramic membrane with clover-leaf design O.D=10 mm L=80 mm	Karnik *et al.*, 2005
α-alumina and Titania	TAMI Industry, Nyons, France	Rectangular plate membranes: (75mm×25mm×2.5 mm) Pore size = 1.0 μm Porosity = 35%	Fievet *et al.*, 2003
α-alumina	Schumacker GmbH (Germany).	Tubular support: I.D = 7 mm O.D = 10 mm L = 250 mm Pore size = 0.2 μm	Tavolaro 2002

Support material	**Commercial producer**	**Details of the membrane support**	**Reference**
α-alumina	Dongsuh Company, Korea	Tubular support: I.D = 6.0 mm O.D = 7.2 mm L = 28 mm Pore size = 1.0 µm Porosity = 40%	Kang and Gavalas 2002
α-alumina	Inocermic and SCT, France	Tubular support: I.D= 7 mm O.D=10 mm L = 30-50 mm Pore size = 5, 200, 500 nm	Bernal *et al.*, 2002
α-alumina	Sen Bool Sintering Co., Korea)	Tubular support: Pore size =10 µm	Hwang *et al.*, 2001
α-alumina	Vel-terop BV, Netherlands	Circular disc shaped support: Diameter = 25 mm T= 2 mm Available pore sizes: 0.08, 0.15, 2 and 9 µm Tubular support: I.D= 8 mm O.D=14 mm Available pore sizes: 2.5 and 9 µm	Romanos *et al.*, 2001
γ-alumina	US Filter	Tubular support: I.D= 7 mm O.D=10 mm L=55 mm Pore size = 5 nm	Tsai *et al.*, 2000
α-alumina	NGK Insulators, Ltd.)	Circular disc shaped support: Diameter = 12 mm Pore size = 0.1 µm	Matsufuj *et al.*, 2000

Support material	Commercial producer	Details of the membrane support	Reference
α-alumina with an inner layer of α-alumina	US Filters	Tubular support: I.D = 7 mm O.D = 10 mm Pore diameter = 200 nm (γ-alumina)	Tuan *et al.*, 1999
α-alumina tubular membrane with an γ-alumina inner surface	US Filters	Tubular support: I.D = 6.5 mm O.D = 10 mm L = 84 mm (cut down length) Pore diameter = 5 nm (γ-alumina)	Jia *et al.*, 1994
ceramic	KPM-Konigliche Porzellan-Manufactur Berlin GmbH, Germany (type P80)	Circular disc shaped support: Diameter = 50 mm T = 3-5 mm Pore size: 0.8 μm Porosity = 45%	Jia *et al.*, 1993
Silica	Microporous Glass, Asahi Glass Inc., Tokyo, Japan	Circular disc shaped support: Φ = 47 mm T = 0.88 mm Pore size: 0.41 μm	Castro *et al.*, 1993
α-alumina	Philips, Elcoma	Circular disc shaped support: Diameter = 39 mm T= 2 – 2.2 mm Pore size: 0.13 μm Porosity = 46%	Leenaars and Burggraaf 1985
α-alumina + SiO_2	Staatliche Porzellan Manufaktur, Berlin, West Germany (type P80)	Circular disc shaped support: Pore size = 0.8 μm Porosity = 45%	Leenaars and Burggraaf 1985

References

Afonso, M.D., Hagmeyer, G. and Gimbel, R., 2001. Streaming Potential Measurements to Assess the Variation of Nanofiltration Membranes Surface Charge with the Concentration of Salt Solutions, *Separation and Purification Technology*, **22-23** 529-541.

Afonso, A., Miranda, J.M. and Campos, J.B.L.M., 2009. Numerical Study of BSA Ultrafiltration in the Limiting Flux Regime - Effect of Variable Physical Properties, *Desalination*, **249**(3) 1139-1150.

Agrafiotis, C. and Tsetsekou, A., 2002. Deposition of Meso-porous γ-alumina Coatings on Ceramic Honeycombs by Sol-Gel Methods, *Journal of the European Ceramic Society*, **22**(4) 423-434.

Ahmad, A.L., Leo, C.P. and Shukor, S.R.A., 2008. Preparation of γ-alumina Thin Layer with Bimodal Pore Size Distribution Diminution of Transport Resistance in Bi-Layered Membrane, *Thin Solid Films*, **516**(12) 4319-4324.

Razi, A.F., Pendashteh, A., Abdullah, L.C., Biak, D.R.A., Madaeni, S.S. and Abidin, Z.Z., 2009. Review of Technologies for Oil and Gas Produced Water Treatment, *Journal of Hazardous Materials*, **170**(2-3) 530-551.

Aimable, A., Buscaglia, M.T., Buscaglia, V. and Bowen, P., 2010. Polymer-assisted Precipitation of ZnO Nanoparticles with Narrow Particle Size Distribution, *Journal of the European Ceramic Society*, **30**(2) 591-598.

Alami-Younssi, S., Larbot, A., Persin, M., Sarrazin, J. and Cot, L., 1994. Gamma Alumina Nanofiltration Membrane Application to the Rejection of Metallic Cations, *Journal of Membrane Science*, **91**(1-2) 87-95.

Alami-Younssi, S., Larbot, A., Persin, M., Sarrazin, J. and Cot, L., 1995. Rejection of Mineral Salts on a Gamma Alumina Nanofiltration Membrane Application to Environmental Process, *Journal of Membrane Science*, **102** 123-129.

Albani, M.I.D. and Arciprete, C.P., 1992. A Study of Pore Size Distribution and Mean Pore Size on Unsupported Gamma-Alumina Membranes Prepared by Modifications Introduced in the Alkoxide Hydrolysis Step, *Journal of Membrane Science*, **69**(1-2) 21-28.

Almandoz, M.C., Marchese, J., Pradanos, P., Palacio, L. and Hernandez, A., 2004. Preparation and Characterization of Non-Supported Microfiltration Membranes from Aluminosilicates, *Journal of Membrane Science*, **241**(1) 95-103.

Anderson, M.A., Gieselmann, M.J. and Xu, Q., 1988. Titania and Alumina Ceramic Membranes, *Journal of Membrane Science*, **39**(3) 243-258.

Arnot, T.C., Field, R.W. and Koltuniewicz, A.B., 2000. Cross-flow and Dead-end Microfiltration of Oily-water Emulsions. Part II. Mechanisms and Modelling of Flux Decline, *Journal of Membrane Science*, **169**(1) 1-15.

Bader, M.S.H., 2007. Seawater versus Produced Water in Oil-Fields Water Injection Operations, *Desalination*, **208**(1-3) 159-168.

Baker, R.H., 2004. Membrane Technology and Applications, Second Edition, John Wiley and Sons Ltd, Chichester, England.

Bandini, S., Drei, J. and Vezzani, D., 2005. The Role of pH and Concentration on the Ion Rejection in Polyamide Nanofiltration Membranes, *Journal of Membrane Science*, **264**(1-2) 65-74.

Barroso, T., Temtem, M., Casimiro, T. and Ricardo, A.A., 2011. Antifouling Performance of Poly(acrylonitrile)-Based Membranes: From Green Synthesis to Application, *The Journal of Supercritical Fluids*, **56**(3) 312-321.

Basso, R.C., Viotto, L.A. and Goncalves, L.A.G., 2006. Cleaning Process in Ceramic Membrane Used for the Ultrafiltration of Crude Soybean Oil, *Desalination*, **200**(1-3) 85-86.

Becht, N.O., Malik, D.J. and Tarleton, E.S., 2008. Evaluation and Comparison of Protein Ultrafiltration Test Results: Dead-End Stirred Cell Compared with a Cross-Flow System, *Separation and Purification Technology*, **62**(1) 228-239.

Belouatek, A., Benderdouche, N., Addou, A., Ouagued, A. and Bettahar, N., 2005. Preparation of Inorganic Supports for Liquid Waste Treatment, *Microporous and Mesoporous Materials*, **85**(1-2) 163-168.

Benito, J.M., Conesa, A., Rubio, F. and Rodriguez, M.A., 2005. Preparation and Characterization of Tubular Ceramic Membranes for Treatment of Oil Emulsions, *Journal of the European Ceramic Society*, **25**(11) 1895-1903.

Bernal, M.P., Coronas, J., Menendez, M. and Santamaria, J., 2002. Characterization of Zeolite Membranes by Measurement of Permeation Fluxes in the Presence of Adsorbable Species, *Industrial & Engineering Chemistry Research*, **41**(20) 5071-5078.

Bhanushali, D., Kloos, S., Kurth C. and Bhattacharyya, D., 2001. Performance of Solvent-Resistant Membranes for Non-Aqueous Systems: Solvent Permeation Results and Modeling, *Journal of Membrane Science,* **189**(1) 1-21.

Bhattacharjee, S. and Bhattacharya, P.K., 1992. Flux Decline Behaviour with Low Molecular Weight Solutes during Ultrafiltration in an Unstirred Batch Cell, *Journal of Membrane Science,* **72**(2) 149-161

Bhide, B.D. and Stern S.A., 1991. A New Evaluation of Membrane Processes Enrichment of Air. II. Effects of Economic Membrane Properties, *Journal of Membrane Science*, **62**(1) 37-58.

Bi, Y.B., Wang, H.F. and Lu, W., 2011. The Influence on the Properties of Microporous Mullite of Adding Different Burning-Out Materials, Advanced Material Research, **214** 84-88.

Boudaira, B., Harabia, A., Bouzerara F. and Condom, S., 2009. Preparation and Characterization of Microfiltration Membranes and their Supports Using Kaolin (DD2) and $CaCO_3$, *Desalination and Water Treatment*, **9**(1-3) 142–148.

Bouzerara, F., Harabi, A., Achour, S. and Larbot, A., 2006. Porous Ceramic Supports for Membranes Prepared from Kaolin and Doloma Mixtures, *Journal of the European Ceramic Society*, **26**(9) 1663-1671.

Bowen, W.R. and Mukhtar, H., 1996. Characterisation and Prediction of Separation Performance of Nanofiltration Membranes, *Journal of Membrane Science*, **112**(2) 263-274.

Brinker, C.J. and Scherer, G.W., 1990. Sol-Gel Science: The Physics and Chemistry of Sol-Gel Processing, Elsevier, San Diego, CA.

Brookes, K., 2008. Economics and the Nano Powder Story that Just Won't Sell, *Metal Powder Report*, **62**(8) 10-12.

Buelna, G. and Lin Y.S., 1999. Sol–gel-Derived Mesoporous γ-alumina Granules, *Microporous and Mesoporous Materials*, 30(2-3) 359-369.

Burggraaf, A.J. and Cot, L., 1996. Fundamentals of Inorganic Membrane Science and Technology, Elsevier, Amsterdam, The Netherlands.

Caro, J., Noack, M., Kolsch, P. and Schafer, R., 2000. Zeolite Membranes - State of Their Development and Perspective, *Microporous and Mesoporous Materials,* **38**(1), 3-24.

Casa, E.J., Guadix, A., Ibanez, R. and Guadix, E.M., 2007. Influence of pH and Salt Concentration on the Cross-Flow Microfiltration of BSA through a Ceramic Membrane. *Biochemical Engineering Journal*, **33**(2) 110-115.

Castellano, M., Turturro, A., Riani, P., Montanari, T., Finocchio, E., Ramis, G. and Busca, G., 2010. Bulk and Surface Properties of Commercial Kaolins, *Applied Clay Science*, **48**(3) 446-454.

Castillo, M.L.G., Beltran, F.H., Fripiat, J.J., Hernandez, A.R., Leon, R.G., Bolanos, J.N., Cervantes, A.T. and Bokhimi, X., 2005. Physicochemical Properties of Aluminas Obtained from Different Aluminum Salts, *Catalysis Today*, **107-108** 874-878.

Castro, R.P., Cohen, Y. and Monbouquette, H.G., 1993. The Permeability Behavior of Polyvinylpyrrolidone-modified Porous Silica Membranes, *Journal of Membrane Science*, **84**(1-2) 151-160

Chakrabarty, B., Ghoshal A.K. and Purkait, M.K., 2008. Ultrafiltration of Stable Oil-in-Water Emulsion by Polysulfone Membrane, *Journal of Membrane Science*, **325**(1) 427-437.

Chakradhar, R.P.S., Nagabhushana, B.M., Chandrappa, G.T., Ramesh, K.P. and Rao, J.L., 2006. Solution Combustion Derived Nanocrystalline Macroporous Wollastonite Ceramics, *Materials Chemistry and Physics*, **95**(1) 169-175.

Chang, C.H., Gopalan, R. and Lin, Y.S., 1994. A Comparative Study on Thermal and Hydrothermal Stability of Alumina, Titania and Zirconia Membranes, *Journal of Membrane Science*, **91**(1-2) 27-45.

Chang, Q., Zhang, L., Liu, X., Peng, D. and Meng, G., 2005. Preparation of Crack-free ZrO_2 Membrane on Al_2O_3 Support with ZrO_2–Al_2O_3 Composite Intermediate Layers, *Journal of Membrane Science*, **250**(1-2) 105-111.

Chen, J., Li, J., Zhan, X., Han X. and Chen, C., 2010. Effect of PEG Additives on Properties and Morphologies of Polyetherimide Membranes Prepared by Phase Inversion, *Frontiers of Chemical Engineering in China*, **4**(3) 300-306.

Chen, W., Peng, J., Su, Y., Zheng, L., Wang, L. and Jiang, Z., 2009. Separation of Oil/water Emulsion using Pluronic F127 Modified Polyethersulfone Ultrafiltration Membranes, *Separation and Purification Technology*, **66**(3) 591-597.

Cheryan, M., 1998. Ultrafiltration and Microfiltration Handbook, Technomic Publishing Company, Basel, Switzerland.

Chowdhury, S.R., Blank, D.H.A. and Elshof, J.E., 2005. Factors Influencing the Transport of Short-Chain Alcohols through Mesoporous γ-Alumina Membranes, *Journal of Physical Chemistry B*, **109**(47), 22141-22146.

Chowdhury, S.R., Schmuhl, R., Keizer, K., Elshof, J.E. and Blank, D.H.A., 2003. Pore Size and Surface Chemistry Effects on the Transport of Hydrophobic and Hydrophilic Solvents through Mesoporous γ-Alumina and Silica MCM-48, *Journal of Membrane Science*, **225**(1-2) 177-186.

Chuah, G.K., Jaenicke, S. and Xu, T.H., 2000. The Effect of Digestion on the Surface Area and Porosity of Alumina, *Microporous and Mesoporous Materials*, **37**(3) 345-353.

Chung, C.V., Buu, N.Q. and Chau, N.H., 2005. Influence of Surface Charge and Solution pH on the Performance Characteristics of a Nanofiltration Membrane, *Science and Technology of Advanced Materials*, **6**(3-4) 246-250.

Colomban, Ph., 1988. Raman Study of the Formation of Transition Alumina Single Crystal from Protonic β/β″ Aluminas, *Journal of Materials Science Letters*, **7**(12) 1324-1326.

Cross, A.D., 1964. An Introduction to Practical IR Spectroscopy, Butterworth, London,

Cui, J., Zhang, X., Liu, H., Liu, S. and Yeung, K.L., 2008. Preparation and Application of Zeolite/Ceramic Microfiltration Membranes for Treatment of Oil Contaminated Water, *Journal of Membrane Science*, **325**(1) 420-426.

Cultrone, G., Navarro, C.R., Sebastian, E., Cazalla O. and Torre, M.J., 2001. Carbonate and Silicate Phase Reactions during Ceramic Firing, *European Journal of Mineralogy*, **13**(3) 621-634.

Cumming, I.W., Holdich, R.G. and Smith, I.D., 2000. The Rejection of Oil by Microfiltration of a Stabilized Kerosene/Water Emulsion, *Journal of Membrane Science*, **169**(1) 147-155.

Darcovich, K., Roussel, D. and Toll, F.N.., 2001. Sintering Effects Related to Filtration Properties of Porous Continuously Gradient Ceramic Structures, *Journal of Membrane Science*, **183**(2) 293-303.

Darcovich, K., Dal-Cin, M.M. and Gros, B., 2009. Membrane Mass Transport Modeling with the Periodic Boundary Condition, *Computers and Chemical Engineering*, **33**(1) 213-224.

De Lange, R.S.A., Hekkink, J.H.A., Keizer, K. and Burggraaf, A.J., 1995. Formation and Characterization of Supported Microporous Ceramic Membranes Prepared by Sol-Gel Modification Techniques, *Journal of Membrane Science*, **99**(1) 57-75,

De Lint, W.B.S. and Benes, N.E., 2005. Separation Properties of γ-alumina Nanofiltration Membranes Compared to Charge Regulation Model Predictions, *Journal of Membrane Science*, **248**(1-2) 149-159.

De Vos, R.M. and Verweij, H., 1998. Improved Performance of Silica Membranes for Gas Separation, *Journal of Membrane Science*, **143**(1-2) 37-51.

Ding, X., Fan, Y. and Xu, N., 2006. A New Route for the Fabrication of TiO_2 Ultrafiltration Membranes with Suspension Derived from a Wet Chemical Synthesis, *Journal of Membrane Science*, **270**(1-2) 179-186.

Dong, Y., Liu, X., Ma, Q. and Meng, G., 2006. Preparation of Cordierite-Based Porous Ceramic Micro-Filtration Membranes Using Waste Fly Ash as the Main Raw Materials, *Journal of Membrane Science*, **285**(1-2) 173-181.

Dong, Y., Feng, X., Dong, D., Wang, S., Yang, J., Gao, J., Liu, X. and Meng, G., 2007. Elaboration and Chemical Corrosion Resistance of Tubular Macro-Porous Cordierite Ceramic Membrane Supports, *Journal of Membrane Science*, **304**(1-2) 65-75.

Dong, Y., Feng, X., Feng, X., Ding, Y., Liu, X. and Meng, G., 2008. Preparation of Low-Cost Mullite Ceramics from Natural Bauxite and Industrial Waste Fly Ash, *Journal of Alloys and Compounds*, **460**(1-2) 599-606.

Ebrahimi, M., Ashaghi, K.S., Engel, L., Willershausen, D., Mund, P., Bolduan, P. and Czermak, P., 2009. Characterization and Application of Different Ceramic Membranes for the Oil-Field Produced Water Treatment, *Desalination*, **245**(1-3) 533-540.

Ebrahimi, M., Willershausen, D., Ashaghi, K.S., Engel, L., Placido. L., Mund, P., Bolduan, P. and Czermak, P., 2010. Investigations on the Use of Different Ceramic Membranes for Efficient Oil-Field Produced Water Treatment, *Desalination*, **250**(3) 991-996.

Elmarraki, Y., Persin, M., Sarrazin, J., Cretin, M. and Larbot, A., 2001. Filtration of Electrolyte Solutions with New TiO_2-$ZnAl_2O_4$ Ultrafiltration Membranes in Relation with the Electric Surface Properties, *Separation and Purification Technology*, **25**(1-3) 493-499.

Erdem, I., Ciftcioglu, M. and Harsha, S., 2004. Preparation of Ceramic Composite Membranes for Protein Separation, *Key Engineering Materials*, **264-268**(8) 2251-2254.

Erdem, I., Ciftcioglu, M. and Harsa, S., 2006. Separation of Whey Components by Using Ceramic Composite Membranes, Desalination, **189**(1-3) 87-91.

Ersoy, B. and Gunay, V., 2004a. Effects of La_2O_3 Addition on the Thermal Stability of γ-Al_2O_3 Gels, *Ceramics International*, **30**(2) 163-170.

Ersoy, B. and Gunay, V., 2004b. Preparation and Characterization of Sol-Gel Derived 4%La_2O_3-Al_2O_3 Ceramic Membrane on Clay-Based Supports, *Key Engineering Materials*, **264-268** 403-406.

Ezzati, A., Gorouhi, E. and Mohammadi, T., 2005. Separation of Water in Oil Emulsions using Microfiltration, *Desalination*, **185**(1-3) 371-382.

Fakhfakh, S., Baklouti, S., Baklouti, S. and Bouaziz, J., 2010. Preparation, Characterization and Application in BSA Solution of Silica Ceramic Membranes, *Desalination*, **262**(1-3) 188-195.

Falamaki, C., Afarani, M.S. and Aghaie, A., 2004a. Initial Sintering Stage Pore Growth Mechanism Applied to Manufacture of Ceramic Membrane Supports, *Journal of the European Ceramic Society*, **24**(8) 2285-2292.

Falamaki, C., Naimi, M. and Aghaie, A., 2004b. Dual Behavior of $CaCO_3$ as a Porosifier and Sintering Aid in the Manufacture of Alumina Membrane/Catalyst Supports, *Journal of the European Ceramic Society*, **24**(10-11) 3195-3201.

Feins, M. and Sirkar, M.K., 2005. Novel Internally Staged Ultrafiltration for Protein Purification, *Journal of Membrane Science*, **248**(1-2) 137-148.

Fievet, P., Sbai, M., Szymczyk, A. and Vidonne, A.**,** 2003. Determining the ζ-potential of Plane Membranes from Tangential Streaming Potential Measurements: Effect of the Membrane Body Conductance, *Journal of Membrane Science*, **226**(1-2) 227-236.

Freeman, N.J., Peel, L.L., Swann, M.J., Cross, G.H., Reeves, A., Brand, S. and Lu, J.R., 2004. Real Time, High Resolution Studies of Protein Adsorption and Structure at the Solid–Liquid Interface Using Dual Polarization Interferometry. *Journal of Physics: Condensed Matter*, **16**(26) 2493-2496.

Frost, R.L., Kloprogge, J., Russell, S.C. and Szetu, J.L., 1999. Dehydroxylation and Structure of Alumina Gels Prepared from Trisecbutoxyaluminium, *Thermochimica Acta*, **329**(1) 47-56.

Fukushima, M., Zhou, Y. and Yoshizawa, Y., 2009. Fabrication and Microstructural Characterization of Porous SiC Membrane Supports with Al_2O_3–Y_2O_3 additives, *Journal of Membrane Science*, **339**(1-2) 78-84.

Furuta, S., Katsuki, H. and Takagi, H., 1994. Preparation and Properties of Fibrous Boehmite Sol and its Application for Thin Porous Membrane, *Journal of Materials Science Letters*, **13**(15) 1077-1080.

Garmash, E.P., Kryuchkov, Y.N. and Pavlikov, V.N., 1995. Ceramic Membranes for Ultra- and Microfiltration (Review), *Glass and Ceramics*, **52**(6) 19-22.

Garrido, L.B. and Aglietti, E.F., 2001. Pressure Filtration and Slip Casting of Mixed Alumina-Zircon Suspensions, *Journal of the European Ceramic Society*, **21**(12) 2259-2266.

Ghose, S., Bhattacharjee, C. and Datta, S., 2000. Simulation of Unstirred Batch Ultrafiltration Process Based on Reversible Pore-Plugging Model, *Journal of Membrane Science*, **169**(1) 29-38.

Ghosh, R. and Cui, Z.F., 1998. Fractionation of BSA and Lysozyme Using Ultrafiltration: Effect of pH and Membrane Pretreatment, *Journal of Membrane Science*, **139**(1) 17-28.

Giacomelli, C.E., Esplandiu, J.M., Ortiz, P.I., Avena, M.J. and De Pauli, C.P., 1999. Ellipsometric Study of Bovine Serum Albumin Adsorbed onto Ti/TiO_2 Electrodes, *Journal of Colloid and Interface Science*, **218**(2) 404-411.

Gonzalez, J.A., Carreras, A.C. and Ruiz, M.D., 2007. Phase Transformations in Clays and Kaolins Produced by Thermal Treatment in Chlorine and Air Atmospheres, *Latin American Applied Research*, **37**(2) 133-139.

Gualtieri, A., Bellotto, M., Artioli G. and Clark, S.M., 1995. Kinetic Study of the Kaolinite-Mullite Reaction Sequence. Part II: Mullite Formation, *Physics and Chemistry of Minerals*, **22**(4) 215-222.

Guizard, C., Ayral A. and Julbe, A., 2002. Potentiality of Organic Solvents Filtration with Ceramic Membranes. A Comparison with Polymer Membranes, *Desalination*, **147**(1-3) 275-280.

Guo, R., Ma, X., Hu, C. and Jiang, Z., 2007. Novel PVA-Silica Nanocomposite Membrane for Pervaporative Dehydration of Ethylene Glycol Aqueous Solution, *Polymer*, **48**(10) 2939-2945.

Haag, S., Burgard, M. and Ernst, B., 2006. Pure Nickel Coating on a Mesoporous Alumina Membrane: Preparation by Electroless Plating and Characterization, *Surface and Coating Technology*, **201**(6) 2166-2173.

Hilal, N., Al-Zoubi, H., Darwish, N.A. and Mohammad A.W., 2005. Nanofiltration of Magnesium Chloride, Sodium Carbonate and Calcium Sulphate in Salt Solutions, *Separation Science and Technology*, **40**(16) 3299-3321.

Ho, W.S.W. and Sirkar, K.K., 1992. Membrane Hand Book, Kluwer Academic Publishers, Van Nostrand Reinhold, New York.

Hochepied, J.F. and Nortier, P., 2002. Influence of Precipitation Conditions (pH and Temperature) on the Morphology and Porosity of Boehmite Particles, *Powder Technology*, **128**(2-3) 268-275.

Hodge, C.A. and Popovici, N.N., 1994. Pollution Control in Fertilizer Production, Marcel Dekker Inc., New York.

Hojamberdiev, M., Eminov, A. and Xu, Y., 2011. Utilization of Muscovite Granite Waste in the Manufacture of Ceramic Tiles, *Ceramics International*, **37**(3) 871-876.

Hsieh, H.P., 1996, Inorganic Membranes for Separation and Reaction, Elsevier, Amsterdam, The Netherlands.

Hua, F.L., Tsang, Y.F., Wang, Y.J., Chan, S.Y., Chuand, H. and Sin, H.N., 2007. Performance Study of Ceramic Microfiltration Membrane for Oily Wastewater Treatment, *Chemical Engineering Journal*, **128**(2-3) 169-175.

Huang, T. and Chen, H., 1995. A Study on the Preparation and Gas Permeation of Porous Alumina Supports, *Separation Science and Technology*, **30**(10) 2189-2209.

Huang, X., Meng, G., Huang, Z. and Geng, J., 1997.Preparation of Unsupported Alumina Membrane by Sol-Gel Techniques, *Journal of Membrane Science*, **133**(2) 145-150.

Huisman, I.H., Tragardh, G., Tragardh, C. and Pihlajamaki, A., 1998. Determining the Zeta-potential of Ceramic Microfiltration Membranes Using the Electroviscous Effect, *Journal of Membrane Science*, **147**(2) 187-194.

Hwang, K.T., Lee, H.S., Lee, S.H., Chung, K.C., Park, S.S. and Le, J.H., 2001. Synthesis of Aluminium Hydrates by a Precipitation Method and Their Use in Coatings for Ceramic Membranes, *Journal of the European Ceramic Society*, **21**(3) 375-380.

Hwang, K.J., Chou, F.Y. and Tung, K.L., 2006. Effects of Operating Conditions on the Performance of Cross-Flow Microfiltration of Fine Particle/Protein Binary Suspension, *Journal of Membrane Science*, **274**(1-2) 183-191.

Hyun, S.H. and Kang, B.S., 1994. Synthesis of Nanoparticulate Silica Composite Membranes by the Pressurized Sol-Gel Technique, *Journal of the American Ceramic Society*, **77**(12) 3093-3098.

Iritani, E., Mukai, Y. and Murase, T., 1995. Upward Dead-End Ultrafiltration of Binary Protein Mixtures, *Separation Science and Technology*, **30**(3) 369-382.

Iritani, E., Mukai, Y. and Hagihara, E., 2002. Measurements and Evaluation of Concentration Distributions in Filter Cake Formed in Dead-End Ultrafiltration of Protein Solutions, *Chemical Engineering Science*, **57**(1) 53-62.

Jakobs, E. and Koros, W.J., 1997. Ceramic Membrane Characterization via the Bubble Point Technique, *Journal of membrane science*, **124**(2) 149-159.

Jayaraman, V., Lin, Y.S., Pakala, M. and Lin, R.Y., 1995. Fabrication of Ultrathin Metallic Membranes on Ceramic Supports by Sputter Deposition, *Journal of Membrane Science*, **99**(1) 89-100.

Jedidi, I., Khemakhem, S., Larbot, A. and Amar, R.B., 2009. Elaboration and Characterisation of Fly Ash Based Mineral Supports for Microfiltration and Ultrafiltration Membranes, *Ceramics International*, **35**(7) 2747-2753.

Jia, M.D., Peinemann, K.V. and Behling, R.D., 1993. Ceramic Zeolite Composite Membranes: Preparation, Characterization and Gas Permeation, *Journal of Membrane Science*, **82**(1-2) 15-26.

Jones, C.D. and Barron, A.R., 2007. Porosity, Crystal Phase, and Morphology of Nanoparticle Derived Alumina as a Function of the Nanoparticle's Carboxylate Substituent, *Materials Chemistry and Physics*, **104**(2-3) 460-471.

Jun-hui, X., Yong, H. and Zhi-peng, X., 2002. Study Of Gel-Tape-Casting Process Of Ceramic Materials, *Materials Science and Engineering A*, **323**(1-2) 336-341.

Kandri, I., Ayral, A., Guizard, C., Ghadraoui, E.H.E. and Cot, L., 1999. Synthesis, Characterization and First Application of New Alumina Hydrosols, *Materials Letters*, **40**(2) 52-58.

Kang, B.S., and Gavalas, G.R., 2002. Intrapore Synthesis of Silicalite Membranes at Temperatures Below 100°C, *Industrial & Engineering Chemistry Research*, **41**(13) 3145-3150.

Karnik, B.S., Davies, S.H., Baumann, M.J. and Masten, S.J., 2005. Fabrication of Catalytic Membranes for the Treatment of Drinking Water Using Combined Ozonation Nanofiltration, *Environmental Science & Technology*, **39**(19) 7656-7661.

Kazemimoghadam, M. and Mohammadi, T., 2007. Synthesis of MFI Zeolite Membranes for Water Desalination, *Desalination*, **206**(1-3) 547-553.

Ke, X.B., Shao, R.F., Zhu, H.Y., Yuan, Y., Yang, D.J., Ratinac, K.R. and Gao, X.P., 2009. Ceramic Membranes for Separation of Proteins and DNA through In Situ Growth of Alumina Nanofibres inside Porous Substrates, *Chemical Communications*, **10** 1264-1266.

Khemakhem, S., Amar, R.B. and Larbot, A., 2007. Synthesis and Characterization of a New Inorganic Ultrafiltration Membrane Composed Entirely of Tunsian Natural Illite Clay, *Desalination*, **206**(1-3) 210-214.

Khider, K., Akretche, D.E. and Larbot, A., 2004. Purification of Water Effluent from a Milk Factory by Ultrafiltration Using Algerian Clay Support, *Desalination*, **167** 147-151.

Kim, J. and Lin, Y.S., 1999. Synthesis and Characterization of Suspension-Derived, Porous Ion-Conducting Ceramic Membranes, *Journal of the American Ceramic Society*, **82**(10) 2641-2646.

Kimura, S. and Sourirajan, S., 1967. Analysis of Data in Reverse Osmosis with Porous Cellulose Acetate Membranes Used, *AIChE Journal*, **13**(3) 497-503.

Kogel, J.E., Trivedi, N.C., Baker, J.S. and Krukowski, S.T., 2006. Industrial Minerals & Rocks: Commodities, Markets and Uses, SME Publisher, Littleton, Colorado.

Kong, J. and Li, K., 1999.Oil Removal from Oil-In-Water Emulsions Using PVDF Membranes, *Separation and Purification Technology*, **16**(1) 83-93.

Koros, W.J. and Mahajan, R., 2000. Pushing the Limits on Possibilities for Large Scale Gas Separation: Which Strategies, *Journal of Membrane Science*, **175**(2) 181-196.

Koros, W.J., Ma, Y.H. and Shimidzu, T., 1996. Terminology for Membranes and Membrane Processes, *Pure and Applied Chemistry*, **68**(7) 1479-1489.

Koter, S., 2006. Determination of the Parameters of the Spiegler-Kedem-Katchalsky Model for Nanofiltration of Single Electrolyte Solutions, *Desalination*, **198**(1-3) 335-345.

Kuzniatsova, T., Mottern, M.L., Shqau, K., Yu, D. and Verweij, H., 2008. Micro-structural Optimization of Supported γ-alumina Membranes, *Journal of Membrane Science*, **316**(1-2) 80-88.

Labbez, C., Fievet, P., Szymczyk, A., Vidonne, A., Foissy, A. and Pagetti, J., 2002. Analysis of the Salt Retention of a Titania Membrane Using the "DSPM" Model: Effect of pH, Salt Concentration and Nature, *Journal of Membrane Science*, **208**(1-2) 315-329.

Lafarga, D., Lafuente, A., Menendez, M. and Santamaria, J., 1998. Thermal Stability of γ-Al_2O_3/α-Al_2O_3 Mesoporous Membranes, *Journal of Membrane Science*, **147**(2) 173-185.

Larbot, A., Alami-Younssi, S., Persin, M., Sarrazin, J., Cot, L., 1994. Preparation of a y-alumina nanofiltration membrane, *Journal of Membrane Science*, **97** 167-173.

Laux, D., Ferrandis, J.Y., Bentama, J. and Rguiti, M., 2005. Ultrasonic Investigation of Ceramic Clay Membranes, *Applied Clay Science*, **32**(1-2) 82-86.

Leenaars, A.F.M., Keizer, K. and Burggraaf, A.J., 1984. The Preparation and Characterization of Alumina Membranes with Ultra-Fine Pores Part 1 Microstructural Investigations on Non-supported Membranes, *Journal of Materials Science*, **19**(4) 1077-1088.

Leenaars, A.F.M. and Burggraaf, A.J., 1985. The Preparation and Characterization of Alumina Membranes with Ultrafine Pores. 2. The Formation of Supported Membranes, *Journal of Colloid and Interface Science*, **105**(1) 27-40.

Leite, E.R., Cerri, J.A., Longo E. and Varela, J.A., 2003. Sintering of Undoped SnO_2, *Ceramica*, **49**(310) 87-91.

Levenstein, R., Hasson, D. and Semiat, R., 1996. Utilization of the Donnan Effect for Improving Electrolyte Separation with Nanofiltration Membranes, *Journal of Membrane Science*, **116**(1) 77-92.

Li, J., Wang, X., Wang, L., Hao, Y., Huang, Y., Zhang, Y., Sun, X. and Liu, X., 2006. Preparation of Alumina Membrane from Aluminium Chloride, *Journal of Membrane Science*, **275**(1-2) 6-11.

Li, K., 2007. Ceramic Membranes for Separation and Reaction, John Wiley & Sons, Ltd, Chichester, England.

Li, L., Liu, N., McPherson, B. and Lee, R., 2008. Influence of Counter Ions on the Reverse Osmosis through MFI Zeolite Membranes: Implications for Produced Water Desalination, *Desalination*, **228**(1-3) 217-225.

Lin, S.H., Hung, C.L. and Juang, R.S., 2008. Effect of Operating Parameters on the Separation of Proteins in Aqueous Solutions by Dead-End Ultrafiltration, *Desalination*, **234**(1-3) 116-125.

Lin, Y.S., De Vries, J. and Burggraaf, A.J., 1991. Thermal Stability and its Improvement of the Alumina Membrane Top-Layers Prepared by Sol-Gel Methods, *Journal of Materials Science*, **26**(3) 715-720.

Liu, Y., Liu, X., Wei, H. and Meng, G., 2001. Porous Mullite Ceramics from National Clay Produced by Gelcasting, *Ceramics International*, **27**(1) 1-7.

Liu, Y., Ma, D., Han, X., Bao, X., Frandsen, W., Wang, D. and Su, D., 2008. Hydrothermal Synthesis of Microscale Boehmite and Gamma Nanoleaves Alumina, *Materials Letters*, **62**(8-9) 1297-1301.

Lobo, A., Cambiella, A., Benito, J.M., Pazos, C. and Coca, J., 2006. Ultrafiltration of Oil-in-Water Emulsions with Ceramic Membranes: Influence of pH and Crossflow Velocity, *Journal of Membrane Science*, **278**(1-2) 328-334.

Luyten, J.,Cooymans, J., Smolders, C., Vercautereq, S.,. Vansant, E.F. and Leysen, R., 1997. Shaping of Multilayer Ceramic Membranes by Dip Coating, *Journal of the European Ceramic Society*, **17**(2-3) 273-279.

Machado, D.R., Hasson, D. and Semiat, R., 1999. Effect of Solvent Properties on Permeate Flow through Nanofiltration Membranes. Part I: Investigation of Parameters Affecting Solvent Flux, *Journal of Membrane Science*, **163**(1) 93-102.

Maleksaeedi, S., Paydar, M.H., Saadat, S. and Ahmadi, H., 2008. In Situ Vibration Enhanced Pressure Slip Casting of Submicrometer Alumina Powders, *Journal of the European Ceramic Society*, **28**(16) 3059-3064.

Mallada, R. and Menendez, M., 2008. Inorganic membranes: Synthesis, Characterization and Applications, Elsevier Science, Amsterdam, The Netherlands.

Mani, T.V., Pillai. P.K., Damodaran, A.D. and Warrier, K.G.K., 1994. Dependence of Calcination Conditions of Boehmite on the Alumina Particulate Characteristics and Sinterability, *Materials Letters*, **19**(5-6) 237-241.

Maruyama, T., Katoh, S., Nakajima, M., Nabetani, H., Abbott, T.P., Shono, A. and Satoh, K., 2001. FT-IR Analysis of BSA Fouled on Ultrafiltration and Microfiltration Membranes, *Journal of Membrane Science*, **192**(1-2) 201-207.

Maryasova, A.G. and Semin, G.L., 1998. Modelling of Pressure-Driven Membrane Separation of Electrolytes. High Temperature Approximation, *Journal of Membrane Science*, **142**(2) 205-212.

Matsufuji, T., Watanabe, K., Nishiyama, N., Egashira, Y., Matsukata, M. and Ueyama, K., 2000. Permeation of Hexane Isomers through an MFI Membrane, *Industrial & Engineering Chemistry Research*, **39**(7) 2434-2438.

Mazzoni, C., Orlandini, F. and Bandini, S., 2009. Role of Electrolyte Type on TiO_2-ZrO_2 Nanofiltration Membranes Performances, *Desalination*, **240**(1-3) 227-235.

McMillan, P. and Piriou, B., 1982. The Structures and Vibrational Spectra of Crystals and Glasses in the Silica-Alumina System, *Journal of Non-Crystalline Solids*, **53**(3) 279-298.

Meng, G., Wang, H., Zheng, W. and Liu, X., 2000. Preparation of Porous Ceramics by Gelcasting Approach, *Materials Letters*, **45**(3-4) 224-227.

Miao, S., Liu, Z., Ma, H., Han, B., Du, J., Sun, Z. and Miao, Z., 2005. Synthesis and Characterization of Mesoporous Aluminosilicate Molecular Sieve from K-Feldspar, *Microporous and Mesoporous Materials*, **83**(1-3) 277-282.

Mishra, D., Anand, S., Panda, R.K. and Das, R.P., 2000. Statistical Optimization of Conditions for the Hydrothermal Precipitation of Boehmite, *Hydrometallurgy*, **58**(2) 169-174.

Mishra, D., Anand, S., Panda, R.K. and Das, R.P., 2002. Effect of Anions during Hydrothermal Preparation of Boehmites, *Materials Letters*, **53**(3) 133-137.

Mohammadi, T. and Pak, A., 2003. Effect of Calcination Temperature of Kaolin as a Support for Zeolite Membranes, *Separation and Purification Technology*, **30**(3) 241-249.

Mohammadi, T., Pak, A., Karbassian, M. and Golshan, M., 2004. Effect of Operating Conditions on Microfiltration of an Oil-water Emulsion by a Kaolin Membrane, *Desalination*, **168** 201-205.

Mohammadi, T., Pak, A., Nourian, Z. and Taherkhani, M., 2005. Experimental Design in Mullite Microfilter Preparation, *Desalination*, **184**(1-3) 57-64.

Moreno, R., Salomoni, A., Stamenkovic, I. and Castanho, S.M., 1999. Colloidal Filtration of Silicon Nitride Aqueous Slips, Part II: Slip Casting and Pressure Casting Performance, *Journal of the European Ceramic Society*, **19**(1) 49-59.

Mottern, M.L., Chiu, W.V., Warchol, Z.T., Shqau, K. and Verweij, H., 2008. High-Performance Membrane Supports: A Colloidal Approach to the Consolidation of Coarse Particles, *International Journal of Hydrogen Energy*, **33**(14) 3903-3914.

Mulder, M., 1997. Basic Principle of Membrane Technology, Second Edition, Kluwer Academic Publishers, Dordrecht, The Netherlands.

Music, S., Dragcevic, D., Popovic, S. and Vdovi, N., 1998. Microstructural Properties of Boehmite Formed Under Hydrothermal Conditions, *Materials Science and Engineering B*, **52**(2-3) 145-153.

Nakatsuka, S. and Michaels, A.S., 1992. Transport and Separation of Proteins by Ultrafiltration through Sorptive and Non-Sorptive Membranes, *Journal of Membrane Science*, **69**(3) 189-211.

Nandi, B.K., Uppaluri, R. and Purkait, M.K., 2008. Preparation and Characterization of Low Cost Ceramic Membranes for Micro-Filtration Applications, *Applied Clay Science*, **42**(1-2) 102-110.

Nandi, B.K., Uppaluri R. and Purkait, M.K., 2009. Treatment of Oily Waste Water Using Low-Cost Ceramic Membrane: Flux Decline Mechanism and Economic Feasibility, *Separation Science and Technology*, **44**(12) 2840-2869.

Nasef, M.M. and Hegazy, E.A., 2004. Preparation And Applications of Ion Exchange Membranes by Radiation-Induced Graft Copolymerization of Polar Monomers onto Non-Polar Films, *Progress in Polymer Science*, **29**(6), 499-561.

Nazzal, F.F., Wiesner, M.R., 1994. pH and Ionic Strength Effects on the Performance of Ceramic Membranes in Water Filtration, *Journal of Membrane Science*, **93**(1) 91-103.

Neelakandan, C., Pugazhenthi, G. and Kumar, A., 2003. Preparation of NO_x Modified PMMA-EGDM Composite Membrane for the Recovery of Chromium (VI), *European Polymer Journal*, **39**(12) 2383-2391.

Noble, R.D. and Stern, S.A., 1995. Membranes Separations Technology: Principles and Applications, Elsevier, Amsterdam, The Netherlands.

Nomura, M., Seshimo, M., Aida, H., Nakatani, K., Gopalakrishnan, S., Sugawara, T., Ishikawa, T., Kawamura, M. and Nakao, S., 2006. Preparation of a Catalyst Composite Silica Membrane Reactor for Steam Reforming Reaction by Using a Counterdiffusion CVD Method, *Industrial & Engineering Chemistry Research*, **45**(11) 3950-3954.

Noordman, T.R., Ketelaar, T.H., Donkers, F. and Wesselingh, J.A., 2002. Concentration and Desalination of Protein Solutions by Ultrafiltration, *Chemical Engineering Science*, **57**(4) 693-703.

Pacewska, B., Ploskonska, O.K. and Szychowski, D., 2005. Influence of Aluminium Precursor on Physico-Chemical Properties of Aluminium Hydroxides and Oxides Part I. AlCl3.6H2O, *Journal of Thermal Analysis and Calorimetry*, **85**(2) 351-359.

Padmaja, P., Krishnapillai, P., Warrier, K.G.K. and Padmanabhan, M., 2004. Adsorption Isotherm and Pore Characteristics of Nano Alumina Derived from Sol-Gel Boehmite, *Journal of Porous Materials*, **11**(3) 147-155.

Palacio, L., Pradanos, P., Calvo, J.I., Kherif, G., Larbot, A. and Hernandez. A., 1998. Fouling, Structure and Charges of a Composite Inorganic Microfiltration Membrane, *Colloids and Surfaces A: Physicochemical and Engineering Aspects*, **138**(2-3) 291-299.

Palmeri, J., Blanc, P., Larbot, A. and David, P., 2000. Hafnia Ceramic Nanofiltration Membranes Part II. Modeling of Pressure-Driven Transport of Neutral Solutes and Ions, *Journal of Membrane Science*, **179**(1-2) 243-266.

Pan, Y., Wang, W., Wang T. and Yao, P., 2007. Fabrication of Carbon Membrane and Microfiltration of Oil-in-Water Emulsion: An Investigation on Fouling Mechanisms, *Separation and Purification Technology,* **57**(2) 388-393.

Panias, D. and Krestou, A., 2007. Effect of Synthesis Parameters on Precipitation of Nanocrystalline Boehmite from Aluminate Solutions, *Powder Technology*, **175**(3) 163-173.

Parks, G.A., 1965. The isoelectric points of solid oxides, solid hydroxides and aqueous hydroxo complex systems, *Chemical Reviews*, **65**(2) 177-198.

Peeters, J.M.M., Boom, J.P., Mulder, M.H.V. and Strathmann, H., 1998. Retention Measurements of Nanofiltration Membranes with Electrolyte Solutions, *Journal of Membrane Science*, **145**(2) 199-209.

Persson, A., Jonsson, A.S. and Zacchi, G., 2003. Transmission of BSA during Cross-Flow Microfiltration: Influence of pH and Salt Concentration, *Journal of Membrane Science*, 223(1-2) 11-21.

Potdar, A., Shukla, A. and Kumar, A., 2002. Effect of Gas Phase Modification of Analcime Zeolite Composite Membrane on Separation of Surfactant by Ultrafiltration, *Journal of Membrane Science*, **210**(2) 209-225.

Prabhakaran, K., Babu, N.R., Kumar, S.R. and Warrier, K.GK., 2002. Freeform Gelcasting of Porous Tubular Alumina Substrate, *Journal of the American Ceramic Society*, **85**(12) 3126-3128.

Pugazhenthi, G. and Kumar, A., 2005. Chromium (VI) Separation from Aqueous Solution Using Anion Exchange Membrane, *AIChE Journal*, **51**(7) 2001-2010.

Pujar, N.S. and Zydney, A.L., 1998. Electrostatic Effects on Protein Partitioning in Size Exclusion Chromatography and Membrane Ultrafiltration, *Journal of Chromatography A*, **796**(2) 229-238.

Qi, H., Fan, Y., Xing, W. and Winnubst, L., 2010. Effect of TiO_2 Doping on the Characteristics of Macroporous Al_2O_3/TiO_2 Membrane Supports, *Journal of the European Ceramic Society*, **30**(6) 1317-1325.

Randon, J., Blanc, P. and Paterson, R., 1995. Modification of Ceramic Membrane Surfaces Using Phosphoric Acid and Alkyl Phosphonic Acids and Its Effects on Ultrafiltration of BSA Protein. *Journal of Membrane Science*, **98**(1-2) 119-129.

Rao, S. and Zydney, A.L., 2006. High Resolution Protein Separations Using Affinity Ultrafiltration With Small Charged Ligands, *Journal of Membrane Science*, **280**(1-2) 781-789.

Reed, J.S, Introduction to the Principles of Ceramic Processing, John Wiley, New York, 1988.

Rios, G.M., Joulie, R., Sarrade, S.J. and Carles, M., 1996. Investigation of Ion Separation by Microporous Nanofiltration Membranes. *AIChE Journal*, **42**(9) 2521-2528.

Rittidech, A. and Tunkasiri, T., 2009. Influence of Heat Treatment in Sintering Process on Characteristics of Al_2O_3-ZrO_2 Ceramics Systems, *American Journal of Applied Sciences*, **6**(2) 309-312.

Romanos, G.E., Steriotis, T.A., Kikkinides, E.S., Kanellopoulos, N.K., Kasselouri, V., Ramsay, J.D.F., Langlois, P. and Kallu, S., 2001. Innovative Methods for Preparation and Testing of Al_2O_3 Supported Silicalite-1 Membranes, *Journal of the European Ceramic Society*, **21**(2) 119-126.

Sachdeva, S. and Kumar, A., 2008. Synthesis and Modeling of Charged Ultrafiltration Membranes of Poly(styrene-co-divinyl benzene) for the Separation of Chromium(VI), *Industrial & Engineering Chemistry Research*, **47**(12) 4236-4250.

Saffaj, N., Younssi, S.A., Albizane, A., Messouadi, A., Bouhria, M., Persin, M., Cretin, M. and Larbot, A., 2004a. Preparation and Characterization of Ultrafiltration Membranes for Toxic Removal from Wastewater, *Desalination*, **168** 259-263.

Saffaj, N., Loukili, H., Younssi, S.A., Albizane, A., Bouhria, Persin, M.M. and Larbot, A., 2004b. Filtration of Solution Containing Heavy Metals And Dyes By Means of Ultrafiltration Membranes Deposited on Support Made of Moroccan Clay, *Desalination*, **168** 301-306.

Saffaj, N., Persin, M., Younsi, S.A., Albizane, A., Cretin, M. and Larbot, A., 2006. Elaboration and Characterization of Microfiltration and Ultrafiltration

Membranes Deposited on Raw Support Prepared from Natural Moroccan Clay: Application to Filtration of Solution Containing Dyes And Salts, *Applied Clay Science*, **31**(1-2) 110-119.

Saksena, S. and Zydney, A.L., 1997. Influence of Protein-Protein Interactions on Bulk Mass Transport during Ultrafiltration, *Journal of Membrane Science*, **125**(1) 93-108.

Santos, L.R.B., Pulcinelli, S.H. and Santilli, C.V., 1997. Formation of SnO_2 Supported Porous Membranes, *Journal of Sol-Gel Science and Technology*, **8**(1-3) 477-481.

Sarkar, A., Rano, R., Mishra K.K. and Sinha, I.N., 2005. Particle Size Distribution Profile of Some Indian Fly Ash - A Comparative Study to Assess their Possible Uses, *Fuel Processing Technology*, **86**(11) 1221-1238.

Sarkar, B. and De, S., 2011. Prediction of Permeate Flux for Turbulent Flow in Cross Flow Electric Field Assisted Ultrafiltration, *Journal of Membrane Science*, **369**(1-2) 77-87.

Sathiyakumar, M. and Gnanam, F.D., 2002. Influence of MnO and TiO_2 Additives on Density, Microstructure and Mechanical Properties of Al_2O_3, *Ceramic International*, **28**(2) 195-200.

Seok, S., Kim, J.H., Choi, K.H. and Hwang, Y.Y., 2006. Preparation of Corrosion Protective Coatings on Galvanized Iron from Aqueous Inorganic–Organic Hybrid Sols by Sol–Gel Method, *Surface & Coatings Technology*, **200**(11) 3468- 3472.

Shah, T.N., Foley, H.C. and Zydney, A.L., 2007. Development and Characterization of Nanoporous Carbon Membranes for Protein Ultrafiltration, *Journal of Membrane Science*, **295**(1-2) 40-49.

Shameri, A.A. and Rong, L.X., 2009. Characterization and Evaluation of Algaof Kaolin Deposits of Yemen for Industrial Application, American Journal of Engineering and Applied Sciences, **2**(2) 292-296.

Shang, W.J., Wang, X.L. and Yu, Y.X., 2006. Theoretical Calculation on the Membrane Potential of Charged Porous Membranes in 1-1, 1-2, 2-1 and 2-2 Electrolyte Solutions, *Journal of Membrane Science*, **285**(1-2) 362-375.

Sheldon, R.A., Arends, I. and Hanefeld U., 2007. Green Chemistry and Catalysis, Wiley-VCH publisher, Weinheim, Germany.

Sheng, G., Chu, L., Zeltner, W.A. and Anderson, M.A., 1992. Nanoparticulate Alumina, Silica and Aluminosilicate Membranes, *Journal of Non-Crystalline Solids*, **147-148** 548-553.

Shqau, K., Mottern, M.L., Yu, D. and Verweij., 2006. Preparation and Properties of Porous α-Al_2O_3 Membrane Supports, *Journal of the American Ceramic Society*, **89**(6) 1790-1794.

Shukla, A. and Kumar, A., 2005. Characterization of Chemically Modified Zeolite-Clay Composite Membranes Using Separation of Trivalent Cations, *Separation and Purification Technology*, **41**(1) 83-89.

Shukla, R., Balakrishnan, M. and Agarwal, G.P., 2000. Bovine Serum Albumin-Hemoglobin Fractionation: Significance of Ultrafiltration System and Feed Solution Characteristics, *Bioseparation*, **9**(1) 7-19.

Singh, N. and Cheryan, M., 1998. Process Design and Economic Analysis of a Ceramic Membrane System for Microfiltration of Corn Starch Hydrolysate, *Journal of Food Engineering*, **38**(1) 57-67.

Skluzacek, J.M., Tejedor, M.I. and Anderson, M.A., 2006. An Iron-Modified Silica Nanofiltration Membrane: Effect of Solution Composition on Salt Rejection, *Microporous and Mesoporous Materials*, **94**(1-3) 288-294.

Spiegler, K.S. and Kedem, O., 1966. Thermodynamics of Hyperfiltration (Reverse Osmosis): Criteria for Efficient Membranes, *Desalination*, **1**(4) 311-326.

Srijaroonrat, P., Julien E. and Aurelle, Y., 1999. Unstable Secondary Oil/Water Emulsion Treatment Using Ultrafiltration: Fouling Control by Backflushing, *Journal of Membrane Science*, **159**(1-2) 11-20.

Steenkamp, G.C., Keizer, K., Neomagus, H.W.J.P. and Krieg, H.M., 2002. Copper (II) Removal from Polluted Water with Alumina/Chitosan Composite Membranes, *Journal of Membrane Science*, **197**(1-2) 147-156.

Stringer, R. and Johnston P., 2001. Chlorine and the Environment: An overview of the Chlorine Industry, Kluwer Academic Publisher, Dordrecht, The Netherlands.

Su, T.J., Lu, J.R., Cui, Z.F., Bellhouse, B.J., Thomas, R.K. and Heenan, R.K., 1999. Identification of the Location of Protein Fouling on Ceramic Membranes Under Dynamic Filtration Conditions, *Journal of Membrane Science*, **163**(2) 265-275.

Sugiyama, K. and Ryu, H.J. and Waseda, Y., 1993. Local Ordering Structure of Meta-Kaolinite and Meta-Dickite by the X-Ray Radial Distribution Function Analysis, *Journal of Materials Science*, **28**(10) 2783-2788.

Tan, B.H., Teng, T.T. and Omar, A.K., 2000. Removal of Dyes and Industrial Dye Wastes by Magnesium Chloride, *Water Research*, **34**(2) 597-601.

Tavolaro, A., 2002. VS-1 Composite Membrane: Preparation and Characterization, *Desalination*, **147**(1-3) 333-338.

Thomas, M.P., Landham, R.R., Butler, E.P., Cowieson, D.R., Barlow, E. and Kilmartin, P., 1991. Inorganic Ultrafiltration Membranes Prepared by a Combination of Anodic Film and Sol-Gel Technologies, *Journal of Membrane Science,* **61** 215-225.

Tsai, C.Y., Tama, S., Lu, Y., and Brinker, C.J., 2000. Dual-layer Asymmetric Microporous Silica Membranes, *Journal of Membrane Science*, **169**(2) 255-268.

Tsuru, T., Urairi., M., Nakao, S.I. and kimura S., 1991. Reverse Osmosis of Single and Mixed Electrolytes with Charged Membranes: Experiment and Analysis, *Journal of Chemical Engineering of Japan*, **24**(4) 518-524.

Tsuru, T., 2001. Inorganic Porous Membranes for Liquid Phase Separation, *Separation and Purification Methods*, **30**(2), 191-220.

Tu, C.H., Wu, L., Wang, D.X. and Wang, X.L., 2010. Prediction of Separation Performance of NF Membranes for Mixed Electrolytes Solution, *Desalination*, **260**(1-3) 218-224.

Tuan, V.A., Falconer, J.L. and Noble, R.D., 1999. Alkali-free ZSM-5 Membranes: Preparation Conditions and Separation Performance, *Industrial & Engineering Chemistry Research*, **38**(10) 3635-3646.

Tung, K.L., Hu, C.C., Li, C.L. and Chuang, C.J., 2007. Investigating Protein Crossflow Ultrafiltration Mechanisms Using Interfacial Phenomena, *Journal of the Chinese Institute of Chemical Engineers*, **38**(3-4) 303-311.

Uhlhorn, R.J.R., Huis, M.H.B.J., Intveld, Keizer K. and Burggraaf, A.J., 1992. Synthesis of Ceramic Membranes. Part I Synthesis of Non-Supported and Supported γ-alumina Membranes without Defects, *Journal of Materials Science*, **27**(2) 527-537.

Unuma, H., Kato, S., Ota, T. and Takahashi, M., 1998. Homogeneous Precipitation Of Alumina Precursors Via Enzymatic Decomposition Of Urea, *Advanced powder Technology*, **9**(2) 181-190.

Urano, H. and Fukuzaki, S., 2000. Conformation of Adsorbed Bovine Serum Albumin Governing its Desorption Behaviour at Alumina-Water Interfaces, *Journal of Bioscience and Bioengineering*, **90**(1) 105-111.

Van Gestel, T., Vandecasteele, C., Buekenhoudt, A., Dotremont, C., Luyten, J., Leysen, R., Van der Bruggen, B. and Maes, G., 2002. Alumina and Titania Multilayer Membranes for Nanofiltration: Preparation, Characterization and Chemical Stability, *Journal of Membrane Science*, **207**(1) 73-89

Varma, H.K., Mani, T.V., Damodaran, A.D., Warrier, K.G.K and Balachandra, U., 1994. Characteristics of Alumina Powders Prepared by Spray-Drying of Boehmite Sol, *Journal of the American Ceramic Society*, **77**(6) 1597-1600.

Vazquez, M.I., Lara, R.D. and Benavente, J., 2005. Modification in the Transport of NaCl and $MgCl_2$ Solutions across a Ceramic Microporous Membrane due to Chemical and Thermal Treatment, *Separation and Purification Technology*, **43**(3) 221-225.

Vercauteren, S., Keizer, K., Vansant, E.F., Luyten, J. and Leysen, R., 1998. Porous Ceramic Membranes: Preparation, Transport Properties and Applications, *Journal of Porous Materials*, **5**(3-4) 241-258.

Wang, P., Huang, P., Xu, N., Shi, J. and Lin, Y.S., 1999. Effects of Sintering on Properties of Alumina Microfiltration Membranes, *Journal of Membrane Science*, **155**(2) 309-314.

Wang, Q.K., Matsuura, T., Feng, C.Y., Weir, M.R., Detellier, C., Rutadinka, E. and Van Mao, R.L., 2001. The Sepiolite Membrane for Ultrafiltration, *Journal of Membrane Science*, **184**(2) 153-163.

Wang, X.L., Wang, W.N. and Wang, D.X., 2002. Experimental Investigation on Separation Performance of Nanofiltration Membranes for Inorganic Electrolyte Solutions, *Desalination*, **145**(1-3) 115-122.

Wang, Y.H., Zhang, Y., Liu, X.Q. and Meng, G.Y., 2006. Microstructure Control of Ceramic Membrane Support from Corundum-Rutile Powder Mixture, *Powder Technology*, **168**(3) 125-133.

Wang, Y.H., Liu, X.Q. and Meng, G.Y., 2007a. Preparation of Asymmetric Pure Titania Ceramic Membranes with Dual Functions, *Materials Science and Engineering A*, **445-446** 611-619.

Wang, Y.H., Zhang, Y., Liu, X.Q. and Meng, G.Y., 2007b. Sol-Coated Preparation and Characterization of Macroporous α-Al_2O_3 Membrane Support,'' Journal of. Sol-Gel Science and Technology, **41**(3) 267-275.

Wang, Y.H., Liu, X.Q. and Meng, G.Y., 2008. Preparation and Properties of Supported 100% Titania Ceramic Membranes, *Materials Research Bulletin*, **43**(6) 1480-1491.

Weir, M.R., Rutinduka, E., Detellier, C., Feng, C.Y., Wang, Q., Matsuura, T. and Le VanMao R.L., 2001. Fabrication, Characterization and Preliminary Testing of All-Inorganic Ultrafiltration Membranes Composed Entirely of a Naturally Occurring Sepiolite Clay Mineral, *Journal of Membrane Science*, **182**(1-2) 41-50.

Whittemore, O.J. and Sipe, J.J., 1974. Growth during the Initial Stages of Sintering Ceramics, *Powder Technology*, **9**(4) 159-164.

Wilharm, C. and Rodgers, V.G.J., 1996. Significance of Duration and Amplitude in Transmembrane Pressure Pulsed Ultrafiltration of Binary Protein Mixtures, *Journal of Membrane Science*, **121**(2) 217-228.

Wu, C., Zhang, S., Yang, D., Wei, J., Yan, C. and Jian, X., 2006. Preparation, Characterization and Application in Wastewater Treatment of a Novel Thermal Stable Composite Membrane, *Journal of Membrane Science*, **279**(1-2) 238-245.

Xu, Y. and Lebrun, R.E., 1999. Investigation of the Solute Separation by Charged Nanofiltration Membrane: Effect of pH, Ionic Strength and Solute Type, *Journal of Membrane Science*, **158**(1-2) 93-104.

Xu, Z., Zhang, L., Chen, N., Lu, W., Zhang, Z. and Wu, Z., 2006. Morphological Characterization of Al_2O_3 Membrane Fabricated by Sol-gel Dip-coating Method, *Journal of Shanghai University*, **10**(6) 553- 557.

Yang, C., Zhang, G., Xu, N. and Shi, J., 1998. Preparation and Application in Oil-water Separation of ZrO_2/α-Al_2O_3 MF membrane, *Journal of Membrane Science*, **142**(2) 235-243.

Yoldas, B.E., 1975a. Alumina Gels that Form Porous Transparant Alumina, *Journal of Materials Science*, **10**(11) 1856-1860.

Yoldas, B.E., 1975b. Alumina Sol Preparation from Alkoxides, *American Ceramic Society Bulletin*, **54**(3) 289-290.

Youm, K.H., Fane, A.G. and Wiley, D.E., 1996. Effects of Natural Convection Instability on Membrane Performance in Dead-End and Cross-Flow Ultrafiltration, *Journal of Membrane Science*, **116**(2) 229-241.

Zeman, L.J. and Zydney, A.L., 1996. Microfiltration and Ultrafiltration: Principles and Applications, CRC Press, Marcel Dekker, New York.

Zeng, W.M and Gao, L., 1999. Sintering Kinetics of α-Al_2O_3 Powder, *Ceramic International*, **25**(8) 723-726.

Zeng, W.M., Gao, L. and Guo, J.K., 1998. A New Sol-Gel Route Using Inorganic Salt for Synthesizing Al_2O_3 Nanopowders, *Nanostructured Materials*, **10**(4) 543-550.

Zhang, H., Quan, X., Chen, S. and Zhao, H., 2006. Fabrication and Characterization of Silica/Titania Nanotubes Composite Membrane with Photocatalytic Capability, *Environmental Science & Technology*, **40**(19) 6104-6109.

Zhang, X., Honkanen, M., Levanen, E. and Mantyla, T., 2008. Transition alumina nanoparticles and nanorods from boehmite nanoflakes, *Journal of Crystal Growth*, **310**(15) 3674-3679.

Zhao, Y., Xing, W., Xu, N. and Wong, F.S., 2005. Effects of Inorganic Electrolytes on Zeta Potentials of Ceramic Microfiltration Membranes, *Separation and Purification Technology*, **42**(2) 117-121.

Zhou, J., Chang, Q., Wang, Y., Wang J. and Meng, G., 2010. Separation of stable Oil-Water Emulsion by the Hydrophilic Nano-sized ZrO_2 Modified Al_2O_3 Microfiltration Membrane, *Separation and Purification Technology*, **75**(3) 243-248.

भारतीय प्रौद्योगिकी संस्थान गुवाहाटी
Indian Institute of Technology Guwahati

LIST OF PUBLICATIONS

International journals

[1] P. Monash and G. Pugazhenthi, Effect of TiO_2 addition on the fabrication of ceramic membrane supports: A study on the separation of oil and bovine serum albumin (BSA) from its solution, *Desalination*, (under Review).

[2] P. Monash and G. Pugazhenthi, Development of ceramic supports derived from low cost clays for membrane applications and its optimization based on sintering temperature, *International Journal of Applied Ceramic Technology*, 8(1) 227-238 (2011).

[3] P. Monash, A. Majhi and G. Pugazhenthi, Separation of BSA using γ-Al_2O_3-clay composite ultrafiltration membrane, *Journal of Chemical Technology and Biotechnology*, 85 (4), 545-554 (2010).

[4] A. Majhi, P. Monash and G. Pugazhenthi, Fabrication and characterization of γ-Al_2O_3-clay composite ultrafiltration membrane for the separation of electrolytes from its aqueous solution, *Journal of Membrane Science*, 340 (1-2), 181-191 (2009).

[5] P. Monash, A. Majhi and G. Pugazhenthi, Characterization of low cost clays for preparation of porous ceramic membrane supports, *International Journal of Chemical Sciences*, 5(4), 1862-1872 (2007).

Conferences

[1] A. Majhi, P. Monash and G. Pugazhenthi, Development of low cost γ-Al_2O_3-clay composite ultrafiltration membrane for separation of bovine serum albumin (BSA), *Euromembrane 2009*, Le Corum, Montpellier, France, September 06-10, 2009.

[2] P. Monash, A. Majhi, P. Balasubramanian, G. Pugazhenthi, A review on treatment of textile plant effluent by membrane separation processes, *Second international conference on "Resource utilization and intelligent systems* (INCRUIS-2008), Kongu Engineering College, Erode, January 3-5, 2008, 351-354.